SOLAR-HYDROGEN SYSTEMS FOR REMOTE AREA POWER SUPPLY

A thesis submitted in fulfillment of the requirements for the degree of Master of Engineering

SUHAIB MUHAMMED ALI

School of Aerospace Mechanical and Manufacturing Engineering

RMIT University

March 2007

Dedicated to my cousin brother, Mulla Mohammad Sabit Ali (1986-2007), whose unfortunate demise has created a permanent vacuum in our entire family

ACKNOWLEDGEMENTS

Throughout my research program, I have gained valuable experience and advice from many people I have interacted with and at this juncture I feel obliged to thank them all for being so helpful to me. First and foremost, I would like to express my sincere gratitude to my supervisor, **Dr. John Andrews** from RMIT University for his continuous support, valuable guidance and fruitful discussions in every aspect of my research work. Without John's guidance, I wonder if I could have able to finish the research. Probably the only thing for which I could consider myself as lucky is that I got John as my supervisor for he is arguably one of the best teachers and I consider him as my role model. Also I would like to thank my second supervisor, Prof. Aliakbar Akbarzadeh from RMIT University a stellar figure in the field of heat pipes, solar desalination who was the first to introduce me to this topic of research.

I would like to dedicate this thesis to my grand parents Mr. Mulla Ahamd Ali and Mrs. Hapsa Khatoon. Most importantly I am highly beholden to my mother, Mrs. Shakera Khatoon who has been my primary source of inspiration and love; my father Mr. Mulla Mohammad Ali for his support and encouragement throughout my life; my elder brother Saad Muhammed Ali, a civil engineer by profession, for his assurance and facilitation of all my paper works leading to my overseas studies; my only sister Umme Ruman and my brother Suhail Muhammed Ali who have always shown their love and encouragement. I am highly to my uncles Dr Liaqat Ali, a senior scientist; Dr Layaque Ali, a renowned physician; Mr Shaukat Ali, a teacher and my aunt Associate Prof. Naima Khatoon from AMU, Aligarh, India, for their constant support and encouraging words. Also I would like to offer my special thanks to my cousins Dr Bushra Liaqat, a dentist by profession and Miss Umme Hani, a student of Phd in Economics at AMU, Aligarh, India.

A very special thanks to Dr Randeep Singh, who can be very well be described as a friend, philosopher and guide for he is the first person whom I consult about both my academic and personal matters. I would also like to acknowledge the RMIT Energy Care group members particularly Bahman Shabani, Biddyut Paul and Arun Kumar and other colleagues in the research office for their assistance whenever required.

DECLARATION

I, Suhaib Muhammed Ali, hereby submit the thesis entitled “Solar hydrogen systems for remote area application” for the degree of Masters by Research and certify that except where due acknowledgement has been made, the work is that of the author alone; the work has not been submitted previously, in whole or in part, for any other academic award and that the content of the thesis is the result of work that has been carried out since the official commencement of the program.

Suhaib Muhammed Ali
31st March 2007

TABLE OF CONTENTS

LIST OF ABBREVIATIONS

RAPS	Remote Area Power Supply
PEM	Proton Exchange Membrane
$\Delta\overline{g}_f$	Gibbs free energy
V_{Ci}	Cut in Voltage
I_{max}	Maximum Current (electrolyser unit)
V_{max}	Maximum Voltage (electrolyser unit)
i_{max}	Maximum Current passing through a single cell
v_{max}	Maximum Voltage across a single cell
i_c	Current drawn by a single cell
m	Slope of I-V curve (electrolyser unit)
N_s	Number of cells in series
N_p	Number of cells in parallel
N	Total number of cells
H_e	Theoretical hydrogen production rate by a single cell
F	Faraday's Constant
η	Faraday's efficiency
H_E	Theoretical production rate by the stack
HHV	Higher Heating Value
LHV	Lower Heating Value
$\mathcal{P}$	Permeability
D	Diffusivity
S	Solubility

LIST OF FIGURES

LIST OF TABLES

EXECUTIVE SUMMARY

Remote area power supply (RAPS) is a potential early market for solar-hydrogen systems because of the comparatively high cost of conventional energy sources such as diesel generators in remote regions isolated from main electricity grid.

The objectives of this project are to:

- Review previous work on renewable energy – hydrogen systems, with special emphasis on remote power supply applications
- Develop a computer simulation model of small-scale solar hydrogen systems for remote energy supply with climatic conditions and the profile of the electrical load to be met as inputs.
- Design, construct and evaluate the performance of a laboratory-scale solar hydrogen system suitable for remote area power supply
- Investigate a number of low-cost options for storage of the hydrogen produced as compressed gas.
- Conduct a preliminary triple bottom line (economic, environmental and social) evaluation of this system compared to conventional RAPS systems employing battery storage or diesel generators.

The technological focus in this study is on a solar-hydrogen system based on a PV array, a Proton Exchange Membrane (PEM) electrolyser and a PEM fuel cell, with the hydrogen storage being carried out at low to medium pressure as compressed gas. It is assumed that the system is to be used for power supply to a remote homestead in south-eastern Australia assuming that is distant from the main electricity and natural gas grids.

In the present work, two experimental solar –hydrogen systems have been designed, constructed, and tested:

- A 50 W PEM electrolyser and 10 W PEM fuel cell system
- A 200 W PEM electrolyser and 500 W PEM fuel cell system.

Experimental data obtained from the PEM electrolysers and PEM fuel cells are compared with the manufacturers' predicted performances, and are used as key inputs to the computer modeling components of this study.

A mathematical model based on Excel spreadsheets and Visual Basic for determining the key characteristics of a solar photovoltaic - hydrogen system for RAPS, given the load to be met and the characteristics of the Proton Exchange Membrane (PEM) electrolyser and PEM fuel cell employed, has been developed. The primary objective of the model is to determine the size of each individual component of the solar-hydrogen system that yields the lowest unit cost of power supplied over a specified period. The model allows two different strategies for determining storage capacity to be compared: 'unconstrained storage', that is, allowing sufficient capacity to store all the hydrogen produced by excess PV power over load; and 'constrained storage', that is, limiting storage capacity to an economic minimum. The minimum unit costs of generated power can be evaluated for a range of constrained-storage capacities assuming the unit cost of all other components, namely electrolyser, fuel cell, and balance of system, remain constant.

The model has been applied to a case study of electricity supply to a remote homestead in south-eastern Australia. All the major parameters such as electrical load requirement and solar radiation for the particular conditions are fed into the model. The model run is carried out for the unconstrained and constrained storage conditions. For each condition the cost of power generation is evaluated by varying the assumed hydrogen storage cost while keeping the rest of the assumed unit costs fixed to typical values found in the literature.

A triple bottom line evaluation methodology covering economic, social and environmental factors has been employed to compare the solar- hydrogen RAPS system to the following alternative systems:

- A diesel generator + battery storage
- A PV array + diesel generator + battery storage
- A PV array + battery storage.

In terms of economics, it was found that a solar-hydrogen system supplying 5 kWh/d in a south-eastern Australian location offers a unit cost of energy in the range of US$1.5-2.5/ kWh depending on the assumed capital cost of storage (US$500/kg for the lower unit cost, US$2000 for the higher unit cost). This cost range compares with an estimated US$ 1.7-1.9 /kWh for a diesel generator – battery system, US$ 2.2-2.3 /kWh for a diesel generator – PV – battery system, and US$ 2.7-2.8 /kWh for a PV – battery system.

The analysis shows that, on the basis of the present capital costs of the main components of a solar-hydrogen RAPS system, a hydrogen storage system with very low losses and a capital cost of US$ 500/kg of hydrogen or less will be needed to make seasonal energy storage attractive and hence obtain the lowest overall unit cost of energy supplied. If this target storage cost can be achieved, a solar-hydrogen system will become an economically attractive proposition.

From environmental aspect, the solar-hydrogen system is the best option compared to the diesel and battery-based RAPS options. In particular, the solar-hydrogen system has zero greenhouse emissions in operation. But a full lifecycle assessment of all the options is still required to estimate embodied greenhouse emissions associated with making system components and disposing or recycling them at the end of their lifetimes.

A key social impact is the level of safety of a solar-hydrogen system compared to the alternatives. Clearly a full safety regimen for safe storage and usage of hydrogen in RAPS systems must be introduced through a new set of standards and regulations. A program of user education will also be required covering potential benefits of solar-hydrogen systems, and safe operating practices. A properly designed solar-hydrogen system should be able to meet the end-use demand over a full year with a high level of reliability, and without requiring regular maintenance, though further field testing and proving of the technology is still required.

A number of experimental investigations of systems for storing hydrogen storage at relatively low pressure, especially those pressure ranges achievable using a PEM electrolyser without external compressor, are reported in the thesis:

- Acrylic cylinders (9.7 litre) for laboratory experiment use

- Fibre reinforced plastic water tanks (225 litre)
- Composite cylinders (for pressures up to 20 bar)
- Low-carbon steel (up to 20 bar) cylinders

The acrylic cylinders and FRP water tank based hydrogen storages are assessed on the basis of mass and volumetric energy density, loss rate, hydrogen permeation, safety and cost per unit mass of hydrogen stored.

The theoretical loss of hydrogen for acrylic system over a period of 50 days was calculated to be around 3% by mass as against an experimentally measured loss of 22% over the same period. Similarly for the FRP water tank the theoretical loss of hydrogen over 45 days was found to be around 5% by mass while actual experimental loss of hydrogen over this period was measured to be almost 11%. There might be some mechanical leaks which escaped the leak testing undetected or developed at a latter stage.

The following recommendations for future work on solar-hydrogen systems for RAPS are made:

- Further experimental testing of the 250 W electrolyser – 500 W fuel cell system should be carried out to measure its performance over an extended period.
- Designing a heat recovery system to use the thermal output of the fuel cell for water heating purposes.
- Investigation of the option of collecting the hydrogen that is ventilated to the atmosphere by the fuel cell during open-ended operation, and burning this to provide additional heat for the hot water system or any other auxiliary requirement.
- Extending the modelling work on solar-hydrogen systems to include:
    - Running scenarios with a more realistic daily load profile that varies from day to day, and season to season, to investigate the effects on system sizing and economics
    - Further sensitivity testing of the results obtained for system component sizes for varying assumed costs of key components, especially the PEM electrolyser and fuel cell.
    - Incorporation into the model the effect of varying ambient temperature on the efficiency of the PV array.

- Research and development into a suitable control system for the overall solar-hydrogen-system should be conducted, covering:
    - Load splitting between final load and electrolyser
    - Switching between hydrogen production and hydrogen utilisation modes
    - Control of the fuel cell subsystem
    - Monitoring the amount of hydrogen in storage.
- Further development work into hydrogen storage systems suitable for stationary applications that have a unit capital cost of US$ 500/kg of hydrogen storage to exploit the full advantage of seasonal storage of hydrogen in solar-hydrogen RAPS systems. Options worthy of further investigation include:
    - Modified FRP, or other suitable high-strength, plastic water tanks for low-pressure storage using the water displacement method, with walls free from joints, the hydrogen outlet taken from a pipe rising from the bottom of the tank through the water to the top, and sensitive hydrogen leak detectors used to test for leaks that might have escaped detection under hydraulic and pneumatic leak tests.
    - Medium-pressure composite gas cylinders
    - Metal hydrides, given that much lower gravimetric and volumetric densities may be practical in RAPS applications than in vehicles.
- The possible use of unitised regenerative fuel cells – a single cell that can operate in either electrolyser or fuel cell mode as required - solar-hydrogen RAPS systems to lower the combined cost of a separate electrolyser and fuel cell. This option is possible since the electrolyser and fuel cell are never required to operate at the same time in a solar-hydrogen system of the type investigated in the present work.
- Extension of the triple bottom line evaluation of solar-hydrogen systems for RAPS with alternatives such as diesel or petrol generators, batteries with or without PV arrays needs to be to cover a life cycle assessment, in particular of embodied greenhouse gas emissions, of all the main components of these systems.

1. INTRODUCTION

1.1 IMPORTANCE OF RENEWABLE-ENERGY HYDROGEN SYSTEMS

The global awareness about the greenhouse effect and potentially adverse climate change has stimulated considerable interest internationally and in Australia in the 'hydrogen economy', where hydrogen is used as a zero-emission fuel for all purposes. On sustainability grounds it is preferable to produce hydrogen from water using renewable energy sources rather than fossil fuels. The principle of sustainable development refers to the necessity for human consumption of energy sources in the short and long term to be in harmony with the environment and look after the needs of future generations (WCED 1987). There weight of evidence suggests that anthropogenic greenhouse gas emissions are resulting in global climate change (IPCC 1995). The development of renewable energy sources and hence rational usage of energy have become the central aim of world energy policy in recent years. International studies have proposed increasing the share of renewable energy in the energy balance to enhance the security of energy supply by reducing the dependence on imported fossil energy sources (Doukas *et al.* 2005), and reducing global greenhouse emissions.

Australia has world's highest per capita greenhouse gas emissions among industrialized nations, and more than double the developed world's average (Passey *et al.* 2005). By 2020, it is estimated that Australia's emissions will be 23% higher than its 1990 level (AGO 2004a), which is much higher than 108% of its 1990 value that Australia agreed to under the Kyoto Protocol. All these factors point to the importance of increasing usage of renewable energy in Australian society. It is in this context that the Australian federal government introduced the Mandatory Renewable Energy Target (MRET) Act in 2001 that required an additional 9500 gigawatt hours of electricity per year by 2010 exclusively provided through renewable sources. Figure 1 shows the schematic diagram of the green-house effect.

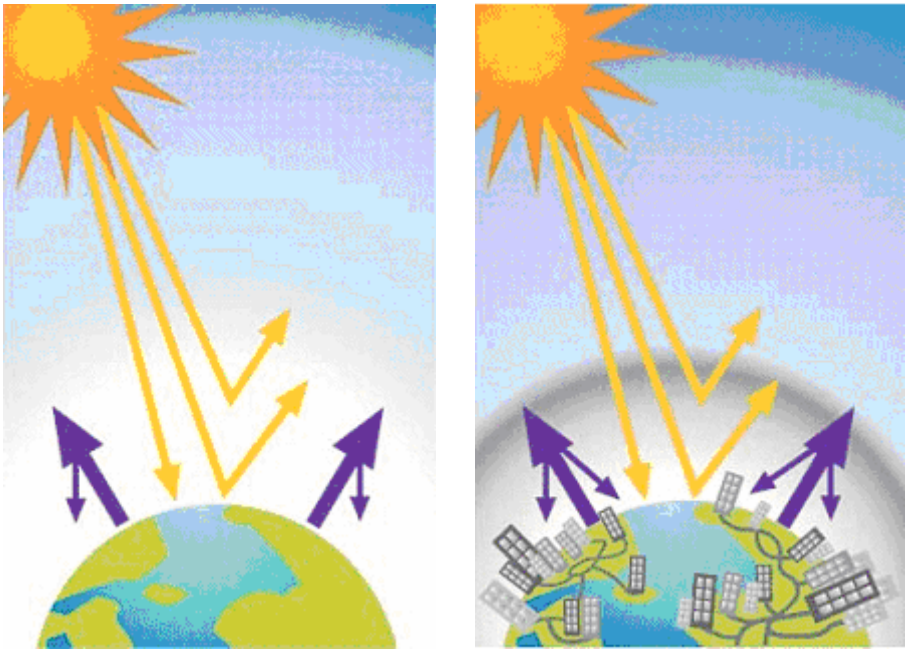

a. Natural effect b. Enhanced effect

Figure 1- Schematic diagram of greenhouse effect. (AGO 2002a)

Renewable energy has the potential to meet the present total world energy demand many times over. The solar radiation falling on 1% of world's desert area is sufficient to meet the energy requirements of the present day world (Zugel and Blackledge 2002). Hydrogen arguably offers the most attractive medium to store some of the solar and other renewables energy input for later usage as a transport fuel or for generating electricity via fuel cells usage, and hence achieves continuity of supply solely from renewable energy sources. The average solar radiation intensity of the entire world is shown in Figure 2. Areas shown in red color receive maximum solar insolations and those areas shown in blue color receive minimum level of solar radiation. The transition of energy from traditional fossil fuel based economy towards a sustainable hydrogen economy is shown in Figure 3 (Dunn 2000). It evident from the Figure 3 at present the market percentage usage of both solid fuels like coal and liquid fuel usage rate are diminishing over the years. On the other hand the market percentage of gas usage is increasing which at present is predominantly based on methane gas. But it is clear that in the latter part of this century hydrogen will become the fuel of the future.

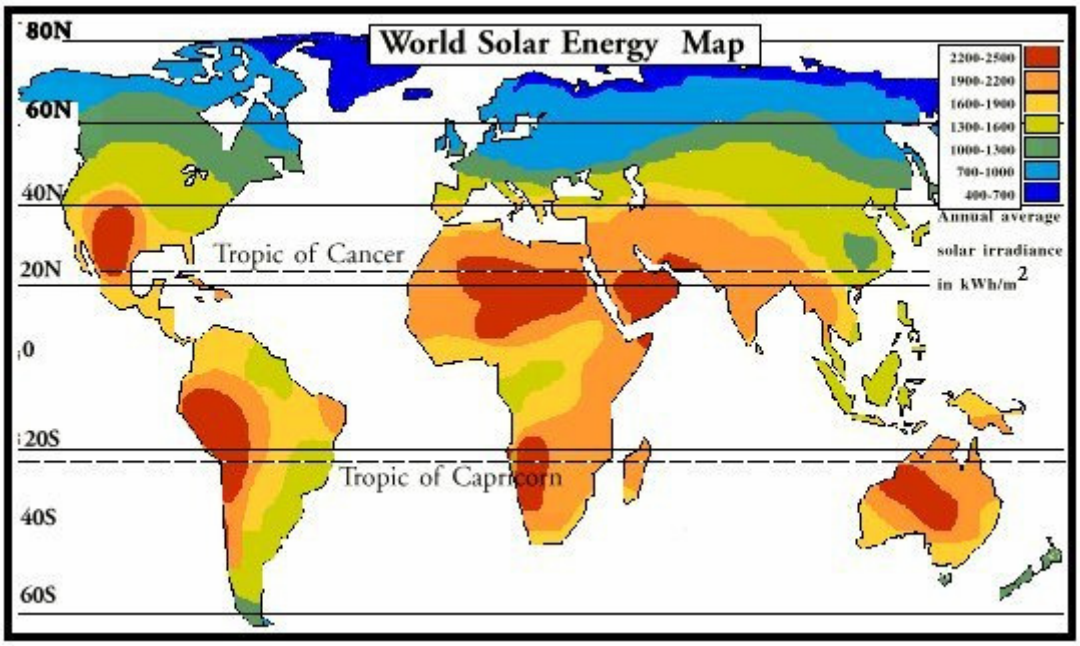

Figure 2- World Solar Energy Map (rise 2007: website)

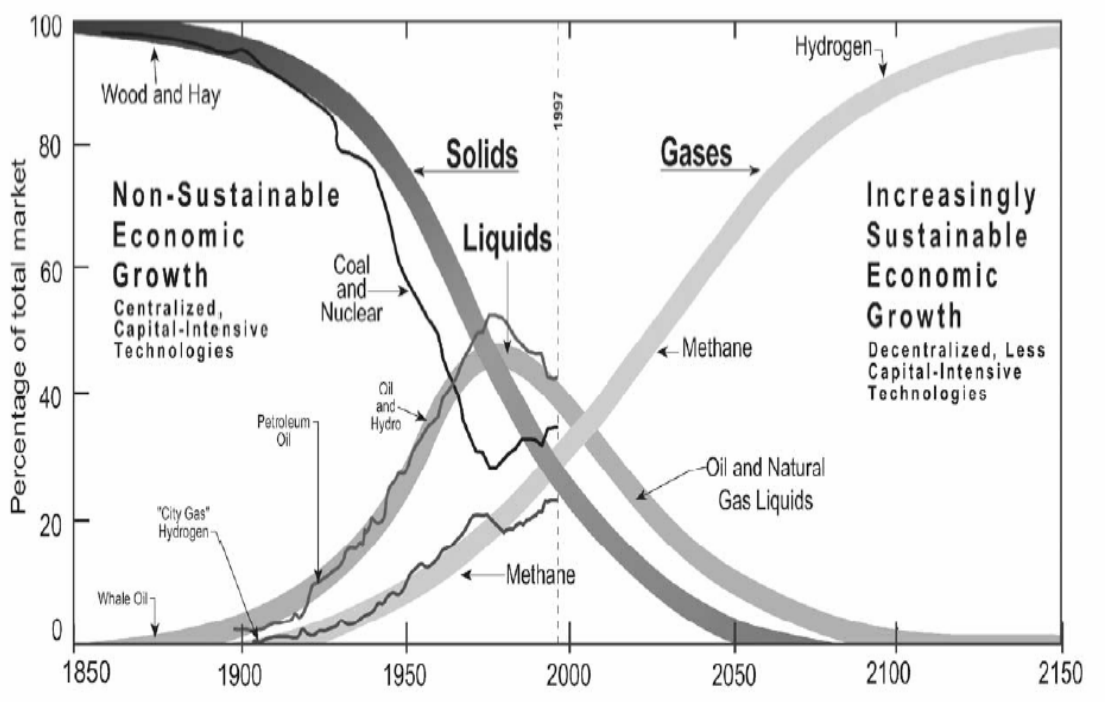

Figure 3 – Global energy system transition (Dunn 2002).

1.2 RAPS AS AN EARLY NICHE MARKET FOR RENEWABLE ENERGY HYDROGEN SYSTEMS

Renewable energy hydrogen systems are one of the most promising alternatives for the off-grid remote areas. Diesel generators with or without batteries can serve remote areas where conventional energy grids do not reach, but they have inherent limitations. Batteries can store electricity only for few days, thereby putting a constraint on the prospect of long duration seasonal storage of energy from summer to winter, while the very nature of remote and inaccessible area makes the supply of diesel fuel expensive and difficult. These limitations can be overcome by renewable-energy hydrogen remote area power supply (RAPS) Systems.

Though commercially available, renewable energy-hydrogen systems are still at an early stage of technological development and are not curretly commercially available. They require continuing research, development and demonstration effort in order to make them cost competitive and user friendly with respect to conventional diesel fuel or battery operated power supply systems.

Australian renewable energy sector supports a significant export oriented industry with 40 % of total revenue derived from export alone (ACRE Green paper 1997). Photovoltaic panels and remote area power supply systems forms the bulk of its expertise. Australia is regarded as a world leader in research in photovoltaics and associated RAPS technologies. There is a vast domestic demand potential of the renewable-energy based RAPS systems in Australia, the Asia Pacific region, and elsewhere internationally, because of the high cost of conventional fuels in remote areas, including remote communities, townships, islands, mining operations, and agricultural operations. . As a regional power, Australia is well suited both economically as well as geographically to exploit this potentially early niche market for renewable-energy hydrogen systems.

1.3 THE MAIN TECHNOLOGICAL OPTIONS FOR RENEWABLE-ENERGY HYDROGEN SYSTEMS FOR RAPS

There are a wide range of technological options that are currently available in the market for renewable energy based hydrogen systems. Photovoltaic panels and aero-generators are extensively used to convert renewable energy into electricity. Also hydroelectric schemes and biomass are widely used.

The electricity produced from a renewable source usually needs to be stored for later use when the primary renewable source is more limited or unavailable. This is particularly the case for solar radiation or wind, which are inherently variable. Instead of storing surplus energy in batteries, it may also be stored by producing hydrogen.

The produced hydrogen can be stored as a compressed gas in metal or composite cylinders at low, medium or high pressure. The higher the pressure of the storage is, the lower the volume required for a given energy content will be, but energy has to expended to compress the hydrogen and the cost of the cylinder per unit volume rise as the storage pressure increases. Alternatively hydrogen is cooled for storage as a liquid in cryogenic tanks. A third storage options is to use solid materials such as metal hydrides or carbon nanotubes that can absorb and desorb hydrogen by varying their pressure and temperature.

The stored hydrogen can be recovered to be used in fuel cell or internal combustion engine to generate electricity at the demand site. There are five main kinds of fuel cells now available in the market: proton exchange membrane fuel cell, alkaline fuel cell, phosphoric acid fuel cell, solid oxide fuel cell, and molten carbonate fuel cell (Larminie and Dicks 2004).

In addition all renewable-energy hydrogen systems require a control system and various power converters and regulators. Collectively this is called the ‘balance of system’ and includes everything in the system apart from the renewable energy source, the hydrogen production system, the hydrogen storage system and the fuel cell or other hydrogen energy converter. The balance of system unit required will vary considerably depending on the renewable energy source used, and the various other main components. It remains

important, however, as the unit that ensures all the components work together, and it often comprises a significant proportion of the overall cost of the system.

1.4 TECHNOLOGICAL FOCUS OF THIS STUDY

In this study the technological focus is on a solar-hydrogen system based on a PV array, a PEM electrolyser and a PEM fuel cell, with the hydrogen storage being carried out at low to medium pressure as compressed gas. The decision to focus on solar PV as the energy source is because of PV's widespread current usage and Australia's high amount of average solar radiation (Figure 3)

For the electrolysis process, a PEM electrolyser is chosen due to it high energy efficiency coupled with no liquid electrolyte, which makes the unit more compact, lightweight and easy to handle compared to conventional alkaline electrolyser. At present the cost of a PEM electrolyser is high but again a mass production of such electrolyser in future is poised to bring it down. The main advantage of using a PEM electrolyser is that it can generate hydrogen at elevated pressure without the need for a separate compressor, i.e. up to 20 bars (Larminie and Dicks 2003). At present commercial hydrogen storage are being carried out in high pressure compressed gas or in liquid state cryogenic cylinder. Both of these processes are expensive and energy intensive and are primarily designed for automobile applications. Since the stationary applications in remote areas can offer ample space, hydrogen storage can be carried out at low pressure large volume tanks. Such tanks will be cost effective which would then its implication on cost of overall system and hence on unit cost of energy supply.

The consumption of hydrogen to regenerate electricity is carried out in a PEM fuel cell. Unlike other fuel cells such as solid-oxide fuel cell, alkaline fuel cells, a PEM fuel cell has the advantage that it operates at low temperature and has relatively higher energy efficiency. It is quite sensitive to the changes in supply rate of reactant which can be controlled as a feed back to the changes in load.

Such a solar hydrogen system is chosen for power supply to a remote homestead in south-eastern Australia assuming such a location to be away from the main electricity and natural gas grids.

1.5 DESIGN AND EVALUATIVE APPROACH (TRIPLE BOTTOM LINE EVALUATION)

The design of solar-hydrogen RAPS systems, and a brief comparison of the system with other types of RAPS systems, is carried out in this thesis using a triple bottom line methodology covering economic, social and environmental factors (Elkington, 1999). The economic comparison is carried out on the basis of lifecycle cost analysis in which an average unit cost of energy supplied is computed taking into account the full lifecycle of each component of the system. The main social factors considered are level of service provided, including reliability; user attitudes and experience; safety; and regulations and standards. The main environmental criterion is greenhouse gas emissions, and brief mention is also made of other environmental impacts such as how to dispose of or recycle toxic materials in batteries.

1.6 OBJECTIVES OF THIS PROJECT

The overall objectives of this project are to:

- Review previous work on renewable energy – hydrogen systems, with special emphasis on remote power supply applications
- Develop a computer simulation model of small-scale solar hydrogen systems for remote energy supply with climatic conditions and the profile of the electrical load to be met as inputs.
- Design, construct and evaluate the performance of a laboratory-scale solar hydrogen system suitable for remote area power supply
- Investigate a number of low-cost options for storage of the hydrogen produced as compressed gas.

- Conduct a preliminary triple bottom line (economic, environmental and social) evaluation of this system compared to conventional RAPS systems employing battery storage or diesel generators.
- Identify components or system aspects requiring further R&D to improve their performance and cost effectiveness.

1.7 RESEARCH QUESTIONS

The specific research questions that are addressed in this thesis are the following:

- What is the optimal design for a PEM-based solar hydrogen system to meet a given profile of annual electricity demand at a remote location?
- What is the most cost-efficient hydrogen storage option for small to medium-scale remote area application?
- How do solar-hydrogen RAPS systems compare with the conventional diesel generator and PV- battery systems from the triple bottom line point of view?
- What improvements in cost and performance are required to make solar-hydrogen systems competitive with conventional RAPS technologies?
- Which system components in solar hydrogen RAPS systems require further R&D?

1.8 OUTCOMES

The research is expected to yield the following outcomes that would be beneficial in further advancement of knowledge in the specified field:

- A working demonstration in RMIT University's Renewable Energy laboratory of a small-scale experimental solar hydrogen system for remote area power supply based on PEM technology
- An evaluation of the technical performance of this system.
- A simulation model useful in designing future solar hydrogen systems.
- A triple bottom line (economic, environmental and social) comparison of this system with conventional RAPS systems employing battery storage or diesel generators.
- Identification of components or system aspects requiring further R&D.

1.9 STRUCTURE OF THESIS

The solar - hydrogen system for RAPS applications that is studied in this thesis is introduced and its technical features explained in Chapter 2. Chapter 3 is dedicated to describing the experimental solar-hydrogen systems that have been designed, constructed and tested in the course of this project. Key parameters and characteristics curves of components for use in subsequent modeling are also identified. Chapter 4 describes the computer-based simulation model of solar-hydrogen RAPS systems, based on Excel and Visual basic, that has been developed in the present study. A case study in which the model is applied to a solar-hydrogen system for meeting the demand of a remote household is presented in Chapter 5. A detailed analysis of a number of potential options for low-lost storage of gaseous hydrogen at low pressures for RAPS applications is given in Chapter 6. This analysis is followed in chapter 7 by a preliminary a triple bottom line comparison of the solar-hydrogen RAPS system studied here with other RAPS options. Conclusions and recommendations arising from the project as a whole are presented in Chapter 8.

2. SOLAR - HYDROGEN SYSTEMS FOR RAPS

2.1 INTRODUCTION

2.1.1 The Remote Area Power supply Market

Energy supply to any application at a location not connected to central electricity grids or gas distribution networks forms the basis of the Remote Area Power Supply (RAPS) market. The main types of application include the following:

- remote households
- remote communities, e.g. Outback Aboriginal communities in Australia, the mountainous tribal belts of India, the islands of the Asia-Pacific and Oceania regions
- remote villages and townships
- telecommunications, meteorological or the satellite facilities
- mines and other remote industrial and agricultural operations

The focus in this study will be on meeting the demands of remote households, but the same principles and technologies are generally applicable to all other RAPS applications.

2.1.2 Conventional Remote Area Power Supply Systems

Conventional remote area power supply systems are either exclusively based on fossil fuels or renewable sources coupled with fossil fuel based power generation systems. Petrol and diesel generators form the most common form of fossil fuel RAPS system. An over view of the different configurations for RAPS application is shown in Table 1. The diesel-battery system is widely found in small to medium ranges of RAPS application

and is a proven matured technology. PV panels are often added to diesel system for systems having a medium to large capacity. Also PV/Wind generators are also installed with battery storage for medium scale RAPA application. Of late hydrogen generation, storage and reuse is being considered as a potential competitor to be added to these sources. Various combination of these energy sources are coupled with hydrogen system for RAPS application. A PV alone with hydrogen is considered a suitable for all three (small-medium-large) scales.

Type of System	**Technological Maturity**	**Scale**
Diesel-Battery	Mature	Small, Medium
PV-Diesel-Battery	Mature	Medium, Large
PV/Aerogen.–Battery	Mature	Medium.
PV-H_2	*New*	*Small, Medium, Large.*
PV/Aerogen-Battery-Diesel	Mature	Medium, Large
PV/Aerogen-H_2	New	Medium, Large
Aerogen.-Diesel gem-Battery	Mature	Medium, Large
Aerogenetor-H_2	New	Large
Micro-hydro-H_2	New	Large

Table 1 Technological options for RAPS application**.** (The configuration discussed in this thesis is mentioned in italic text).

2.1.3 Renewable Energy Hydrogen System for Remote Area Power Supply

RAPS applications vary according to the location and power and energy demands of the user. A number of renewable-energy technology options are available for such applications. Solar photovoltaic and wind power systems are the most commonly deployed, but befouls and micro-hydro units are possible alternative sources of renewable

energy. At present, different combinations of PV panels, aero generator, and bio-fuel coupled with battery storage are generally employed.

Solar-hydrogen systems with their renewable energy source, decentralized on-site hydrogen generation and storage, and reuse of the stored hydrogen in fuel cells offer a completely autonomous RAPS system that enables uninterruptible power supply to the load. Solar-hydrogen systems ability to be completely independent of an electricity grid or any form of fossil-fuel based back-up makes then highly suitable to supply the power for the remote area applications. Also their lower environmental impact and higher reliability are among their advantages over conventional battery or diesel-supported systems.

Among renewable-energy based RAPS systems there are a number of different technological options that are suitable for different load requirements and locations with varying availability of renewable energy sources. It is generally found that solar and wind are the preferred source of renewable energy for small to medium scale RAPS applications (Shakya *et al.*2004). Wind energy is specially preferred for small energy demands where as a hybrid solar-wind combination is recommended for medium scale demand range if the wind energy alone is not sufficient to meet the energy demand or for economical considerations. A solar based RAPS system is preferred if the location receives a fair amount of solar insolation. The reliability and low maintenance cost (no moving parts) associated with photovoltaic panels puts itself as a preferable option for remote area applications. Unlike wind the solar insolation is more consistent and predictable for a particular location.

2.2 SOLAR-HYDROGEN RAPS SYSTEMS: CURRENT STATUS

Remote area power supply (RAPS) is a potential early market for renewable energy – hydrogen systems because of the relatively high costs of conventional energy sources such as diesel generators in regions remote from the main electricity grid. A typical solar hydrogen system is shown in Figure 4. Some experimental and demonstration solar-

hydrogen systems in the power range 1.5 kW to 250 kW have been built internationally (Khole *et al.* 2003) Generally photovoltaic cells have been used as the source of renewable energy, and Proton Exchange Membrane (PEM) fuel cells to convert stored hydrogen back to electricity. Increasingly PEM electrolysers are also being employed in RAPS applications (Ali *et al.*2005; Kolhe *et al.* 2003). A number of simulation models of solar-hydrogen systems have also been reported in the literature (Andrews *et al.* 2005; Lehman *et al.* 1994). Hydrogen production by electrolysis is an existing technology that serves a high-value industrial and medical market. An increase in efficiency coupled with a decline in cost, are the keys to adapting this technology to meet energy-related applications in the future. Among all existing options, alkaline electrolysis is the most mature technology for most commercial systems in use today. At present PEM electrolysis systems are expensive; they are poised to mirror the cost reduction and improvements for fuel cells (Schatz Energy Research Center 2003).

.

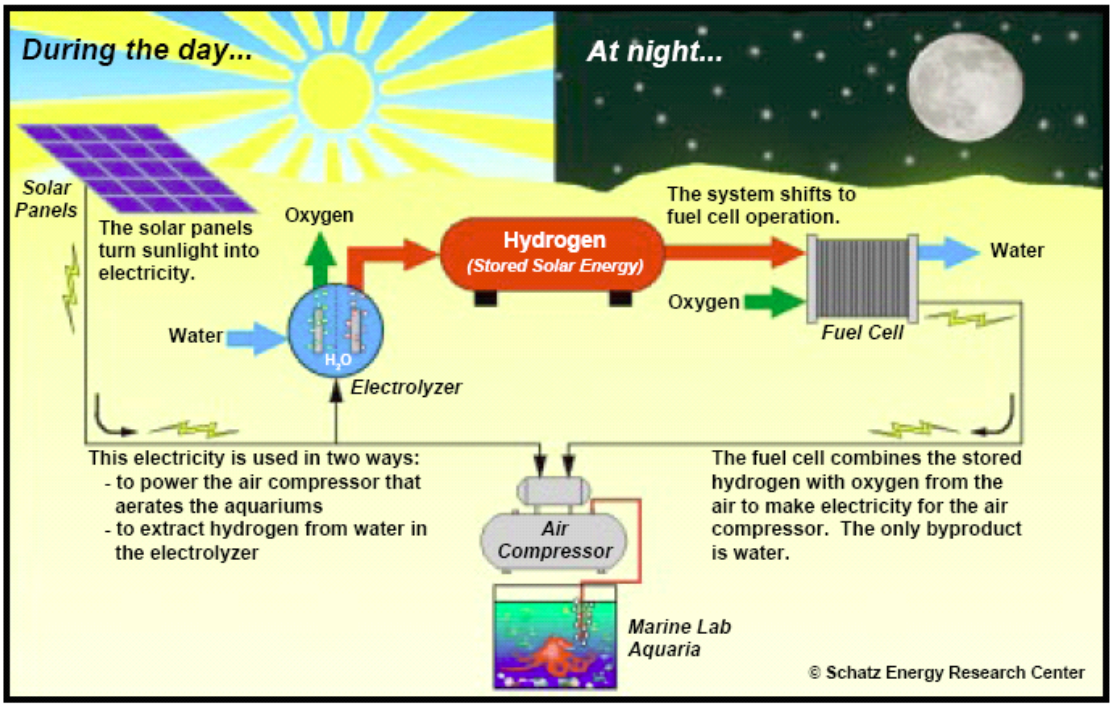

Figure 4- A typical present day solar hydrogen system (Schatz Energy Research Center 2003).

Some experimental and demonstration solar–hydrogen systems in the power range of 1.5 kW to 250 kW have been built internationally (Agbossou *et al.* 2004; Lehman *et al.*1994). Generally photovoltaic cells have been used as the source of the renewable energy and proton exchange membrane (PEM) fuel cells to convert stored hydrogen back to electricity. Increasingly PEM electrolysers are also being employed in RAPS applications (Suchan 2000). RAPS applications can broadly be categorized as those systems dedicated to off grid remote areas and other standalone power supply systems. As hydrogen is not an energy source occurring in its naturally elemental form, it needs to be produced from the others sources i.e. water, ammonia or hydrogen rich hydro-carbons like methane or natural gas. Though several methods have been developed for production of hydrogen from renewable energy sources, the most promising option that currently provides practical solution is electrolysis of water (Barbir 2005).

As far as safety issues are concerned, quite contrary to the general public perception, hydrogen is as safe as any other common fuels (Barbir 1999). Ogden and Williums (1989) evaluated the solar hydrogen options and concluded that hydrogen could be economically produced from larger PV power plants if the cost of PV could be brought to $0.2 to $0.4/ Watt. An operating experience with PV hydrogen system was mentioned by Lehman et al. (1994). A simulation of solar hydrogen system for different location was done by Torres et al (1998). Vosen and Keller (1999) made an optimisation of system performance and cost control for a stand alone solar-hydrogen power system. El-Shatter (2002) designed and simulated a hybrid PV/fuel cell system. Wang, Nehrir and Nelson (2002) designed a Simulink-based model for a standalone wind-PV fuel cell operating system. Veziroglu and Barbir (1992) compared hydrogen over conventional fuels based upon some criteria i.e. versatility, utilization efficiency, environmental compatibility safety and economy. The results from this study indicated that hydrogen has the overall merit factor. It was found to have the most versatile convertibility at the user end, efficient, environmentally most compatible, one of the safest and cost effective fuel to society.

Numerous studies have been conducted into self-sufficient small-scale solar hydrogen systems over the past few years. For example, Lehman and Chamberlain (1991) conducted the feasibility of a small-scale self-sufficient solar-hydrogen system employing alkaline electrolyser and PEM fuel cells with metal hydride based hydrogen storage system. Even

though a higher volumetric density was reported but the higher cost of metal hydride makes this system unsuitable for solar H_2 systems. Santarelli (2003) has demonstrated a number of RAPS systems dedicated to remote area power supply i.e. non grid connected applications.

2.3 REMOTE POWER SUPPLY

The average daily energy requirement for RAPS applications ranges from 2 – 10 kWh for a remote homestead to 100 kWh or more for larger agricultural or industrial installations. Some mines or rural industrial enterprises can have daily energy demands in the MWh range or even higher.

The profiles of the electrical power demand of remote household in Australia have been examined previously. For example, the Sustainable Energy Development Office (SEDO, 2002) estimated the demand of a typical small remote homestead with modest energy needs using statistical data on the likely appliances in the household and their daily usage in summer and winter. All of the electrical energy appliances were assumed to be used carefully. The details of the estimated usage are given in Table 2. There is a small difference in electrical load requirement between summer (6.2 kWh/day) and winter (5.3 kWh/day). This could be due to difference in electrical appliance usage.

Appliance/Equipment	Power Ratings (W)	Number of Units	Total power rating (W)	Usage time(hr/day)		Daily usage (Wh/day)	
				Summer	Winter	Summer	Winter
Compact fluorescent lamp	20	5		3	4	300	400
Refrigerator	200	1	200	10	8	2000	1600
Microwave	800	1	800	0.5	0.5	400	400
Microwave's digital clock	5	1	5	24	24	120	120
Toaster	600	1	600	0.08	0.08	48	48
Television	150	1	150	3	3	450	450
Video recorder	100	1	100	3	3	300	300
Video standby and clock	10	1	10	24	24	240	240
Stereo	80	1	80	3	3	240	240
Washing machine	700	1	700	0.5	0.5	350	350
Incandescent lights	60	5	300	2	3	600	900
Power tools	800	1	800	0.14	0.14	112	112
Vacuum cleaner	1000	1	1000	0.14	0.14	140	140
Computer	100	1	100	0.25	0.25	25	25
Ceiling fan	150	2	300	3	0	900	0
Total Peak Power			**1900**	**Total Daily Energy**		**6225**	**5325**

Table 2-Typical Australian homestead daily power requirements. (Research institute for sustainable energy Australia 2006).

There is also an Australian standard relating to the energy demand for a remote Australian homestead, namely AS 4509.2. This standard has been developed assuming all the heating and cooking processes utilise bottled LPG gas, so do not add to electricity demand. The details of the electrical power usage in this standard are presented in Table 3.

Appliance	Model	No.	Cont. Real Power (Watts)	Surge apparent Power (Watts)	Usage Time (hr/day)	Daily Energy use = Watts X Hours
Kitchen						
Refrigerator	F&P C190 (ii)	1	94	1536	13.4	1260
Freezer	None					
Light	Single Fluorescent	1	36	40	4	144
Toaster	Sunbeam	1	900	900	0.1	90
Living Area						
Lights	Performer	1	20	23	4	80
Reading	-	1	40	46	1	40
Television	Gold star 34cm	1	40	65	3	120
Radio	Kambrook	1	6	10	4	24
Lights	Performer	1	16	18	2	32
Study/Office:						
Desk Light	Kambrook	1	30	34	0.5	15
Computer	Pearl 486	1	20		3	60
Bedroom 1						
Lights	Performer	1	16	18	1	16
Lights	Performer	1	16	18	1	16
Laundry						
Washing Machine	Fisher & Paykel	1	200	1600	1	57
Iron	Sunbeam	1	1800	1800	0.5	257
Lights	Performer	1	16	18	1	16
Bathroom						
Lights	Performer	1	16	18	2	32
Fan	Kambrook	1	40	80	0.5	20
Workshop/ Other*:*						
Total Daily Energy Use						**2280**

Table 3- Energy demand for a typical small remote Australian house. (Australian Standards AS4509.2)

The values mentioned in Table 3 are specific to a very small remote household in rural outback. The total daily energy use is much smaller (2.28 kWh) as compared to a daily use of 6.225 kWh recommended by SEDO. The difference could be due to the fact that SEDO recommendations are for an average household not specifically a remote homestead one.

This study will focus on a typical demand for a remote household in south eastern Australia. It is assumed that bottled is not available for cooking purpose so a relatively higher daily energy (5kWh) requirement than the recommended Australian Standards for remote household is considered for the case study.

2.4 THE SOLAR-HYDROGEN SYSTEM STUDIED

2.4.1 System Configuration

The basic solar-hydrogen system for RAPS applications studied in this thesis is a stand-alone system comprising a photovoltaic array, a PEM electrolyser and fuel cell and storage of hydrogen gas in low-pressure containers. A schematic of the system is shown in the Figure 6, and the logic of its mode of operation is described in Figure 6.

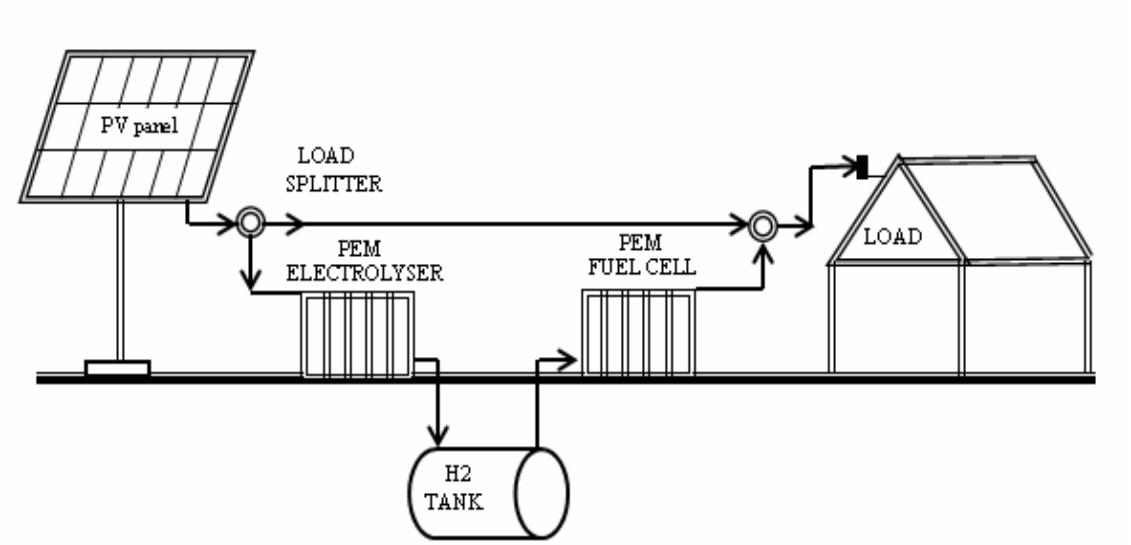

Figure 5- A schematic diagram of the solar-hydrogen system showing its main components

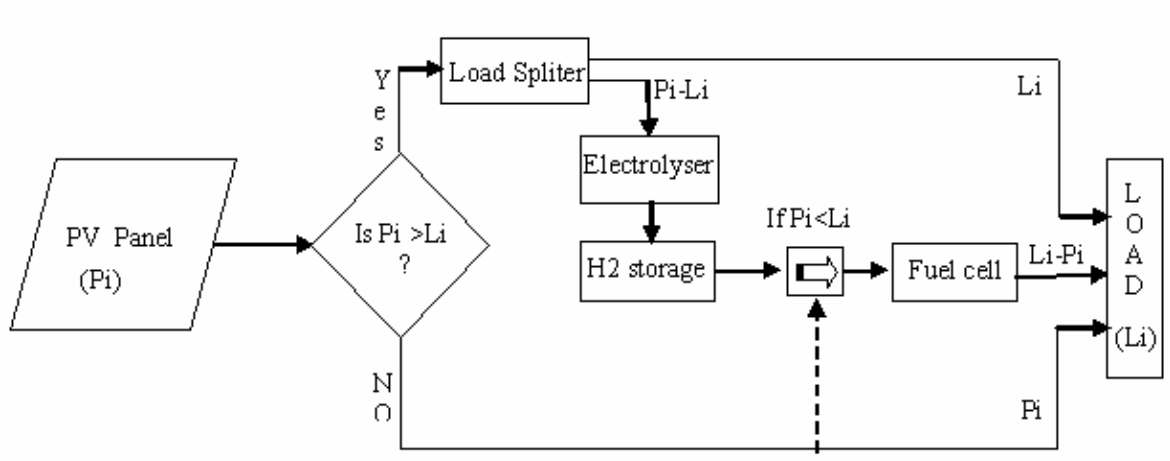

Figure 6-Mode of operation of the solar-hydrogen system

Solar-hydrogen systems for RAPS applications can be divided into two basic types depending on the fraction of the total load that is met from by drawing energy from the storage system. In the type 1, the electrical power from the PV panel is supplied directly to the load, and only the excess power over the instantaneous demand is utilised by the electrolyser for the production of hydrogen. In the type 2, all the available electrical energy from the PV panels is fed to the electrolyser to generate the hydrogen, and subsequently the load at the user end is exclusively drawn from the fuel cell.

Each of these two system types has its relative advantages and disadvantages that can be outlined as follows:

- The first type has the inherent advantage of being the more energy-efficient system so that a smaller PV array and smaller hydrogen storage capacity are required compared to type 2. This advantage arises since in the type 1 system only a fraction of the total load is supplied via the electrolyser-storage-fuel cell system, which inevitably will lead to energy losses, while in the type 2 system all the load is supplied via this storage system with consequently greater energy losses.
- The type 1 system minimises the working hours of operation of both the electrolyser and fuel cell, hence extending their lifetimes, since these units are only working some of the time.
- In the type 2 system, the electrolyser is working whenever there is sunlight, and the fuel cell at all times there is any load.
- The type 2 system eliminates the extra cost of the load-splitter as there is no bypassing of power directly from the panel to the load.
- The type 2 system may be more suited to applications with rapidly varying loads, since it may in practice be difficult to switch quickly between supplying all power directly to the load and some to the electrolyser, and to switch the fuel cell on and off over short intervals.
- The type 2 system would also be suited to an application where all (or most of) the load was at night when there is no sunlight.

The advent of proton exchange membrane (PEM) electrolysers and fuel cells with quick response times to changing inputs and loads has made the type 1 system both technically

possible and more attractive. Therefore, in the present work the focus will be on this system type 1.

2.4.2 System components

The basic solar-hydrogen system for RAPS applications that is studied in this thesis thus has the following major components:

- PV Panel
- Load splitter
- PEM electrolyser
- Hydrogen storage
- PEM fuel cell
- Balance of system.

2.4.3 Photovoltaic Panels

Photovoltaic panels act as a renewable source of direct-current electricity free of any associated running cost. With continuous decrease in initial cost and simultaneous improvement in efficiency, their usage is poised to become more extensive (Nafeh 2002). PV panels are made from a large number of individual cells connected in series and parallel configurations. The standard type of PV cell consists of a p-n junction semiconductor with a photosensitive n-layer (Figure 7).

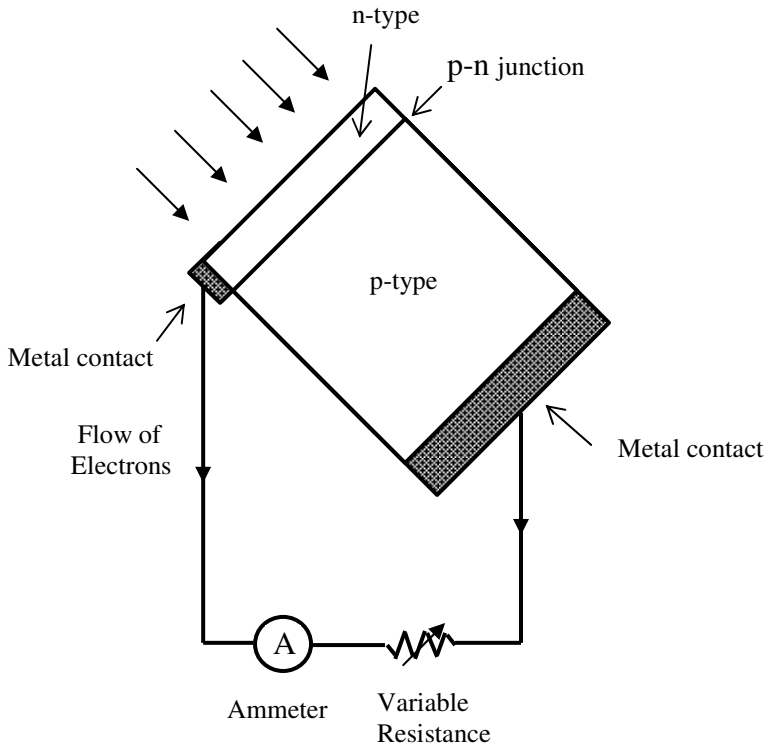

Figure 7 - Working mechanism for a PV cell.

When a photon strikes this layer, it can provide enough energy to an otherwise stable electron to overcome the band energy gap of the material. The band energy gap is defined as the energy difference between the conduction band and valence band of the material. In a typical PV cell, semiconductors with n-type and p-type materials are placed side by side forming a p-n junction. In the n-type semiconductor material electrons are free to move at room temperature, while in the p-type material positively-charged holes are freely moving at normal temperatures. A p-n junction operates as a diode. When a spectrum of photons with energy higher than the band gap energy of the semiconductor strikes this diode, the number of free electrons in the p type material and holes in the n type are considerably increased. When these released free electrons and positive holes reach the p-n junction, an electric field is generated across the junction. This induced electric field drives a current if both the p and n type semiconductors are connected externally, thereby providing a useful source of direct-current electric energy (Masters GM 2004).

The electrical output of a PV panel can be calculated from its characteristics and the solar radiation incident on its surface. The total solar radiation incident on the panel can be regarded as a summation of following three components:

- Direct normal solar radiation (I_b)
- Diffuse solar radiation (I_d)
- Reflected global radiation (I_R)

The general equation for relationship between current and voltage of a PV cell is given by

$$I = I_{ph} - I_d - \frac{V_d}{R_p} = I_{ph} - I_r \left\{ e^{\left[\frac{q(V+IR_s)}{AKT} \right]} - 1 \right\} - \left(\frac{V + IR_s}{R_p} \right) \quad \text{----------[Eq 2.1]}$$

Where I = PV cell out put current (A), V= PV output voltage, I_{ph} = photo current, I_d =diode current, I_r= reverse saturation current, q = charge of electron, A ideality factor. K= Boltzman constant and T = cell operating temperature k.

The photo current is directly proportional to the incident solar radiation and also depends on cell temperature

$$I_{ph}(G_a, T) = I_{sc(Ts)} \frac{G_a}{G_{as}} \left[1 + K_0 (T - T_s \right] \quad \text{----------[Eq 2.2]}$$

Where Ga is the solar radiation, T is the cell operating temperature, also dependent on incident irradiance. $I_{sc(Ts)}$ = short circuit current on standard test conditions. G_{as} is standard irradiance (1000 W/m^2), K_0 = short circuit current temperature coefficient. The cell operating current is approximately proportional to the incident solar radiation and is given by

$$T = T_a + C_t G_a \quad \text{----------[Eq 2.3]}$$

where C_t is constant = $\dfrac{NOCT(^0C) - 20}{800 \, W/m^2}$

NOCT is normal operating cell temperature, which is generally given by the manufacture specifications.

2.4.4 Load Splitter and control system

The allocation of the PV power output to the various components of the system according to varying conditions is achieved by using a load splitter. When the PV output is greater than the load ($P_i > L_i$), the load is met directly and entirely by the PV array. The surplus power over the load (P_i-L_i) is diverted by the load splitter to the electrolyser for generation of hydrogen gas.

If on the other hand the PV output is less than the load (that is, $P_i < L_i$), then the load splitter ensures P_i is supplied to the load, while the rest of the load (L_i-P_i) must now be drawn from the fuel cell. The splitting of the PV output according to the prevailing conditions can be accomplished by a feedback connection provided through the current-voltage regulation channel available in the conventional data loggers (such as the Data Taker DT 500, or DT 800 units).

2.4.5 Electrolyser

2.4.5.1 Types of Electrolyser

Hydrogen is generally generated via electrolysis by allowing electricity to pass between two electrodes in contact with water. The water molecule is broken down resulting in the formation of hydrogen and oxygen molecules respectively.

H_2O + electrical energy $\longrightarrow$ H_2 +1/2 O_2

There are several methods that have been developed for production of hydrogen by electrolysis namely:

- Alkaline electrolysis
- Acidic electrolysis
- Low-temperature PEM electrolysis
- Thermo-chemical electrolysis
- Photochemical electrolysis
- Biochemical electrolysis

Out of these options, the most commonly used methods to date are alkaline electrolysis and PEM electrolysis. The alkaline (KOH) electrolyser is often preferred for hydrogen generation due to its high conductivity. These alkaline electrolysers can be unipolar where the electrolysers resemble a water tank like structure with electrodes being connected in parallel whereas bipolar electrolyser is similar to a filter press structure (Ivy 2004). The liquid electrolyte with its complications of non- uniform charge distribution, problems associated with handling, and high energy consumption per unit hydrogen production (due to a high cell resistance) are some of the disadvantages associated with alkaline electrolysers (Hydrogen Technology Research Center HYTREC report 2006: website). Generally liquid electrolytes in which electrodes are immersed for the reaction to occur result in a low effective contact area between electrode and electrolyte, and a large distance between electrodes that resists the flow of ions due its ohmic resistance (Larminie and Dicks 2003). The advent of solid polymer or proton exchange membrane based electrolysers has overcome some of these those short comings.

2.4.5.2 PEM electrolyser

In a PEM electrolyser, a solid polymer membrane acts as the ion-conducting electrolyte, in place of the aqueous solution of an alkaline electrolyser. The polymer membrane conducts the flow of H^+ ions from the anode to cathode where formation of hydrogen molecules occurs (Barbir 2005). Figure 8 shows working model of a PEM electrolyser.

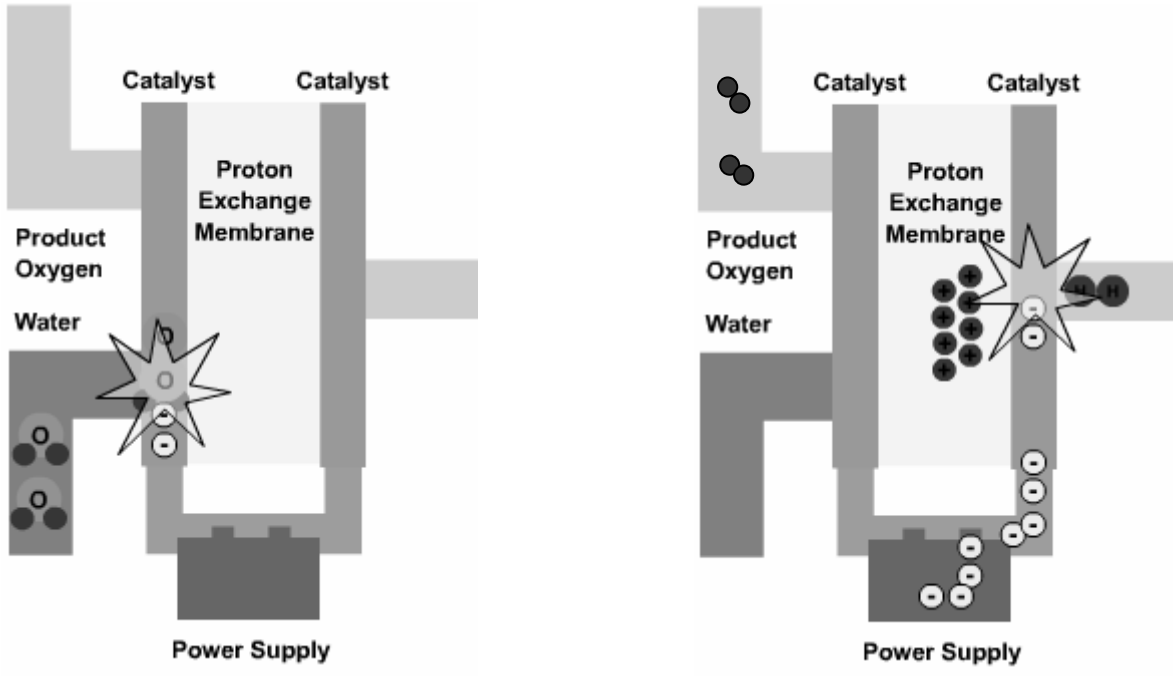

a. Water molecule splitting **b.** Recombination of hydrogen molecule

Figure 8- Schematic diagram of a PEM electrolyser working mechanism initial (a) and final (b) stages of reaction.

Invented by Willard Thomas Grubb and Lee Niedrach in early 1960, the proton exchange membrane (PEM) successfully eliminated the problems such as continuous circulation of electrolyte, a nonuniform distribution ionic current, and high cell resistance associated with conventional liquid (KOH) electrolytes etc. The proton exchange membrane allows the electrolysis process to take place in a solid electrolyte, and has the following additional advantages over conventional alkaline electrolysers:

- ability to cope with a variable power input
- a higher purity level of the produced hydrogen
- higher rates of hydrogen production per unit mass and volume of the electrolyser unit
- an option of getting compressed hydrogen directly delivered without the requirement of a mechanical compressor
- increased level of safety and ecological cleanliness
- lower costs per unit mass of hydrogen produced
- regular replacement of liquid electrolyte is avoided as the electrolyte is entirely solid state and does not degrade
- an energy efficiency almost 10% higher (Grigoriev *et al.* 2007)

Moreover there are some inherent advantages associated with PEM electrolysers when used with renewable energy sources. The characteristic current- voltage curve of a PEM electrolyser is such that there is a possibility with appropriate series – parallel stacking of getting a high power transfer from the PV panel to PEM electrolyser with direct coupling, thus eliminating the requirement for an expensive maximum power point tracker, and the use of a dc/dc converter (Paul and Andrews 2007).

Operational performance data for some of the larger PEM electrolyser units that are commercially available are provided in Table 4. The Proton HOGEN H series has got a maximum delivery pressure of 218 psig with a hydrogen production rate of 6 kg/hr. The peak power corresponding to the maximum production rate is 38 kW. The Proton HOGEN 20 - 40 are relatively smaller scale as compared to H series or Proton HOGEN 380. The Proton HOGEN 20 has got a minimum hydrogen production rate of 05.kg/hr with peak power corresponding to maximum H_2 production rate is just 3kW. The largest among them is the Proton HOGEN 380 with a hydrogen production rate of 10 kg/hr with peak power corresponding to maximum production rate being 63 kW. The purity level for all of these electrolysers are 99.999%.

Model Manufacturer	Hydrogen Production Rate	H2-delivery Pressure	Energy Requirements	Peak Power corresponding to max H2 prod.	H2 Purity level
	(kg/hr)	psig	(kWh/kg)	(kW)	(%)
Proton HOGEN H Series	6	218	70.1	38	99.999
Proton HOGEN 20	0.5	200	62.3	3	99.999
Proton HOGEN 40	1	200	62.3	6	99.999
Proton HOGEN 380	10	200	70.1	63	99.999

Table 4- Working Performance some of the large scale PEM electrolysers (Source: Ivy 2004).

For all the reasons outlined in this subsection, the present study focuses exclusively on the use of a PEM electrolyser in the solar-hydrogen system investigated.

2.4.5.3 Theoretical characteristics of PEM electrolyser

The decomposition of water molecule into hydrogen and oxygen is achieved by passing a d.c. electric current through the PEM electrolyser:

$$2H_2O \rightarrow 2H_2 + O_2 \qquad \Delta\overline{g}_f > 0 \qquad \text{[Eq. 2.1]}$$

Where $\Delta\overline{g}_f$ is the Gibbs free energy of the water decomposition reaction. The positive sign of $\Delta\overline{g}_f$ indicates the reaction is endothermic, i.e. it requires an energy input to proceed in the forward direction. A certain minimum electric voltage V_{Ci} , called the cut in voltage, must be applied to initiate this reaction, and thereafter cell current increases approximately linearly with increasing applied voltage up to its maximum allowed current (I_{max} occurring at V_{max}), as shown in Figure 9.

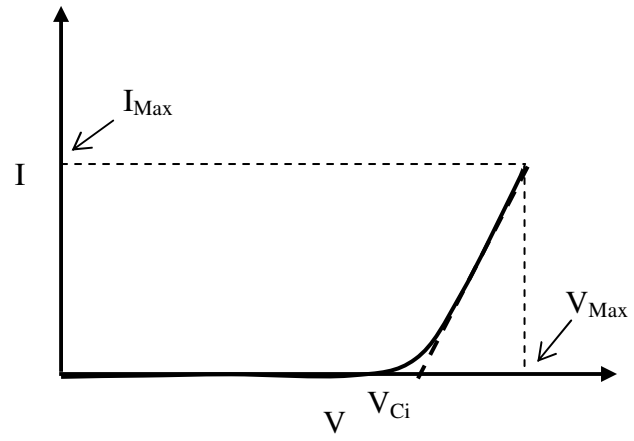

Figure 9-Current density versus Voltage characteristic curves for PEM electrolyser.

For most PEM electrolysers, the linear approximation to the V-I curve is a good one over its allowed operating range, and Vci can be taken as the intercept of this straight line with the voltage axis. The constant slope of the V-I curve is then given by

$$m = \frac{i_{Max}}{(V_{Max} - V_{Ci})} \qquad \text{[Eq. 2.1]}$$

The current drawn by the single cell can be expressed

$i_c = (Vc\text{-}V_{ci})/m_c$,

Or the voltage can be expressed in terms of current as

$$v_c = \frac{i_c}{m_c} + v_{ci} \qquad \text{[Eq. 2.2]}$$

Individual PEM electrolyser cells can be connected in series and/or parallel configurations to get an electrolyser stack of higher hydrogen production capacity and with a maximum voltage and current as required.

The power consumed by one single cell is

$p = v_{Max} \times i_{Max}$

Total stack power, P_s, thus can be expressed in terms of the individual cell current (i_c) and voltage (v_c) as follows:

$$P_s = V_s \times I_s = N_p i_c \times N_s v_c = N i_c v_c \quad , \qquad \text{[Eq. 2.3]}$$

where N_p and N_s are the number of cells in parallel and series respectively, and N is the total number of cells in the stack (that is, N_p x N_s).

The stack power can be expressed in terms of instantaneous current i_c and cell voltage v_c as follows:

$$P_s = N \times i_c \times v_c$$

$$= N \times i_c \times (\frac{i_c}{m_c} + v_{co})$$

Hence the following quadratic function for i_c can be obtained:

$$i_c^{\,2} + m_c v_{co} i_c - \frac{m_c P_s}{N} = 0 \qquad \text{[Eq.2.4]}$$

Solving this quadratic equation for i_c yields:

$$\therefore\ i_c = \frac{-m_c v_{co} + \sqrt{(m_c v_{co})^2 + \frac{4 m_c P_s}{N}}}{2} \qquad \text{[Eq 2.4]}$$

The negative root is neglected as it is not physically relevant in this case.

According to Faraday's first law, the theoretical hydrogen production rate, H_e, is given by:

$$H_e = \frac{Currentdrawn}{FaradayConst \times (electron/molH_2)} \text{ mol/sec}$$

$$= \frac{i_c}{1000F} \text{ kg/sec} \qquad \text{[Eq.2.5]}$$

Where F is Faraday's constant equal to 96 485 C/mol. For the release of 1 molecule of hydrogen, two electrons must pass around the external circuit. Hence the electrons consumed per molecule (often written as z) is 2.

The rate of hydrogen production is best expressed as a mass per unit time rather than volume per unit time, so that the energy content is independent of the pressure of the gas.

Henceforth in this thesis the rate of hydrogen production and consumption will generally be expressed in kg/s.

In practice, not all the hydrogen produced in an electrolyser by a given cell current is collected, as a result of crossover of hydrogen produced back through the membrane or other pathway, leakage, and the passage of some electrons through the membrane without taking part in the decomposition reaction (Larminie and Dicks 2003). The Faraday efficiency, η of an electrolyser is defined as the ratio of the actual hydrogen produced to the theoretical value of hydrogen generated by the given cell current. The actual hydrogen production rate is then given for a single cell by:

$$H_e = \frac{\eta \times i_c}{1000Fz} \quad \text{kg/s} \quad \text{where z = 2} \qquad \text{[Eq.2.6]}$$

For a stack of N such cells in series in a series – parallel combination such that the same current flows through each cell, the total hydrogen production rate will be N times that for a single cell. In practice parallel combination of cells are normally replaced by single cells with larger cell area in series, since the latter have a lower cost than the equivalent number of single cells in parallel.

Hence the rate of hydrogen production for the electrolyser stack is:

$$H_E = \frac{N \times \eta \times i_c}{1000Fz} \quad \text{kg/s}$$

where the value of i_c can be found analytically from equation 2.4. Therefore the rate of hydrogen production from the electrolyser is:

$$H_E = \frac{N\eta}{2000Fz}\left[\sqrt{(m_c v_{co})^2 + \frac{4m_c P_s}{N}} - m_c v_{co}\right] \quad \text{kg/s}$$

Substituting the value of *F and z* with 96485 and 2 as defined earlier respectively,

$$H_E = 1.866\times10^{-5} N_E \eta\left[\sqrt{(m_c v_{co})^2 + \frac{4m_c P_s}{N}} - m_c v_{co}\right] \quad \text{kg/s} \qquad \text{[Eq. 2.7]}$$

The energy efficiency of an electrolyser is the ratio of the energy content of the hydrogen produced per sec to the power consumed. Hence in terms of the high heating value of hydrogen (HHV_H)

$$\eta_{energy} = \frac{E_{hydrogen}}{E_{electric}} = \frac{H_E \times HHV_{H_2}}{P_s} \quad \text{[Eq. 2.8]}$$

where HHV_{H2} is the higher heating value of hydrogen.

Alternatively at STP conditions for the electrolytic action, the thermo-neutral voltage is 1.48 V and the minimum reversible voltage is 1.23 V. Since the reaction is endothermic in nature, it draws heat from the surroundings when voltage applied across the electrode terminal is in the range of 1.23 V to 1.48 V. At 1.48 V the reaction becomes thermo neutral with the surroundings and any further increase in applied voltage will result in rise in temperature. In real conditions the minimum value of applied voltage where the electrolytic action initiates is generally found to be in the range of 1.6 - 2 V. If v_c, is the operating voltage for a single cell electrolyser then the energy efficiency of the electrolyser is,

$$\eta_{Electrolyser} = \frac{1.48}{v_c} \quad \text{[Eq. 2.8]}$$

2.4.6 Hydrogen Storage

2.4.6.1 Introduction

Storage of hydrogen is a key to the implementation of hydrogen technology in any of its applications. Hydrogen is the first element of the periodic table. With an atomic number of one, it is one of the lightest elements having a mass density of 0.08245 kg m^{-3} at atmospheric pressure. The very low boiling point of hydrogen, -253^0 C, ensures that it can only exist in gaseous form at standard temperature and pressure (STP) conditions. Hydrogen can be stored in all three phases: as a gas, a liquid at temperatures less than -253° C, or in certain solid media (such as metal hydrides).

Hydrogen storage as compressed gas and in cryogenic tanks as liquid are both established technologies. Both solid and liquid-phase hydrogen storage need parasitic energy for filling and from the tank or substrates. Cryogenic tank storage is quite an energy-intensive process demanding about 25% of the energy content of the stored hydrogen as a parasitic energy requirement (Tzimas *et al.*2003). Solid-state hydrogen storage has emerged in recent years as an attractive alternative compared to the gas or liquid storage due to its greater potential

for volumetric energy density as well as improved safety. The adsorption and desorption cycle of some metal hydrides may be well matched to the operating condition of small scale RAPS systems (Hagstrom *et al.* 1995). The other widely-mentioned solid-state storage option of carbon nanotubes is yet to be demonstrated as a practical solution (REF).

2.4.6.2 Storage as Compressed gas

Hydrogen gas is generally stored at high pressures (above 250 bars) in thick-walled cylinders made from high-strength materials. The European Integrated Hydrogen Project (EIHP 2003), which is developing global regulatory standards for hydrogen testing and certification of hydrogen fueling infrastructure components and systems, has catagorised compressed vessels for hydrogen storage can be grouped as follows:

- Type I: metal cylinder;
- Type II: load-bearing metal liner hoop wrapped with resin-impregnated continuous filament;
- Type III: non-load bearing metal liner, axially and hoop wrapped with resin-impregnated continuous filament;
- Type IV: non-load bearing non-metal linear axially and hoop wrapped with resin-impregnated continuous filament.

The type of metal used in Type I to III systems is usually stainless steel. Type IV cylinders are made from advanced composite materials and are the most technologically advanced option for lightweight hydrogen storage as compressed gas (Tzimas *et al.* 2003). Type IV cylinder structure can be divided into two sections: the liner and the composite section. The liner acts essentially as a barrier for hydrogen diffusion through the walls, whereas the composite structure ensures the mechanical integrity of the storage container. The reliability of this type of structure, and its design and safety specifications, are still being investigated (Tzimas *et al.* 2003). Irani (2000) has proposed the extension of these techniques for designing complex shaped tank with optimal use of material. Also some of the manufacturers of tanks for compressed natural gas have developed composite tanks for hydrogen storage, for example, Dynetek GmbH (using a stainless steel liner in a type II cylinders), and Faber in Italy (using metallic liner) (Tzimas et al 2003). Franzky (2002)

reported that Dynetek's latest high-pressure hydrogen storage cylinders have been tested for a storage pressure of 825 bar. These cylinders are purpose-built hydrogen storages for stationary applications with a nominal storage capacity of 170 litres, service pressure of 825 bar, maximum fill pressure of 1024 bar. The liner section of these cylinders consists of seamlessly formed, aerospace-grade aluminum with-out any weld points. This specially designed liner reportedly performs a better seal compared to other contemporary methods. Quantum Technologies and General Motors in a joint partnership have also designed a composite tank for storage of hydrogen up to a nominal pressure of 700 bar (Tzimas et al. 2003). Figure 10 shows the details of a compressed hydrogen gas cylinder.

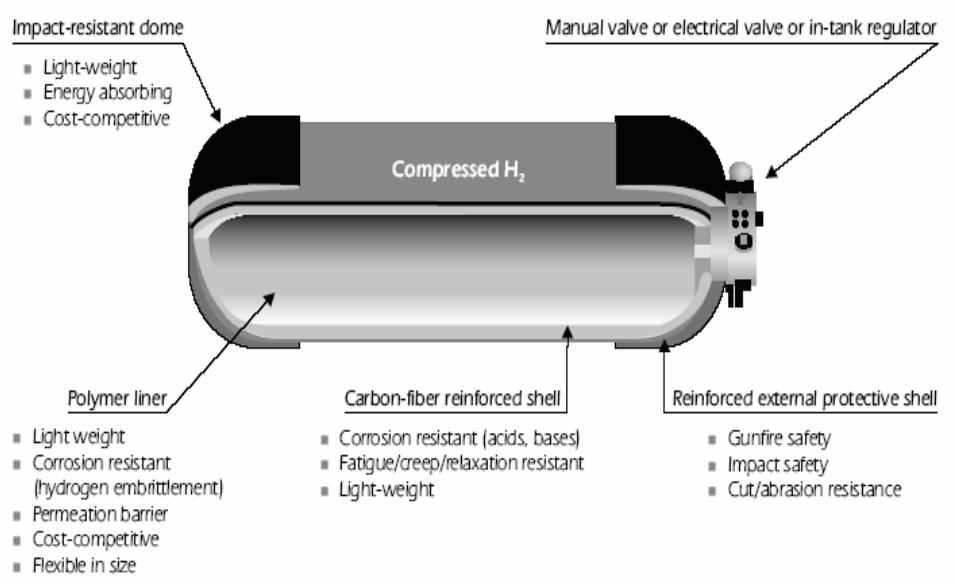

Figure 10- Compressed Hydrogen gas cylinder (Tzimas *et al*. 2003)

2.4.6.3 Hydrogen Storage in Liquid form

Liquid hydrogen has a greater energy density than high pressure compressed hydrogen gas thus providing an attractive storage option. At present liquid hydrogen is used in space-craft, military aircraft and a number of experimental and demonstration cars.

Though liquid hydrogen storage has proved to be effective, it has following inherent disadvantages (Tzimas et al. 2003):

- The energy required for the liquefaction from STP constitutes just over 25% of the energy content of the hydrogen stored in the tank
- Accurate temperature control is needed to avoid any possible overpressure.
- Evaporation loss of hydrogen (boil-off) occurs from the container. Normal hydrogen always exists in two allotropic forms: namely ortho-hydrogen and par-hydrogen. With the reduction of temperature the existing ortho-hydrogen transforms into para hydrogen, which releases some energy. If the concentration of ortho-hydrogen remains above equilibrium concentration after liquefaction, it eventually converts to para-hydrogen and the process induces evaporation loss. The shape and size of the container, i.e., surface-to-volume ratio, plays a critical role in the evaporation loss. Smaller containers due to their larger surface-to-volume ratio suffer greater hydrogen evaporation loss.
- Expensive cryogenic vessels are required to maintain the temperature inside at less than -252.7 °C, i.e., below the boiling point of hydrogen.

The cryogenic tanks for hydrogen storage are generally double-walled metallic vessels with thermal insulation placed in between the walls. Wolf (2002) has recommended that all three modes of heat transfer - radiation convection and conduction - be taken into account when designing a cryogenic vessel to minimise thermal losses. A multi-layered material with spacers in between each layer acts as an insulating barrier between the cryogenic hydrogen and the external wall. This inner layer forms a complete inner vessel and is mounted within the outer vessel by specially designed fixtures and the resulting spaces between inner and outer vessel is evacuated to minimise possible heat leakages. Hydrogen

storage in cryogenic tank is also being carried out at low pressures which have potential to reduce the weight by using composite materials. Tzimas (2003) has further predicted that such lightweight composite cryogenic hydrogen storage vessels the specific energy of storage mass can reach that of conventional petroleum fuel storage tanks.

2.4.6.4 Storage in Metal hydrides

Various metallic alloys have a tendency to adsorb hydrogen. These alloys, collectively termed metal hydrides, form a chemical compound with hydrogen at relatively low pressure (typically in the order of 2-5 bars). In a metal hydride cylinder, during the hydrogen filling process heat is released and conversely heat is generated as pressure is reduced by opening the outlet valve of the cylinder. Hydrogen molecules are initially absorbed on the surface of the metal alloy followed by their dissociation into individual atoms strongly bound to the metal atoms (Tzimas *et al.* 2003). The alloy is so chosen in order to optimize both the weight and the recovery temperature of hydrogen. The process of hydrogen filling in and out from the hydride cylinder is cyclic in nature and it has no damaging impact on net storage capacity (Tzimas *et al.* 2003).

In principle hydrogen storage in solid metal hydrides is relatively safe, due to the low pressures involved as compared to compressed gas, and the inherent separation from oxygen and protection from ignition sources. The dissociation pressure in the alloy is a temperature dependent property (Tzimas et al. 2003).

Metal hydrides can be classified as follows (Tzimas et al. 2003):

- Interstitial metal hydrides (Zr-Ti-Ni alloys): These hydrides are having a storage capacity of 1.8 wt% with a hydrogen dissociation temperature of 60-70 ° C.
- Activated magnesium rich powders: It has a weight density of (5-6 wt %) at a dissociation temperature of 260-280° C at 1 bar filling pressure.
- Complex light-metal hydrides (alanates): Theses alanates have relatively higher i.e. 5-8 wt. % density. But the release of hydrogen occurs at relatively low pressure. For lab-scale purpose alanates offer good prospects due to its dissociation temperature of 180° C at 1 bar delivery pressure

2.4.6.5 Storage Option Discussed In This Study

The conventional methods for storage of hydrogen discussed above such as LIST AGAIN are most suited to applications such as automobiles and submarines where limited space is available. Hence a high volumetric energy density for hydrogen storage is essential. By contrast, in many remote area power supply (RAPS) applications there is ample space for hydrogen storages with relatively large volumes. Hence it may be most cost-effective to store hydrogen at low to medium pressures achievable by using PEM electrolysers directly to generate the hydrogen at the required pressure. A separate electrically-driven gas compressor would then not be required, with a consequent saving in total system costs and gain in the net electricity produced.

In this thesis, the scope is confined to investigating hydrogen storage in gaseous form. In particular, preliminary experimental investigations into a number of low-cost low-pressure storage options, namely acrylic cylinders for laboratory use, plastic tanks designed originally for water storage, are conducted. Also the possible adaptation for hydrogen storage of commercially-available purpose-built metal hydrogen cylinders and composite cylinders originally designed for LPG storage is briefly discussed. The storage pressure in all these options is in the low to medium range, that is, 1 -10 bar.

2.4.7 Fuel cell

2.4.7.1 Types of Fuel cell

The history of the hydrogen fuel cell goes back to 1880. William Grove demonstrated the basic principle of producing a voltage by combining the hydrogen and oxygen generated from the electrolysis process to reform water and a small amount of heat.

The main types of fuel cell and their characteristics and typical applications are listed in Table 5. Even though at present alkaline fuel cell is most matured and cost effective

technology, PEM fuel cell is becoming more popular due to its higher efficiency, easy to handle and its response time (to change in reactant mass flow) is quickest. For remote applications the properties of PEM fuel cell are most suited and hence in this thesis the focus is primarily concentrated on PEM electrolyser.

Types of fuel cells	**Mobile ion**	**Operating temperature**	**Applications**
Alkaline (AFC)	OH^-	50-200° C	Space vehicles
Proton exchange membrane (PEMFC)	H^+	30-100° C	Vehicles and CHP(Combined heat power) systems
Direct methanol (DMFC)	H^+	20-90° C	Suitable for portable electronic systems of low power
Phosphoric acid (PAFC)	H^+	220° C	Large numbers of 200-kW CHP systems
Molten Carbonate (MCFC)	CO_3^{-2}	650° C	Large-scale CHP up to MW capacity
Solid oxide (SOFC)	O^{2-}	500-1000° C	Suitable for a wide range 2 kW to multi-MW.

Table 5- Types of fuel cell. (Larminie and Dicks 2006).

2.4.7.2 PEM Fuel cell

In hydrogen fuel cells with a liquid electrolyte in which the electrodes are immersed for the reaction to proceed, the generated current is small since the effective contact area between the reactant gases, the electrodes and the electrolyte is low, and there is a large distance between electrodes leading to a high ohmic resistance to the flow of H^+ ions.

The proton exchange membrane (PEM) fuel cell overcomes these limitations by employing a thin solid polymer electrolyte sandwiched between two porous plate electrodes. The PEM fuel cell was developed by General Electric and was first used by NASA in a manned Gemini space vehicle in 1960 (REF). As in a PEM electrolyser, the solid polymer electrolyte in a PEM fuel cell is a good conductor of protons (H^+ ions) but has a very high resistance to electron flow. The electrolyte is thus solid and immobile so that the system is inherently simple. The reactions that take place at the cathode and anode are shown in Figure 11, and these are the reverse reactions to those in a PEM electrolyser.

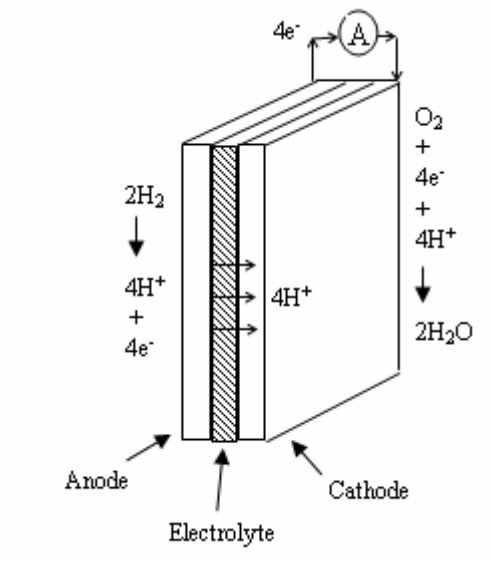

$$H_2 + \tfrac{1}{2} O_2 = H_2O + \text{Energy released}$$

Figure 11- Basic reactions occurring across a PEM fuel cell.

The membrane in a PEM fuel cell is a sulphonated fluoropolymer, most commonly the proprietary material Nafion made by Dupont. The basic polymer is polyethylene with all hydrogen atoms substituted with fluorine, which is called poly tetrafluoroethylene (PTFE) or Teflon (Larminie and Dicks 2006). For the electrolyte of a PEM fuel cell the PTFE is then sulphonated by attaching side chains of SO_3^{--} ions. The strong bond between carbon and fluorine makes Nafion resistant to chemical attack, and it is strongly hydrophobic in nature so that product water is easily driven out of the membrane of the fuel cell. But the other parts of the material are hydrophilic in nature, which allows the proper humidification of the membrane that is absolutely critical for the reaction to proceed. The critical properties of a PEM membrane can be summarised as follows:

- highly resistant to chemical attack
- mechanically strong enough to be made into thin films

- acidic in nature.
- can absorb large quantities of water to enable easy conduction of protons.
- Has a very high resistance to electron flow

A 10 W PEM fuel cell made by BCS Fuel Cells is shown in Figure 12.

Figure 12 PEMFC 10 cell stack BCS fuel cell at RMIT Renewable Energy Lab.

2.4.7.3 Theoretical characteristics of PEM fuel cell

The basic reaction that takes place in the PEM fuel cell is:

$$H_2 + \frac{1}{2} O_2 \longrightarrow H_2O \quad \text{(liquid)} \qquad \triangle g_f = -228.2 \text{ kJ mol}^{-1} \text{ at } 80\,^0\text{C} \qquad \text{[Eq 2.9]}$$

$$\triangle g_f = \triangle g_{f\,(\text{Products})} - \triangle g_{f\,(\text{Reactants})}$$

Where $\triangle g_{f,}$ is the Gibbs free energy of formation. The negative sign indicates that the forward process of forming water is exothermic in nature. It is this free energy that is used to generate electrical energy from the cell. A typical voltage current curve is shown in Figure 13.

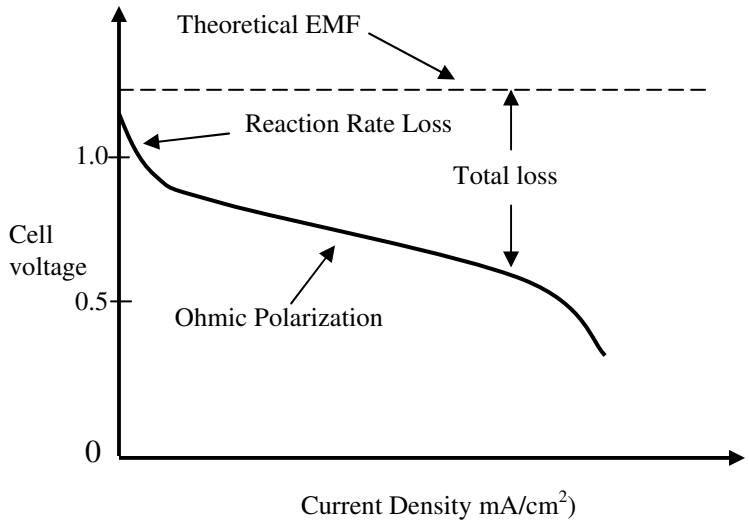

Figure 13 V-I characteristics curves for a PEM fuel cell.

In a PEMFC, for each of hydrogen molecule consumed, two electrons pass round the external circuit. Hence for one mole of hydrogen used, $2N_A$ electrons of pass through the external circuit, where N_A is Avogadro's number. If '–e' is the charge on one electron, then the total charge that flows in the external circuit per mole of hydrogen consumed is

$$-2\,Ne = -2\,F \text{ coulombs}$$

Where F= N_A. e = 96 485 coulombs/mol is the charge of one mole of electrons, and is called Faraday's constant.

If V is the voltage of the fuel cell, then the electrical work done moving this charge round the circuit is

$$\text{Electrical work done} = \text{Charge} \times \text{Voltage}$$

$$= -2\,FV \quad \text{joules}$$

For the process to be reversible there are no energy losses and all of the Gibbs free energy is converted to electrical energy. Hence

$$\triangle \bar{g}_f = -2\,F.V$$

Thus

$$V = -\triangle \bar{g}_f / 2F \qquad \text{[Eq. 2.10]}$$

This equation gives the electromotive force or reversible open circuit voltage for the PEMFC.

The value of $\triangle \bar{g}_f$ corresponds to LHV. In a low temperature fuel cell since the product water is in liquid form, HHV is used and the $\triangle \bar{g}_f$ can be replaced by $\triangle \bar{h}_f$ and the voltage obtained will be the theoretical maximum value. This is limited by the enthalpy of formation h_f.

Hence, $V_{max} = - \triangle \bar{h}_f / 2F$ [Eq. 2.11]

Thus the efficiency μ_f, can be evaluated as ratio of actual voltage generated over theoretical maximum voltage

$$\text{Since } \frac{\triangle \bar{h}_f}{2F} = 1.48 \text{ volt,}$$

$$\Rightarrow \mu_f = \frac{V_{ac}}{1.48} \times 100\,\% \qquad \text{[Eq.2.12]}$$

Now the rate of hydrogen consumption by the fuel cell, *HFC*

$$HFC = \frac{I}{2F} \quad \text{g.mol/sec}$$

$$= \frac{I}{1000F} \quad \text{kg/sec} \quad \text{---------- [Eq. 2.13]}$$

However, in practice not all the hydrogen input to the fuel cell is consumed in the cell reaction, since there will be losses of hydrogen due to fuel crossover through the membrane as well, as some hydrogen coming out of the fuel cell unused. The fuel utilisation factor μ_f is defined as is the ratio of hydrogen fuel actually used to the total hydrogen fuel input. Hence actual hydrogen consumption by the fuel cell will be given by

$$HFC\ (I) = \frac{1}{\mu_f} \frac{I}{1000F} \quad \text{kg/sec.} \qquad \text{[Eq. 2.14]}$$

The current density versus voltage curve of a PEM fuel cell is shown in Figure 14. The straight portion of the curve indicates the ohmic loss occurring at various current densities. The initial sharp drop in voltage can be attributed to activation potential. At higher current

density, at its other extreme the sudden drop in voltage could be due to the fuel cross over (Larminie and Dicks 2003).

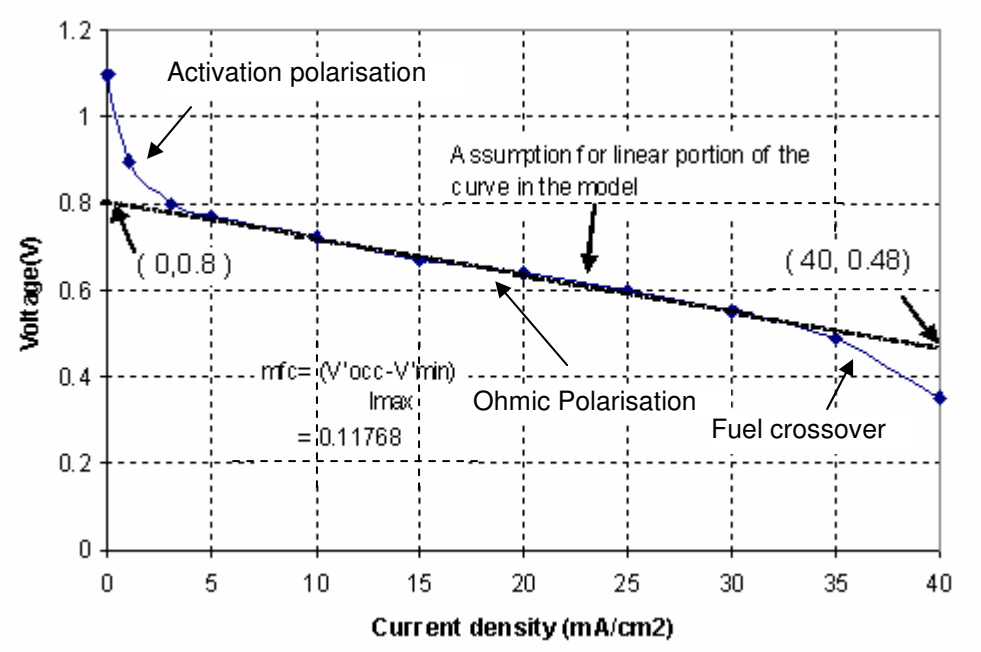

Figure 14- Current-Voltage characteristic of a low temperature PEM fuel cell.

The power generated by the PEM fuel cell can be expressed as the product of the cell voltage and current.

Hence,

$$P = V \times I \qquad \text{[Eq.2.15]}$$

Since for most of the duration, the operational current density lies in the ohmic resistance region, the curve is approximated to be linear through out its range. At extreme low solar insolations and/or when PV panel just fails to provide the load directly, only for those hours the actual performance differs from the approximated values.

On the basis of this linear approximation, the cell voltage over the linear portion of the V-I graph can be expressed simply as:

$$V = -\frac{I(V'_{oc} - V'_{\min})}{I_{\max}} + V_{oc}$$

$$= V_{oc} - m_{fc} \times I \qquad \text{[Eq.2.16]}$$

Substituting for V in Eq.2.15 gives:

$$\therefore P = (V_{oc} - m_{fc} \times I) \times I$$

$$\Rightarrow \quad I^2 m_{fc} - V_{oc} I + P = 0 \qquad \text{[Eq.2.17]}$$

Solving the quadratic equation for 'I' in terms of 'P' gives

$$I = \frac{-(-V_{oc}) \pm \sqrt{(-V_{oc})^2 - 4m_{fc}P}}{2m_{fc}}$$

$$\Rightarrow \quad I = \frac{V_{oc} \pm \sqrt{V^2{}_{oc} - 4m_{fc}P}}{2m_{fc}} \qquad \text{[Eq.2.18]}$$

Substituting for I from Eq (2.18) in Eq (2.14) gives

$$HFC\ (P) = \frac{1}{\mu_f} \frac{(V_{oc} \pm \sqrt{V^2{}_{oc} - 4m_{fc}P})}{2000.F.m_{fc}} \quad \text{kg/sec} \qquad \text{[Eq.2.19]}$$

Hence the net hydrogen consumption by the fuel cell is,

$$H_{fc,i} = \frac{3.6 \times N}{mu \times F}\left[\frac{V_{0cc}}{2 \times m_{fc}} - \sqrt{\left(\frac{V_{occ}}{2 \times m_{fc}}\right)^2 - \frac{FC_{s,i}}{N \times m_{fc}}}\right] \qquad \text{[Eq.2.21]}$$

2.4.8 Balance of System

Apart from the major components that have now been described, all other components and accessories needed for the system are grouped in the Balance of the System. Among these the most prominent components are the following:

- the load splitter
- the overall control unit for the solar-hydrogen system that must use information about prevailing conditions of PV output and load to switch the system between its various modes of operation:
    - PV system supplying all load with any surplus power going to electrolyser; fuel cell switched off
    - PV system supply part of the load with the remainder supplied by the fuel cell; electrolyser switched off
    - Fuel cell supplying all the load; electrolyser switched off
- Solenoid valves to control gas flow from the electrolyser into the storage, and from storage into the fuel cell
- A cooling system for the fuel cell
- Safety cut-outs in the event of hydrogen leakage or other risk factor

The design, construction, testing, performance evaluation and costing of the balance of system for a solar-hydrogen system of the kind studied in this thesis are still tasks requiring a lot more attention, since these costs of the balance of system are likely to be a significant proportion of the total system costs. These tasks, however, are outside the scope of the present thesis.

3. EXPERIMENTAL SOLAR-HYDROGEN SYSTEMS

3.1 SOLAR HYDROGEN SYSTEM STUDIED

In the present work at RMIT Renewable energy laboratory, various experimental solar-hydrogen systems have been designed and constructed. The experimental data obtained from the PEM electrolysers and PEM fuel cells were obtained and compared with the manufacturers predicted performances. The evaluated performance and characteristics of the PEM electrolyser and PEM fuel cells are used as an input in the mathematical model created using Excel and Visual basic.

In this chapter, two of these experimental systems are described:

- A 50 W electrolyser and 10 W fuel cell system
- A 200 W electrolyser and 500 W fuel cell system

The main components of these system, including the PV panels and hydrogen storage system are explained. The results of experiments conducted on the system are reported, for subsequent use as key inputs to the computer modeling components of this study.

3.2 PV PANELS

3.2.1 PV specifications

Both the experimental solar-hydrogen systems studied derive their power for photovoltaic arrays at the RMIT Renewable Energy Laboratory. Four of the panels with a total area 2.25 m^2 are separately connected in parallel and provide a 24 V of dc power for use inside the laboratory. Four of these PV panels are separately connected in parallel which acts as the source of conversion from solar energy to electrical energy.

The source has been used to supply power to the two solar hydrogen systems used in the present study. The BP solar PV modules are certified by CEC503 (European Commission) as presented in the Table 6.

Name	Peak power (W)	Nominal Voltage (V)	Number of cells	Peak Voltage (V)	Peak current (A)	Open circuit voltage (V)	Short circuit current (A)
BP275	75	12	36	17	4.45	21.40	4.75

Table 6- PV panel specification by European commission.

Standard test conditions:

Description	Parameters	Value
Intensity of solar radiation	Insolation (W/m^2)	1000
Spectral Density	Air Mass (AM)	1.5
Operating Temperature	Cell Temperature (°C)	25

Table 7- Standard test conditions for PV panel specification.

The dimensions of PV panel are of (1188mm x 530mm x 38.5mm) and each weighing 7.5 kg. The angle of tilt is kept 38° due north as per the local latitude of Melbourne.

3.2.2 Experimental V-I Curve

Measurements of the characteristic voltage-current curve of the PV array were made using the experimental set up shown in Figure 16. The experiment was conducted on a clear cloud free sunny day with the solar radiation being fairly constant. The V-I values obtained and the associated insolation and calculated power input and overall energy conversion are shown in Table 8.

Volt	Current	Power Output	Insolation	Area	Efficiency
(V)	(A)	(Watt)	(Watt/m2)	(m^2)	(η%)
3	3.79	11.37	1010	2.25	0.50
4.1	3.78	15.498	1008	2.25	0.68
6.6	3.76	24.816	1008	2.25	1.09
11.4	3.75	42.75	1010	2.25	1.88
16.5	3.73	61.545	1009	2.25	2.71
21.3	3.72	79.236	1013	2.25	3.48
26.3	3.7	97.31	1009	2.25	4.29
31.7	3.64	115.388	1006	2.25	5.10
36	3.61	129.96	966	2.25	5.98
40.5	3.54	143.37	977	2.25	6.52
45.2	3.52	159.104	967	2.25	7.31
50.2	3.46	173.692	957	2.25	8.07
55.5	3.37	187.035	963	2.25	8.63
60.1	3.28	197.128	963	2.25	9.10
63.7	3.1	197.47	966	2.25	9.09
66.3	2.87	190.281	951	2.25	8.89
68.9	2.59	178.451	949	2.25	8.36
70.4	2.39	168.256	945	2.25	7.91
71.7	2.13	152.721	932	2.25	7.28
73.2	1.88	137.616	943	2.25	6.49
74.3	1.65	122.595	949	2.25	5.74
75.5	1.22	92.11	954	2.25	4.29
77	0.77	59.29	932	2.25	2.83
79	0	0	0	2.25	0.00

Table 8- Experimental values for voltage and current observed.

The graph between voltage and current characteristic obtained from the experiments at RMIT renewable energy lab is shown in Figure 15.

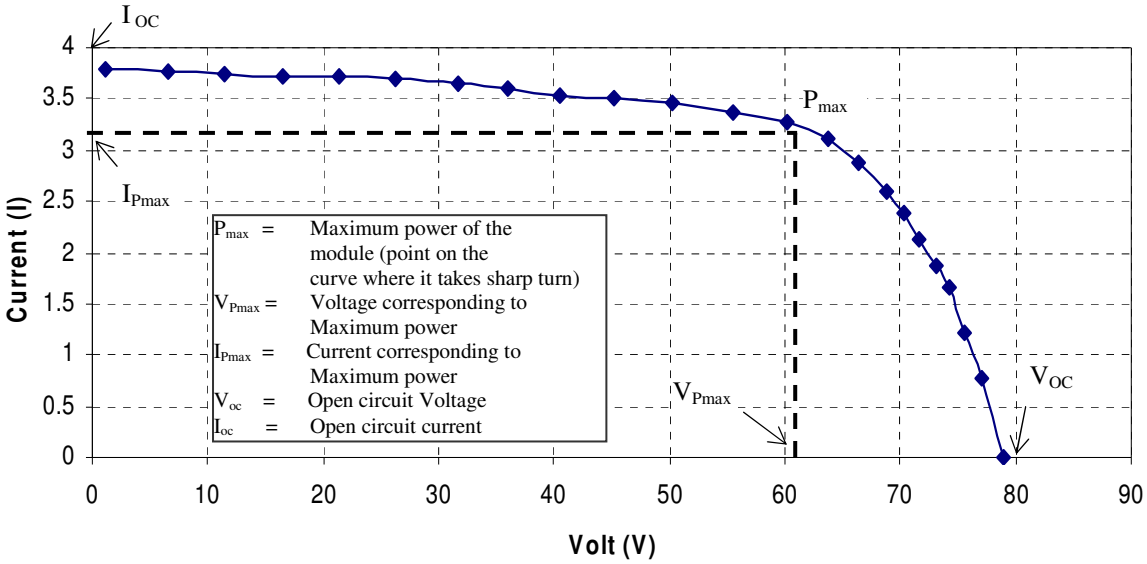

Figure 15- V-I characteristic obtained from the experiments at RMIT renewable energy lab. (NOTE: The values are taken on a clear sunny day (cloud free) with the solar insolation being in the range of 932-1014 watt/m^2)

Experiments performed on these PV panels suggest the fact that a factor of less than 10 % energy conversion is attained. This could be due to the life time based degradation of efficiency. Although a number of PV panels are available in the market with higher efficiency of 15% (latest researchers have achieved as high as 21%), a conservative value of 10 % efficiency is incorporated in the model for all calculation purpose.

3.3 50 W ELECTROLYSER AND 10 W FUEL CELL SYSTEM

3.3.1 System Design

A 50 W electrolyser - 10 W fuel cell system has been designed and assembled with its storage system built in our workshop as part of the present project. The existing PV panels of the Renewable Energy Laboratory described in section 3.2 are used for electrolytic hydrogen generation. A commercially available PEM electrolyser unit supplied by h-tec and a fuel cell supplied by BCS are employed in the experimental rig. A schematic diagram of the overall system is shown in Figure 17. The main components are described in the following sections

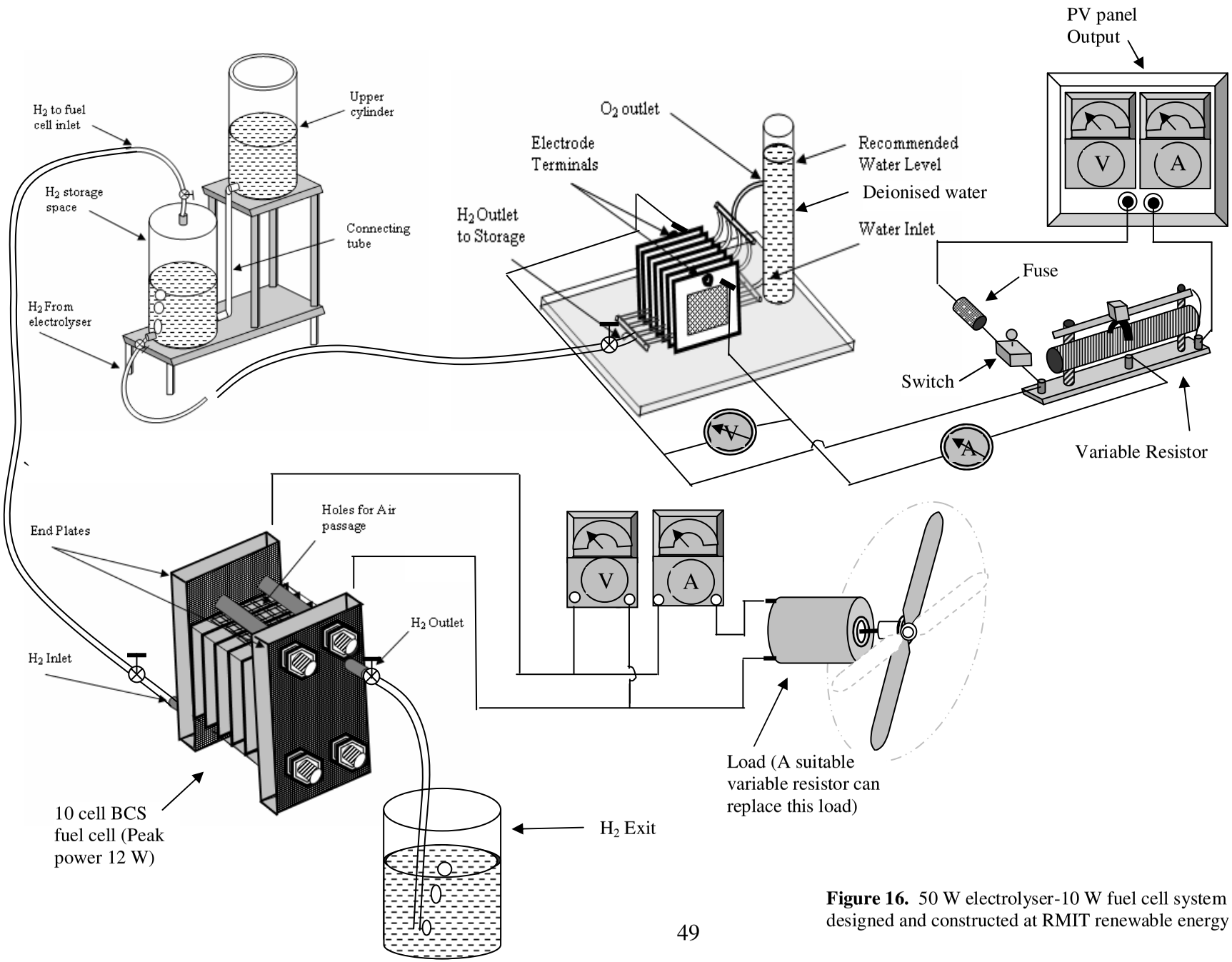

Figure 16. 50 W electrolyser-10 W fuel cell system designed and constructed at RMIT renewable energy lab.

3.3.2 The 50 W h-tec electrolyser

3.3.2.1 Specifications

An h-tec STAXX7 PEM electrolyser stack was used to generate hydrogen using the electric power available from the PV terminal output (Figure 17). A variable-resistor was used to bring down the voltage and current available from the out put terminal of the PV down to the permissible limit of the electrolyser stack (14V).

Component	Electrolyser staXX7
Dimensions	190 x 264 x 200 mm
Weight	1.486 g
Electrode area	16 cm^2
Power	50 W at 14 V DC
Permissible voltage	10.5-14 V DC
Permissible current	0-4.0 A DC
H_2 Production	230 cm^3/ min (8.33 x 10^{-8} kg/min)

Table 9- Electrolyser Specification.

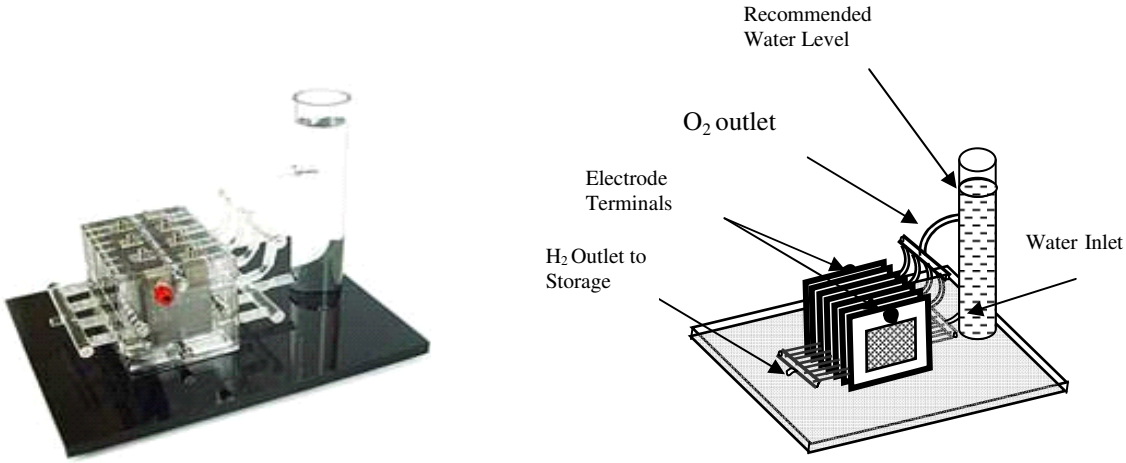

Figure 17- H-tec Electrolyser (7 cell, 50 W, 14 Vdc).

3.3.2.2 Experimental results

A series of experimental test were conducted on this PEM electrolyser to evaluate its performance within the permissible input voltage range and obtain performance characteristic for use in the computer modeling component of the study. The experimental set up used is shown in Figure 18. The corresponding voltage-current characteristic curve is plotted in Figure 20.

Voltage (V)	Current (A)	Voltage (V)	Current (A)
7.28	0	11.4	1.08
7.95	0	11.5	1.23
8.37	0	11.67	1.45
8.7	0	11.7	1.51
9.26	0	11.79	1.64
9.7	0	11.91	1.83
9.96	0	12.04	2.03
10.13	0	12.22	2.31
10.25	0.02	12.31	2.46
10.35	0.04	12.37	2.57
10.42	0.07	12.52	2.81
10.52	0.13	12.61	2.97
10.56	0.15	12.68	3.1
10.65	0.22	12.78	3.26
10.7	0.26	12.9	3.45
10.77	0.32	12.96	3.56
10.87	0.44	13.02	3.65
10.98	0.54	13.08	3.74
11.09	0.68	13.13	3.82
11.18	0.88	13.16	3.89
11.28	0.92	13.2	3.92

Table 10- Experimental data obtained for I-V values for7 cell h-tec electrolyser (50 w)

The best straight line fit to the data in the linear portion of the I-V curve, that is, for voltages in the range of 11.0 to 13.2 volts was obtained using the excel curve fitting (add trend line). The slope of this straight line approximation to the curve was found to be 3.6 A/V. Since the individual cells are in series the same amount of current is drawn across all the individual cells. The area of an individual cell is divided by this amount to determine the slope of current density and voltage and ($A/m^2/V$). This experimentally determined value for m_c is the theoretical I-V curve given earlier in equation 2.2. It is used as an input to the system modeling. As a precautionary measure a further increase in voltage supplyover13.2 V was avoided as voltages greater than the maximum permissible limit of 14 V can lead to an excessive current densities resulting in deterioration of membranes of the electrolyser.

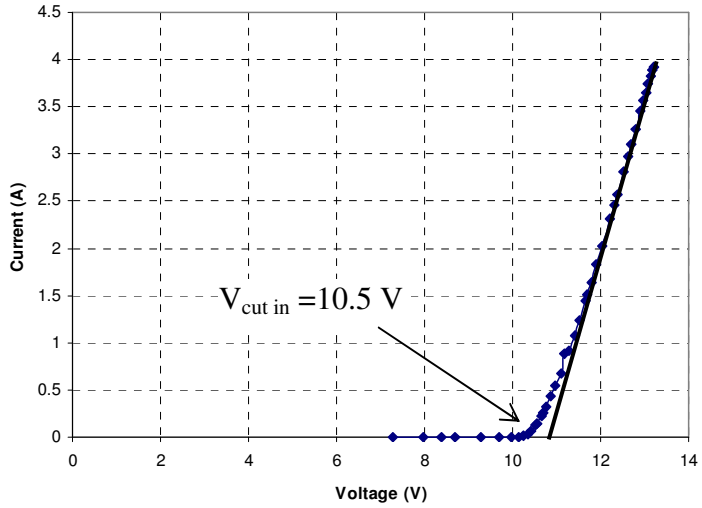

Figure 18- Current versus Voltage curves for the experimental 7 cell h-tec electrolyser.

In a second experiment, the rate of hydrogen production by the electrolyser was measured for a range of applied voltage and currents drawn. The rate of hydrogen production was obtained by measuring the time taken for a fixed volume of hydrogen (60 cm^3) to be produced. As explained in chapter 2 section 2.4.5, the volume of hydrogen generation is proportional to the current drawn by the electrolyser. The energy content of the produced hydrogen is then compared with the power supplied to the electrolyser to determine the energy efficiency of the electrolyser. The actual production rate of hydrogen is then compared with the theoretical hydrogen production rate to evaluate the Faraday efficiency (of the electrolyser at the level of electrical power input as explained in chapter 2 section

2.4.5. The results obtained for the rate of hydrogen production, Faraday efficiency, and energy efficiency for power inputs in the range of 6 W to 40 W are presented in the Table 11.

Voltage	Current	Volume of H_2	Time taken	Rate of H2 prod.	Power supplied	Faraday eff.	Energy eff.
(V)	(A)	(cm^3)	(Sec)	$x10^{-7}$ (kg/sec)	(W)	η_{farad}	η_{energy}
12.62	3.10	60	23.62	2.26	39.12	82.09	82.58
12.56	3.03	60	24.00	2.22	38.05	82.48	83.55
12.18	2.41	60	30.38	1.75	29.35	85.05	85.55
12.16	2.39	60	31.51	1.69	29.06	85.19	83.33
11.70	1.65	60	45.26	1.17	19.30	88.54	87.34
11.69	1.63	60	45.70	1.16	19.05	88.62	87.63
11.14	0.82	60	89.34	0.59	9.13	92.99	93.46
11.13	0.81	60	90.66	0.58	9.01	93.08	93.37
10.96	0.59	60	127.58	0.41	6.46	94.52	92.52
10.94	0.58	60	134.20	0.39	6.34	94.69	89.62

Table 11 Result table for experimental evaluation of Faraday efficiency and energy efficiency of the electrolyser.

3.3.3 Hydrogen Storage in Acrylic Cylinder

The hydrogen generated by the electrolyser in this system is stored in an acrylic cylinder using the standard displacement technique (Figure 21). The material is the chemical compound named polymethylmethacrylate commercially known as Plexiglas. The details of both physical and chemical properties of acrylic material are shown in Table 1 in Appendix. A small volume (10-15 $\times 10^3$ cm^3) of hydrogen storage is chosen for for laboratory requirements. The storage system comprises two acrylic cylinders (Dia of 150 mm, height 500 mm) at different levels so that as hydrogen is collected over water in the lower cylinder and the resultant water displaced, flows into the second cylinder which is open to the atmosphere at the top (Figure 19). Similar transparent acrylic cylinders are used in many of the small scale demonstration solar-hydrogen systems now available

commercially, such as H-tec. Appropriate piping and connections for this mechanism is needed in order to facilitate the smooth passage of incoming hydrogen and subsequent regulation of stored hydrogen during fuel cell operations.

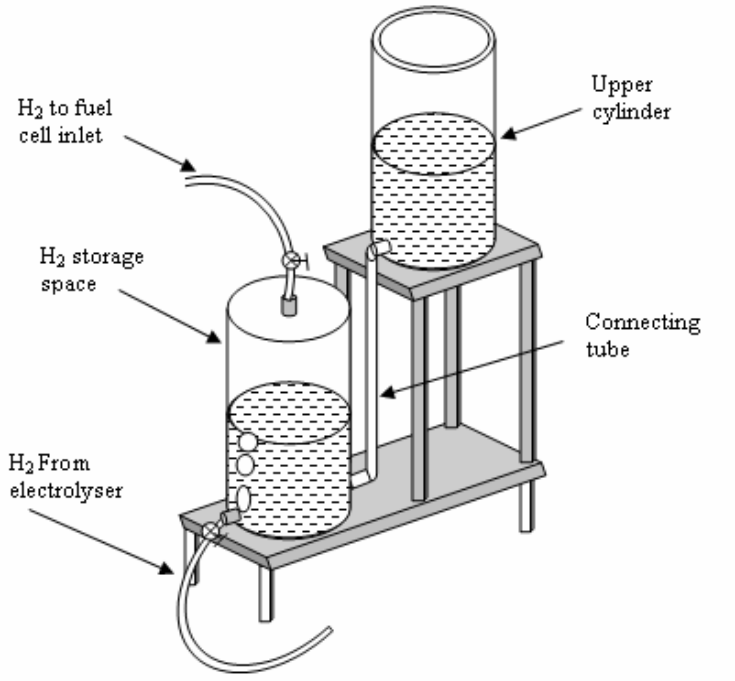

Figure 19 – Acrylic cylinder based hydrogen storage system.

The cylinders are originally cut out of large acrylic tubes and separate end plates are placed on the top and bottom section of the tubes to form a complete cylinder. The cylinders are of dimension diameter, Φ = 150 mm and height, H = 500 mm, thickness of the wall, t = 3 mm, and thickness of the end plate, T = 5 mm. From a 5 mm thick square acrylic plate (250 mm x 250 mm), circular end-plates are sliced out using Band-Saw in the RMIT workshop. The bottom cylinder is designed to have three connections i.e. hydrogen inlet, water passage on the sideways (on the wall of the cylinder) while hydrogen outlet on the top of the end-plate.

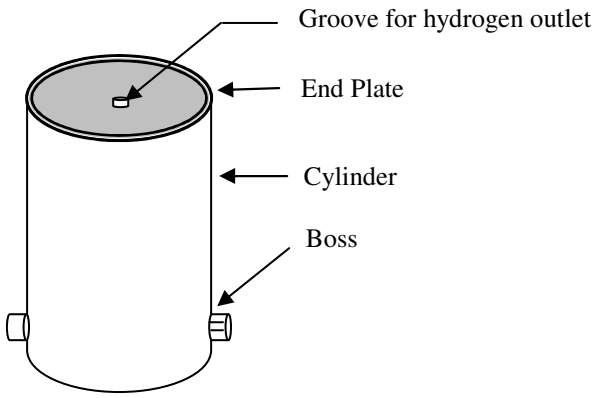

Figure 20 – Bottom cylinder with Boss and end-plate groove

The connections on the wall are provided by employing a concentric boss (acrylic material) to provide extra strength to the connections and making the joints leak proof. A special type of glue, suggested by the acrylic-supplier is used to attach the boss to the main body of the cylinder. The acrylic material-specific glue named "WELD.ON" 3 is clear, water thin, which acts as very fast curing solvent for gluing acrylic substance. This glue is also used to fix the end-plates to the main body of the acrylic cylinder. The fittings are provided across the groove on the end plate as well as the holes across the boss-cylinder wall joints. The upper cylinder just holds the displaced water and hence it requires the passage for water regulation only. The entire system is placed in a stand designed according to the height of the storage cylinders as shown in Figure 20. The stand structure consists of cast iron rods and plates. The level for upper cylinder is raised to provide a greater height of water column to pressurise the stored hydrogen.

The system is assembled with proper connecting pipes (¼ inch outer Dia, PFT tube) and plug valves (¼ inch Dia) from Swagelok. The details of which are shown in Figure 21 and Table 12 describes the details specification of the parts. These hydrogen compatible valves and pipes are capable of sustaining a pressure of 100 psi which is well above the desired working pressure for the system.

a. Valve

b. Connector

c. Tube

Name	Part No	Descriptions
Valve	PFA-43S4	PFA Plug Valve, 1/4 in. Swagelok Tube Fitting
Connector	PFA-220-1-2	PFA Swagelok Tube Fitting, Male Connector, 1/8 in. Tube Fitting x 1/8 in. Male NPT
Tube	PFA-T10M-1M-30M	PFA Tubing, 10 mm OD x 1 mm Wall x 30 Meters

Table 12 – Components parts and description (Swagelok)

Figure 21 – Valves and fittings used in acrylic based hydrogen systems. (Swagelok, Melbourne)

The entire assembly is then tested for leakage as the various joints and connections are considered as a potential source for hydrogen escape.

Prior to the storage of actual hydrogen, a hydrostatic leak test followed by pneumatic leak testing of the acrylic cylinder was carried out to ensure a fail-safe mechanical leak proof storage system. Both the pressure testings are carried out at relatively low pressures i.e. with in the range of working pressure. It is always recommended to carry out these leak tests at the initial stages before the storing of actual hydrogen to avoid future complications that could stall the functioning of the entire system. Water being an incompressible in nature ensures uniform transmission of applied test pressure across the whole cylinder.

Hydrostatic leak testing was carried out by exerting a pressure of water column of 4m high (6 psi). The height of the water column was so chosen to employ a factor of safety of 2 corresponding to the actual storage pressure of 3 psi (the input pressure conditions required by our larger,500 watt fuel cell unit). Initially a number of leakages came out from the

tube fittings which were immediately taken care of by sealing the press fit areas. As the height of the tube containing water is raised by feeding water from mains utility lines, failure of the system (water leaking right from the joints between the cover plate and acrylic tube) was observed.

The cover plate was removed and the surface between the plate and acrylic cylinder was conditioned with sand paper and a relatively denser layer of silicon glue was applied to re-assemble the cylinder system. The system was left isolated for duration of (24 hour) to ensure complete settlement of bond between the treated surfaces. Again the water pressure was applied up to the desired pressure of 6 psi. The system was left isolated for couple of days and the water column was monitored. At the end of 2 days, there was no decrease in water column and no leakage was observed from the acrylic cylinder. This ensured that there is apparently no mechanical leak existing in side the system with in the experimental pressure of 6 psi (actual storage pressure being 3 psi).

The hydrostatic testing of the acrylic system was followed by the pneumatic test where an air pressure of 6 psi was applied to the test cylinder by a commercially available pneumatic compressor (portable compressor widely used in automobile cars). A converter (AC-DC) was used to run the compressor till the desired test pressure was attained inside the cylinder. A pressure gauge was connected to the outlet of the cylinder to observe the applied pressure. The compressor was turned off and the system was left isolated for some duration. Surprisingly a quick drop in pressure level was observed. The entire system was pressurized again and was immersed in a large container filled with water to detect possible leakage in the form of bubbles coming out of the water. It was the connection with in the tubes (press fitting) from where the air bubbles were coming rather than from the actual test cylinder. After properly fixing the connection of the tube, there was no air bubbles observed hence no leakage from the system was ensured. Also the pressure gauge showed no drop in test pressure.

Both the hydrostatic and pneumatic leak tests were successful in avoiding the possible mechanical leak from the acrylic cylinder at the desired pressure. Then the cylinder was employed for the actual storage of hydrogen generated by our electrolyser bank.

3.3.4 The 10 W BCS Fuel Cell

3.3.4.1 Specifications

A 10 cell BCS fuel cell (10 W) is used to generate power by utilising the stored H_2 (Figure 22). The H_2 supply is regulated by a control valve while O_2 is consumed via natural convective air across the passage designed for air flow. The flow of hydrogen has a direct regulating impact over the current and hence the power generation. Specifications of for standard parameters for a BCS fuel cell is shown in the Table 13.

Power out put	10-12 W
Reactants	H_2/air
Operating temp	70° C
Electrode area	10 cm^2
Mode of H_2 flow	Parallel
Operating Pressure	0-3 psi
Number of cells	10
Model of air flow	Convection.

Table 13- Standard Specifications for 10 W BCS fuel cell.

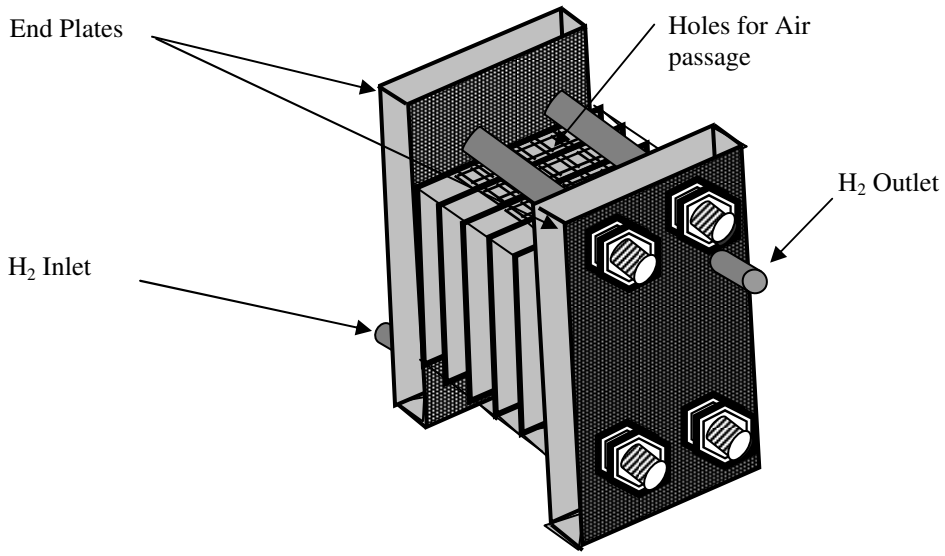

Figure 22- 10 Watt BCS PEM fuel cell stack.

A variable load is required to properly match the generated current. The flow of current is proportional to the hydrogen supplied while the upper limit of the current generation is limited by the specifically designed PEM membrane. (With a fixed % by density concentration of catalysts corresponding to maximum permissible current densities per cell area).The fuel cell functions both in dead-end and open-end operations while dead end operation requiring opening of the outlet valve after some interval (15-30 sec).

3.3.4.2 Manufacturer's performance curves

The 10 W BCS fuel cell manufacture's predicted performance is shown in Figure 23. The stack current varies from 0-2 Amp with a corresponding variation in voltage from 9.5 volt to 7 volt. The power generated by the fuel cell reaches from zero to a maximum value of 12 Watt. The stack potential curve maintains a straight line.

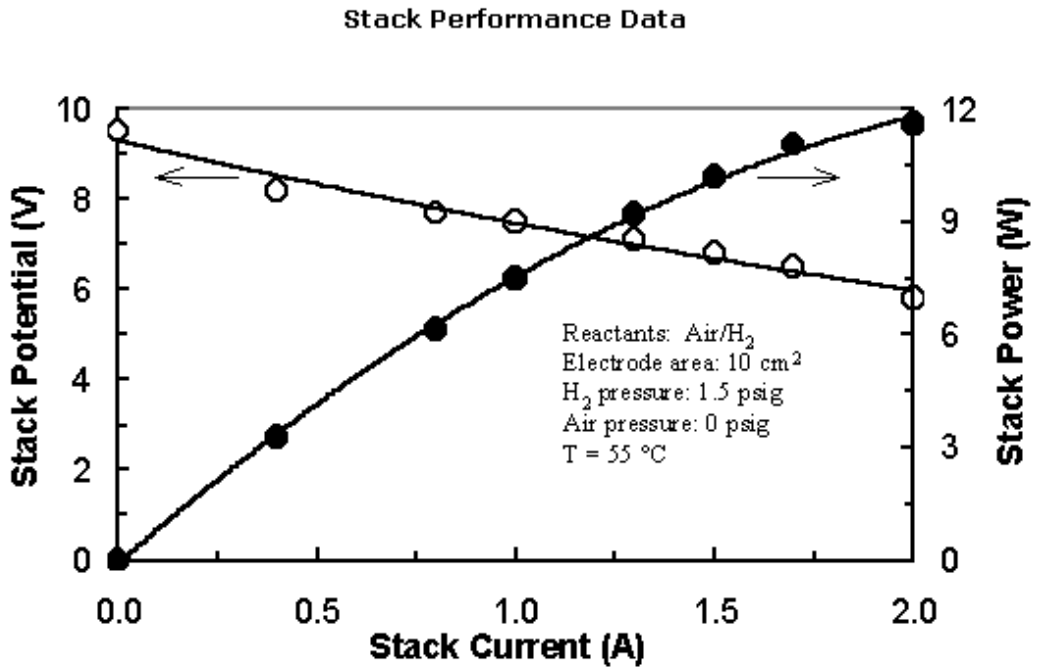

Figure 23- Performance curves of the BCS 10W fuel cell (BCS, 2004 fuel cell manual for 10 cell 10 W stacks).

The current generation is slightly improved when flow of hydrogen is increased from its stoichiometric values (Table14). Apart from these occasional drop in voltage occurs. This can be possibly due to insufficient flow of hydrogen or blockage of channels due to excessive accumulation of water.

Current (A)	0.2	0.5	0.7	1.0	1.2	1.5	1.8	2.0
H_2 flow(1:1) (ml/min)	12.6	31.6	44.3	63.3	75.9	94.9	113.9	126.6
H_2 flow (1:1.2) (ml/min)	15.1	37.9	53.2	76.0	91.0	113.9	136.7	115.9

Table 14. Stoichiometry chart for hydrogen flow in the BCS 10 W fuel cell (BCS, 2004 fuel cell manual for 10 cell 10 W stacks).BCS Fuel cell manual)

3.3.4.3 Experimentally measured performance curves

To evaluate the current–voltage characteristics of a PEM fuel cell, a series of experiments were conducted on the 10 W BCS fuel cell. The corresponding values are reported in Table 15. The maximum voltage obtained from the fuel cell is 7.6 volt with a low current of 0.19 A. At the other extreme, a voltage of 3.7 volt was obtained against a current of 1.25A. The amount of hydrogen consumed was kept constant ($50cm^3$) for each set of readings while time taken for that amount hydrogen consumption were recorded. The Faraday efficiency was evaluated to be in the range of 0.58 to 0.91 whereas energy efficiency was found to be in the range of 0.22 to 0.34. These values are lower than the manufacturer's predicted performance. This could be due to the fact that the manual opening of hydrogen exit valve from the fuel cell could have been more than the actual desired amount. This is evident from the Faraday efficiency. Also there could be degradation in performance of the fuel cell over the years. Improper humidification or load drawn can also have negative impact on the performance of the fuel cell (Larminie and Dicks 2003).

Volt.	**I**	**Power**	**H2 Cons.**	**Actual H2 cons.**	**Time**	**Actual H2 consum. rate**	**Theo. H2 consum. per cell**	**Theo.H2 consum. in the stack**	**Farad. η**	**Energy η**
(V)	(A)	(W)	cm3	$x10^{-8}$kg	(Sec)	$x10^{-8}$ kg/sec	$x10^{-7}$ kg/sec	$x10^{-6}$ kg/sec	%	%
7.6	0.19	1.444	50	4.23	126.53	3.34	2.49	2.49	0.58	0.30
7.5	0.22	1.65	50	4.23	113.76	3.71	2.59	2.59	0.61	0.31
7.4	0.27	1.998	50	4.23	101.86	4.15	2.85	2.85	0.67	0.33
7.1	0.36	2.556	50	4.23	82.11	5.15	3.06	3.06	0.72	0.34
6.8	0.4	2.72	50	4.23	76.38	5.54	3.16	3.16	0.74	0.34
6.6	0.46	3.036	50	4.23	68.45	6.18	3.26	3.26	0.77	0.34
6.3	0.54	3.402	50	4.23	59.81	7.07	3.34	3.34	0.79	0.33
6	0.61	3.66	50	4.23	56.04	7.55	3.54	3.54	0.83	0.33
5.1	0.86	4.386	50	4.23	41.56	1.01	3.70	3.70	0.87	0.30
4.5	1.06	4.77	50	4.23	34.07	1.24	3.74	3.74	0.88	0.26
3.7	1.25	4.625	50	4.23	29.77	1.42	3.85	3.85	0.91	0.22

Table 15- Experimental data obtained from the BCS 10 Watt fuel cell.

The values for the current versus voltage and current versus power are plotted in Figure 25. The profile of both the voltage and power curves are similar to manufacture's predicted performance though the actual amount varies significantly.

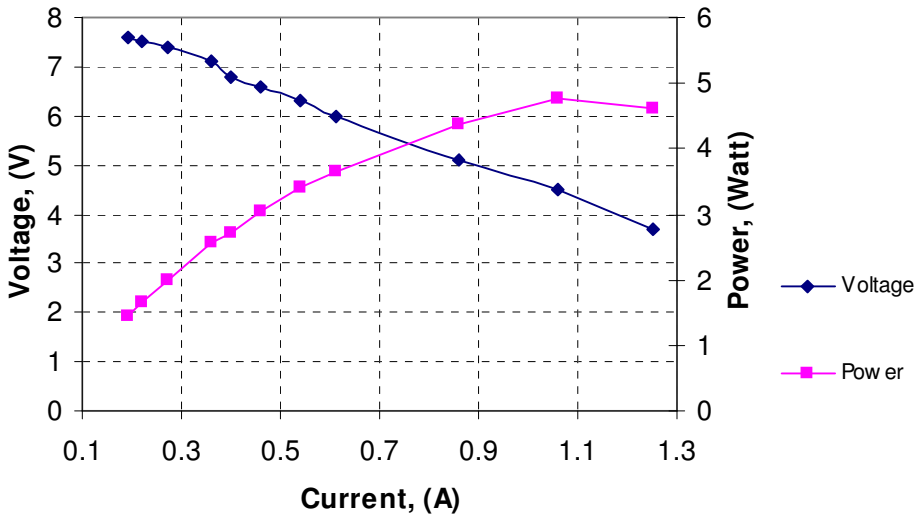

Figure 24-Current versus voltage and corresponding current versus power for the BCS 10 W fuel cell are plotted.

3.4 A 500 W_e SOLAR HYDROGEN SYSTEM

3.4.1 System description

A larger scale solar hydrogen system was designed and assembled inline with the earlier mentioned small scale solar hydrogen system. A larger 300W PV panels are coupled to a 250 W electrolyser bank consisting five individual 50W PEM electrolyser units to generate hydrogen. The generated hydrogen is stored in a larger low pressure 225 liters plastic water tank. The storage mechanism was designed to deliver hydrogen at higher pressure (4 psi) just sufficient to run a larger fuel cell unit.

3.4.2 PV Panel

As a next step a larger scale solar hydrogen system was designed. Since the existing PV panels are having a combined capacity of 2 KW (Figure 25), while the single module used for smaller system is having a capacity of 300 Watts.

Figure 25- Renewable energy lab, SAMME, RMIT**.**

These solar modules are fed back to the mains grid connection. One single panel with 300 W is separately taken as the source for the larger scale solar hydrogen system.

3.4.3 250 W Bank of H-tech Electrolysers

The 250W bank of H-tec Electrolysers was constructed in order to obtain a higher rate of hydrogen production. Each single unit has a production rate of 230 N cm^3/min. Five such units were combined to generate a higher hydrogen production for the usage in larger fuel cells via a larger storage sub-system. The combined total power required by these cells is 250 W (5x50 W) (Figure 26). The electrolyser units are kept on a large wooden plank facing each other and the hydrogen exit from each unit are connected to an inclined central header pipe resting on a supporting rod. The header pipe was kept inclined to avoid interlocking of hydrogen bubbles with in the tube particularly at low level of hydrogen production range.

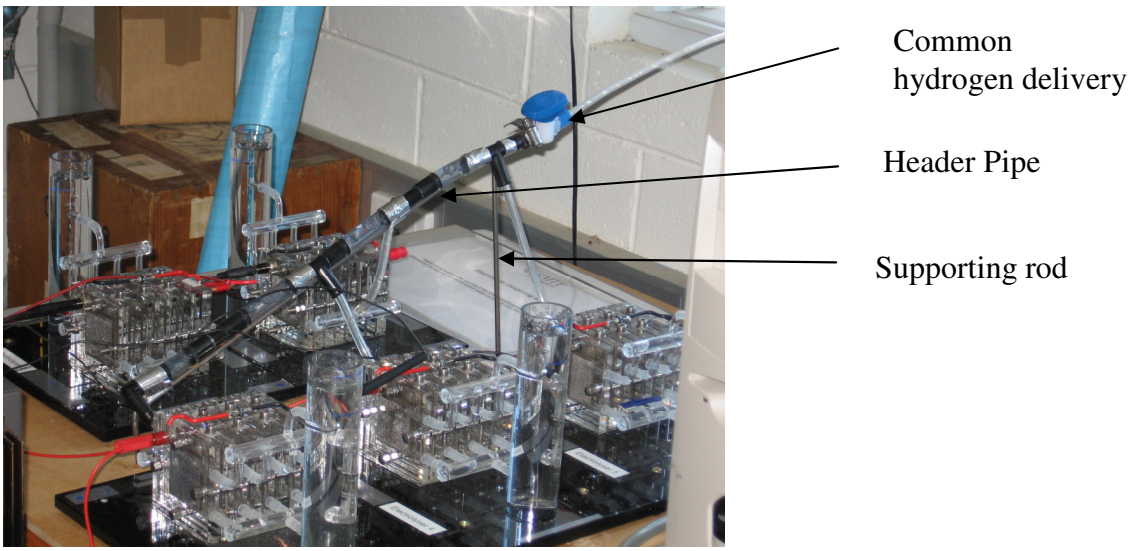

Figure 26- 250 W Electrolyser bank (5 units of 50 W electrolyers connected via a common central hydrogen output)

3.4.4 Storage systems

3.4.4.1 Plastic Water Tank Storage

The storage of hydrogen gas generated by the electrolyser bank, was so chosen after considering a number of factors such as

- hydrogen generation capacity of electrolyser bank
- hydrogen consumption requirements of fuel cell
- efficient hydrogen storage (minimum permeation of hydrogen across the wall) and its commercial availability.

The 250 W electrolyser bank has a capacity to generate hydrogen of 1.15 N.lit /min and the fuel cell consumes 3 N.lit/min of hydrogen. So a relatively large volume of 225 N.lit/min commercially available Fibre-reinforced plastic (FRP) tank (originally designed for water storage) for hydrogen storage is chosen. The storage mechanism is similar to acrylic cylinder that is water displacement technique. Two similar FRP tanks of same volume are chosen. These tanks are made of food grade fiberglass resins designed to Australian Standard AS 2634-1985 (Tank world 2005).

The tanks are bilaterally symmetrical along horizontal axis with two inverted equal half conical-subsections being welded to form the complete shape (Figure 27). The top cover of the tanks were originally fitted with a water filters. The filter was removed and replaced by a 5 mm fibre glass plate. This 5 mm fibre glass plate was both glued and tightened by fourteen fasteners placed radially along the periphery of the top section. Before the top plate is fixed, hole connectors (Dia, Φ = 1 inch) are connected at the top and bottom section of the wall. These hole connectors were supplied by the manufacturer. And a suitable reduction of area corresponding to hydrogen delivery tube from electrolyser, (Dia, Φ= 4 mm) was accomplished by attaching male-female connector. Apart from the top plate modifications and hole connectors, there were some specific changes incorporated in the tanks. The specific design changes carried out in the upper tank is shown in Figure 27. The upper tank primarily collects the displaced water from the bottom of the cylinder. A vertical transparent tube is fitted in this tank which enables the detection of actual water

level present in the tank. This can be approximated to be the actual volume of hydrogen present in the bottom tank.

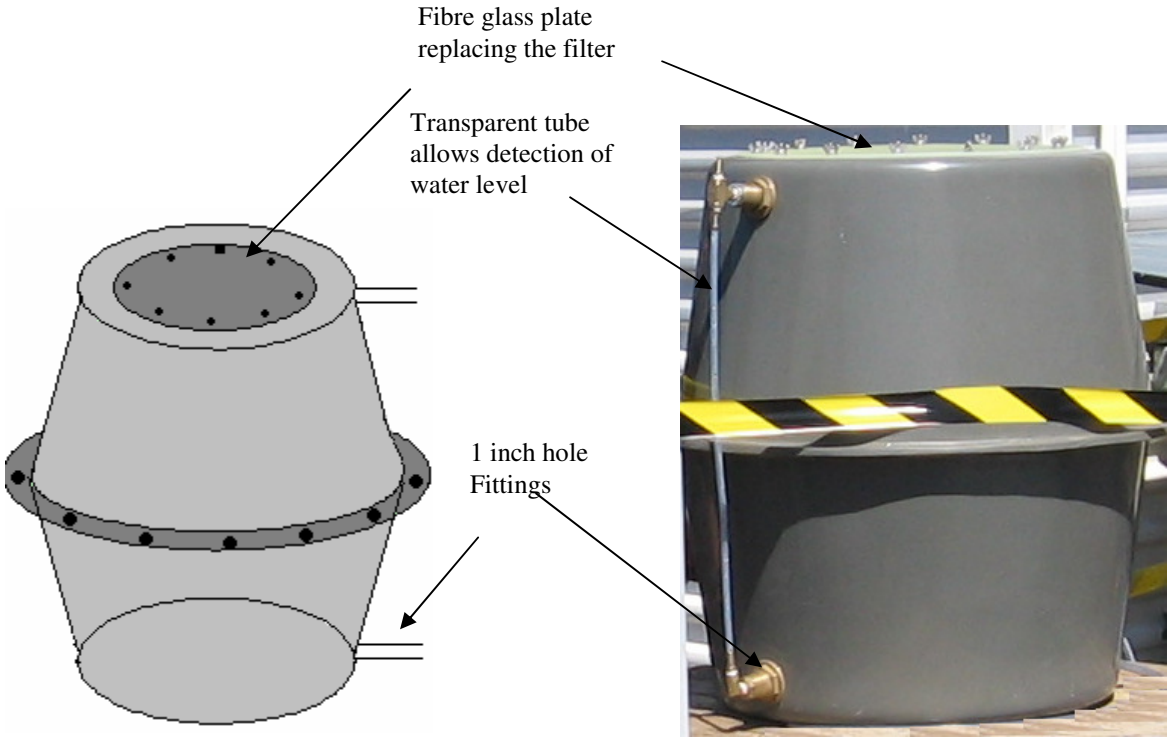

Figure 27- 225 liter fiber reinforced plastic (FRP) water tank (upper tank primarily collects displaced water) used in hydrogen storage mechanism.

The bottom tank is the main hydrogen storage component where the generated hydrogen from the electrolyser is stored. This tank is initially filled with water. The hydrogen from electrolyser is allowed to enter the tank from its bottom and is collected over the water. The incoming hydrogen displaces the existing water in the bottom tank to the upper tank via a connecting tube which joins the bottom and top tank. The bottom tank with design consideration is shown in Figure 28. The hydrogen exit from the storage tank requires some technical modifications i.e. enhanced safety precautions along the pipelines. A flashback arrestor is installed at the delivery point to avoid any kind of flame propagation back into the storage tank along the pipeline assembly leading to fuel cell. The working principle of flashback arrestor is similar to a spring fitted non-returning valve that does not allow buildup of back pressure thus it is able to prevent flame propagation.

a. Flash back arrestor

b. Pressure gauge

c. Connector

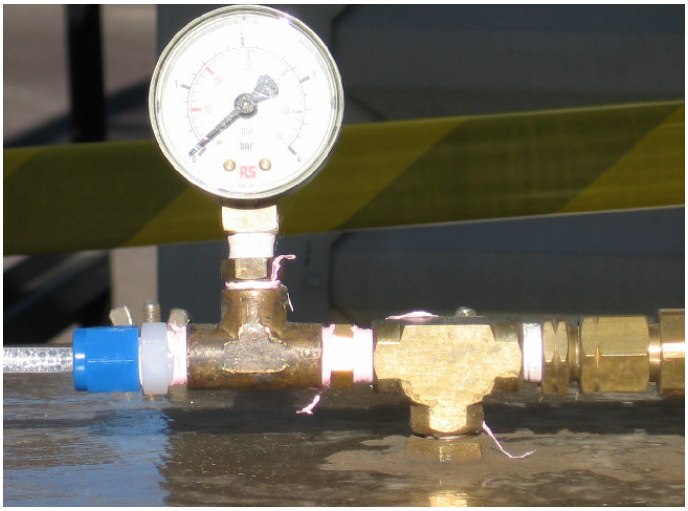

d. Pipe assembly at hydrogen outlet from bottom tank

Figure 28 a. Flash back arrestor, b. Pressure gauge, c. Connector, d. Pipeline assembly at hydrogen outlet from the bottom tank

The pressure gauge has the operating range of 0-4 bar and in the event of impasse of pipeline; it shows the rise in pressure inside the tank. A complete list of parts and description is shown in the Table 16.

Name	Part Number	Description	Company
Flash back Arrestor	561313	Re-settable flashback arrestors offer safety against flame propagation.	Fuel cell store
Pressure gauge	777104	B/ENTRY GAUGE 0-4 BAR	RS Australia
Connector	PFA-220-1-2	PFA Swagelok Tube Fitting, Male Connector, 1/8 in. Tube Fitting x 1/8 in. Male NPT	Swagelok

Table 16- Component parts and description of hydrogen outlet assembly at the bottom tank.

The bottom tank is completely wrapped with metallic foil to avoid any kind of static charge accumulation that can act as a potential source of ignition. Figure 29 shows a view of bottom tank incorporating all design requirements for lightning and static charge protection.

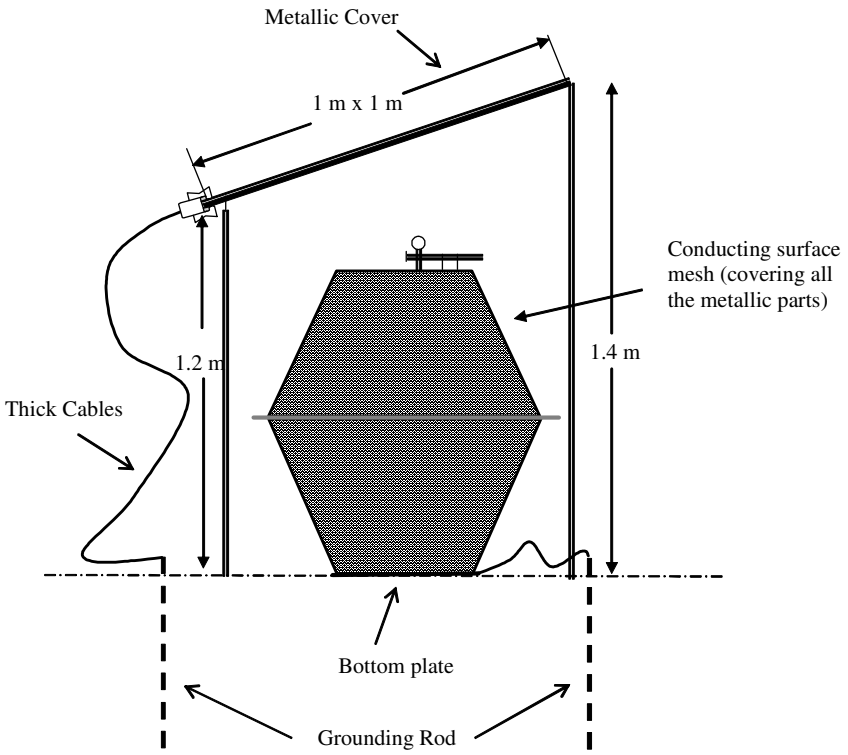

a. Schematic diagram of the bottom tank with required protections

b. Bottom tank

Figure 29- Bottom tank integrated with both lightning and static charge protections.

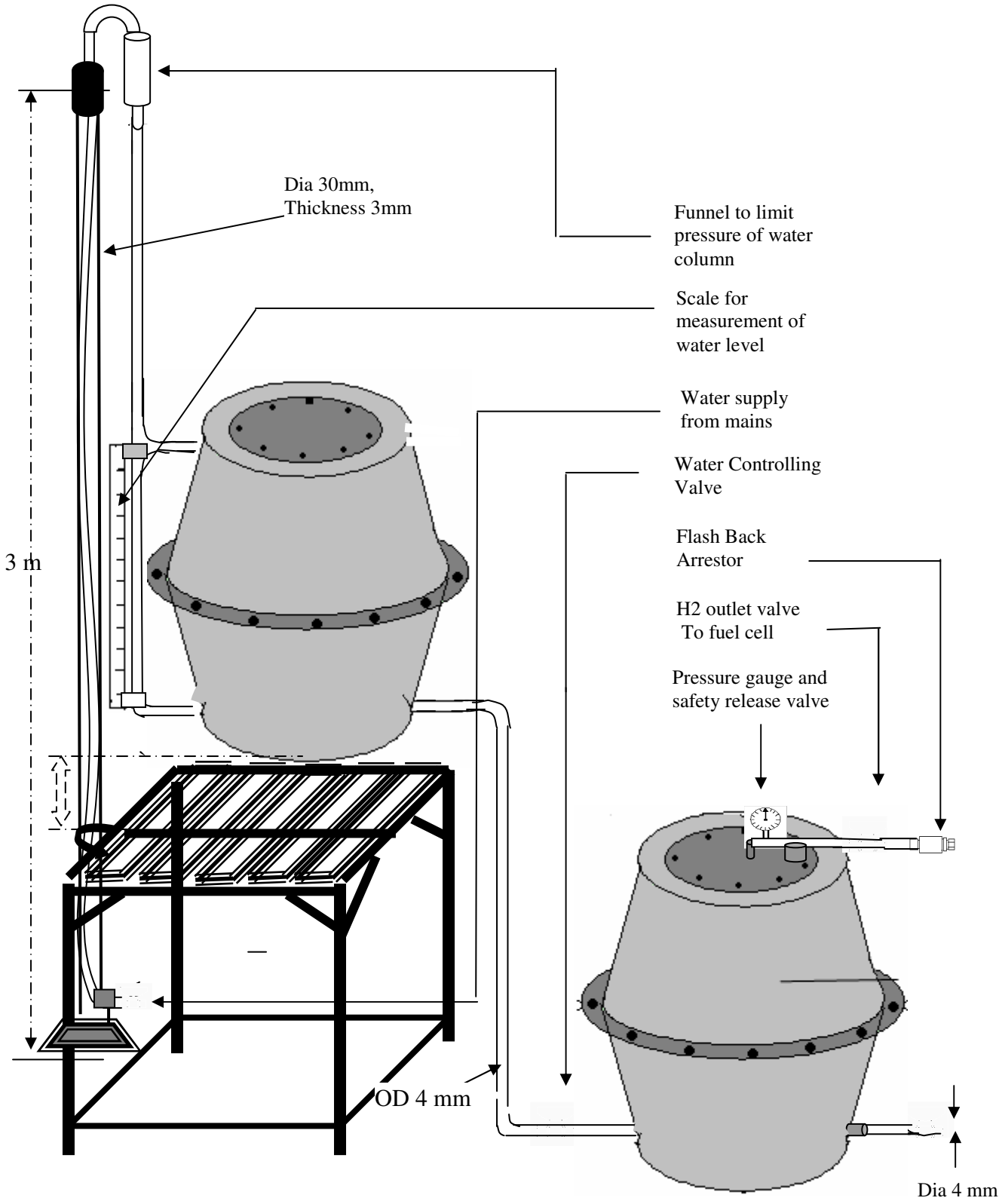

Figure 30- Hydrogen storage in water tank based on displacement technique.

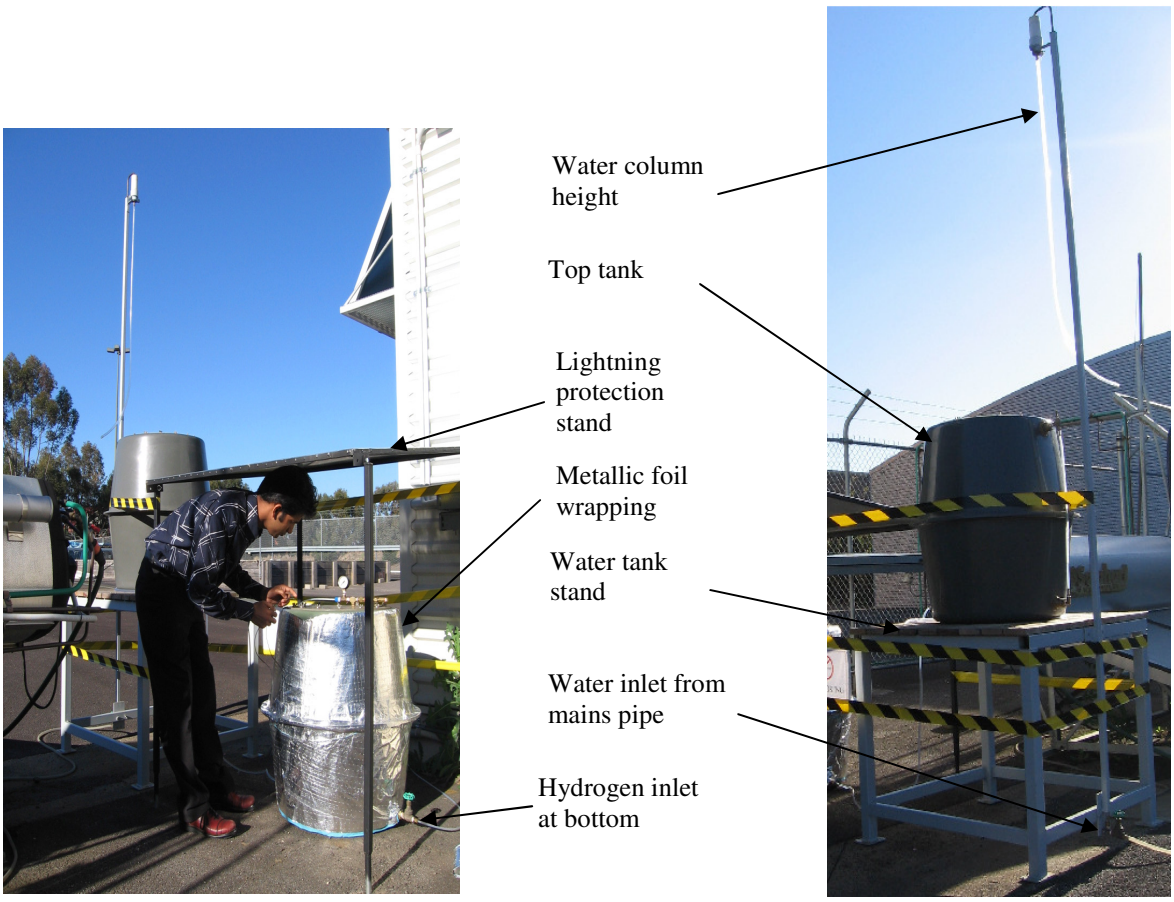

Figure 31- 225 litre FRP tank based hydrogen storage system integrated with necessary lightning and static charge protections.

3.4.5 500 W BCS Fuel cell

A 32 cell, 500 W BCS fuel cell was chosen for the higher amount of power generation from the stored hydrogen (Figure 32). The rate of hydrogen consumption is about 3 liters/min. Either the air or oxygen can be used. Below 200 W of power generation, cooling is carried out by the four set of fans which acts as a parasitic load. Between 200-500 W of power generation, external water cooling (with a water flow rate of 4-6 lit/min) is required.

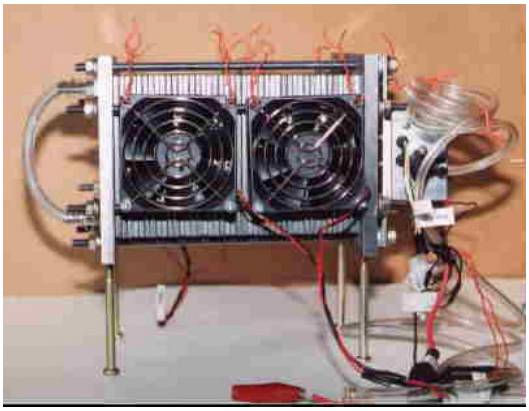

Figure 32- 500 W BCS fuel cell.

Stack specifications

Number of cells: 32, Electrode area: 64 cm^2, Reactants H_2/air, H_2/O_2, Power output: 500W.Operating temperature: 65° C. Operating Pressure: 0-7 psig hydrogen.

4. MODELLING OF SOLAR-HYDROGEN SYSTEMS FOR REMOTE POWER

4.1 INTRODUCTION

This chapter describes a mathematical model based on Excel spreadsheets for determining the key characteristics of a solar photovoltaic - hydrogen system for remote area power supply (RAPS) given the load to be met and the characteristics of the Proton Exchange Membrane (PEM) electrolyser and PEM fuel cell employed.

The primary objective of the model is to determine the size of each individual component of the solar-hydrogen system that yields the lowest unit cost of power supplied over a specified period. The model thus determines the economically-optimal area of PV panels and capacities of the electrolyser, fuel cell and hydrogen storage to meet a given annual load profile. Since volume constraints for hydrogen storage systems are generally more relaxed in RAPS applications compared to vehicles, a possible reduction in unit cost of power generation via low-pressure and hence low-cost storage capacity is analysed. The model allows two different strategies for determining storage capacity to be compared: 'unconstrained storage', that is, allowing sufficient capacity to store all the hydrogen produced by excess PV power over load; and 'constrained storage', that is, limiting storage capacity to an economic minimum. The minimum unit costs of generated power can be evaluated for a range of constrained-storage capacities assuming the unit cost of all other components, namely electrolyser, fuel cell, and balance of system, remain constant.

A schematic of the basic solar-hydrogen system modelled is given in Figure 33. The system is similar to the experimental systems described in chapter 3. This spreadsheet model uses the key characteristics of the individual components of the system to simulate the performance of the complete solar-hydrogen system.

The present chapter provides a detailed description of the spreadsheet model. Section 4.2 gives a brief guide to the overall model. Section 4.3 explains the technical performance evaluation sheet of the model. Section 4.4 is dedicated to the cost analysis part of the

model, while section 4.5 explains how the results are placed in a tabulated format in the worksheet 3.

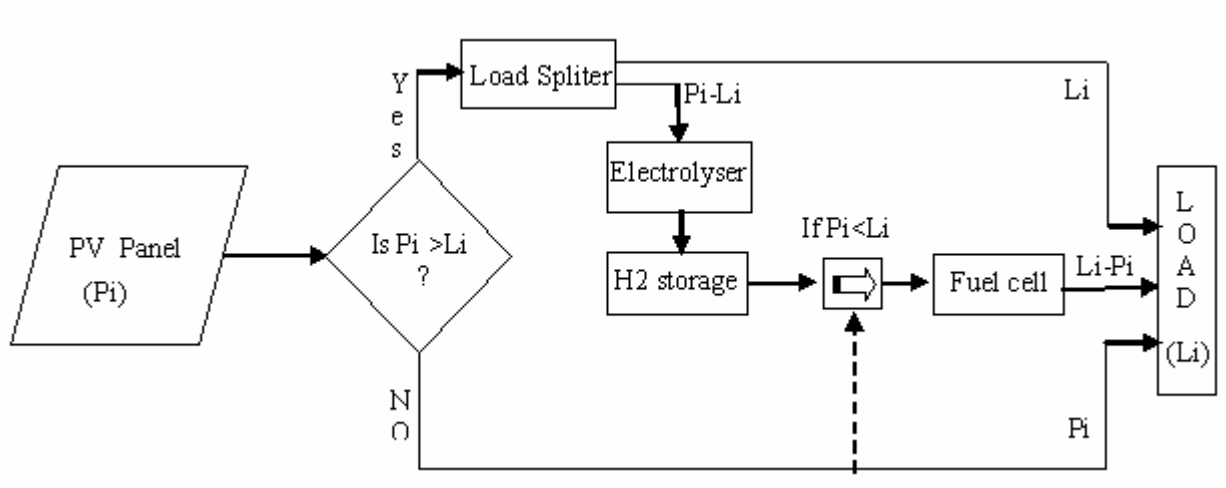

Figure 33 Schematic diagram of basic solar-hydrogen system for RAPS application.

Section 4.6 specifies the various scenario conditions that can be investigated, namely:

- unconstrained storage,
- unconstrained storage without limiting the capacity of electrolyser, and
- constrained storage both with and without limiting the capacity of the electrolyser.

Section 4.7 explains various graphs the model can generate as model output.

4.2 GUIDE TO SPREADSHEET MODEL

The spreadsheet model is designed to simulate the actual performance of the overall solar-hydrogen system in meeting a specified load profile over a year. It is a simple yet powerful tool to determine the minimum size of the system components given the available input solar isolation and load requirement as inputs. While evaluating the component sizes, the model can also incorporate costs, thereby enabling an optimum techno-economic value for each of the system components – that is, the size of each component to yield the lowest average unit cost energy generated over the system lifetime. Variation in component unit costs and their effects on the rest of the system and overall unit power costs can be analysed in detail. The model is constructed exclusively using Excel and the Visual Basic

so that it can be used by a wide range of interested analyst. Excel is used to carry out all the mathematical functions while Visual Basic is employed for all the repetitive substitution of values for different set of conditions, that is, the iterative procedure employed. The basic structure of the model is shown in Figure 34.

The model is broadly divided into three active worksheets:

- Technical Performance Evaluation -Worksheet 1
- Economic analysis - Worksheet 2
- Result Table and Graphs - Worksheet 3

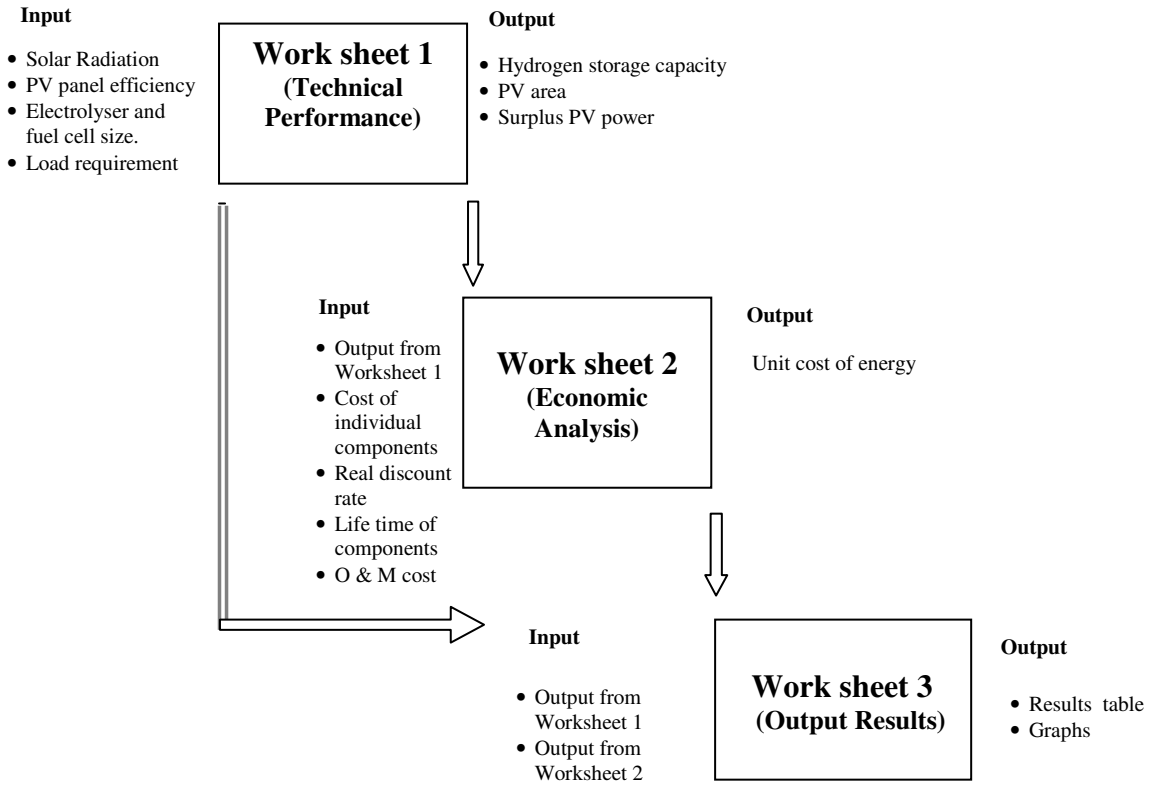

Figure 34- Basic structure of the spreadsheet model.

Worksheet 1 (Technical Performance Evaluation) allows the user to select all the input assumptions for a particular model run (Table 17-18). The parameters that need to be input are:

- Solar radiation for the location of the system (hourly values in MJ/ m^2 in a typical year over a horizontal surface)
- Energy efficiency of the PV array
- Specifications and characteristics of the electrolyser and fuel cell
- Capacity of the storage tank (in kg of hydrogen)
- The electrical load requirements for each hour of the year

Also ambient temperature could be provided as an input parameter as it affects the overall efficiency of the PV array but this is not done in the basic form of model. The model simulates the performance of the system on an hourly basis throughout the year. The main outputs are:

- The minimum array area sufficient for the load to be met at all times.
- The annual surplus of PV supplied energy over the total load.
- The minimum capacity of capacity of the hydrogen storage that will allow the load to be met.
- The energy efficiency of the electrolyser and fuel cell in each hour of operation.

Worksheet 2 (Economic analysis) evaluates the average unit cost of power generation over the systems lifetime. It receives input data about component sizes from Worksheet 1 and along with unit cost assumptions for the components, their life time and a nominal discount rate is considered as an input. The resultant average unit costs of power generation for various set of conditions are put in a tabulated format in the next worksheet.

Worksheet 3 (Results table and graphs) presents all the final outputs of a model run. It gives the sizes of all the system components and the overall average unit cost of power generation over the system's lifetime. The relationship between hydrogen storage capacity and PV array size is analysed. The unit cost of power supplied is plotted against various set of storage capacity. The most economically optimal conditions among the available options are identified. Unit storage cost is also considered as a primary variable along with the storage capacity.

4.3 WORKSHEET 1 (TECHNICAL PERFORMANCE EVALUATION)

4.3.1 Hourly Solar Radiation Input

The total global solar radiation incident on a horizontal plane for each hour of a typical year is required to feed the model. The solar insolation is expressed in $MJ/m^2/h$. the 8760 (24 x 365) values are entered in the column C rows 42 to 8801 of the Worksheet 1 (Figure 26). If only an hourly global solar radiation for an average day in each month is available, the same 24 average values can be entered for all the days of that month as an approximation to the real situation.

4.3.2 Load Profile

The hourly loads in kWh that the solar-hydrogen RAPS system must supply are inserted for each hourly period for each day of the year in column G cells 42 to 8801 of Worksheet 1 (Figure 35). Any set of hourly loads for a year can be accommodated by the model, but of course variations within each hour are not considered. Unless the application has been monitored for a whole year or more, data on the variation of load on an hourly basis for a full year are unlikely to be available. In that case, standardised hourly load profiles for an average day in a year, or an average day in summer and winter have to be used, and entered in column C for all the days to which they apply.

4.3.3 PV Array Model

The PV array model computes the hourly electrical energy supplied to the solar-hydrogen system given the hourly global insolation in column C and the mean ambient temperature over that hour input in column D. If the PV panels are inclined at angle Φ, to the horizontal focusing north (southern hemisphere), the total radiation incident on the panels can be

found from the global insolation on the horizontal surface (column D) using the formula shown in section 2.4.3.

In the absence of hourly ambient temperature readings and detailed PV cell characteristics. An approximation to the energy efficiency of the PV panels can be made by using an annual average figure, erring on the conservative side.

The energy supplied by unit area of the PV panel pi, column E cell 34, is calculated in kWh/m^2. Total energy supplied by the panel Pi, column F cell 34, in kWh is then derived by multiplying energy supplied per unit area by the total PV area receiving the solar radiation.

The load requirement is given in column G cell 34 on an hourly basis. Surplus power SP_i, column H cell 34, is simply the difference between energy supplied by the panel Pi and load requirement Li for that hour. $SP_i = P_i - L_i$.

	A	B	C	D	E	F	G	H	I	J	K	L	M	N	O	P	Q
1	RENEWABLE ENERGY (PV) - HYDROGEN RAPS SYSTEM MODEL																
2	**Input parameters**										**Ouput**						
3	STORAGE TANK										PV PANEL AREA					18.35	Sq.m
4	Maximum volume of storage tank (kg)				Tmax	13.49377	kg of H2				Initial start of mass of hydrogen required					6.96	kg of H2 gas
5	PV PANEL										Maximum capacity of the storage tank (mass of hydrogen)					13.49	kg of H2 gas
6	PV panel at latitude angle to horizontal				38 degree						Total load supplied in a year					1825.00	kWh
7	Total area of PV panels				A	18.34655	m2				Load supplied directly by the PV panel					779.34	kWh
8	Energy efficiency of PV array				PVeff	0.1					Load supplied by the fuel cell					1045.66	kWh
9	Hydrogen in storage at beginning of hour 0				C0	0	kg of H2										
10	Single cycle efficiency of H2 storage system				ε	100	%	Assummed to be 100% eficient			**Load Profile**						
11	ELECTROLYSER																
12	Assume 50 V dc, 1		Faraday efficiency		eta	0.95											
13			Slope I-V (linear part) graph		m	7.2	amps/volts	Based on 7cell h-tec electrolyser									
14			Cut in voltage		Vcutin	1.5	volts										
15			Number of cells in series		NSE	33		Max Inout Volatge assumed 50 Vdc									
16			Number of cells in parallel		NPE	42											
17			Total number of cells		NE	1386		Based on max power input of 10 kW									
18	FUEL CELL																
19	Assume 50 V dc, 1		Fuel utilisation coefficient		mu	0.95											
20			Voc,cell		Vocc	0.92	volts										
21			Voltage at max current, cell		Vmin	0.6	volts										
22			Max operating current per c		Imax	1	amps	Based on BCS 10 W fuelcell									
23			(Vocc-Vmin)/Imax		mfc	0.1534	V/A	NB inverse units to electrolyser curve									
24			Number of cells in series		NS	54		50 V dc max output									
25			Number of cells in parallel		NP	308											
26			Total number of cells, NP*NS		N	16632											
27																	
28	**Date**	**Hour**	**Insolation**	**Ambient temperature**	**Energy supplied per unit area of PV**	**Total energy supplied by panel**	**Load**	**Surplus power (mean over hour)**	**Effective surplus power that can be utilzed by the**	**Hydrogen produced by electrolyser**	**Actual power consumed by the elctrolyser**	**Load supplied directly by PV**	**Load supplied by fuel cell**	**Hydrogen used by fuel cell from storage**	**Hydrogen stored**	**Energy Efficiency of electrolyser**	**Energy efficiency of fuel cell (HHV)**
29			**MJ/m2**	**C**	**kWh/m2**	**kWh**	**kWh**	**kWh**	**kWh**	**kg/h**	**kWh**	**kWh**	**kWh**	**kg/h**	**kg**	**%**	**%**
30		i	Si	Ti	pi	Pi	Li	SPi=Pi - Li	ESPi	Hei	Pac	PVsd,i	FCSUPPLYi	HFCi	Ci	N elec	N fc
31										if Spi >0			if Spi>or=0	HFCi(Li-Pi)	IF Spi>or=0		
32										HEi = ...			FCSUPPLYi=0		=Hei+C (i-1)		
33										Else HEi=0			Else =Li-Pi		ELSE IF Spi<0		
34															=C(i-1)-HFCi		

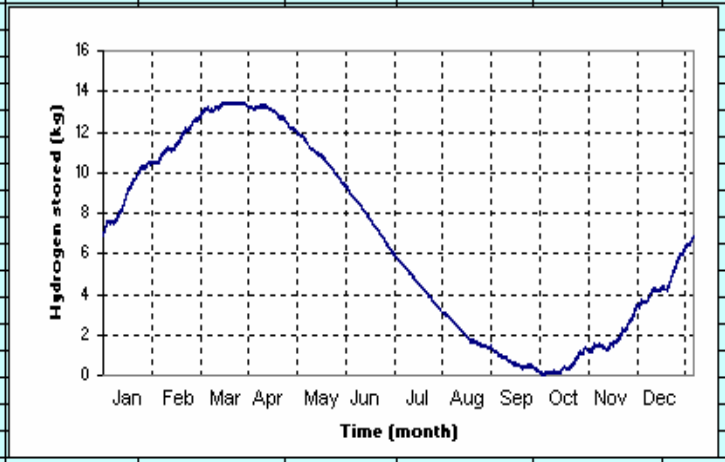

Table 17-'Technical Performance evaluation' section of the Model.

	A	B	C	D	E	F	G	H	I	J	K	L	M	N	O	P	Q
34	Date	Hour	Insolation	Ambient temperature	Energy supplied per unit area of PV	Total energy supplied by panel	Load	Surplus power (mean over hour)	Effective surplus power that can be utilzed by the	Hydrogen produced by electrolyser	Actual power consumed by the elctrolyser	Load supplied directly by PV	Load supplied by fuel cell	Hydrogen used by fuel cell from storage	Hydrogen stored	Energy Efficiency of electrolyser	Energy efficiency of fuel cell (HHV)
35			MJ/m2	C	kWh/m2	kWh	kWh	kWh	kWh	kg/h	kWh	kWh	kWh	kg/h	kg	%	%
36		i	Si	Ti	pi	Pi	Li	SPi=Pi - Li	ESPi	Hei	Pac	PVsd,i	FCSUPPLYi	HFCi	Ci	N elec	N fc
37										if Spi >0			if Spi>or=0	HFCi(Li-Pi)	IF Spi>or=0		
38										HEi = ...			FCSUPPLYi=0		=Hei+C (i-1)		
39										Else HEi=0			Else =Li-Pi		ELSE IF Spi<0		
40															=C(i-1)-HFCi		
41															6.957144937		
42	1-Jan	1	0		0	0	0.1448187	-0.1448187	0	0	0	0	0.144818708	0.0061922	6.950952766	0	58.9
43		2	0		0	0	0.1298005	-0.1298005	0	0	0	0	0.129800472	0.0055491	6.945403659	0	58.9
44		3	0		0	0	0.1265823	-0.1265823	0	0	0	0	0.126582278	0.0054113	6.939992323	0	58.9
45		4	0		0	0	0.1287277	-0.1287277	0	0	0	0	0.128727741	0.0055032	6.934489141	0	58.9
46		5	0		0	0	0.1394551	-0.1394551	0	0	0	0	0.139455053	0.0059625	6.92852666	0	58.9
8777		8736	0		0	0	0.1823643	-0.1823643	0	0	0	0	0.1823643	0.0078008	6.751822192	0	58.9
8778	31-Dec	8737	0		0	0	0.1448187	-0.1448187	0	0	0	0	0.144818708	0.0061922	6.745630021	0	58.9
8779		8738	0		0	0	0.1298005	-0.1298005	0	0	0	0	0.129800472	0.0055491	6.740080914	0	58.9
8780		8739	0		0	0	0.1265823	-0.1265823	0	0	0	0	0.126582278	0.0054113	6.734669578	0	58.9
8781		8740	0		0	0	0.1287277	-0.1287277	0	0	0	0	0.128727741	0.0055032	6.729166396	0	58.9
8782		8741	0		0	0	0.1394551	-0.1394551	0	0	0	0	0.139455053	0.0059625	6.723203915	0	58.9
8783		8742	0.026098		0.00072	0.0133	0.1823643	-0.1690641	0	0	0	0.013300228	0.169064072	0.0072308	6.715973139	0	58.9
8784		8743	0.328803		0.00913	0.167567	0.2789101	-0.1113434	0	0	0	0.167566666	0.111343439	0.0047591	6.711214051	0	58.9
8785		8744	0.91353		0.02538	0.465559	0.3003647	0.1651942	0.1651942	0.00387622	0.165194213	0.300364729	0	2.901E-16	6.71509027	93.15452671	0.0
8786		8745	1.806108		0.05017	0.92044	0.2681828	0.6522574	0.6522574	0.01499318	0.652257399	0.268182793	0	2.901E-16	6.730083446	91.25677963	0.0
8787		8746	2.587124		0.07186	1.318467	0.2360009	1.0824657	1.0824657	0.02445799	1.082465653	0.236000858	0	2.901E-16	6.754541434	89.70096607	0.0
8788		8747	3.222548		0.08952	1.642295	0.2145462	1.4277491	1.4277491	0.03183644	1.427749078	0.214546235	0	2.901E-16	6.786377873	88.52442085	0.0
8789		8748	3.67156		0.10199	1.871124	0.1930916	1.678032	1.678032	0.03707228	1.678032039	0.193091611	0	2.901E-16	6.823450156	87.70807771	0.0
8790		8749	3.892886		0.10814	1.983917	0.187728	1.7961893	1.7961893	0.03951285	1.796189252	0.187727955	0	2.901E-16	6.862963008	87.33268078	0.0
8791		8750	3.870217		0.10751	1.972364	0.1823643	1.7900002	1.7900002	0.0393855	1.790000189	0.1823643	0	2.901E-16	6.902348508	87.35218993	0.0
8792		8751	3.536498		0.09824	1.802292	0.171637	1.6306555	1.6306555	0.03608816	1.630655511	0.171636988	0	2.901E-16	6.938436667	87.86036582	0.0
8793		8752	3.046078		0.08461	1.552362	0.1727097	1.3796518	1.3796518	0.03081966	1.379651835	0.172709719	0	2.901E-16	6.969256323	88.68471709	0.0
8794		8753	2.152502		0.05979	1.096972	0.1930916	0.9038801	0.9038801	0.02056705	0.903880085	0.193091611	0	2.901E-16	6.989823371	90.33408693	0.0
8795		8754	1.149776		0.03194	0.585956	0.2413645	0.3445916	0.3445916	0.00802346	0.34459161	0.241364514	0	2.901E-16	6.997846835	92.43740194	0.0
8796		8755	0.962285		0.02673	0.490406	0.2789101	0.2114957	0.2114957	0.00495269	0.211495668	0.278910105	0	2.901E-16	7.002799527	92.96732034	0.0
8797		8756	0.294561		0.00818	0.150116	0.2799828	-0.1298668	0	0	0	0.150116042	0.129866795	0.0055519	6.99724758	0	58.9
8798		8757	0.024398		0.00068	0.012434	0.2681828	-0.2557489	0	0	0	0.012433863	0.25574893	0.0109486	6.986298932	0	58.8
8799		8758	0		0	0	0.2628191	-0.2628191	0	0	0	0	0.262819138	0.0112522	6.975046732	0	58.8
8800		8759	0		0	0	0.2360009	-0.2360009	0	0	0	0	0.236000858	0.010101	6.964945693	0	58.9
8801		8760	0		0	0	0.1823643	-0.1823643	0	0	0	0	0.1823643	0.0078008	6.957144937	0	58.9
8802	Total		5456.304255		151.564	2780.676	1825	955.67632	2001.3344	44.7433898	1972.089257	779.3418932	1045.658107	44.74339			58.9
8803	Max Val		3.861141		0.10725	1.967739	0.3003647	1.8607399	1.8607399	0.04083795	1.860739891	0.300364729	0.300364729	0.012865			
8804														0.1488446			
8805								During summer the peak storage reaches to a value of (in kg) =							13.49377227		
8806								During winter the cumulative storage comes down to a value of (in kg) =							-1.83371E-13		
8807								Diffrence between Max Storage and Min Storage values in a year =							13.49377227		

Table 18- Results obtained for unconstrained storage conditions. (Spread Sheet Model)

4.3.4 Electrolyser model

The electrolyser modeled is rated as 50 V dc and 10 kW; that is, if a voltage potential of 50 V is applied across this electrolyser; all the available power is consumed to produce hydrogen. The higher power rating is used to extend the usage of all of the excess power available from the PV panel. For both PEM electrolysers and fuel cells the system efficiency is independent of scaling (Crockett *et al.* 1995). *Faraday efficiency*, defined as 'η' is the ratio of the actual hydrogen production to that of theoretical production and is assumed to be 95 % in the model. Different values can be used if desired. The Faraday efficiency is less than 100% because of fuel crossover across the membrane. *Slope*, ('m') is the ratio of current and voltage. The value of 'm' mentioned in column F (cell 19) is taken from the experiments performed on the 7 cell h-tec electrolyser. The cut-in voltage (Vcut-in', located in column F cell 20) is the minimum voltage applied across a single cell at which production of hydrogen starts. This cut-in voltage is just above the thermo-neutral voltage 1.48 V of a water molecule. Since the 7-cell electrolyser starts generating hydrogen at 10.5 volt, the cut-in voltage across a single cell is evaluated as 1.5 volts i.e. $(10.5 \div 7)$. Number of cells in series 'NSE' is expressed in column F cell 21. If the maximum volt of 50 V dc can be applied across the terminal, the stack needs (50 V $\div$1.5 V) 33 cells in series. Number of cells in parallel 'NPE' is shown in column F cell 22. The total number of cells that are stacked in the electrolyser is shown in column F cell 23.

Hydrogen produced by the electrolyser, $H_{e,i}$ (column J cell 35), is expressed in kg/h. It depends on two conditions: the effective excess surplus power available $P_{es,i}$, and the remaining available storage volume $(T_{\max} - C_{i-1})$. C_{i-1} is the net hydrogen stored or filled in the storage tank till $(i-1)^{th}$ hour.

$$\left.\begin{aligned} H_{e,i} &= H_{es,i} \quad \textit{if} \quad P_{es,i} > 0 \;\&\; H_{es,i} \le T_{\max} - C_{i-1} \\ &= T_{\max} - C_{i-1} \quad \textit{for} \quad H_{es,i} \ge T_{\max} - C_{i-1} \end{aligned}\right\} \qquad \text{[Eq 4.2]}$$

where $H_{es,i}$ = hydrogen production due to the effective surplus power alone

$$H_{es,i} = 1.866\times10^{-5}\times eta\times NE\left[\sqrt{\left\{m^2\times V_{cut,in}{}^2+\frac{4\times m\times P_{es,i}\times 1000}{NE}\right\}}-m\times V_{cut,in}\right] \quad \text{[Eq 4.3]}$$

For details refer to Eq.2.6, chapter 2.

Actual power consumed by the electrolyser $P_{ac,i}$ (column K cell 34) is the amount of surplus power that is utilised by the electrolyser to produce the hydrogen generated at the i^{th} hour.

$$P_{ac,i} = \frac{\left[\left\{\frac{H_{e,i}}{\left(1.866\times10^{-5}\times eta\times NE\right)}+\left(m\times V_{cut,in}\right)\right\}^2-\left(m\times V_{cut,in}\right)^2\right]\times NE}{4\times m\times 1000}$$

$$\Rightarrow P_{ac,i} = \frac{\left[\left\{\frac{H_{e,i}}{\left(1.866\times10^{-5}\times eta\times NE\right)}\right\}^2+\frac{2\times H_{e,i}\times m\times V_{cut,in}}{\left(1.866\times10^{-5}\times eta\times NE\right)}\right]\times NE}{4000\times m} \quad \text{[Eq 4.4]}$$

Where $H_{e,i}$ = hydrogen produced by the electrolyser. The rest of the parameters are same as defined earlier (for details refer to Eq 2.6 chapter 2)

Power supplied directly by the PV panel to the load end $PV_{sd,}$ is shown in column L cell 34. The load is always directly connected to the PV panel. It is only the excess available power that is utilised by the electrolyser.

4.3.5 Hydrogen Storage

The net hydrogen storage at the end of ith hour (in kg) *Ci* is given in column O cell 34, At the end of each hour the net hydrogen accumulated in the storage tank is evaluated. Hence net hydrogen storage *Ci* is calculated by the following formula:

$$\left.\begin{aligned} C_i &= C_{i-1} + H_{e,i} \quad if \quad S_{p,i} \geq 0 \\ &= C_{i-1} - H_{fc,i} \quad if \quad S_{p,i} < 0 \end{aligned}\right\} \qquad \text{[Eq 4.5]}$$

Where = C_{i-1} is the net hydrogen present at the end of the previous hour. $H_{e,i}$ is the hydrogen generated by the electrolyser for the ith hour operation. $H_{fc,i}$ is the hydrogen consumed by the fuel cell for the duration of the i th hour.

4.3.6 Fuel cell Model

The fuel cell is also modeled as having same maximum power ratings as the electrolyser, that is, 50 V dc, 10 kW however these values can be altered to accommodate a fuel cell of higher capacity. Fuel utilisation coefficient defined as 'μ', mentioned in column F cell 25 is the ratio of actual hydrogen utilised to that of total hydrogen consumed from the storage tank. Since most of the fuel cells employ open-ended operation, the loss of hydrogen via open end is incorporated in fuel utilization co-efficient. Dead-end operated fuel cells having higher fuel utilization coefficients, but this mode has negative effects on water management of the fuel cell stack (Larminie and Dicks 2005). Open circuit voltage for a single cell (Vocc, column F cell 26) can be evaluated as total voltage output over the number of cells in the fuel cell stack. Voltage at maximum cell current (V_{min}, column F cell 27) is the voltage across a single cell corresponding to the maximum current drawn by the load. The V_{min} for a single cell corresponds to voltage output when current drawn is maximum**.** The maximum operating current for a single cell is shown as I_{max}, column F cell 28. This value is based on design of a PEM membrane's current-carrying density by the manufacturer of the BCS fuel cell. Slope of the Voltage /Current curve (mfc', column F cell 29) is evaluated as 0.1534 as mfc= $(V_{occ}-V_{min})/I_{max}$. Number of cells in series, column F cell 30 defined as 'NS' is taken as 54. Since maximum rated out put is 50 Vdc and Vocc

is 0.92 volt, 'NS' is calculated as $50 \div 0.92 = 54$. Number of cells in parallel, column F cell 31, is determined as 308 based on maximum rated power output of fuel cell of 10 kW. Thus the total number of cells is NS×NP =1632.

Load supplied by the fuel cell $FC_{s\,i}$ is given in column M cell 34. If the excess surplus power $PV_{sd,i}$ is greater than zero, then load supplied by the fuel cell $FC_{s,\,i}$ is zero, that is, the fuel cell is turned off. For the rest of the period, it is simply the difference of the load requirement *Li* and energy available at the PV terminal *Pi*.

Hydrogen consumed by the fuel cell from the storage tank to generate the required power to supply the demand in kg/hr ($H_{fc,\,i}$, column N cell 34) is calculated as:

$$H_{fc,i} = \frac{3.6 \times N}{mu \times F}\left[\frac{V_{0cc}}{2 \times m_{fc}} - \sqrt{\left(\frac{V_{occ}}{2 \times m_{fc}}\right)^2 - \frac{FC_{s,i}}{N \times m_{fc}}}\right] \quad \text{(Refer chapter 2, Eq.2.21)}$$

Where $FC_{s,\,i}$ is the power supplied by the fuel cell to the load. F is the Faraday's constant, is defined as the charge content of 1 mole of electrons, that is, 96 485 C mol^{-1}.Vocc is the open circuit voltage of the fuel cell. 'N' is the total number of the cells, '*mu*' and '*mfc*' are fuel utilization coefficient and slope of *V-I* curve respectively.

4.3.7 Energy Efficiency of Electrolyser and Fuel cell

Energy efficiency of the electrolyser (N_{elec} column P cell 34) is defined as the ratio of energy content based on the high heating value (HHV) of the hydrogen produced and the total energy input to the electrolyser, per unit time:

$$N_{elec} = \frac{\left(H_{e,i} \times 142.9\right)}{\left(P_{apc,i} \times 3.6\right)} \times 100 \quad \text{If} \quad E_{sp,i} > 0 \;\&\; P_{apc,i} > 0\text{, else, } = 0 \qquad \text{[Eq 4.6]}$$

The energy efficiency of the fuel cell (column Q cell 34) is defined as the ratio of energy supplied by the fuel cell to the energy content of hydrogen consumed, per unit time.

$$N_{fc} = \frac{\left(FC_{s,i} \times 3.6\right)}{\left(H_{fc,i} \times 142.92\right)} \times 100 \qquad \text{If} \quad FC_{s,i} > 0 \text{, else, } = 0 \qquad \text{[Eq 4.7]}$$

4.3.8 Computational Procedure

The logical details of the computational procedure used in Worksheet 1 are shown in the flow chart in Figure 35.

The input parameters are initially fed to the model, including hourly solar radiation, and hourly load to be met. The capacity of the electrolyser is set such that all of the surplus PV power can used by the electrolyser to generate hydrogen. The storage capacity is kept unconstrained, so that all of the hydrogen generated is stored. Initial random trial values for the storage capacity T_{max} and the PV area are typed in and the model run subsequently re-adjusts to correct values. The fuel cell capacity is set so that it is just sufficient to meet the demand at peak hours. The start-up amount of hydrogen in storage, C_0, is set to zero.

The value of the PV area that is just sufficient to allow all the load to be met continuously throughout the year is then found by an iterative procedure. The indicator of whether the load is met is the amount of hydrogen in storage at the end of the year after a run of the model through a whole year. Thus if initially $C_0 = 0$, then $C_0 = 0$ too indicates that the PV area is exactly right for the system to meet the annual load. The iterative procedure is executed in Excel using the command, Tools/Add in/Solver to vary the value of PV area until the value in the target cell C_{8760} is zero.

When the required value of PV area is found, the storage capacity needed, T_{max} is determined by the amount of stored hydrogen when it reaches its peak during summer. In addition, on the basis of the results, a graph of hydrogen storage versus time over the year is displayed in the top right of the worksheet. The difference between the peak and trough of the curve gives the exact size of the storage tank, without any allowance for contingency. Any changes to the input variables are directly reflected on this graph.

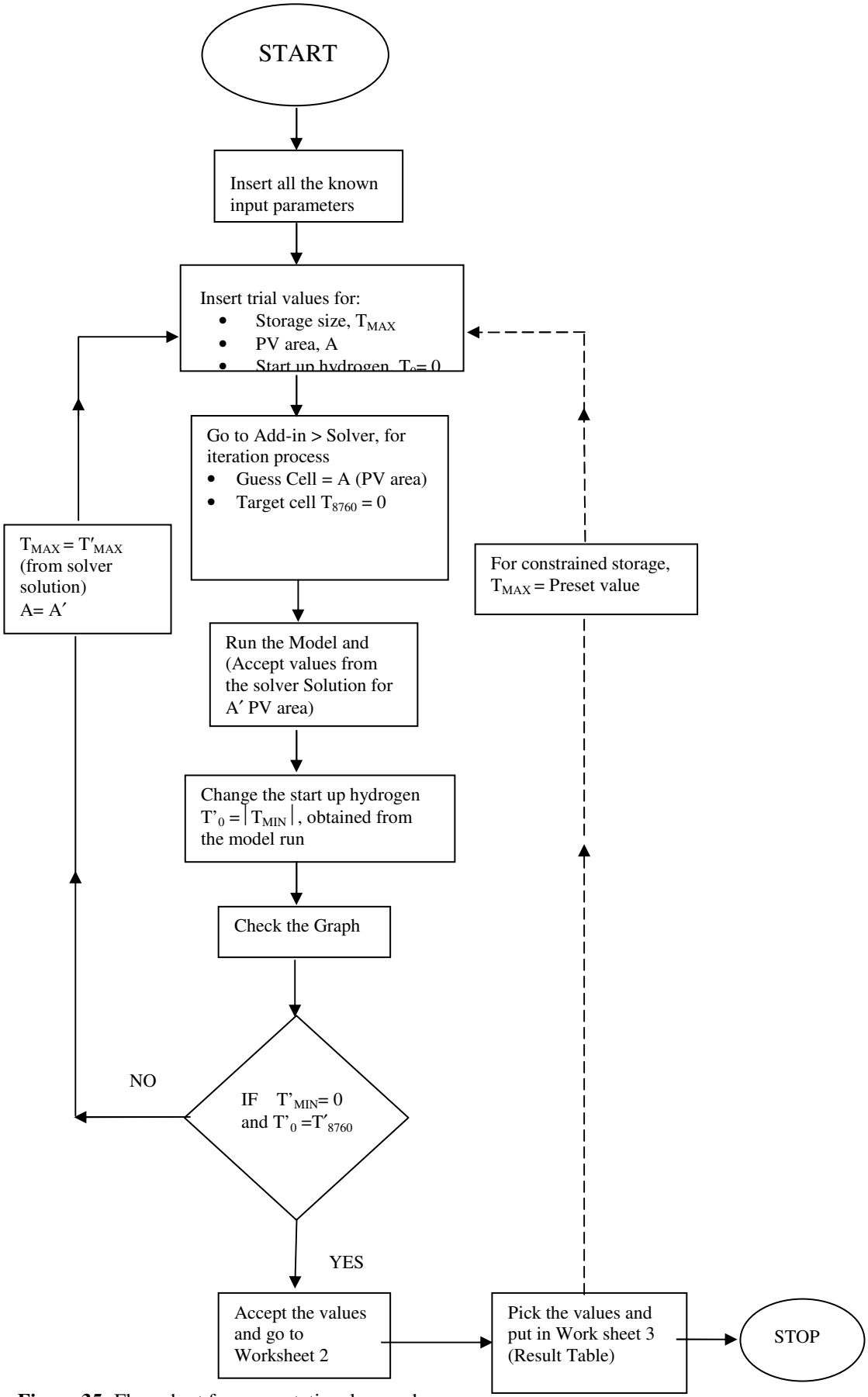

Figure 35- Flow chart for computational procedure.

order to make the operation cyclic, the amount of hydrogen stored at the end of the year is supplied to the storage at the start of the year C_0. This is done to keep a non-negative value for the actual amount of hydrogen stored. The actual hydrogen storage is plotted against time the upper right hand corner and it gives the actual profile of hydrogen storage for whole year. The values of minimum storage capacity needed and PV panel area are carried over to Worksheet 2 for the economic analysis. The cell representing the of PV area, A and storage size, T_{max} are connected actively (internally fed) to Worksheet 2.

4.3.9 Initial hydrogen volume

In order to run the system to complete a cycle continuously each year, it is essential to avoid the hydrogen storage tank from becoming completely devoid of hydrogen gas at any point of operation. This condition arises specifically during winter where insufficient solar radiation leads to increased reliance on the fuel cell for supplying the load and hence greater hydrogen consumption from the storage tank. Thus a certain particular mass of hydrogen must be fed into the storage tank at the start of the year to enable the continuous operation of the system. This initial mass of hydrogen depends upon the running conditions and component sizes as well as the time chosen for the start of the year. Starting with 10% more mass than the estimated minimum required is an initial suggested safe practice, but further experience with actual systems will be needed to establish a firm value. Account must also be taken of the estimated loss rate, and annual variation in insolation and load, in setting the excess value. The storage capacity calculated by the model will then have to be increased by an amount equal to this margin for safety and contingency.

4.3.10 Maximum volume of the tank needed

In the model the storage tank size calculated (column A cell 4) is specific to a particular set of operating conditions and system sizes. For example, an increase in PV cell area lowers the minimum tank size limit, since a higher proportion of the load over the year is met directly by the PV array.

4.3.11 Cumulative load for entire year

The cumulative load over the year is the sum of the hourly loads over the 8760 hours in a year (column A cell 5). This value is changed according to the demand profile that is required to be met as there could be both daily as well as seasonal variation in the load requirement.

4.3.12 Load supplied directly by the panel

This is the PV power in kWh that is directly supplied to the demand side (cited in column A cell 6), and it is dependent on the PV cell area.

4.3.13 Load supplied by the fuel cell

The cumulative annual load supplied by the fuel cell by drawing on stored hydrogen usage is displayed in column A cell 7. For all those hours when there is insufficient solar radiation to meet the demand profile directly from the panel, the fuel cell is operated to meet the load requirements.

4.4 WORKSHEET 2 (COST ANALYSIS)

Worksheet 2 (Table 19) is dedicated to the cost analysis of the system, using the flowing results from worksheet 1 are as inputs:

- Area of PV panel required
- Load supplied by the PV panel
- Maximum value of surplus power
- Maximum power generated by the fuel cell
- Storage tank capacity (kg)

PV panel size (A) is obtained from worksheet 1 and is entered in Worksheet 2 column E cell 3.

The total load supplied by the PV panel for the duration of entire year (Li) is entered in column E cell 4. It includes both the power directly supplied to the load and surplus power available to the electrolyser.

Maximum value of surplus power available from the panel (SP_i) (column E cell 5) gives an indication of the power rating of electrolyser needed for the system. Maximum load in kW (column E cell 7) is the rated power of the fuel cell, and is set equal to the maximum hourly peak demand over the year. (In practice a surplus over peak demand would be required, but here the model is calculating in effect the unit costs of a system precisely matched to the demand.)

Size of storage tank needed T_{max} is shown in column E cell 10. The size is expressed in kg of hydrogen as this mass is independent of storage pressure. Subsequently the corresponding volume of hydrogen, and hence the volume of the storage tank, can be calculated given the storage pressure and ambient temperature.

Apart from these input parameters regarding system component size, the unit costs of system components such as the PV array, electrolyser, hydrogen storage system, fuel cell and balance of system (including a control unit) must also be input to worksheet 2. These values may be taken from the scientific and commercial-product literature, or set by the user of the model to investigate a range of scenarios regarding future cost movements.

System components are listed in column A cell 12 followed by the relative cost of components per unit size in column B cell 12 (all units are in US$). The assumed unit cost values (a range) of hydrogen storage are typed in column B cell 19 to cell 25. Unit costs are multiplied by component size for each component to obtain the total capital cost of the component. No economies of scale are assumed. Total capital cost of the component, $C_{t,}$ is mentioned in column D cell 12.

A real discount% rate is incorporated in column E cell 12. Average life times, mentioned in column F cell 14 to cell 18 of electrolyser and fuel cell are obtained from the literatures.

A capital recovery factor CRF_{PV} (column G cell 12) is used to convert the capital cost to an equivalent annualized cost at the set discount rate and taking into account the lifetime of the component. The CRF_{PV} is calculated as:

$$CRF_{PV} = \frac{d}{100} \times \left(\frac{1}{1 - (1 + 0.01 \times d)^{-n}} \right) \quad \text{[Eq 4.8]}$$

Where d = annual discount rate % and 'n 'is the life period (Kazim 2005).

Annual capital recovery amount ACR_{PV} (column H cell 12) is the product of capital recovery factor and the total capital cost of the component, C_t.

$$\text{Hence } ACR_{PV} = CRF_{PV} \times C_t \quad \text{[Eq 4.9]}$$

The operating and maintenance cost is nominally taken as 2% of the total capital cost for each of the components. Alternative values may be inserted if desired.

The total annualised cost is the summation of annual capital recovery amount, and annual operating and maintenance cost. Finally the unit cost of energy supplied (in US$/kWh) is evaluated by dividing the total annualised cost of all the system components by the cumulative annual load supplied.

4.5 SCENARIO CONDITIONS

4.5.1 Basic Conditions

The model can be used to investigate system sizing and economics under a number of different conditions:

- Unconstrained storage, in which all the surplus PV power over the load is used to generate hydrogen, all of which is stored.

- Constrained storage, in which all the surplus PV power over the load is potentially able to generate hydrogen, but the preset storage capacity limits the amount of hydrogen produced that is actually stored
- Unconstrained storage while limiting the capacity of the electrolyser.
- Constrained storage while limiting the capacity of the electrolyser.

These conditions are explained further in the following subsections. The use of the model under these conditions will be illustrated in the case study in the next chapter.

4.5.2 Unconstrained storage while utilising all the surplus PV power

Unconstrained storage is the simplest of the four conditions, and is used in the most general and initial model run to establish the basic system sizing parameters, irrespective of economically optimal conditions. Its defining features are that all the surplus PV power over the load is used by the electrolyser to produce hydrogen that is all stored. The electrolyser capacity is thus just sufficient to utilise all of the available surplus PV power, and there is just enough storage capacity to accommodate all the hydrogen produced.

4.5.3 Constrained storage with no limitations on electrolyser capacity

In constrained storage, the storage capacity an input to the model run is limited to a certain preset value that is less than the storage capacity needed in the unconstrained storage condition. The corresponding PV area is again found in the model run by the iteration process done by the “solver” described in section 4.1. The capacity of electrolyser is changed to the corresponding maximum available surplus power.

A number of different preset storage capacities are input for the model runs and the corresponding results are displayed in the relevant sections of the Result table. For solar-hydrogen systems meeting household loads, the present values of constrained storage capacity are typically varied from an initial storage size of 13 kg of hydrogen by steps down of 1 kg to a final value of 1 kg.

4.5.4 Unconstrained storage with limited capacity electrolyser

In unconstrained storage with limited electrolyser capacity, the condition is the same as for unconstrained storage in that the storage capacity accommodates all the hydrogen generated, but now the capacity of electrolyser is set below the maximum value of available surplus power. This lowers the capital cost of the electrsolyser employed and in turn lowers the required storage capacity. But these cost reductions are at the expense of the additional PV area that is required. Though it is not as energy efficient unconstrained storage the decrease in capital cost of electrolyser and storage may lead to lower unit costs of power. .

For solar-hydrogen systems examined in this study, it has been found that the capacity of the electrolyser may be varied from 2 kW down to 1.5 kW in steps of 0.1 kW. Below a certain minimum electrsolyser capacity it becomes impossible to meet the load continuously no matter what the PV area is.

4.5.5 Constrained storage with limited capacity electrolyser

The final condition is constraining both the storage capacity and the electrolyser capacity. There are again minimum capacities for both these components below which the system cannot meet the load continuously. But exploring capacities below the values found in unconstrained storage may yield lower unit costs of power, depending on the relative unit costs of PV panels, electrolysers and hydrogen storage assumed

	A	B	C	D	E	F	G	H	I	J	K
1	**COST EVALUATION**										
2	**Input Parameters**										
3	PV panel area required			A	18.15648292	m2					
4	Total load supplied by the PV for the entire			L_i	2563.120123	kWh					
5	Maximum value of surplus power			SP_i	1.839573916	kW					
6	Total suplus power for the whole year			ΣSP_i	737.7551317	kW					
7	Maximum value of load supplied by fuel cel			FCSUPPLYi	0.300364729	kW					
8	Total load supplied by the fuel cell for the w			ΣFCSUPPLY	859.8228648	kW					
9	Higher heating value of Hydrogen			HHV	3.55	kWh/m^3					
10	volume of tank size needed			Tmax	9.761455822	kg					
11	Maximum tank pressure			P_{tank}	2	bar					
12	System component	Relative cost of the component per unit size	Component characteristic size	Total cost (Ct	Discount rate (d)	Life time (n)	Capital recovery factor, CRFpv	Annual capital recovery amount	Operating and Maintenance cost	Annual cost	Unit cost of power generated
13		(USD)	(kW)	(USD)	(%)	(years)		(USD)	(USD)	(USD)	(USD)
14	Photovoltaic	5000	1.815648292	9078.24146	5	25	0.07095246	644.1235394	181.5648292	825.6883686	
15	Electrolyser	3000	1.839573916	5518.72175	5	20	0.08024259	442.8365111	110.374435	553.2109461	
16	Fuel cell	6000	0.300364729	1802.18837	5	15	0.09634229	173.6269504	36.04376743	209.6707179	
17	Balance of System cost.	6000	1	6000	5	25	0.07095246	425.7147438	120	545.7147438	
18	Storage Tank										
19		2000	13.70890098	27417.802	5	25	0.07095246	1945.360423	548.3560392	2493.716462	2.53538401
20		1750	13.70890098	23990.5767	5	25	0.07095246	1702.19037	479.8115343	2182.001904	2.36461567
21		1500	13.70890098	20563.3515	5	25	0.07095246	1459.020317	411.2670294	1870.287347	2.19384733
22		1250	13.70890098	17136.1262	5	25	0.07095246	1215.850264	342.7225245	1558.572789	2.02307898
23		1000	13.70890098	13708.901	5	25	0.07095246	972.6802114	274.1780196	1246.858231	1.85231064
24		750	13.70890098	10281.6757	5	25	0.07095246	729.5101586	205.6335147	935.1436733	1.68154229
25		500	13.70890098	6854.45049	5	25	0.07095246	486.3401057	137.0890098	623.4291155	1.51077395
26											

Table 19- Cost analysis -Worksheet 2

4.5 WORKSHEET 3 (RESULT TABLE)

Results obtained from the Worksheet 1 (Technical performance evaluation) and Worksheet 2 (Cost evaluation), are summarised in both tabulated as well as graphical forms in the worksheet 3 (Table 20-21). Worksheet 3 is activated with Visual Basic programming (macros connected) where a background program is connected as a macro in the upper right corner under the text as "Display Result". When the macro is run, it collects all the data from the previous two work sheets and displays the results in the uppermost section of the Result table. The data are then taken to the desired section of worksheet 3.

Alternatively these data obtained from the Worksheet 1 and Worksheet 2 can be manually copied and pasted at the desired location in the Worksheet 3.The various sections of Worksheet 3 are shown in Figures 38 and 39. The worksheet is divided into three different sections where logical steps are taken towards finding the lowest unit cost of power supply over the year. Initially all the results are displayed by the macro in a single row cell 5 for a specific set of readings. Then the results are copied and pasted in their respective places as defined in the header columns. In the result table the individual columns are dedicated to desired parameters for each set of readings.

Storage size is shown in the column A cell 3. At first the execution of the model is done for the unconstrained storage, where the storage size is determined by the difference in values between maximum and minimum level of storage limits in the storage tank in the whole year of operation (from column O cell 8807 in worksheet 1). For subsequent runs under the constrained storage condition, the storage size is preset to a lower value that has been provided to the model as an input parameter in worksheet 1.

The PV panel area in a particular run is cited in the column B cell 3 (obtained from column F cell 13 of Worksheet 1).

Maximum surplus power is displayed in column C cell 3. This is the surplus power that is available during peak solar insolation. It gives an indication about the maximum capacity of the PEM electrolyser that should be used to convert all of the excess solar radiation into useful energy storage in terms of hydrogen. If the capacity of the electrolyser is greater

than the maximum surplus power then, it will result in an increase in capital cost without having any impact on energy efficiency. The value of maximum surplus power is expressed in kW as the input insolations are provided on an hourly basis. The unit cost of energy supplied by the solar-hydrogen system is displayed in the columns D-to-J Cell 3 for their corresponding assumed unit storage costs.

	A	B	C	D	E	F	G	H	I	J	K
1					**RESULT TABLE**						
2											
3	Storage size fixed	Coresponding PV area	Maximum surplus power available	unit cost with a unit storage cost of US$2000/kg.	unit cost with a unit storage cost of US$1750/kg.	Unit cost with a unit storage cost of US$1500/kg	Unit cost with a unit storage cost of US$1250/kg	Unit cost with a unit storage cost of US$1000/kg	unit cost with a unit storage cost of US$750/kg.	unit cost with a unit storage cost of US$500/kg.	Display Results
4	(kg)	(m2)	(kwh)	(US$/Kw)	(US$/Kw)	(US$/Kw)	(US$/Kw)	(US$/Kw)	(US$/Kw)	(US$/Kw)	
5	13.4937723	18.3465479	1.860739891	2.4627361667	2.2946476275	2.1265590882	1.9584705490	1.7903820097	1.6222934705	1.4542049312	
6	**Constrained storage without limiting the electrolyser size (Electrolyser power rating = Maximum surplus available power).**										
7	Storage size fixed	Coresponding PV area	Maximum surplus power available	unit cost of power supply with a storage cost of US$2000/kg.	unit cost of power supply with a storage cost of US$1750/kg.	unit cost of power supply with a storage cost of US$1500/kg.	unit cost of power supply with a storage cost of US$1250/kg.	unit cost of power supply with a storage cost of US$1000/kg.	unit cost of power supply with a storage cost of US$750/kg.	unit cost of power supply with a storage cost of US$500/kg.	
8	(kg)	(m2)	(kwh)	(US$/Kw)	(US$/Kw)	(US$/Kw)	(US$/Kw)	(US$/Kw)	(US$/Kw)	(US$/Kw)	
9	13.494	18.347	1.861	2.522	2.354	2.186	2.018	1.850	1.682	1.514	
10	13	18.784	1.909	2.492	2.330	2.168	2.006	1.844	1.682	1.520	
11	12	19.681	2.009	2.431	2.282	2.132	1.983	1.833	1.684	1.534	
12	11	20.697	2.122	2.375	2.238	2.101	1.964	1.827	1.690	1.553	
13	10	21.759	2.241	2.322	2.197	2.072	1.948	1.823	1.699	1.574	
14	9	22.903	2.368	2.271	2.159	2.047	1.935	1.823	1.711	1.599	
15	8	24.097	2.501	2.223	2.124	2.024	1.924	1.825	1.725	1.626	
16	7	25.731	2.683	2.194	2.107	2.020	1.933	1.846	1.759	1.671	
17	6	27.396	2.868	2.167	2.092	2.017	1.943	1.868	1.793	1.718	
18	5	29.213	3.071	2.146	2.084	2.021	1.959	1.897	1.834	1.772	
19	4	31.043	3.275	2.125	2.075	2.026	1.976	1.926	1.876	1.826	
20	3	32.921	3.484	2.107	2.070	2.032	1.995	1.957	1.920	1.883	
21	2	35.962	3.822	2.139	2.114	2.089	2.064	2.039	2.014	1.989	
22	1	40.353	4.311	2.229	2.217	2.204	2.192	2.179	2.167	2.154	

Table 20- Results obtained for the constrained storage conditions. (Note; the result for unconstrained storage is mentioned at the first row for the constrained storage result).

	A	B	C	D	E	F	G	H	I	J
23	**Unconstrained storage with limiting the electrolyser size as input parameters. (Storage size = 13.4937723 Kg)**									
24	Electrolyser Power Rating	Coresponding PV area	Maximum surplus power available	unit cost of power supply with a storage cost of US$2000/kg.	unit cost of power supply with a storage cost of US$1750/kg.	unit cost of power supply with a storage cost of US$1500/kg.	unit cost of power supply with a storage cost of US$1250/kg.	unit cost of power supply with a storage cost of US$1000/kg.	unit cost of power supply with a storage cost of US$750/kg.	unit cost of power supply with a storage cost of US$500/kg.
25	(kW)	(m2)	(kwh)	(US$/Kw)	(US$/Kw)	(US$/Kw)	(US$/Kw)	(US$/Kw)	(US$/Kw)	(US$/Kw)
26	1.861	18.347	1.861	2.522	2.354	2.186	2.018	1.850	1.682	1.514
27	1.800	18.347	1.861	2.512	2.344	2.176	2.008	1.840	1.672	1.504
28	1.700	18.347	1.861	2.496	2.328	2.160	1.991	1.823	1.655	1.487
29	1.600	18.347	1.861	2.479	2.311	2.143	1.975	1.807	1.639	1.471
30	1.500	18.347	1.861	2.463	2.295	2.127	1.958	1.790	1.622	1.454
31	Any further reduction in electrolyser capacity will result in insufficient hydrogen production,which makes the system unable to become cylic in operation over a year.									
32	**Constrained storage with limiting the size of electrolyser to 1.5 kW**									
33	Storage size fixed	Coresponding PV area	Maximum surplus power available	unit cost with a fixed size of electrolyser of 1.5kw and storage cost of US$2000/kg.	unit cost with a fixed size of electrolyser of 1.5kw and storage cost of US$1750/kg.	Unit cost with a fixed elctrolyser of 1.5 kw and storage cost of US$1500/kg	Unit cost with a fixed elctrolyser of 1.5 kw and storage cost of US$1250/kg	Unit cost with a fixed elctrolyser of 1.5 kw and storage cost of US$1000/kg	unit cost with a fixed electrolyserof 1 kw and storage cost of US$750/kg.	unit cost with a fixed electrolyserof 1 kw and storage cost of US$500/kg.
34	(kg)	(m2)	(kwh)	(US$/Kw)	(US$/Kw)	(US$/Kw)	(US$/Kw)	(US$/Kw)	(US$/Kw)	(US$/Kw)
35	13.494	18.347	1.861	2.463	2.295	2.127	1.958	1.790	1.622	1.454
36	13	18.784	1.909	2.424	2.262	2.101	1.939	1.777	1.615	1.453
37	12	19.681	2.009	2.347	2.198	2.048	1.899	1.749	1.600	1.450
38	11	20.699	2.123	2.273	2.136	1.999	1.862	1.725	1.588	1.451
39	10	21.759	2.241	2.200	2.075	1.950	1.826	1.701	1.577	1.452
40	9	22.904	2.368	2.128	2.016	1.904	1.792	1.680	1.568	1.456
41	8	24.097	2.501	2.059	1.959	1.859	1.760	1.660	1.560	1.461
42	7	25.731	2.683	2.000	1.912	1.825	1.738	1.651	1.564	1.476
43	6	27.396	2.868	1.941	1.867	1.792	1.717	1.642	1.568	1.493
44	5	29.224	3.072	1.887	1.825	1.763	1.700	1.638	1.576	1.514
45	4	31.087	3.280	1.834	1.784	1.734	1.685	1.635	1.585	1.535
46	3	33.039	3.497	1.783	1.746	1.708	1.671	1.634	1.596	1.559
47	2	36.174	3.846	1.761	1.737	1.712	1.687	1.662	1.637	1.612
48	1	40.896	4.372	1.779	1.767	1.755	1.742	1.730	1.717	1.705

Table 21-Results obtained with limiting the value of electrolyser size for both constrained and unconstrained storage

5. APPLICATION OF MODEL TO A REMOTE HOUSEHOLD

5.1 CASE STUDY : STAND-ALONE POWER SUPPLY TO A REMOTE HOUSE HOLD

5.1.1 Introduction

This chapter presents an application of the model to a case study of electricity supply to a remote homestead in south-eastern Australia. All the major parameters such as electrical load requirement and solar radiation for the particular conditions are fed into the model. The model run is carried out for various conditions described in chapter 4 and their implications for unit cost of power generation are examined. For each condition the cost of power generation is evaluated by varying the assumed hydrogen storage cost while keeping the rest of the assumed unit costs fixed to typical values found in the literature. Hydrogen storage cost is specifically chosen as a variable parameter as it comprises a substantial portion of total system cost, i.e., up to 40 % in some cases (Andrews *et al.* 2005). The storage of hydrogen gas is assumed to be carried out in low-pressure and hence low-cost cylinders. A certain target value for unit storage cost is established as a guide for the discussion on developing low-cost storage systems in chapter 6.

Section 5.2 explains the details of both the input and output parameters for Worksheet 1 and Worksheet 2. Section 5.3 describes the results obtained from the model run.

5.1.2 Load profile for the remote household

In this case study, a daily average electrical power requirement of 5 kWh is assumed based on a conservative approach to overall electrical energy usage. The variation in hourly demand over a day is simulated according to a typical demand cycle obtained from the literature (Nelson *et al.* 2005) and adapted to the 5 kWh total daily demand. This particular profile was chosen considering the fact that household electricity demand normally has two peaks, in the morning and evening, while for the rest of the period maintaining a lower level. In other words, the load profile closely matches to a real scenario where such variations in load requirement are apparent. The hourly values for a daily load of 5 kWh are shown in Table 22 presented graphically in Figure 36. As a first approximation, the same daily load and hourly load profile are assumed for all days in the year. The model itself, however, can be used with any hourly load profile over a year, if such data are available.

Hour	Load (kWh)	Hour (Continued)	Load (kWh)
1	0.14	13	0.19
2	0.13	14	0.18
3	**0.13**	15	0.17
4	0.13	16	0.17
5	0.14	17	0.19
6	0.18	18	0.24
7	0.28	19	0.28
8	**0.30**	20	0.28
9	0.27	21	0.27
10	0.24	22	0.26
11	0.21	23	0.24
12	0.19	24	0.18

Table 22- Load profile provided as in input to the spread sheet model. (Note: The maximum and min load are shown in bold fonts).

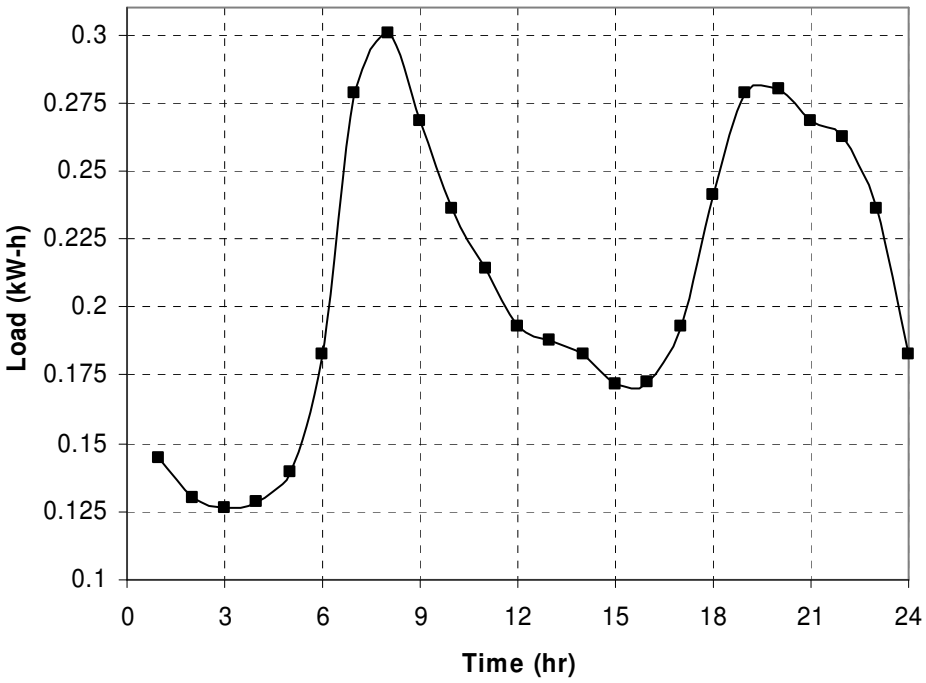

Figure 36- Daily average load assumed in the model. (Note: The peak of this load profile curve determines the max power rating of the fuel cell.

5.1.3 Hourly incident solar radiation

In this case study the location is assumed to be Melbourne 38 degrees south local latitude. The average half-hourly solar hourly radiation corresponding to the local latitude for Melbourne was obtained from Bureau of Meteorology, Australia (for the year 2002). These data were converted to hourly averages and provided as in input in the column C cells 42-8801.

5.1.4 PV panel efficiency

The PV panel efficiency is evaluated as the ratio of electrical energy out to the radiation incident on a horizontal surface. It is widely found in the literatures to be in the range of 12-15%. One of the major factor that affects the PV panel efficiency is the cell temperature. This decrease in PV panel efficiency is proportional to the difference between cell temperature and its reference temperature. From the experiments conducted in RMIT lab, the efficiency was found to be around 10%. So in the present model for the calculation purpose a conservative approach of 10% efficiency is employed for the PV panel. This assumption is consistent with real situation where even age factor has also negative impact on PV panel efficiency. However any suitable value according to the user's preference can be employed in the model.

5.1.5 Electrolyser capacity

The capacity of the electrolyser should ideally be rated high enough to accommodate all the excess surplus power available from the PV panel. As explained in section 4.3.3, the model is designed to accommodate any value between 0-10 kW. For this particular daily load requirement of 5 kWh, the required rated value of the electrolyser fluctuates within the range of 1-2 kW depending upon the storage – electrolyser capacity condition being examined (section 4).

5.1.6 Fuel cell capacity

The fuel cell capacity is determined by the peak load requirement. For this particular case study with an average daily load requirement of 5 kWh along with a load usage pattern described earlier (Figure 41), the peak demand load is 0.3 kWh per hour. Hence a fuel cell capacity of 0.3 kW is used in this case study. This is an idealised assumption in that no sharp peaks in demand are assumed above the hourly average maximum demand. In addition no allowance is made for an excess capacity to allow the contingencies such as an unexpected large loads and variation in peak load from year to year.

5.1.7 Cost Factors

The capital cost for each of the solar hydrogen components are assumed based on the values accepted in the literatures. The unit cost of all the system components are shown in Table .The PV panel costs is found to be US$ 5000/kW where as the PEM electrolyser being US$ 3000/kW. Both the fuel cell and balance of system which includes inverter and auxiliary equipments are assumed as US$ 6000. The hydrogen storage cost is assumed to be varying from US$2000/kg down to our target cost of US$ 500.

Components	**Unit Cost**
	US$/kW
Photovoltaic	5000
Electrolyser	3000
Fuel cell	6000
Balance of System cost.	6000
Storage Tank	2000-to-500/kg of H_2

Table 23- Unit costs of system components.

The life period of PV panel and hydrogen storage are 25 years while that of PEM electrolyser is taken as 20 years and fuel cell of 15 years (Andrews *et al*. 2005).

5.2 MODEL OUTPUT

5.2.1 Unconstrained storage

The first condition to be employed is unconstrained storage. All the excess surplus power from the PV panel is used for the generation of hydrogen. The storage capacity is kept unconstrained, thereby obtaining the minimum size of photovoltaic area that will be needed to fulfill the total demand requirements over successive years. Any further reduction in the size of PV area would prevent the system meeting the demand requirement, as the amount of stored hydrogen becomes negative. The size of hydrogen storage tank corresponding to the size of PV area is the optimum value with respect to the energy efficiency of the overall system, since all of the surplus power available from the PV panel is completely used by the electrolyser to produce hydrogen. The electrolyser capacity is just enough to accept the available maximum surplus power. The principal model outputs for the unconstrained storage condition are given in Table 24.

Parameters	Model Output	Location in the Model	
		Column	Cell
PV area	18.34 m^2	P	3
Hydrogen Storage	13.1 kg	F	4
Initial Start-up hydrogen required	6.5 kg	P	4
Cumulative Load Supplied	1825 kWh	P	6
Load Supplied by the PV panel	779.4 kWh	P	7
Load supplied by the Fuel cell	1045.6 kWh	P	8

Table 24: The principal model outputs for the unconstrained storage condition

The PV panel area was initially assumed to be 20 m^2 at the beginning of the model run. The execution of model run leads the solver to iterate this PV panel area to obtain the desired result. For the present scenario of unconstrained storage, the model run yields a value of 18.34 m^2 of PV panel size. This is shown in cell 3 column P.

The hydrogen storage capacity was initially taken as a trial value of 10 kg. This can be any random value and is provided just to feed the model prior to the execution of the model run. The model run corrects this to the desired result that satisfies all the conditions. For the present scenario of unconstrained conditions with a 5 kWh load requirements, the model gives a result for hydrogen storage capacity of 13.1 kg. This value is shown in cell 4 column F.

Once all the basic input parameters are fed in, the model run is performed using the computational procedure explained in chapter 4 (section 4.3.8). The solutions provided by the solver are accepted. The level of hydrogen during winter, when it reaches the nadir, is selected as an equivalent to the initial start-up hydrogen that needs to be provided to avoid the level of hydrogen from becoming a non-negative quantity. Also the level of hydrogen at the end of the year will become equal to that at the start of the year if this value is employed. The initial mass of hydrogen (shown in Column F cell 3) is about 6.95 kg for this particular case study of 5 kWh daily requirements and the start of operation being 1st January. The profile of hydrogen storage for the complete year is shown in Figure 37. The sinusoidal curve shows that there is a substantial amount of hydrogen storage between summer to winter is taking place. During the hotter days of March-April the level of hydrogen present in the storage tank reaches its maximum capacity. The storage tank becomes almost empty during the September-October period, after the extended period over winter when solar radiation is low and heavy reliance on stored hydrogen and the fuel cell must be made.

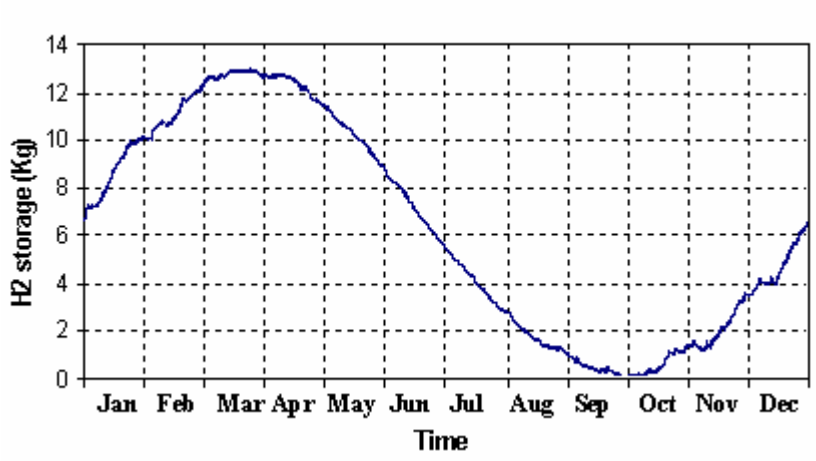

Figure 37- Hydrogen storage profile for unconstrained storage condition.

Cumulative load for the entire year is the summation of all the hourly electrical demand of the household for the entire year. In this case study an average daily load of 5 kWh is assumed, which yields a cumulative load of 1825 kWh. This value clearly has a critical influence in the evaluation of unit cost of power.

The total load directly supplied by the panel is 779.4.5 kWh (shown in column E cell 6). This value indicates the actual power that is directly met by the PV panels. Greater the amount of this value less will be the hour for which the fuel cell is required to run. This value is a function of input parameters such as solar radiation and PV panel area. Rest of the excess PV panel output is used to generate hydrogen.

The load supplied by the fuel cell is 1045.6 kWh (shown in column C cell 7). It indicates the total amount of load, including those hours of partial power supply in conjunction with PV or completely by the fuel cell alone, fed by stored hydrogen via fuel cell. Hence an overall 42% of the annual load is met by the PV array and rest 58 % by using hydrogen from storage in the fuel cell (Note: Load is not uniform hence these % variations are different from ratio between insolation hours and non-insolation hours).

Under the unconstrained storage condition, the unit cost of power supplied by the solar-hydrogen system varies from $1.43/kWh for a unit storage cost of $500/kg of hydrogen to $2.42/kWh for a unit storage cost of $2000/kg. The unit cost of power versus unit storage cost is plotted corresponding to the unconstrained storage conditions in Figure 38.

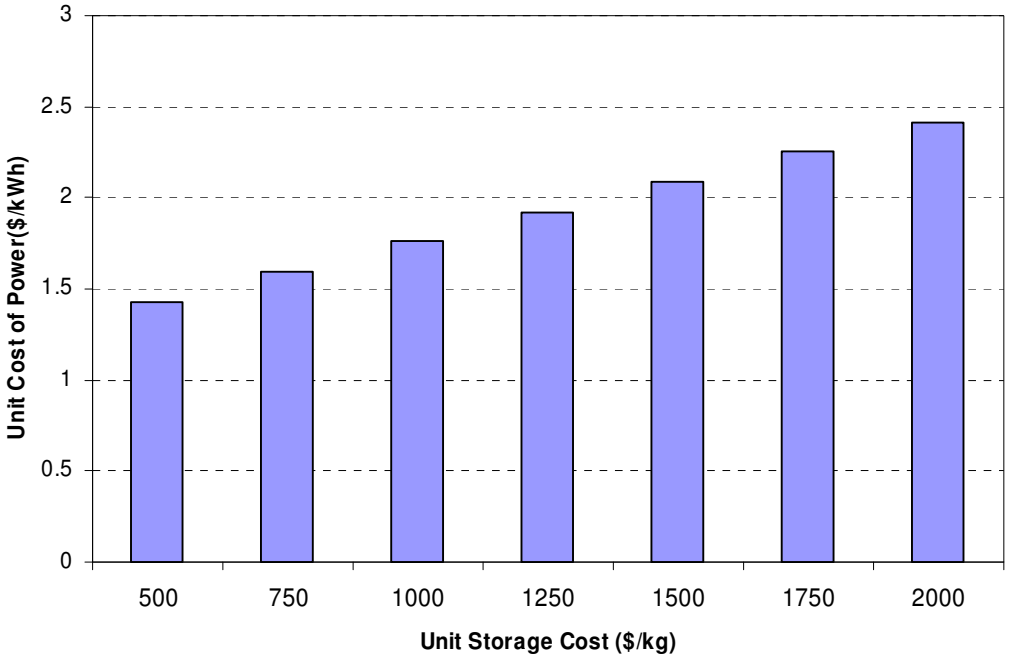

Figure 38-Unit cost of power as function of unit storage cost.

5.2.2 Constrained Storage

The objective in constraining the hydrogen storage capacity of the system is to seek a balance between PV panel cost and the total storage cost that yields a lower unit cost of power than the normal unconstrained storage conditions. Since storage capacity is lowered a relatively larger PV panel area is required to fulfill the demand and replenish the amount of hydrogen in storage after a draw down during periods of low solar insolation. The net effect on unit costs of power depends on the relative capital costs of the PV panel and the hydrogen storage required.

The results from the model for the required PV area with variation of the preset storage capacity are shown in Figure 39. It is clear that, at the lower end of the constrained storage range, a sharp rise in PV area is required. This is due to the fact that there is a greater need to provide power directly to the load rather than by drawing on hydrogen and using the fuel cell. The curve becomes even steeper if the storage size is reduced further down from the 1 kg size limit. From the model it was found that if containment is down further down to 0.1 kg, no amount of increment in PV panel size however large it may be wont be able to meet the demand.

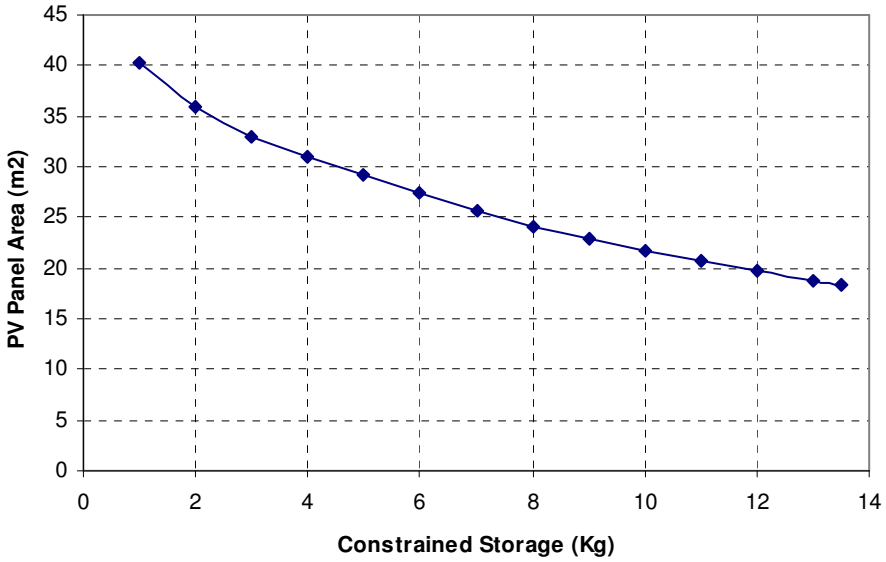

Figure 39-PV panel area as a function of Constrained Storage

As the capacity of electrolyser is not limited the entire excess surplus power is utilised to produce hydrogen. The higher capacity of electrolyser to utilise the excess power leads to an increase in capital cost of electrolyser. The constraining of storage was carried out by lowering the storage capacity by 1 kg in each set of model runs. The actual hydrogen storage profile for each of these conditions is plotted in Figure 40. For the constrained storage condition, storage size versus maximum surplus power is plotted in Figure 41.

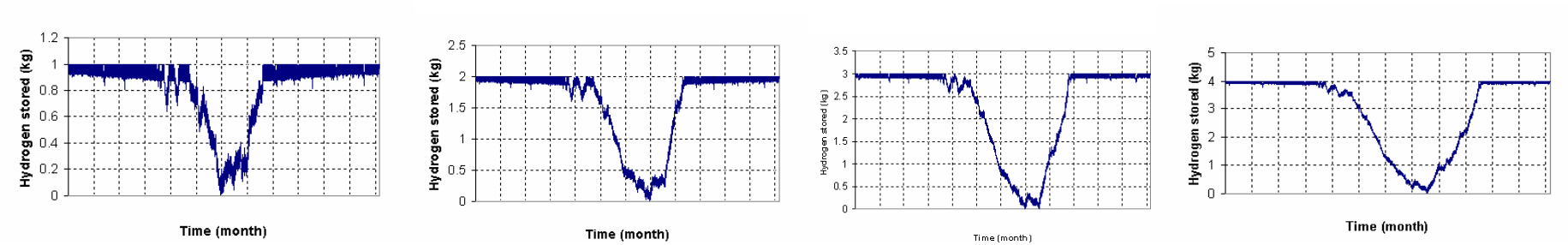

a. 1 kg b. 2 kg c. 3 kg d. 4 kg

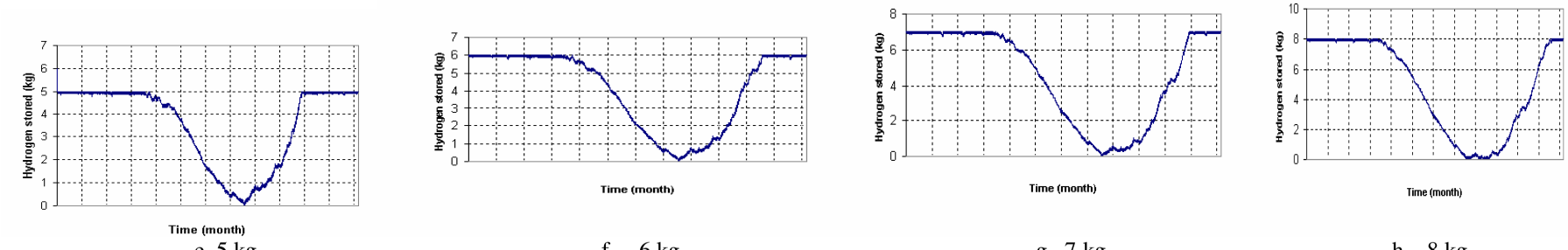

e. 5 kg f. 6 kg g. 7 kg h. 8 kg

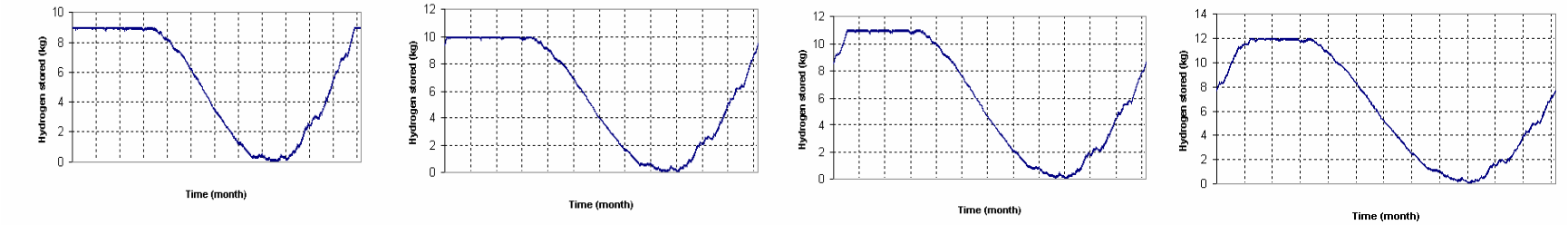

i. 9 kg j. 10 kg k. 11 kg l. 12 kg

Figure 40- Hydrogen storage profile obtained from the model corresponding to various constrained storage conditions

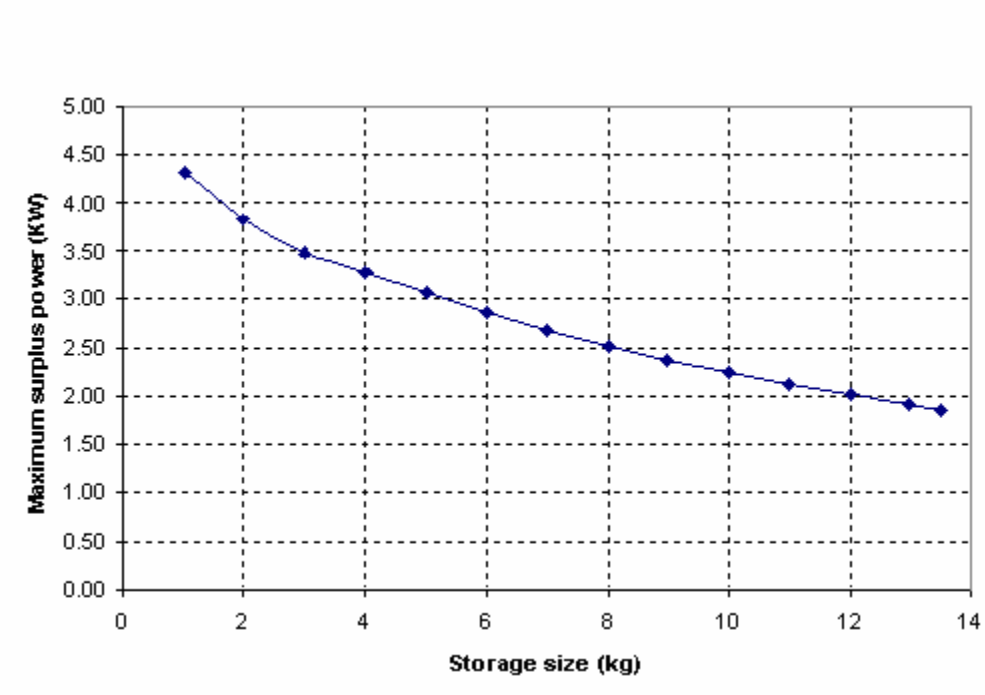

Figure 41 -Maximum surplus power as a function of Storage size.

The hydrogen storage profile for a constrained storage of 3 kg preset value is shown in Figure 42. From the graph it is evident that for most of the year the level of hydrogen stays near its full capacity. The thickness of the plotted line, reflecting short-term minor fluctuations in storage level, corresponds to the daily hydrogen requirement that is easily replenished by the larger PV panel almost on a daily basis. In winter, however, there is a relatively rapid draw down on the hydrogen stored until the lowest point is reached over July and August when the winter insolation is at a minimum. In fact the effective storage of hydrogen occurs just for the few months, that is, from June to September. The seasonal storage of energy is thus very much more restricted than in the unconstrained storage condition.

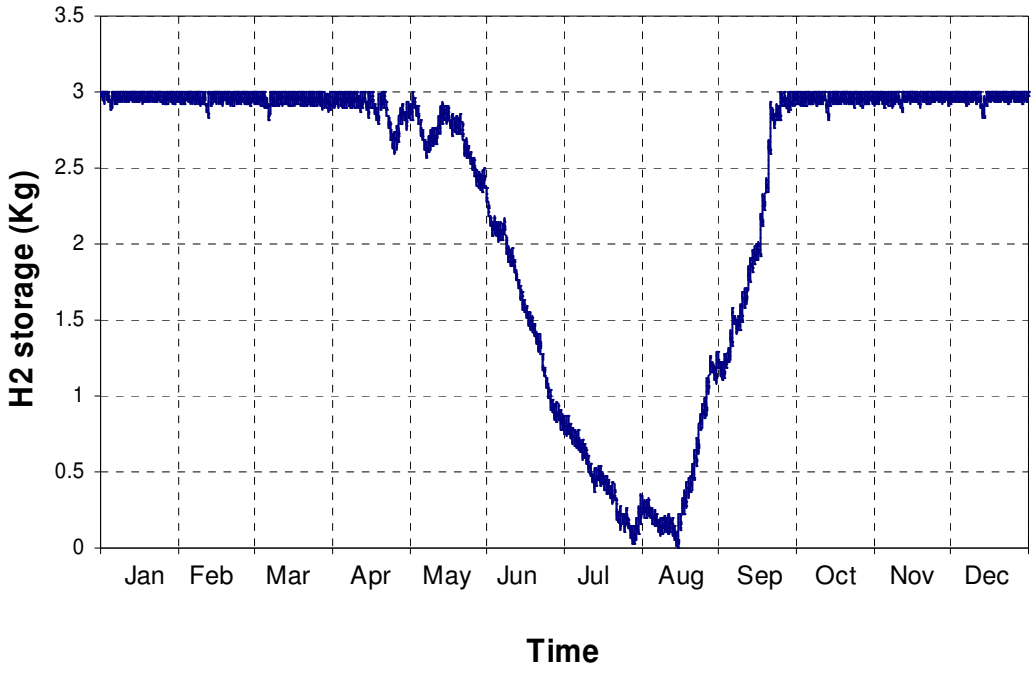

Figure 42- Hydrogen storage profile for a constrained storage of 3 kg storage capacity.

The model outputs for the unit cost power against the constrained storage preset value for a series of different unit storage cost are plotted in Figure 42. Unit storage costs ranging from US$ 2000/kg to US$ 500/kg are assumed. The graph shows the trend of economically optimal points – that is, the points where the unit costs of power attain their minimum value for that particular preset value. The location of the economic optimum shifts towards higher preset storage capacities, and eventually the unconstrained condition, with the decrease in unit storage cost. From the graph it is observed that an economic minimum is attained at a storage size of 3 kg for a unit storage cost of US$ 2000/kg. On the other hand for a unit storage cost of US$ 500, the economic optimum is attained at the storage size of 13.2 kg, which is the unconstrained storage capacity. As the unit storage cost decreases, the optimum system employs an increasing amount of season-to-season energy storage.

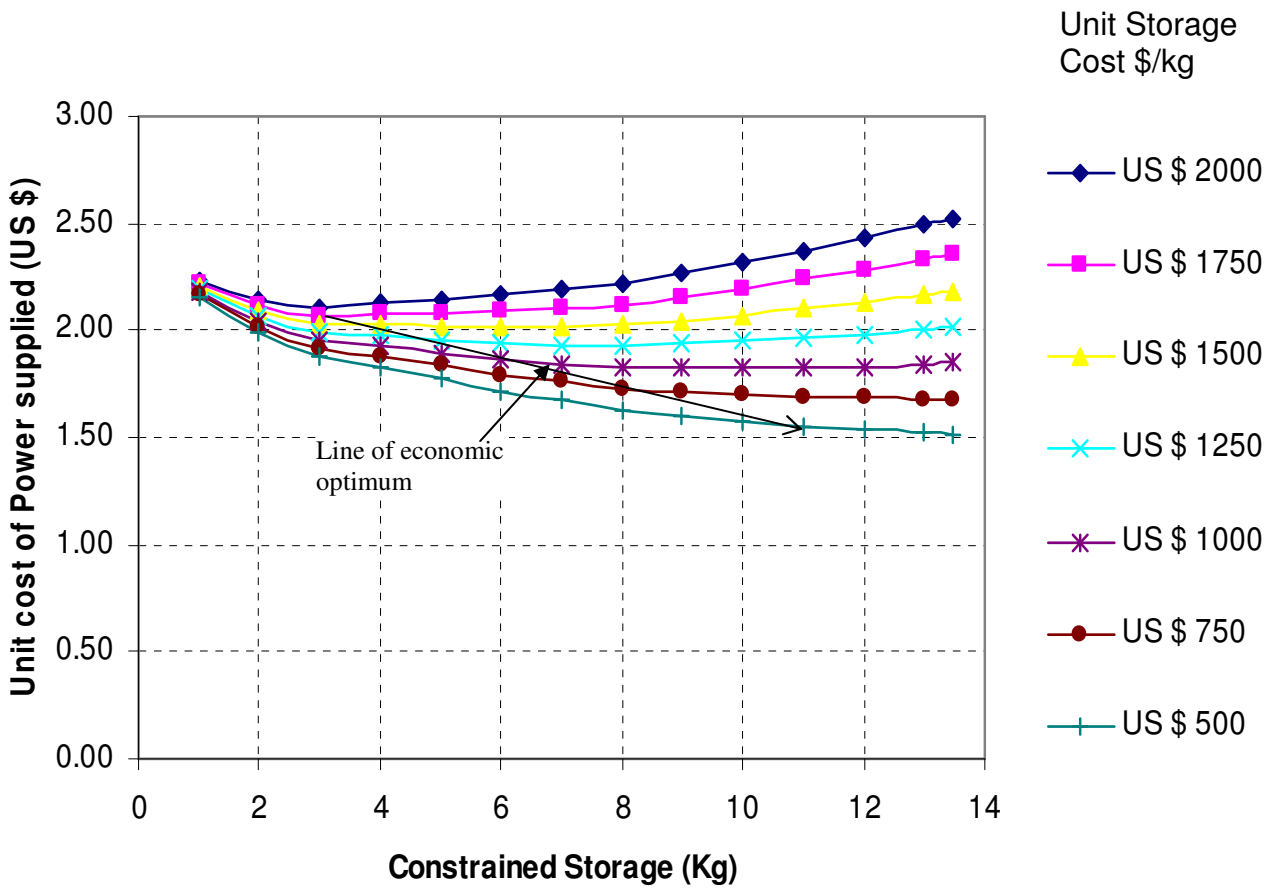

Figure 43-Unit cost of power as function of constrained storage capacity for various unit costs of storage.

The economically optimal unit cost of power is plotted against the unit storage cost in Figure 43. The decline in unit cost of power as the storage cost is reduced is due to the fact that increasing storage capacities become economically beneficial leading to more season-to-season storage, and hence a lower required PV area hence PV cost. This effect is more evident as the lowest assumed storage cost of US $500 is approached. Minimum unit cost of power as a function of unit storage cost, where the constrained storage capacity is set to its economically optimal value is plotted in Figure 44.

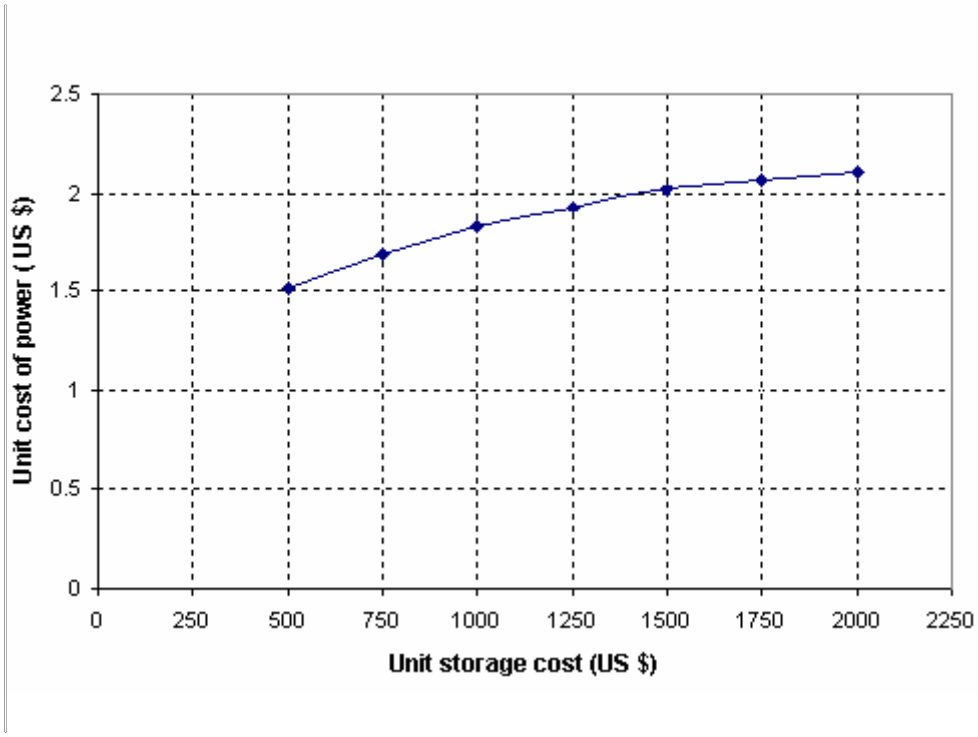

Figure 44- Minimum unit cost of power as a function of unit storage cost, where the constrained storage capacity is set to its economically optimal value.

5.2.3 Unconstrained storage with limited electrolyser capacity

In the previous conditions the rating of the electrolyser has been set high to accept the maximum surplus power available, so that all of the excess PV power over load can be converted to hydrogen. Though this is an efficient process from an energy utilisation point of view, yet from the model runs it is found that smaller electrolyser capacities can still enable the system to meet the load for the whole year while giving a lower unit cost. This is due to the fact that the stated maximum surplus power of 1.7 kW is available only for very few days, and for most days the surplus power available is less than 1.35 kW. Hence by limiting the electrolyser to 1.35 kW instead of the previous 1.7 kW, a marginally lower unit cost of power is obtained, with the rest of the input parameters in the unconstrained storage condition being kept constant.

The unit cost of power for unconstrained storage with limited electrolyser capacity is thus plotted for a series of unit storage costs in Figure 45.

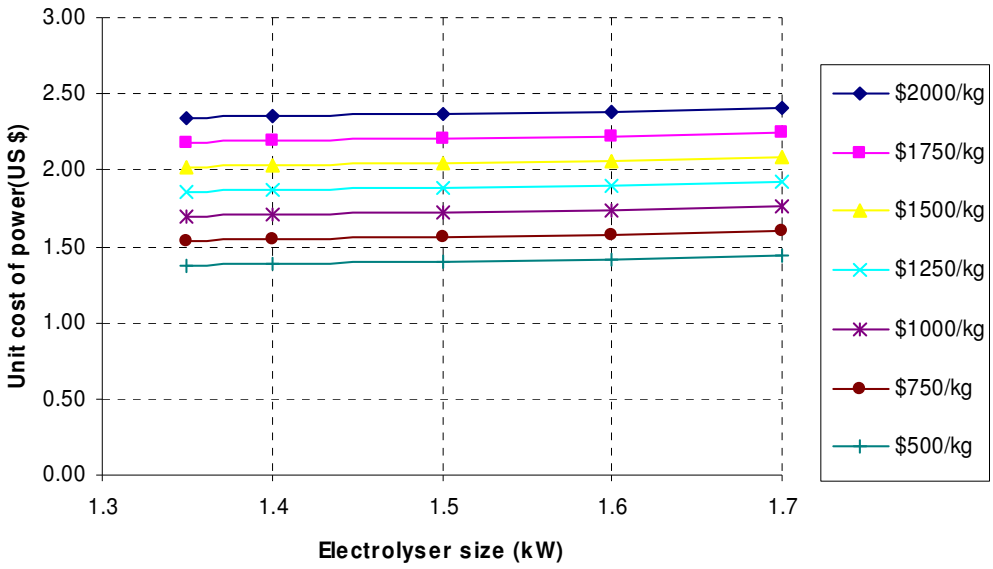

Figure 45-Unit cost of power as a function of Electrolyser power.

The slightly inclined nature of each graph shows a small but uniform overall lowering of unit cost of power is obtained as the capacity of the electrolyser is lowered. From the result table of Worksheet 3 it is also found that any further reduction in electrolyser capacity fails to make the operation cyclic for a complete year, and is thus not an acceptable solution.

5.2.4 Constrained storage with limited electrolyser capacity

Constrained storage conditions along with a limited electrolyser capacity offer a further lowering of unit cost of power compared to no electrolyser capacity limitation being employed. Since in case of constrained storage in which the storage capacity is further lowered, the required PV area increases, so does the excess surplus power. On an average day a larger PV panel area is able to provide substantial power even at low levels of solar insolation (early morning and later afternoon hours), whereas around noon when insolation is high, excess power from the panel is often not utilised as the hydrogen storage is likely to be full. This limited capacity of storage can be filled easily with a lower-capacity electrolyser without hampering the desired performance, but of course there will be changes to the storage profile.

Graph of PV area versus Storage for constrained storage with limited capacity of electrolyser is shown in Figure 52.

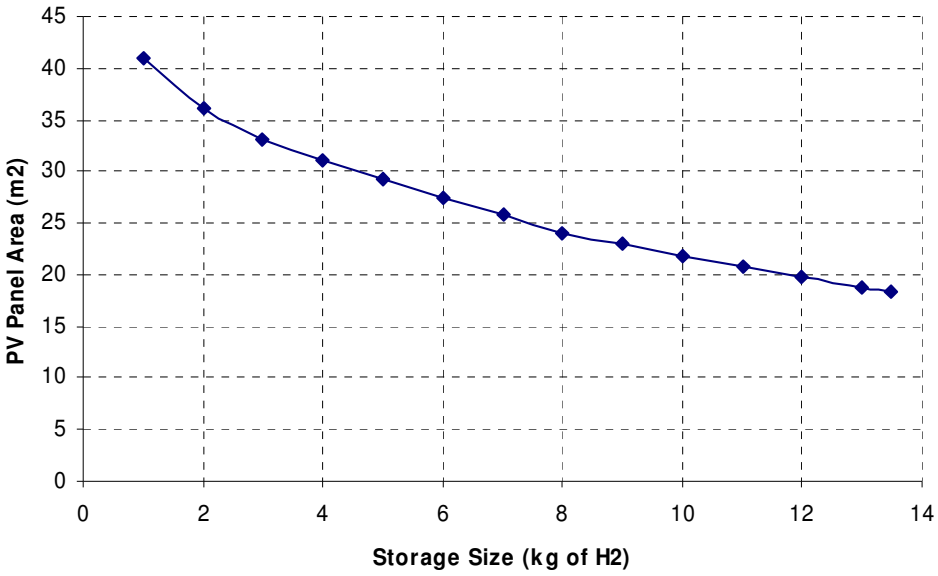

Figure 46- PV area versus Storage size

The identical nature of the curve for PV panel area for both cases i.e. for a fixed 1.5 kW electrolyser (Figure 46) and electrolyser capacity equal to maximum surplus power (Figure 41) shows the fact that at constrained storage vis a vis higher PV panel area doesn't necessarily yields the equivalent greater production of hydrogen from electrolyser as limited storage restricts the hydrogen generation. As the electrolyser capacity is confined to 1.35 kW, at lower range of constrained storage 1kg, the sharp rise in surplus power 4.5kW shows that a large amount of energy coming out of panel is left unused by the electrolyser. This should be avoided from an energy utilisation point of view, yet the overall reduction in unit cost of power due to a lower net storage cost, proves to be more advantageous economically.

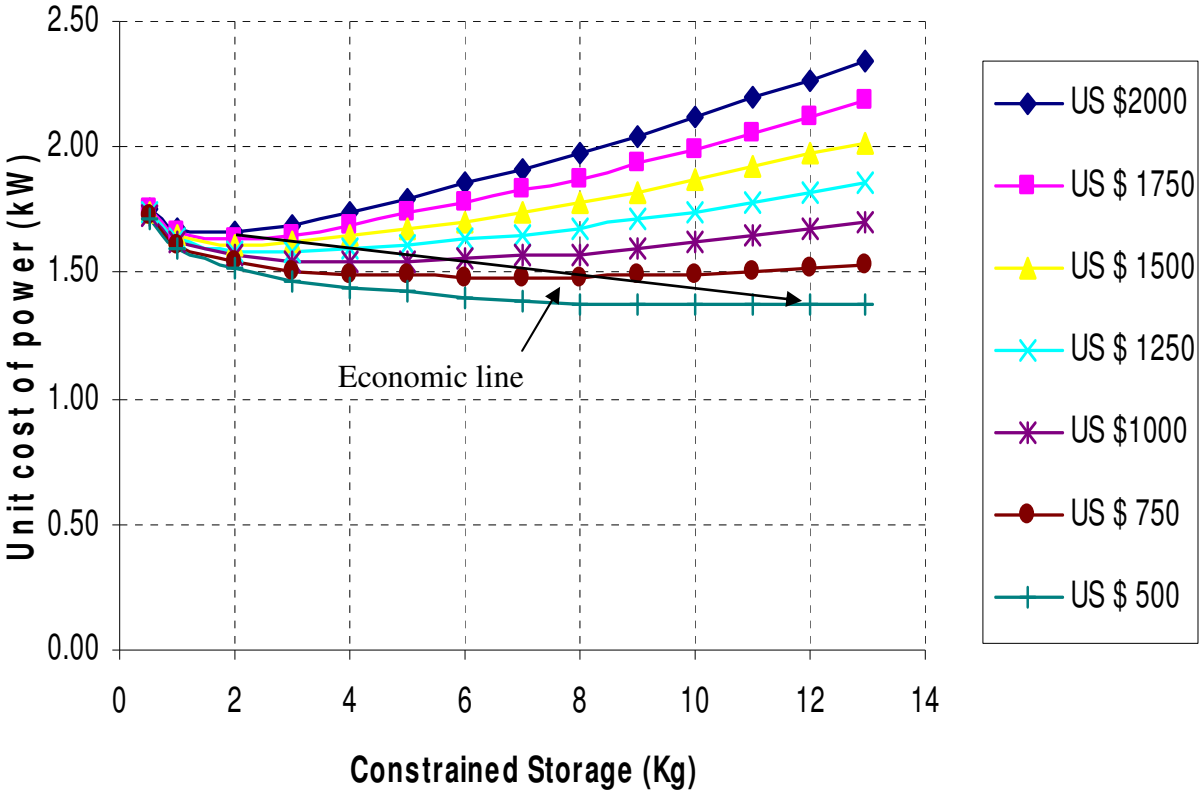

Figure 47-Unit Cost of Power against Constrained Storage (kg) with a limited electrolyser size of 1.35 kW

The variation of unit cost of power with constrained storage size for a limited electrolyser capacity of 1.35 kW and a range of unit storage costs is shown in Figure 47. The economically optimal condition is attained at a storage size of 2 kg for unit storage of US $ 2000, while it is at 12 kg for a unit storage cost of US $ 500. At 12 kg storage the unit cost of power becomes a minimum of US $ 1.45/ kWh. For the intermediate storage range of 8 kg with a unit storage cost of US$ 750/kg, the economic optimum unit cost of power becomes US$ 1.56/kWh. So in order to reach the economically optimum condition constrainment of storage along with an electrolyser capacity limited to 1.35 kW is considered the most viable option.

5.3 CONCLUSION

In this case study of electricity supply to a remote household in south-eastern Australia, the simulation model of a solar-hydrogen system that has been developed in this project has been used to estimate the sizes of system components such as PV area, hydrogen storage capacity and fuel cell capacity, and then find the specifications of the system that yields the lowest unit cost of power.

In the unconstrained storage condition, a PV area of 18.3 m^2 is required and a storage capacity of 13.1 kg of hydrogen. A substantial amount of hydrogen storage between from summer to winter takes place. 42% of the annual load is met by the PV array and 58% by using hydrogen from storage in the fuel cell. The unit cost of power supplied varies from $1.43/kWh for a unit storage cost of $500/kg of hydrogen to $2.42/kWh at $2000/kg.

In constrained storage, the required PV area rises sharply as the preset storage capacity is lowered, since there is a greater need to provide power directly to the load rather than by drawing on hydrogen from storage and using the fuel cell.

The analysis here has shown that, on the basis of the present capital costs of the main components of a solar-hydrogen RAPS system, a hydrogen storage system with very low losses that has a capital cost of US$ 500/kg of hydrogen or less will be needed to make seasonal energy storage attractive and hence obtain the lowest overall unit cost of energy supplied.

6. LOW-COST HYDROGEN STORAGE OPTIONS

6.1 EVALUATION CRITERIA

The storage options investigated for hydrogen storage at relatively low pressure, especially those pressure ranges achievable using a PEM electrolyser itself as the compressor, are worth investigating for RAPS applications in the drive to achieve lowest-cost storage solutions. Low-pressure storage thus permits hydrogen gas from an electrolyser to be transferred directly to the storage vessel without the need of an external compressor and its associated parasitic electrical power consumption. Shapiro has found that the use of PEM electrolysers directly for hydrogen compression has a significant net energy advantage over use of a separate electrically-driven compressor (Aurora & Duffy 2005). The analysis in the previous chapter indicates that, if the cost of storage can be cut to US $500/kg, season-to-season storage becomes feasible and unit power costs in the order of US$ 1/kWh for stand-alone solar-hydrogen RAPS systems can be achieved.

The various technological options for storing the hydrogen can be compared using a range of criteria. The primary criteria that will be used in the present chapter to evaluate the options most suitable for RAPS are the following:

- mass and volumetric energy densities;
- loss rates through mechanical leaks, diffusion through and permeation of the container walls, and through water (in the case of the water displacement method)
- safety; and
- costs per unit mass of hydrogen stored.

6.2 ENERGY DENSITY AND VOLUME REQUIREMENTS

Hydrogen is the most abundant element of the universe and constitutes 91% of our solar system by mass. It is also the second most abundant element in the sea and the ninth most abundant element in the earth's crust (Tzimas *et al.* 2003). Hydrogen has a very low density both in gaseous and liquid form. As a gas, its density is 0.089 kg/m^3 at STP conditions – that is, 7% of the density of air – and in liquid state (at -252.7° C and 100 kPa pressure), 70.8 kg/m^3, only 7% of the density of water (Tzimas *et al.* 2003).

The density of gaseous hydrogen at elevated pressure and varying temperature can be estimated from Van der Waals equation:

$$\left(P + n^2 \frac{\alpha}{V^2}\right)\left(\frac{V}{n} - \beta\right) = RT \qquad \text{Eq.6.1}$$

where P, V, T and R represent pressure, volume, temperature and the universal gas constant (8.314 kJ/kmol.K) respectively, and n is the number of moles present. The constants α and β are empirically determined. For hydrogen the values of α = 0.0244 Pa (m^3)^2 mole^{-2} and β = 0.0266 x10^{-3} m^3 mol^{-1} respectively are normally used (Tzimas *et al.* 2003). Alternatively the deviation of hydrogen gas from an ideal gas can be accommodated by introducing a 'compressibility factor' Z into the ideal gas equation. The corresponding equation of state is then:

$$PV = nZRT \qquad \text{Eq.6.2}$$

Where the compressibility factor Z can be determined experimentally. Z depends on the temperature and pressure of the hydrogen.

The volume ratio of gaseous hydrogen at 25°C and liquid hydrogen at -252.7 °C for a given mass at ambient pressure (101.325 kPa) is 848; and at 25° C the volume ratio of hydrogen at 1 bar and compressed hydrogen at 700 bar is 440. The variation of hydrogen

density as a function of pressure using the various approximations to the equation of state is shown in Figure 48.

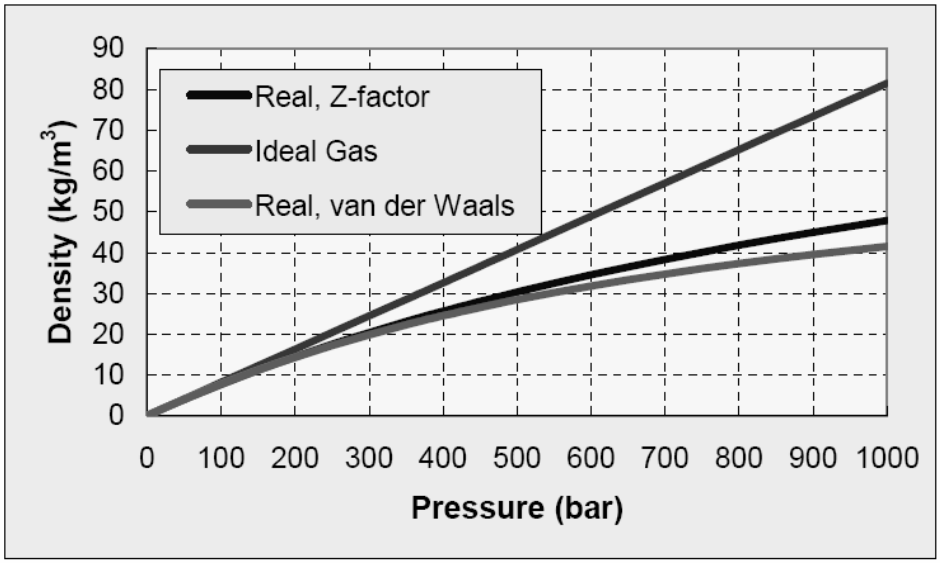

Figure 48 – Pressure versus density of hydrogen gas at ambient temperature of 25° C using various approximations to the equation of state (Source Tzimas *et al.* 2003).

To evaluate the performance of hydrogen storage systems, a number of quantitative metrics are useful. Firstly there is the mass energy density or gravimetric energy density, which is the energy per unit mass (e.g. in MJ/kg) of hydrogen. The gravimetric energy density of hydrogen depends only on its temperature and phase of the product water, and is otherwise independent of the characteristics of the storage system. The higher heating value (HHV), also commonly known as gross calorific value of a fuel, is defined as the total amount of energy (heat) released by the combustion of its unit mass (initially at 25°C) while the formation of product water is in liquid state (Larminie and Dicks 2003)

When hydrogen is reacted with oxygen to form water vapour at 298.15 K or 25° C, the reaction and corresponding heats of formation are as follows (Larminie and Dicks 2003):

$H_{2\,(g)} + ½\ O_{2\,(g)} \longleftrightarrow H_2O_{\,(g)} \qquad \Delta H_{298.15\,K} = -241.826\ kJ/\ mol$ --------Eq (6.3)

$H_{2\,(g)} + ½\ O_{2\,(g)} \longleftrightarrow H_2O_{\,(l)} \qquad \Delta H_{298.15\ K} = -285.830\ kJ/\ mol$ --------Eq (6.4)

The heat of formation is higher when the reaction product is in liquid water rather than water vapor since the latent heat of vaporisation is recovered as the water condenses from vapour to liquid. The lower heating value (LHV) of hydrogen, corresponding to reaction product in the form of water vapor, is 241.826 kJ/mol, while the higher heating value (HHV), corresponding to formation of liquid water, is higher at 285.830 kJ/mol.

The mass energy densities of hydrogen at 25° C are 119.716 MJ/kg (LHV) and 141.500 MJ/kg (HHV), that is, the energy density per mole divided by the molecular mass (2x 10^{-3} kg) (Tzimas *et al.* 2003),. Generally the HHV of hydrogen is evaluated at 25°C or 20°C under normal atmospheric conditions, at 15°C (standard conditions according to the International Organisation for Standardisation (ISO) or at 0°C (standard condition according to International Union of Pure and Applied Chemistry IUPAC) (Tzimas *et al.* 2003). The product of density (kg/m^3) and energy density by mass (MJ/kg) of hydrogen results in volumetric energy density. The variation of the volumetric energy density of hydrogen with pressure at a constant temperature of 25° C is shown in Figure 49. It is evident that within practically-achievable pressure ranges the volumetric energy density of gaseous hydrogen cannot exceed the volumetric energy density of liquid hydrogen.

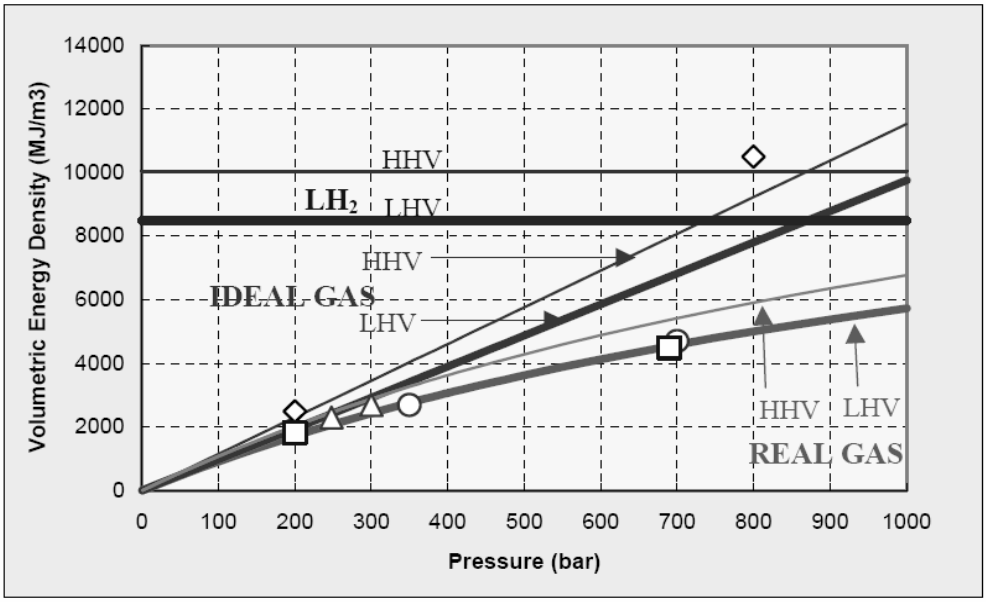

Figure 49 – Volumetric energy density of gaseous and liquid hydrogen as a function of pressure. The continuous lines corresponds to calculated values whereas the points refer to measured values (Tzimas *et al.* 2003)

Hydrogen has the highest mass energy density of all the fuels, that is, almost three times that of gasoline. The mass energy density of hydrogen is compared with other hydrocarbon fuels in Figure 50 (Thomas and James 1998). On the other hand hydrogen has the lowest values of volumetric energy density compared to other hydrocarbon fuels. The value of volumetric energy density of hydrogen in comparison to other hydrocarbon fuels is shown in Figure 51. The deviation in properties of hydrogen from ideal gas behavior increases at pressures above 100 bar, that is, the compressibility factor, plays a dominant role (Figure 49).

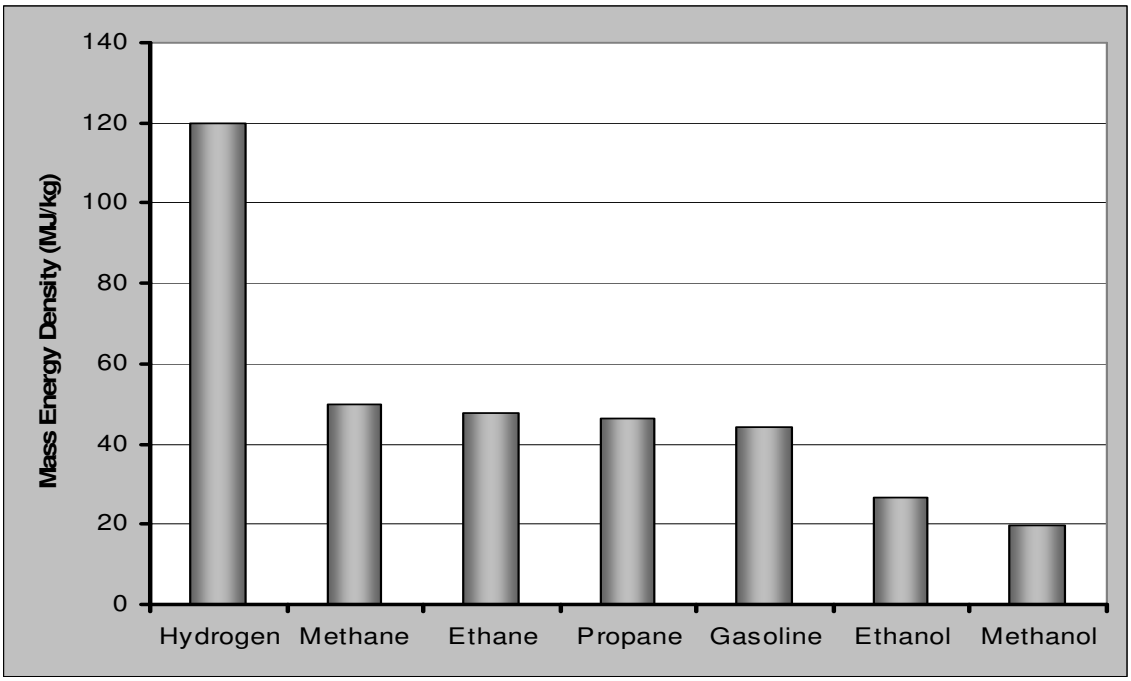

Figure 50 – Mass energy density of hydrogen compared to other hydrocarbon fuels. (Thomas and Ramon 2000)

Since volume constraints for hydrogen storage systems are generally more relaxed in RAPS applications compared to vehicles, relatively large volume and hence low pressure hydrogen storage may often be accommodated. Relatively low-pressure high-volume hydrogen storage systems may therefore have substantial economical advantages over purpose-built high-pressure hydrogen storage system in these applications (Ali and Andrews 2005)

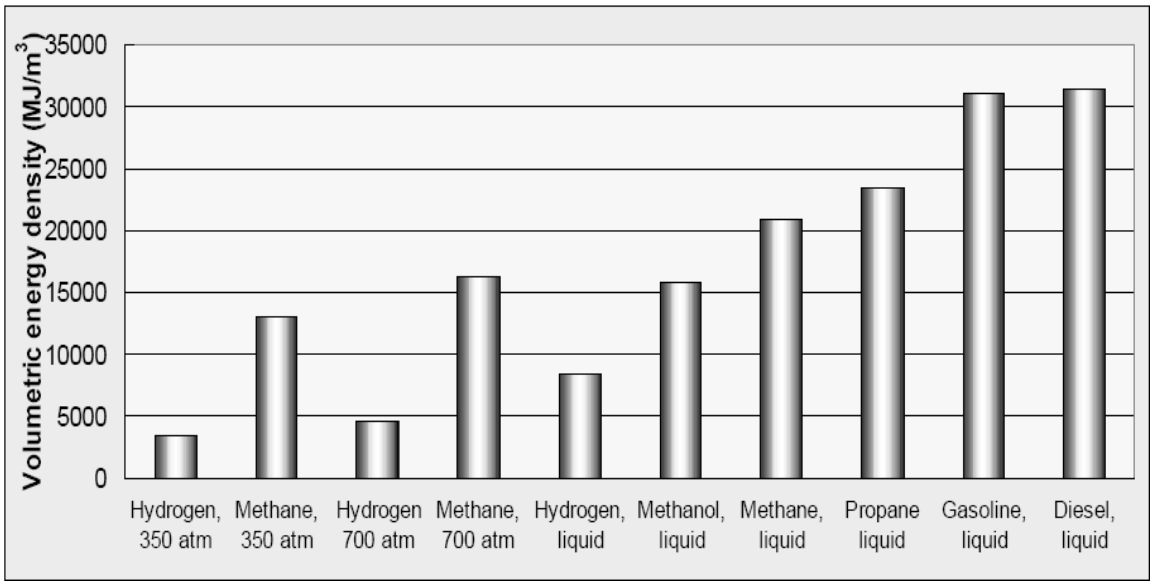

Figure 51 – Volumetric energy density of hydrogen compared to other hydro carbon fuels. (Tzimas *et al.*2003)

6.3 LOSS PROCESSES IN HYDROGEN GAS STORAGES

6.3.1 Types of Loss Process

Efficient storage of hydrogen is characterised by minimal losses present in the system. Gaseous hydrogen with its small molecular size has a great tendency to escape at joints or valves, and even through the walls of the cylinder.

The storage options considered in this study are analysed for various possible losses that might allow the escape of stored hydrogen. Such losses could be due to mechanical leaks or hydrogen permeation of the walls of the storage cylinder. There is also the possibility of hydrogen loss through absorption in and desorption from the water used in the storage system in the case of a water displacement storage system.

6.3.2 Mechanical Leaks

The mechanical leakages at valves, joints or other physical passage in the container can be detected by conventional leak detection mechanisms for gases. Great care must be taken to minimise leaks at joints between materials, fittings, valves or pipe connections, as will be

seen later. Measures that can be taken include both hydrostatic and pneumatic leak testing, as were discussed in relation to the design of acrylic and plastic tank hydrogen storage vessels in chapter 3 (section 3.3.3).

6.3.3 Diffusion through polymers

Diffusion of hydrogen gas is defined as the flux of hydrogen particles through a specimen. The usual units of this flux are thus mols/ m^2 /s, or kg/ m^2 /s. The nature of this flux varies depending on whether there is any chemical reaction between the hydrogen and the material of the medium or not (Shelby 1996). Physical diffusion refers to the diffusion of gas that does not chemically interact with the material of the wall. This is the case for hydrogen diffusion through polymers, in which the relatively open molecular structures enhance the prospects of the comparatively small hydrogen molecules to move through the material. Physical diffusion can be treated as a "random walk" of atoms or molecules through the interstices of the network across the wall material (Shelby 1996).

The diffusion of small molecules into the specimen is a function of both the material of specimen and the diffusant. Factors that affect the process of diffusion include:

- Molecular size and physical state of the diffusant
- Morphology of the specimen material
- Solubility limit of the solute with in the specimen
- Volatility of the solute
- Interfacial energies of the monolayer films (Crank 1968).

Fick's first law of diffusion is that: "The process of diffusion in isotropic substances through unit area of a section is proportional to the concentration gradient measured normal to the section" (Crank 1968), or

$$J = - D(\Delta C/\Delta x) \quad \text{----------} \quad \text{(Eq 6.5)}$$

where J is the mass flux (mol/m^2)/s, D is the diffusivity, a measure of the readiness with which the diffusion process takes place, and ΔC (mols/m^3) the difference in concentration of the diffusant across a section of material of thickness Δx (m).

When hydrogen gas is introduced into a container, some hydrogen diffuses into the walls and the concentration of hydrogen in the wall material builds up. A solid polymer, for example, has a tendency to absorb gaseous hydrogen. The solubility of gaseous hydrogen dissolved in the solid polymer is generally expressed by Henry's law, which states that: "The amount of gas which dissolves in a specified volume of a liquid/solid at constant temperature is almost directly proportional to the partial pressure of that gas in the gas phase" (Shelby 1996). That is:

$H_{dissolved} = S \times P$ ---------- (Eq. 6.6)

Where $H_{dissolved}$ = the amount of hydrogen that is dissolved (in mols/m^3 or mols/cm^3)

S = solubility coefficient (in mols/m^3, kPa or mols/cm^3.atm)

P = partial pressure of gas above the solvent surface (stored hydrogen)

At present not much work or experimental for values of solubility for hydrogen in acrylic material is reported in the literature (Benson *et al*. 2004). A typical value of solubility of hydrogen in vitreous silica is 0.94×10^{17} molecules/cm^3-atm, or 0.150 mols/m^3-kPa. For calculation purposes, hydrogen solubility in an acrylic polymer will be assumed here to be the same as that in vitreous silica. The local concentration of the hydrogen gas is determined by the solubility and partial pressure of the gas in the surrounding atmosphere.

As the diffusion of hydrogen into the walls of a polymer container proceeds, the concentration of hydrogen in the material increases, but there remains a decrease in concentration with distance into the wall material from the inner wall. As the concentration of hydrogen builds up in the wall near the outer surface, hydrogen begins to escape through the wall into the surrounding atmosphere. It is the migration of hydrogen molecules right through the wall of the container to the outside environment that is termed as permeation.

The flow rate of hydrogen through the walls once steady-state flow is attained is determined by the permeability of the wall material to hydrogen. Stefan and Exner in 1870 (Shelby 1996) demonstrated that the permeability of a membrane (that is, the flux transmitted per unit pressure gradient) is proportional to the product of the solubility coefficient (S) and Fick's diffusion coefficient (D), that is:

$$\mathcal{P} = D \times S \qquad \text{Eq.6.7}$$

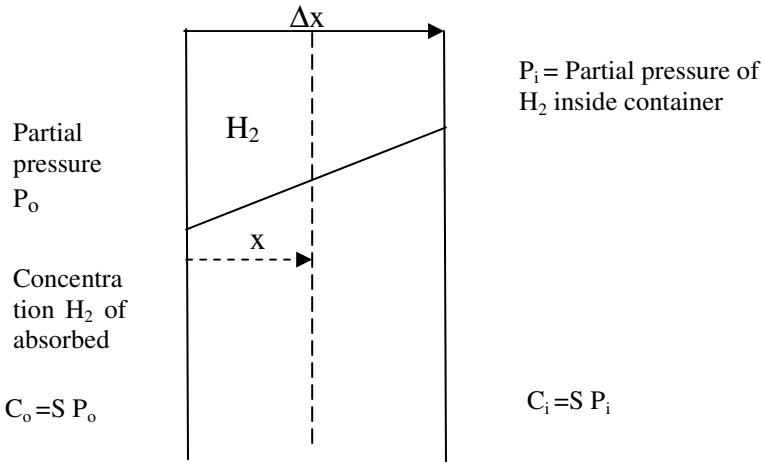

Figure 52 – Schematic diagram of permeation process

A simple derivation of this relationship is as follows (Benson *et al.* 2004). On the assumption of a linear fall in concentration of hydrogen across the wall, the local concentration gradient at all points, $dc/dx = \Delta C/\Delta x = (Ci - C_0)/\Delta x$, is constant (Figure 52).

From Fick's law of diffusion (Eq 6.5):

$J(x) = - D (dC/dx) = - D (C_i - C_o)/\Delta x$

But $C_0 = S P_0$ and $Ci = S P_i$

$J(x) = - D.S. (Pi-P_o)/\Delta x$

$= - DS (\Delta P/\Delta x)$

Permeability $\mathcal{P}$ is defined as follows (Shelby 1996):

$J= - \mathcal{P} (\Delta p/\Delta x)$

$\therefore \mathcal{P} = DS$ Eq 6.8

The permeability $\mathcal{P}$ is generally expressed in the units

$$\frac{cm^3(STP)\times cm}{cm^2\times \sec\times cm.of.Hg} \text{ or } \frac{kg\times m}{m^2\times \sec\times kPa}.$$

In summary then, the flux of hydrogen atoms or molecules through the material, and hence the time necessary to reach the steady state flow, is determined by the diffusion coefficient D. The solubility S refers to the dissolved gas concentration per unit applied pressure. While permeability determines the net flow of gas molecules right through the material after the steady state is attained.

Benson (2004) stated that the values of hydrogen permeability for acrylic plastic are not available in the literature but can be approximated using other gas–polymer interactions: "The lack of data could mean that hydrogen is not soluble in PMMA, as there is a wide variety of data on gas permeability in PMMA for other gasses. For most polymers, though, the permeability for hydrogen is about three times the permeability for oxygen when neither interacts with the film" (Benson *et al.* 2004). On this basis, the permeability of hydrogen across acrylic is assumed in the calculations conducted here to be:

$$\mathcal{P} = 3\times10^{-11}\ \frac{cm^3(STP)\times cm}{cm^2\times \sec\times cm.of.Hg}$$

$$= 1.8754\times10^{-16}\ \frac{kg\times m}{m^2\times \sec\times kPa}$$

The analysis in this subsection will be used later in this chapter (subsection 6.5.1.2) to obtain a theoretical estimate of the loss of hydrogen through the walls and endplates of the acrylic and fibre reinforced plastic vessels used to store hydrogen in the experimental solar-hydrogen systems constructed and tested as part of this project.

6.3.4 Diffusion through metals

Diffusion of hydrogen through metals occurs readily. But unlike in polymers, the process of hydrogen diffusion in metals is chemical in nature, as the diffusion usually requires dissociation of hydrogen molecules at the surface of the metal. It is the hydrogen atoms that penetrate the metal wall rather than the hydrogen molecules. Most of the metals are almost impermeable to the inert gases. It is hydrogen alone that diffuses rapidly through most metals through a dissociation or chemical diffusion process (Shelby 1996).

So the solubility of hydrogen in metals is best described not by Henry's law, but instead by Sievert's Law, for chemical diffusion, namely:

$$C = SP^{1/2} \quad \text{----------} \quad (4)$$

where C is the concentration of the dissolved gas hydrogen, S is the solubility and P is the gas pressure (Shelby 1996). At low pressures, the square root of pressure term tends towards the Henry's Law of solubility ($H_{dissolved} = S \times P$) (Shelby 1996). At very low pressures, the rate of dissociation becomes so slow that the overall movement of hydrogen gas across the wall is not controlled by the actual diffusion but by the dissociation process itself. At high temperatures, dissociation occurs with in a gaseous phase without the involvement of metal surface. Also sometimes formation of metal-oxide and metal hydride films at the surface affects the diffusion process (Shelby 1996).

6.4 SAFETY ANALYSIS

6.4.1 Flammability

Like all other fuels, hydrogen is an energetic material that possesses fire and explosion risks. In a closed chamber if hydrogen is exposed to air, a potentially explosive flammable mixture is formed. If the burning of hydrogen is constrained, the resulting rise in temperature and pressure can lead to an explosion. Compared to gasoline, hydrogen has a greater tendency to detonate but this effect is insignificant in open spaces.

Since hydrogen is colourless and odourless, it is difficult to detect a hydrogen leakage. In some cases – for example, a collision in an open space – a hydrogen-powered vehicle poses less of a hazard than a traditional gasoline-powered vehicle due to the reduced risk of a flammable fuel leak. This is due to the fact that the light hydrogen gas molecules rapidly disperse in to the atmosphere unlike conventional gasoline which spills over and hence causes greater hazardous situation.

Prevention and control of accidental formation of flammable hydrogen-air mixtures, particularly in storage systems, are necessary for the safe operation of solar-hydrogen systems. A concentration of hydrogen in air between 4% (lower flammability limit) to 75% (upper flammability limit) forms a potentially dangerous flammable mixture (Alcock *et al.*

2001). For the safety of operating plant and equipment adequate understanding of the overpressures generated in an accidental situation is essential. The safe handling and use of hydrogen requires an acknowledgement of its physical properties in each of the forms in which it is stored, that is, as a low to medium pressure gas for the solar-hydrogen systems investigated in the present project.

Under certain circumstances hydrogen proves to be safer than conventional fuels, but in other circumstances it is more dangerous. A comparison according to specific conditions and the same criteria is needed for a meaningful assessment. Cadwallader and Herring (1999) qualitatively analysed and compared the properties of hydrogen to those of methane and propane. From their experiments, they came to the conclusion that hydrogen is less dangerous than propane while being more dangerous than methane. They concluded that:

- in confined spaces hydrogen was quickest to form a flammable mixture and that it has the lowest ignition energy
- in vented spaces it resulted in virtually no flammable mixtures whereas methane gave a small flammable mixture and propane formed a large flammable mixture (Cadwallader and Herring 1999).

However, this assessment is not the sole criteria of the aforementioned conclusion as there exist other particular situations where a higher leak frequency may be observed for hydrogen compared to other gases. In relatively-congested areas ignition of a flammable mixture of hydrogen may lead to generation of significantly higher over-pressures, hence the risk of detonation may become higher than for either methane or propane.

A general comparison of fuel hazards purely on the basis of relative energy contents of the fuels is given by DTI (1997). This approach also has its limitations since hydrogen with less amount of energy content per unit volume than methane can cause a more damaging impact under conditions leading to detonation, while methane may not detonate at all in such circumstances.

Hydrogen has much wider flammable limits in air compared to methane, propane or gasoline, with the minimum ignition energy being about an order of magnitude less than the other fuels (Alcock *et al.* 2001), as shown in Table 25.

	Hydrogen	Methane	Propane	Gasoline
Flammability limits (vol. % in air) Lower limit (LFL) Upper limit (UFL)	 4 75	 5.3 15	 2.1 9.5	 1 7.8
Minimum ignition energy (mJ)	0.02	0.29	0.26	0.24

Table 25- Comparison of Flammability limits against other fuels (Alcock *et al.* 2001)

The broad flammability range of hydrogen is in principle a disadvantage in relation to the potential risks associated with it. But there is only a minor difference between the lower flammable limits of hydrogen and methane whereas those for propane and gasoline are even lower. The lower flammable limits (LFL) are of particular importance in accidental circumstances when ignition sources with sufficient energy content are often present to ignite a fuel-air mixture. In case of low momentum release the dispersion characteristics of hydrogen makes less formation of a flammable mixture less likely compared to other fuels. Furthermore the LFL of 4% is valid for upward propagating flames while an actual flammable limit of 9-10% is observed for downward propagating flames (Alcock *et al.* 2001). In case of methane, the difference between LFLs for upward and downward propagating flames is found to be less i.e. 5.3 % versus 5.6% by volume (Table 25). As far as lower ignition energy is concerned, a minimum level of the stoichiometric composition 29% by volume is needed.. But at the LFL the ignition energy for hydrogen is of same order of methane. Almost all of the accidental ignition sources – such as unprotected flames, electrostatic sparks, or spark from striking objects – contain more energy than the lower ignition energy of hydrogen, methane, propane or gasoline.

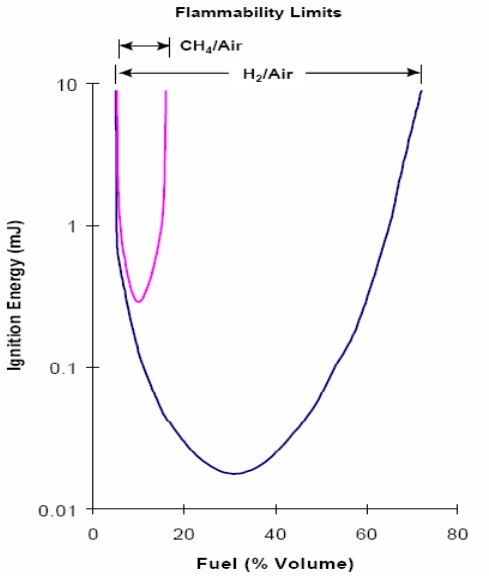

Figure 53-Ignition energy V/S Fuel % Volume (Alcock *et al.* 2001).

Another important factor is the minimum auto-ignition temperature (Alcock *et al* 2001). Hydrogen has a higher auto-ignition temperature than methane, propane or gasoline (Figure 53). But this auto-ignition temperature depends on the nature of the heat surface. The minimum value of auto-ignition temperature for hydrogen is observed if a heated glass vessel is used. In case of heated air or nichrome wire, however, methane, propane have higher auto-ignition temperatures than hydrogen.

	Hydrogen	Methane	Propane	Gasoline
Autoignition Temperatures (°C)				
Minimum	585	540	487	228-471
Heated air jet (0.4 cm diameter)	670	1220	885	1040
Nichrome wire	750	1220	1050	

Table 26- Comparison of auto-ignition temperature (Alcock *et al.* 2001).

From the above facts, it can be concluded that in the event of spill, gaseous hydrogen will form a flammable mixture in air more rapidly than methane due to its higher buoyancy. But this very rapid mixing also leads to quick dispersal of hydrogen, resulting in a much shorter duration of the flammable mixture. Despite having a relatively higher upper flammable limit, the much higher buoyancy of hydrogen in air brings the mixture down to a limit below the lower flammable limit very quickly.

6.4.2 Hydrogen combustion

Hydrogen-based flames with their lower radiant heat and no soot formation are different in their effects from hydrocarbon-based flames. . Hydrogen flames have a higher flame temperature, and are invisible since there is no smoke and the combustion product is water vapour. The heat from the hydrogen flames is emitted in narrow infra-red bands, mainly from water vapour and carbon dioxide (Alcock *et al* 2001). Also most of the radiated heat is normally absorbed by the surrounding atmospheric water vapour and carbon dioxide. The adiabatic flame temperature of hydrogen is higher than methane, propane but less than gasoline (Table 27).

	Hydrogen	Methane	Propane	Gasoline
Adiabatic Flame Temperature in Air (K)	2318	2158	2198	2470
% Thermal Energy Radiated from Flame to Surroundings*	5 to 10	10 to 33	10 to 50	10 to 50

Table 27- Comparison of adiabatic flame temperature and thermal energy radiation of hydrogen and hydrocarbon fuel flames (Alcock *et al.* 2001)

If the propagation of a flame is obstructed by a narrow critical passage, it extinguishes because of heat transfer and/or free radical loss becoming enough to prevent flame propagation. The largest gap that can prevent the flame propagation is called quenching gap. This quenching gap is a function of gas composition, temperature, and pressure and passage geometry (Alcock *et. al* 2001). Hydrogen-induced flames have a very small quenching gap compared to other fuels. The design of flashback arrestors to prevent flame propagation in a pipe back from an application is principally based on this quenching gap measurement. Under NTP conditions, the quenching gap for hydrogen induced flame is 0.6mm compared to 2 mm for methane, propane and gasoline (Alcock *et. al* 2001), that is, a tighter design requirement for gaseous hydrogen systems.

Detonation pressure rise (20:1) of hydrogen gas is less likely than a deflagration explosion pressure rise (8:1) as the minimum ignition energy required for detonation is high (in the

10 kJ range), the minimum concentration of the detonable limit is higher, and the detonable range is narrower than its flammable range (Table 28) (Alcock *et. al* 2001).

	Hydrogen	Methane	Propane	Gasoline
Detonability limits (vol. % in air)				
Lower limit (LDL)	11-18	6.3	3.1	1.1
Upper limit (UDL)	59	13.5	7	3.3
Maximum burning velocity (m/s)	3.46	0.43	0.47	
Concentration at maximum (vol. %)	42.5	10.2	4.3	
Burning velocity at stoichiometric (m/s)	2.37	0.42	0.46	0.42
Concentration at stoichiometric (vol. %)	29.5	9.5	4.1	1.8

Table 28 – Comparison of detonation limit (Alcock *et al.* 2001)

In open-air conditions detonation of flammable hydrogen mixture is less likely to occur than with the other fuels because a higher-energy ignition source is required and a much greater mixture limit of 18% mass is needed as opposed to 4% mass. The storage options mentioned in this thesis i.e. low pressure hydrogen storage in plastic tank or medium pressure (up to 20 bar) storage in composite or metallic cylinder have their own safety considerations specially the potential source of ignition in an otherwise electrical circuit surrounding the solar hydrogen system.

6.4.3 Tendency to Leak

Hydrogen has a relatively greater tendency to leak from a containment vessel and associated piping than other gaseous fuels. The flow parameters, relative leak rates on both volumetric and energy basis are shown in Table 29 (Alcock *et al.* 2001). The diffusion coefficient of hydrogen in air at NTP is much higher (0.61 cm^2/s) as compared to methane (0.16 cm^2/s) or propane (0.12 cm^2/s). The ratio of specific heat of hydrogen at NTP is 1.308 where for methane and propane it is 1.383 and 1.14 respectively. On a volumetric basis for diffusion in subsonic flow, the relative leak rates of methane and propane as compared to hydrogen are 0.26 and 0.20 and for laminar flow it is 0.77 and 1.11 respectively while for turbulent flow the relative leak rate ratio becomes 0.35 and 0.21 respectively. Similarly at sonic flow the relative leak rates become 0.34 and 0.20 respectively.

On the other hand on an energy basis the relative leak rates for subsonic diffusion of methane and propane as compared to hydrogen becomes 0.87 and 1.63. For laminar flow, as compared to hydrogen the relative leak rates are 2.66 for methane and a much higher value of 9.38 for propane while that for turbulent flow conditions it is 1.18 for methane and 1.80 for propane. For sonic flow the relative leak ratio between methane and hydrogen is 1.14 and between propane and hydrogen is 1.63.

	Hydrogen, H_2	Methane, CH_4	Propane, C_3H_8
Flow Parameters:			
Diffusion coefficient in air at NTP[a] (cm^2/s)	0.61	0.16	0.12
Viscosity at NTP ($g/cm\text{-}s \times 10^{-5}$)	89	11.7	80
Density at NTP (kg/m^3)	0.0838	0.6512	1.870
Ratio of specific heats, Cp/Cv at NTP	1.308	1.383	1.14
Relative leak rates (volumetric):			
Subsonic flow			
Diffusion	1	0.26	0.20
Laminar Flow	1	0.77	1.11
Turbulent Flow	1	0.35	0.21
Sonic flow	1	0.34	0.20
Relative leak rates (energy basis[b]):			
Subsonic flow			
Diffusion	1	0.87	1.63
Laminar Flow	1	2.66	9.38
Turbulent Flow	1	1.18	1.80
Sonic flow	1	1.14	1.63

Table 29- Comparison of Flow rates for hydrogen (Alcock *et al*. 2001)

6.4.4 Hydrogen embrittlement

If high strength steels are exposed to hydrogen for elongated duration, the mechanical properties of the material deteriorate due to the phenomena called embrittlement. Otherwise ductile steel thus becomes brittle in nature after prolonged exposure to hydrogen and hence a hydrogen storage vessel made from such a material has increased risks over time of developing fractures. Proper selection of material is essential to avoid these risks. Low carbon steel with a Brinell hardness of less than 200 is generally recommended for steel cylinders used to store compressed hydrogen (Pyle 1997).

6.4.5 Dispersion

Hydrogen when released disperses more rapidly into the atmosphere than methane, propane or gasoline due to the fact that it is more buoyant and diffusive in nature (Alcock *et. al* 2001). This is a positive factor for the safety of gaseous hydrogen systems.

But in the case of release of cryogenic liquid hydrogen, the vapour cloud initially formed is heavier than the surrounding air. At low concentrations the density of hydrogen-air mixture is similar to that of air hence the buoyancy effect becomes insignificant. Also for high momentum release buoyancy becomes less effective as the direction of release becomes the determining factor on the direction of formation of cloud.

6.5 STORAGE OPTIONS INVESTIGATED

6.5.1 Acrylic cylinder

6.5.1.1 System design and features

The design and construction of a hydrogen-storage system in the present study using acrylic cylinders for laboratory-scale experiments is explained in section 3.3.3. The pressure of the hydrogen stored is atmospheric pressure plus the head pressure due to the difference in water levels in the two cylinders. Since atmospheric pressure is equivalent to about a 10 m head of water and the height of the cylinders is only 0.5 m, this system stores hydrogen at only just over atmospheric pressure. Importantly atmospheric pressure also acts on the outside surfaces of the lower storage cylinder so the pressure difference the vessel has to withstand is only the head due to the difference in water levels. This type of arrangement provides a self regulating, reliable and safe mechanism for hydrogen storage on the scale required in many laboratory experiments. The total cost of an 8 litre storage system of this kind including piping and valves is approximately $AU 160 (almost $US 120).

In this section the theoretical hydrogen loss rate as a result of permeation of the walls of the container, and through the water of the storage system, will be estimated and then compared with experimental measurements of the actual loss rate.

6.5.1.2 Mass and volumetric energy densities

The hydrogen that is stored in acrylic cylinder is just above atmospheric pressure. The density of hydrogen stored is 0.09 kg/m^3. The volumetric energy density of hydrogen is 12.7 MJ/m^3. The mass energy density of hydrogen is 142 MJ/kg. The weight of acrylic cylinder is 450 gm. The volume of hydrogen stored is 9.7x 10^{-3} m^3. The cylinder at STP will hold 0.8 gm of hydrogen. Hence a gravimetric energy density of hydrogen based on HHV for the acrylic tank will be of 0.227 MJ/kg of storage system. Of course this amount is just for small laboratory purposes.

6.5.1.3 Theoretical Evaluation of hydrogen Loss

The diffusion of hydrogen molecules through the acrylic material can be estimated theoretically as follows. Since the top end-plate of the lower gas storage cylinder has a different thickness to the cylinder wall, losses across this end plate occur at a different rate. Also the bottom-end plate is not in direct contact with stored hydrogen as a layer of water is always present. Hence hydrogen cannot escape through the bottom plate.

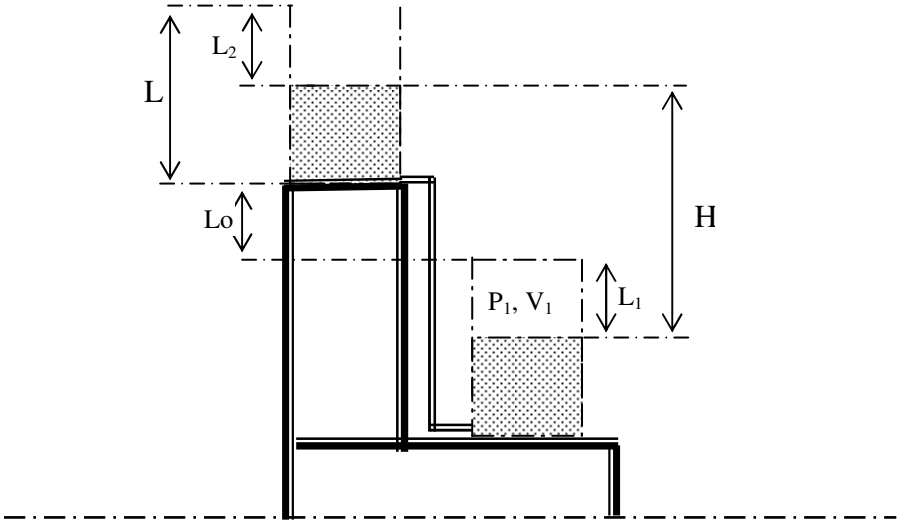

Figure 54 – Level of water column in the cylinders

The dimensions of the acrylic storage cylinder are internal radius r = 75 mm; height h = 550 mm; wall thickness t = 3 mm; and end-plate thickness, T = 5 mm (Figure 54). The total surface area exposed to hydrogen diffusion can be divided into two parts, namely:

- the side surface area, $A_{side} = 2\pi rho = 2 \times 3.14 \times 0.075 \times 0.55 = 0.259\ m^2$
- and the top-end surface area, $A_{top} = \pi r^2 = 3.14 \times 0.075^2 = 0.017\ m^2$
- total exposed area = $0.276\ m^2$.

The concentration of hydrogen inside the cylinder, C_i , can be evaluated at these low pressures using the ideal gas equation PV=mRT, where P, V, m, T are storage pressure

(summation of atmospheric pressure and pressure due to height of water column, in kPa), volume of the cylinder (m^3), moles of hydrogen, and Kelvin temperature (K) respectively. R is the universal gas constant.

Hence the number of moles of hydrogen present inside the cylinder $m_{H2} = 0.379$ mol. Since molar mass of hydrogen is 2 gm, 0.379 mols of hydrogen will weigh =0.795 gm or 0.000795 kg of hydrogen. Hence concentration of hydrogen inside the cylinder $C_i = 7.95 \times 10^{-4}$ kg. The outside concentration and partial pressure of hydrogen in the atmosphere is considered as negligibly small.

Hence the flux of hydrogen in our experimental acrylic cylinder can be calculated as follows. The initial pressure of hydrogen gas mixture inside the chamber $P_{mix} = 112.4$ kPa. The difference in height of water level between the two cylinders is of the order of 1 metre. Since there is water vapor present, the net pressure exerted on the wall is the summation of partial pressure of water vapor and hydrogen. The saturated vapor pressure of water vapor $P_{H2O\ sat}$ at 15° C = 1.7051 kPa and at 20° C = 2.339 kPa. By interpolating the values the saturated vapor pressure of water at the initial hydrogen storage temperature of 15.7 °C is evaluated to be 1.8 kPa. So the partial pressure of hydrogen gas alone is $p_{H2} = p_{mix} - p_{H2o\ sat}$ = (112.4-1.78649) kPa = 110.613 kPa.

The flux of hydrogen through the side wall of the cylinder (thickness = 0.003 m), is given $J_{wall} = \mathcal{P} \times (\Delta p/\Delta x)$.

From the earlier analysis (section 6.3.3) a value for permeability of

$$\mathcal{P} = 1.8754 \times 10^{-16} \frac{kg \times m}{m^2 \times \sec \times kPa}$$

will be assumed. Hence

$$J_{wall} = 1.8754 \times 10^{-16} \frac{kg \times m}{m^2 \times \sec \times kPa} \times \frac{110.613 kPa}{0.003 m}$$

$$= 6.915 \times 10^{-12}\ kg/m^2/\sec$$

Loss across the wall $Loss_{wall} = J_{wall} \times 2 \times 3.142 \times 0.075 \times 0.55$

$= 1.792 \times 10^{-12}$ kg/sec

$J_{top} = 4.149 \times 10^{-12}$ kg/m^2/sec (for a thickness of 5 mm),

Loss across the top plate = $J_{top} \times 3.142 \times 0.075^2$ kg/ sec $= 7.332 \times 10^{-14}$ kg/sec

Total loss per sec = $\text{Loss}_{wall} + \text{Loss}_{top} = 1.8658 \times 10^{-12}$ kg/sec

Loss per day = Total loss per sec x time

$= 1.8658 \times 10^{-12}$ (kg/sec) x 60 x 60 x 24

$= 1.612 \times 10^{-7}$ kg

Assuming conditions stay approximately constant, total loss over 50 days = $1.612 \times 10^{-7} \times 50 = 8.0603 \times 10^{-6}$ kg

Percentage of loss in 50 days = $(8.0603 \times 10^{-6} / 0.000795) \times 100 = 1.01$ %

In addition to the permeation of hydrogen through the acrylic wall, there is a small amount of hydrogen that is dissolved in water and subsequently permeates to the atmosphere via the water column inside the cylinder, as the water is exposed to atmosphere in the upper cylinder. The amount of hydrogen that is dissolved in water can be evaluated as follows.

The mole fraction of solubility of hydrogen in water at 298.15 K and 101.325 kPa partial pressure is 1.411×10^{-5} (Scharlin *et al.* 1998). Temperature and pressure corrections are small enough to be neglected. Hence 1.411×10^{-5} moles of hydrogen are present in 1 mole of water.

1 mole of hydrogen weighs 2 g and 1 mol of water 18 g. So $2 \times 1.411 \times 10^{-5}$ g of hydrogen is present in 18 g of water. Conversely 18 gm of water contains 2.822×10^{-5} g of hydrogen.

1000 gm of water will contain $\frac{2.822 \times 10^{-5}}{18} \times 1000$ gm of hydrogen

1 litre of water will contain 1.567×10^{-3} g of hydrogen

Hence 9.7 litre of water will contain $= 9.7 \times 1.567 \times 10^{-3}$ g $= 1.52 \times 10^{-2}$ g

Therefore the percentage of the mass of hydrogen originally in the acrylic cylinder that will dissolve in the water

$$= \frac{1.52 \times 10^{-2}}{0.795} \times 100\ \% = 1.9\ \%$$

Next the loss rate of hydrogen by diffusion through the water columns to the outside atmosphere at the top of the upper cylinder will be calculated.

The diffusivity of hydrogen in water is quoted by Adriaens *et al*. (2003) as
$D_w = 5 \times 10^{-5}\ cm^2/s$

The permeability of the hydrogen through the water columns $\mathcal{P}_w$ can be calculated from the solubility mole faction mentioned earlier and the diffusivity of hydrogen in water using the relationship:

$\mathcal{P}_w = D_w \times S_w$

S_w = Concentration of hydrogen in water / pressure

$= 1.567 \times 10^{-6}/1.013\ kg/m^3/\ kPa$

$= 1.546 \times 10^{-6}\ kg/m^3/\ kPa$

Permeability $\mathcal{P} = 5 \times 10^{-9}\ (m^2/s) \times 1.546 \times 10^{-6}\ (kg/m^3/\ kPa)$

$= 7.7325 \times 10^{-20}\ kg.m/m^2/s/kPa$

The flux of hydrogen through water column of height 1 m, with the area exposed to hydrogen being equal to base area of cylinder, can be calculated using the permeability factor, by a similar method to that used for the acrylic wall calculations:

$J_w = P_w \times (\Delta p_w/\Delta x_w)$

$= 7.7325 \times 10^{-20} \times (110.613/\ 1)\ kg/m^2/\ sec$

$= 8.553 \times 10^{-18}\ kg/m^2/\ sec$

Loss of hydrogen through water $= J_w \times A_w$

$= 8.553 \times 10^{-18}\ (kg/m^2/\ sec) \times 0.00177\ m^2$

$= 1.511 \times 10^{-19}\ kg/sec$

Amount of hydrogen that would have been lost for the duration of observational period of 50 days, is equal to = Loss/sec x time

$$= 6.53 \times 10^{-13} \text{ kg}$$

This amount is small enough to be neglected. Only the hydrogen that is initially dissolved in water till saturation contributes significantly to the total loss of hydrogen from the storage system.

The overall results of the loss calculation are summarised in Table 30 .The net loss of hydrogen can be taken as the summation of hydrogen permeation across the acrylic cylinder walls and the amount that is dissolved in water. It is evident that the amount dissolved in water is in fact more than the permeation through the wall. The amount of hydrogen that would have escaped thought the water is small (6.53×10^{-13} kg) enough to be neglected.

Size	**PartialPres-sure**	**H_2 storage capacity**	**Permeability co-efficient**	**Loss of H_2 in a day**	**% loss of H_2 in 50 days**	**% total loss including solubility factor**
m	(kPa)	(Kg)	Kg.m/m^2/sec/kPa	kg	%	%
r=0.075 h=0.55 t= 0.003	110.63	0.000795	1.87×10^{-16}	$1.61x10^{-7}$	1.013%	2.923 %

Table 30-The %loss of hydrogen in the acrylic storage cylinder for a period of 50 days.

6.5.1.4 Experimental Loss Measurements

The experimental loss measurement of stored hydrogen was carried out by generating hydrogen from the 50 W PEM electrolyser with the electrical power being supplied from the PV panel. For details of the system refer to section Chapter 3. An ohmic resistor was connected in parallel to the electrolyser to stabilise the current flow with in the acceptable limits for input voltage and current. The storage chamber was initially completely evacuated and water was poured into the system via the upper tank till it eventually filled the bottom tank entirely. The electrolyser was run till the storage chamber was completely filled with hydrogen. The hydrogen output or delivery point from the storage cylinder was fixed with a pressure transducer to monitor the exact pressure variations of the stored hydrogen. The transducer was connected to data-logger (DT800) which stores the data. The final pressure variation is displayed in the monitor. A schematic diagram of the experimental set up is shown in Figure 55.

The pressure transducer, used for the measurement of gas pressure inside the hydrogen storage container, was initially calibrated using a dead weight tester as shown in Figure 56. The principle of a dead weight tester is based on Pascal's law of uniform pressure distribution across a liquid. At one end of the dead weight tester, a known dead weight is placed over a piston head, which exerts pressure on the liquid, i.e. oil, inside it. The oil is compressed using a rotating screw type piston mechanism.

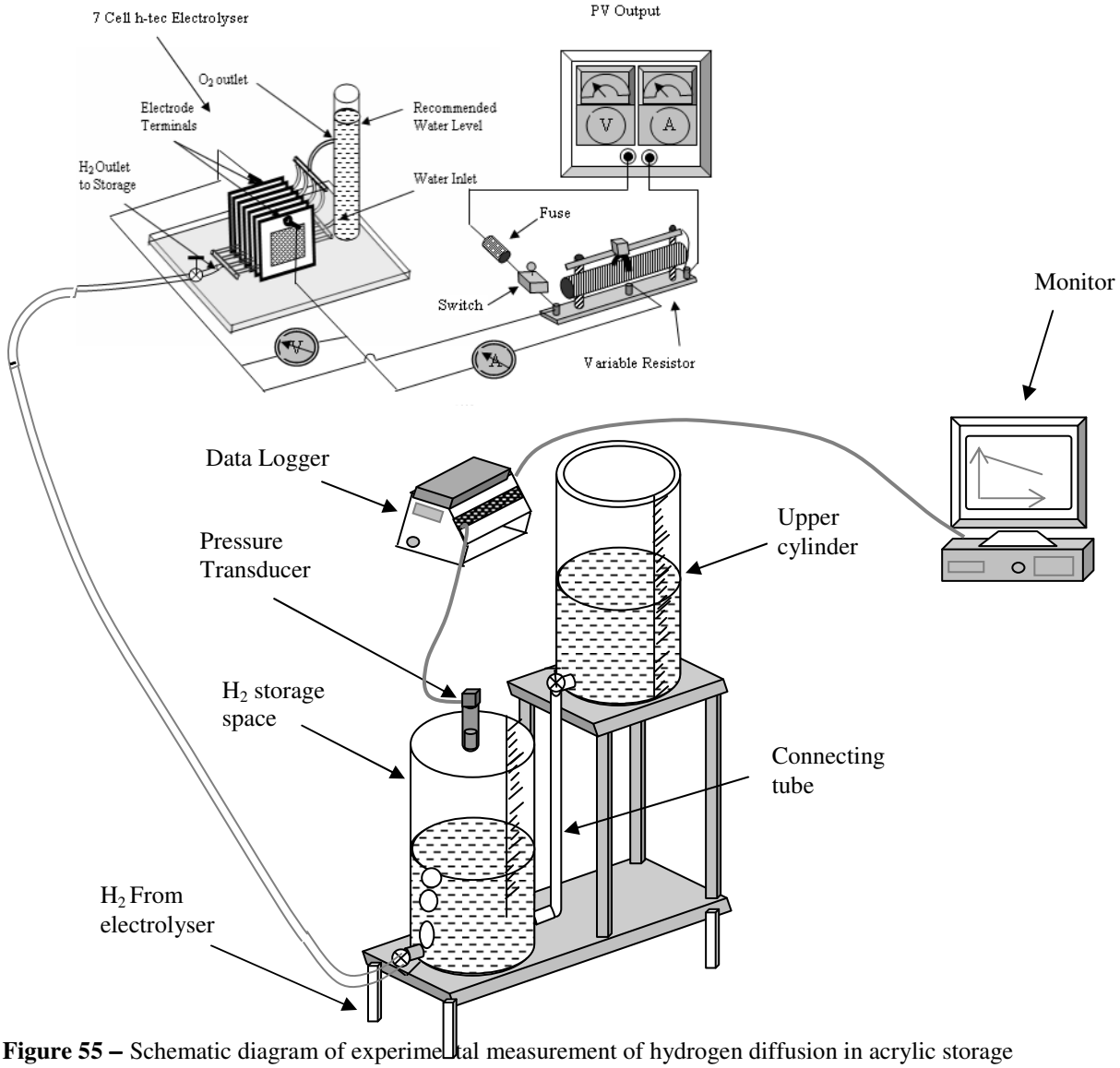

Figure 55 – Schematic diagram of experimental measurement of hydrogen diffusion in acrylic storage subsystem**.**

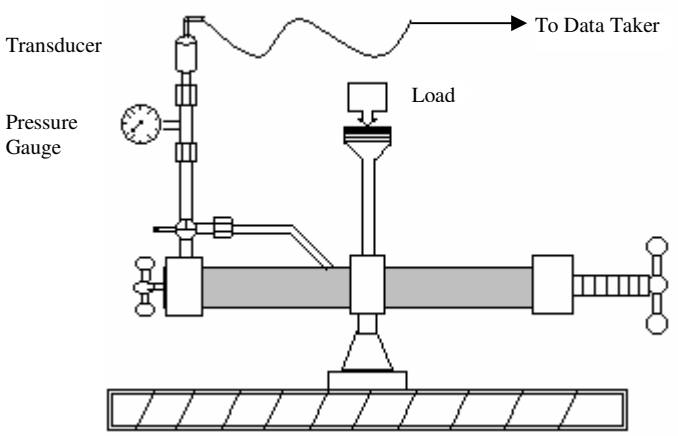

Figure 56 -Schematic diagram of Dead-weight tester

Since the oil is incompressible, the pressure is uniformly distributed across the whole volume of liquid in accordance with Pascal's Law of pressure. The other end of the dead weight tester is provided with a pressure gauge and a port for the pressure transducer. When the applied pressure becomes just sufficient to lift the dead weight, the pressure is recorded simultaneously by from the pressure gauge as well as pressure transducer. The exerted pressure due to the dead weight is displayed by the pressure transducer, which is connected to the data logger-computer system. A series of readings corresponding to the different dead weight loadings were obtained and these are plotted in Figure 57.

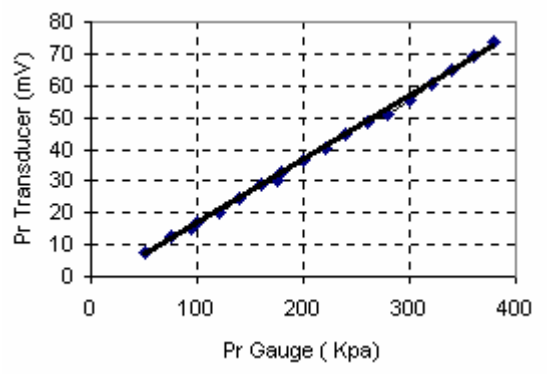

Figure 57-Pressure transducer versus Pressure gauge readings for different set of dead weight.

The profile of the graph is linear which indicates that with an appropriate multiplying factor the pressure transducer can be calibrated to indicate the readings in pressure units. Figure 58 shows the graph between dead weight pressure and pressure transducer.

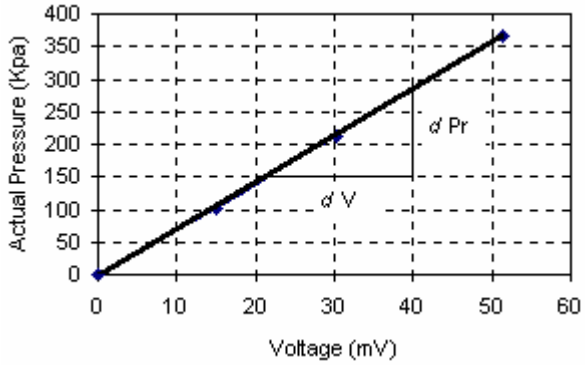

Figure 58– Actual pressure versus Transducer Voltage for same set of dead weight.

Actual applied pressure is evaluated as the dead weight over its effective surface area,

(Pressure $_{actual}$ = Load/Area). The area of the span over which dead weight is placed is evaluated as A= $\pi D^2/4$, where D is the diameter of the plunger i.e.7mm. The equation of the trend line can be approximated as liner with a value of slope m =5.118 with zero intercept i.e. line passes through origin as shown in Figure 59. The value of slope is taken as calibration factor, which is multiplied, to the readings obtained by the pressure transducer in mV to provide actual pressure in kPa.

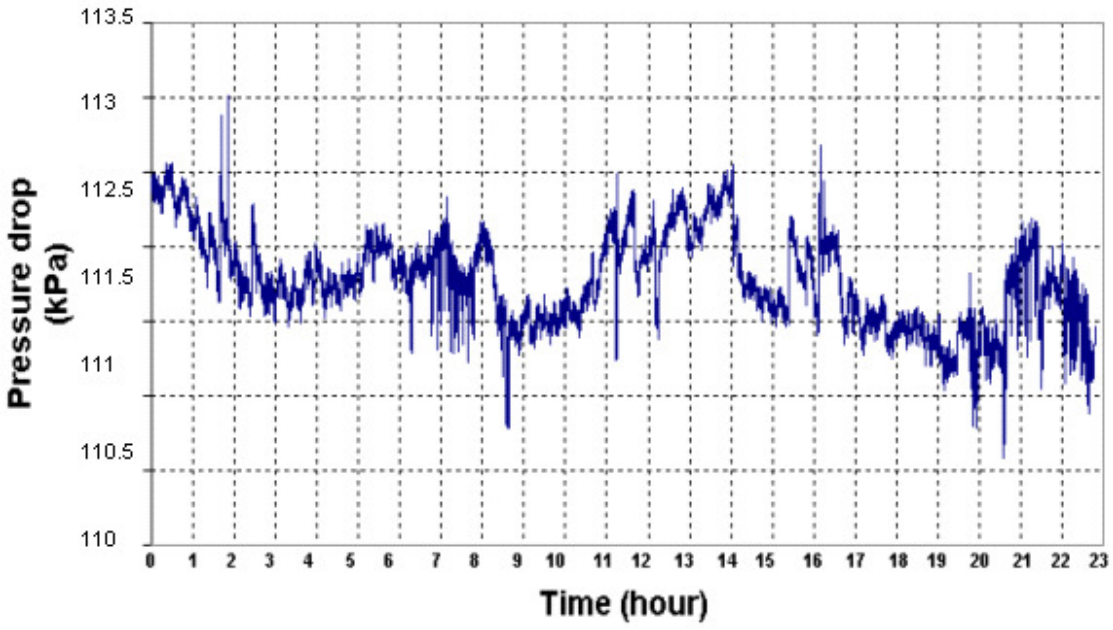

Figure 59- Short term pressure fluctuation of stored hydrogen inside the acrylic cylinder

The pressure inside the storage cylinder was continuously recorded via the data logger and fed to the computer. The observations were recorded for short term durations lasting in the order of couple of days. The data recorded for the periods between 20th to 21st Sep 06 is shown in Figure 59.

The following observations were made. A mass of hydrogen introduced into the storage cylinder at the beginning of the period of the experiment was kept under investigation for duration of 50 days, that is, a period comparable to that which would be needed for season-to-season storage of hydrogen. No hydrogen was added to the cylinder over the experimental period.

All the primary data - height of water column, level of hydrogen present in the cylinder, ambient temperature and atmospheric pressure – were recorded at about 3 pm in every two days. The hydrogen storage pressure corresponding to these conditions was calculated as the sum of atmospheric pressure and the pressure due to the difference in heights of the water levels in the tow cylinders (see Figure 54). The mass of hydrogen present inside the storage chamber is calculated from the volume, temperature and pressure using the ideal gas law.

The experimental data obtained and the quantities calculated from these data are presented in Table 31.

Time	**Vol. of H_2**	**Atm. temp**	**Atm. Pr**	**Diff in hgt of water columns**	**Pr. due to water column**	**Actual storage pr.**	**Mass of H_2 stored**
Date	***m^3***	***K***	***kPa***	***m***	***kPa***	***kPa***	***gm***
23-Aug-06	0.00831	288.5	101.61	1.1006	10.79	112.4	0.781
25-Aug-06	0.00825	285.5	101.96	1.0965	10.75	112.71	0.784
27-Aug-06	0.00819	287.8	101.89	1.0904	10.69	112.58	0.771
29-Aug-06	0.00812	289.3	103.24	1.0843	10.63	113.87	0.770
31-Aug-06	0.00806	295	102.35	1.0781	10.57	112.92	0.746
2-Sep-06	0.008	297.9	101.33	1.0741	10.53	111.86	0.727
4-Sep-06	0.00793	287.9	102.08	1.0669	10.46	112.54	0.747
6-Sep-06	0.00788	284.4	101.69	1.0628	10.42	112.11	0.747
8-Sep-06	0.00781	286.8	102.08	1.0567	10.36	112.44	0.738
10-Sep-06	0.00775	287.7	103.51	1.0516	10.31	113.82	0.739
12-Sep-06	0.0077	293	103.34	1.0465	10.26	113.6	0.720
14-Sep-06	0.00762	293.5	102.65	1.0404	10.2	112.85	0.707
16-Sep-06	0.00759	290.9	102.66	1.0353	10.15	112.81	0.711
18-Sep-06	0.0075	291.3	101.89	1.0292	10.09	111.98	0.695
20-Sep-06	0.00745	290.6	101.13	1.0231	10.03	111.16	0.687
22-Sep-06	0.00739	296.2	99.81	1.0169	9.97	109.78	0.661
24-Sep-06	0.00731	285.3	100.66	1.0108	9.91	110.57	0.676
26-Sep-06	0.00727	316.8	101.88	1.0047	9.85	111.73	0.672
28-Sep-06	0.0072	292	101.95	0.9996	9.8	111.75	0.666
30-Sep-06	0.00715	289.2	102.17	0.9935	9.74	111.91	0.668
2-Oct-06	0.0071	290.2	102.31	0.9863	9.67	111.98	0.659
4-Oct-06	0.00701	301.6	101.51	0.9812	9.62	111.13	0.624
6-Oct-06	0.00695	293.8	102.24	0.9741	9.55	111.79	0.639
8-Oct-06	0.0069	287.5	102.74	0.969	9.5	112.24	0.645
10-Oct-06	0.00682	296.4	102.78	0.9629	9.44	112.22	0.624
12-Oct-06	0.00678	308.8	101.3	0.9568	9.38	110.68	0.587
14-Oct-06	0.00671	308.8	101.73	0.9517	9.33	111.06	0.561

Table 31 Experimental data for pressure variation of hydrogen in acrylic cylinder are taken at approximately 3 pm on every alternate day**.**

The variation of atmospheric pressure and the pressure drop due to the difference in heights of the two water columns are plotted against time in Figure 60. The near parallel trend of the curves (absolute pressure and gauge pressure) shows there is a very slow but steady drop in the pressure of the hydrogen stored. The relatively constant rate of fall in hydrogen storage pressure due to the reducing height of the water column is shown in Figure 61.

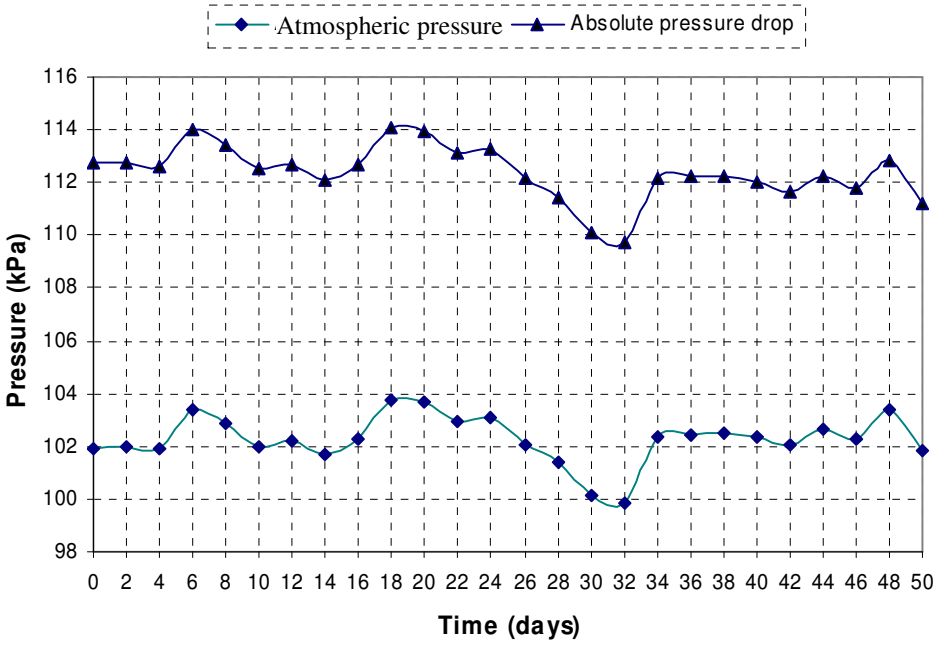

Figure 60- Atmospheric pressure, and total pressure (atmospheric plus pressure due to difference in height of water columns) of the hydrogen stored in the acrylic cylinder plotted against time**.**

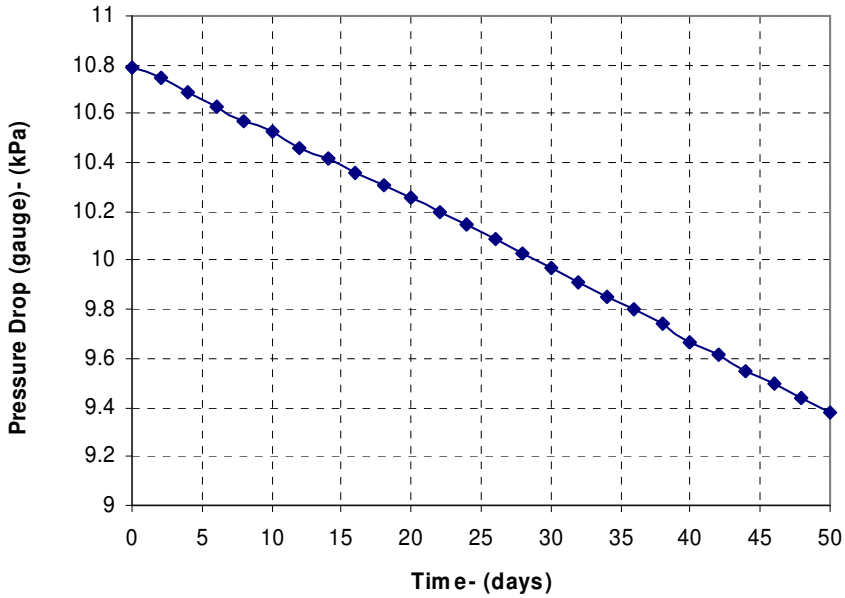

Figure 61- Pressure change due to decrease in water column over the observation period.

The volume of hydrogen present in the storage chamber is plotted against time in Figure 62. There is a steady fall in the volume of hydrogen stored. However, to find out the rate of loss of hydrogen the mass of the hydrogen in the storage vessel must be calculated from the volume taking into account the changing temperature and pressure over time.

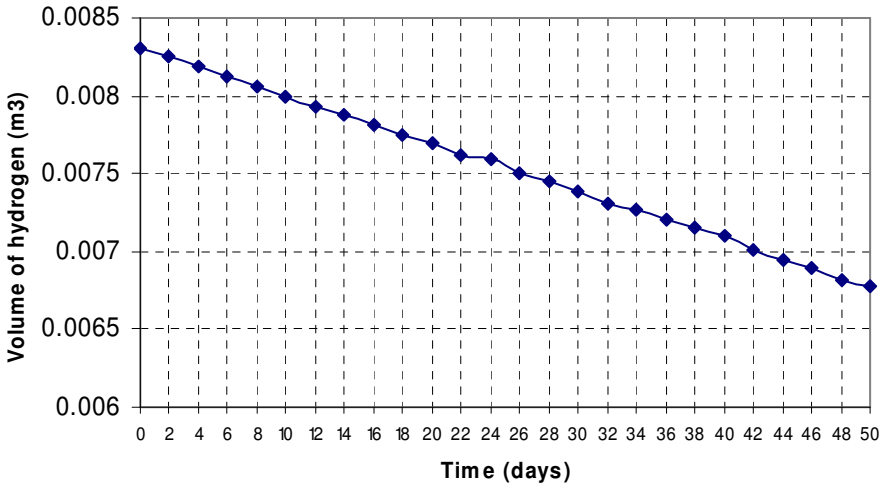

Figure 62- Actual volume of hydrogen stored versus time.

The mass of hydrogen present inside the storage cylinder is plotted against time in Figure 63. A decreasing trend is observed in the graph, indicating that hydrogen is being continuously lost from the storage. The minor deviation in some points from the trend line is probably due to small errors in reading the heights of water in the cylinders as a result of parallax effects.

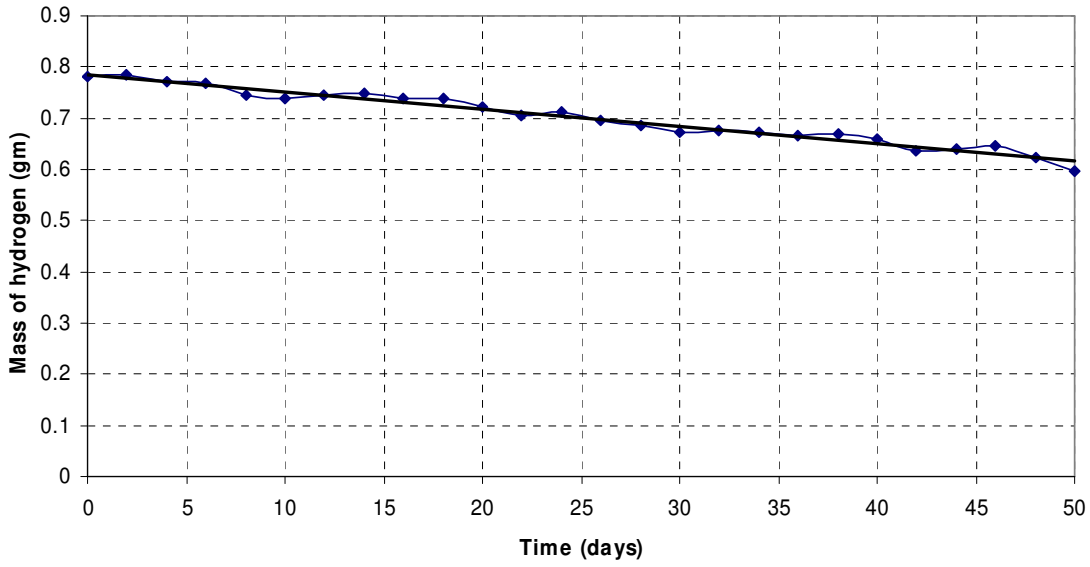

Figure 63- Mass of hydrogen present in the storage chamber plotted against time.

The initial and final masses of hydrogen in the acrylic storage cylinder were 0.781 g and 0.561 g respectively (Table 21), so that over 50 days the total loss of hydrogen was 0.22 g. Hence 22% of the original mass of hydrogen stored was lost over this period. This percentage loss is about seven times greater than the theoretical total loss over the same period due to permeation of the walls and top of the cylinder, the solubility of the hydrogen in the water, and the permeation of hydrogen through the water column (sub-section 6.5.1.2).

As was stated earlier, there remains some uncertainty about the values of the diffusivity, solubility and permeability coefficients used in the theoretical analysis. If these values are approximately correct, however, the most likely explanation of the disparity between actual and theoretical loss rates is hydrogen leakage through the valve, connections, and possibly the glued joint between the acrylic top plate and the cylinder. Small leaks that occur when the cylinder is filled with hydrogen would not be detected by the hydrostatic and pneumatic leak tests conducted on the cylinder prior to it being filled with hydrogen. Over 50 days, however, the cumulative effect of such leaks would be substantial.

6.5.1.5 Safety analysis

The pressure of hydrogen stored is atmospheric plus the head due to the difference in water levels in the two cylinders. Since atmospheric pressure is equivalent to about a 10 m head of water and the height of the cylinders is only 550 cm, this system stores hydrogen at only just over atmospheric pressure (about 1.1 bar). Importantly atmospheric pressure also acts on the outside surfaces of the lower storage cylinder so the pressure difference the vessel has to withstand – that is, the gauge pressure – is only the head due to the difference in water levels (about 0.1 bar). This type of arrangement provides a self-regulating, reliable and safe mechanism for hydrogen storage on the scale required in many laboratory experiments.

6.5.1.6 Unit costs

If we assume the hydrogen is at atmospheric pressure and 25 C, the system can store just 0.0008 kg of hydrogen, or 0.02 kWh of electrical energy. The total cost of a 10 litre storage system of this kind including piping and valves is approximately $US 120. Hence the cost per kg is $US 150,000 or $6000/kWh. This unit cost is enormous compared to the target values established in Chapter 5, but this is of course a purpose-built and very small-scale hydrogen storage system.

6.5.1.7 Design and procedural improvements

The acrylic cylinder hydrogen storage system investigated here can be significantly improved by some design modifications to minimise the chances of hydrogen escape via mechanical joints or valves.

Firstly, it would clearly be advantageous to have a complete cylinder molded with a continuous surface, that is, with the sides running without joins into the ends. There would thus be no glued joins between end plates and the sides, which are one possible source of leaks.

Secondly a fitting at the top of the storage cylinder could be avoided by fitting a vertical pipe to draw off hydrogen gas into the cylinder through the bottom, rising through water to just below the top of cylinder.

Thirdly, the use of special sensitive hydrogen leak detectors to test for leaks around any remaining joints, valves and fittings would allow a very low loss rate to be obtained.

6.5.2 Fibre Reinforced Plastic Tank

6.5.2.1 System Design and Features

A larger-volume fibre reinforced plastic (FRP) tank for storing hydrogen was described in chapter 3 section 3.4. This system, with further development and testing, is a candidate for providing low-pressure low-cost hydrogen storage for RAPS applications. In principle the FRP water tank system is similar to the acrylic storage system evaluated in the previous subsection, except that the volume of hydrogen stored is much larger, 225 litres approximately, corresponding to a hydrogen mass of 0.018 kg at atmospheric pressure.

Each of the plastic tanks is formed by welding two conical sections together (Figure 64). The dimensional details of the water tank are as follows:

Outer central diameter, $D_0 = 0.77$ m

External base diameter, $d_0 = 0.57$ m

Outer height, $H = 0.79$ m

Thickness, $t = 0.005$ m

Height of the extended upper half of the cone, $H_L = 1.482$ m

Height of an imaginary cone with diameter equal to the top tank base, $H_T = 1.09$m

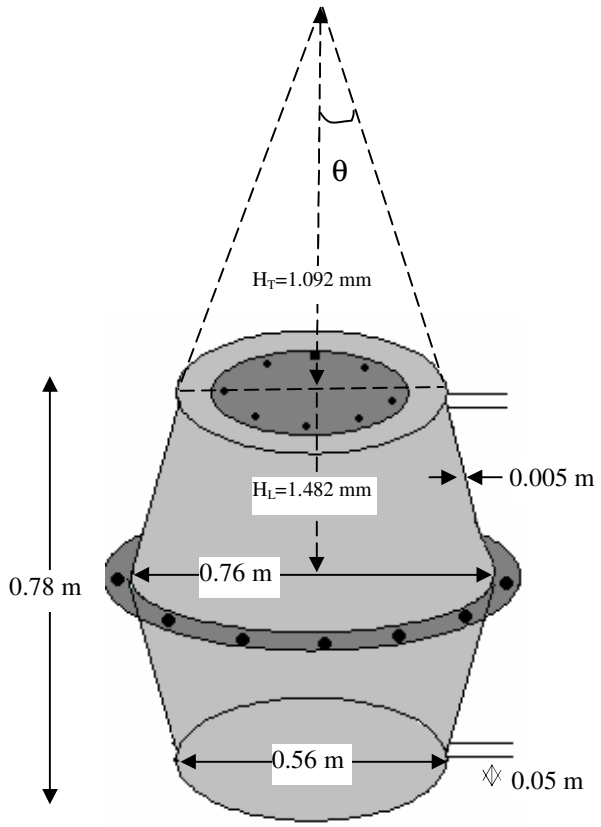

Figure 64 – Dimensions of the FRP water tank. (Note: Internal dimensions are adjusted against thickness).

6.5.2.2 Mass and volumetric energy densities

The hydrogen that is stored in acrylic cylinder is just above atmospheric pressure. The density of hydrogen stored is 0.09 kg/m^3. The volumetric energy density of hydrogen is 12.7 MJ/m^3. The mass energy density of hydrogen is 142 MJ/kg. The weight of the water tank is 5 kg. The volume of hydrogen stored is 225 litre at STP conditions. Hence the gravimetric energy based on HHV is found to be 0.511 MJ/kg for the FRP tank system.

6.5.2.3 Theoretical evaluation of hydrogen loss

A similar procedure to that used for the acrylic storage system can be used to calculate the theoretical loss rate of this plastic tank storage system over a period of 45 days, the period over which losses were also measured experimentally.

The volume of the storage tank is the sum of the volumes of the two half conical sub-sections:

$$V_{1/2\ section} = 1/3\ \pi\ (R_c^2\ H_L - R_b^2\ H_T)$$
$$= 0.134\ m^3$$

Hence the total volume of the tank $V = 2 \times V_{1/2\ section} = 0.268\ m^3$.

Similarly the total surface area of the tank through which hydrogen can diffuse is the sum of the side areas and the area of the top. The side surface area of the upper half,

$$A_{1/2\ Side} = A_{Extended\ top} - A_{\ Imaginary}$$

$$A_{Extended\ top} = \pi\ R_c H_L$$
$$= 3.14 \times 0.28 \times (0.28^2 + 1.092^2)^{1/2}$$
$$= 1.823\ m^2$$
$$A_{\ Imaginary} = \pi\ R_b H_T$$
$$= 3.14 \times 0.38 \times (0.38^2 + 1.48^2)^{\frac{1}{2}}$$
$$= 0.991\ m^2$$
$$\therefore\ A_{1/2\ Side} = A_{Extended\ top} - A_{\ Imaginary} = 1.823\ m^2 - 0.991\ m^2 = 0.832\ m^2$$

Hence the total side surface area of the tank, $A_S = 2 \times A_{1/2\ Side} = 1.664\ m^2$

The area of the top surface $A_T = \pi R_b^2 = 0.246\ m^2$. Since the bottom layer is always covered with water, it is only the top layer that will be exposed to hydrogen permeation. Hence the actual area exposed to hydrogen permeation, $A = A_S + A_T = 1.91\ m^2$.

The permeability of hydrogen in fibre reinforced plastic can be taken as (Benson et al. 2003)

$P_T = 1.5 \times 10^{-13}\ cm^3.\ cm\ cm^{-2}\ s^{-1}\ Pa^{-1}$

$=3.2 \times 10^{-18}\ kg.m/(m^2.s.kPa)$

From the permeability equation (Eq. 6.6 section 6.3.3):

$J_T = P_T \times (\Delta P_T/\Delta x)$

$J_T = 3.2 \times 10^{-18}$ kg.m/m2.sec.Kpa x 105.307/0.003 kPa/m

$= 3.29169E\text{-}14\ kg/m^2/sec$

Loss per sec $H_{loss/sec} = 3.29169E\text{-}14 \times kg/m^2/sec \times 1.91\ m^2$

$= 8.097 \times 10^{-15}\ kg/sec$

Hence loss in 45 days $= 3.148 \times 10^{-8}\ kg$

Percentage loss in 45 days $= (3.148 \times 10^{-8}/0.013) \times 100 = 0.0018\%$.

The mass of hydrogen that will be lost due to dissolving in the water can be calculated using the same method as for the acrylic system. 1 litre of water contains 1.567×10^{-3} g of hydrogen, so that 225 litre of water contains $225 \times 1.567 \times 10^{-3} = 3.52 \times 10^{-4}$ kg of hydrogen. Hence around 4.7 % of the hydrogen in the storage originally is dissolved in the water. The relatively higher quantity of dissolved hydrogen could be due to the fact that for an increase in volume of the container. The permeation of hydrogen through the water is likely again to be negligibly small compared to the other losses (as evaluated earlier in case of acrylic cylinder).

The total loss of hydrogen over 45 days due to permeation of the walls and the solubility of hydrogen in water is thus estimated to be around 4.7 % of the initial mass stored, the loss due to solubility of hydrogen in water being the dominant term.

6.5.2.4 Experimental Results

The storage of hydrogen in water tank was experimentally investigated for a period of 45 days. In the beginning, hydrogen was generated via the 250 W electrolyser bank and stored in the water tank. Once enough hydrogen was produced, the electrolyser was shut down, no more hydrogen was added to the storage, and the storage system was kept under investigation. The ambient temperature and pressure and the level of water column were recorded. The method of calculating the mass of hydrogen stored in the plastic tank at any given time was the same as that used for the acrylic storage system.

The data obtained are presented in Table 32 , and a graph for mass of hydrogen in storage against time is plotted in Figure 65. From the graph, an intimal rapid drop in mass of hydrogen is observed. Initially it was assumed that the drop in water column and hence mass of hydrogen stored was due to permeability of the vessel. But a minute leak at one of the joints was detected by applying a soap solution on all the connections. Accordingly a thick layer of glue (silica-gel) was applied at the leaking point. It resulted in a much improved performance, as can be observed in Figure 69, as the height of the water column and hence mass of stored hydrogen became far more stable.

Date (2006-7)	Ambient temp	Atmospheric Pressure	Height of water level	Volume of Hydrogen	Moles of Hydrogen Present	Mass of Hydrogen
	Deg C	*kPa*	*m*	*m^3*	*mol*	*g*
5-Nov	14.000	100.900	0.435	0.158	6.689	13.378
6-Nov	17.400	101.100	0.440	0.160	6.713	13.425
7-Nov	12.100	101.200	0.435	0.158	6.753	13.507
8-Nov	13.000	100.000	0.436	0.159	6.670	13.340
9-Nov	13.900	100.800	0.435	0.158	6.684	13.369
10-Nov	13.500	101.000	0.437	0.159	6.743	13.486
11-Nov	13.100	100.200	0.438	0.159	6.717	13.434
12-Nov	18.200	99.700	0.440	0.160	6.601	13.203
13-Nov	16.400	99.600	0.401	0.143	5.933	11.866
14-Nov	17.000	99.400	0.390	0.134	5.544	11.087
15-Nov	9.900	99.590	0.370	0.126	5.314	10.629
16-Nov	10.400	101.400	0.355	0.119	5.119	10.239
17-Nov	14.000	101.400	0.348	0.116	4.927	9.854
18-Nov	14.000	101.300	0.320	0.104	4.423	8.846
19-Nov	16.000	100.800	0.303	0.097	4.072	8.144
20-Nov	20.000	99.900	0.293	0.093	3.825	7.650
21-Nov	33.000	99.400	0.290	0.092	3.598	7.196
22-Nov	17.000	100.600	0.275	0.086	3.598	7.196
23-Nov	11.000	101.100	0.270	0.084	3.610	7.220
24-Nov	16.000	100.500	0.270	0.084	3.526	7.053
25-Nov	10.000	100.600	0.265	0.082	3.523	7.046
26-Nov	10.500	100.900	0.266	0.083	3.544	7.087
27-Nov	11.000	100.200	0.267	0.083	3.529	7.058
28-Nov	13.000	100.300	0.269	0.084	3.540	7.080
29-Nov	17.000	100.700	0.270	0.084	3.521	7.043
30-Nov	23.000	99.500	0.273	0.085	3.448	6.895
1-Dec	17.000	99.700	0.270	0.084	3.486	6.973
2-Dec	15.000	100.500	0.265	0.082	3.459	6.917
3-Dec	11.600	101.100	0.260	0.081	3.440	6.880
4-Dec	15.700	100.400	0.265	0.082	3.447	6.893
5-Dec	21.200	99.800	0.270	0.084	3.440	6.880
6-Dec	16.500	100.900	0.267	0.083	3.486	6.973
7-Dec	10.800	101.050	0.263	0.082	3.496	6.993
8-Dec	11.800	101.300	0.261	0.081	3.460	6.921
9-Dec	22.300	99.800	0.272	0.085	3.458	6.917
10-Dec	21.400	100.300	0.270	0.084	3.455	6.910
11-Dec	9.900	101.600	0.258	0.080	3.445	6.890
12-Dec	9.700	101.200	0.259	0.080	3.450	6.900
13-Dec	16.000	99.900	0.263	0.082	3.394	6.789
14-Dec	11.600	100.700	0.258	0.080	3.394	6.788
15-Dec	10.800	101.400	0.256	0.079	3.395	6.790
16-Dec	12.200	101.040	0.258	0.080	3.398	6.797
17-Dec	13.500	101.060	0.257	0.079	3.368	6.735
18-Dec	15.000	101.080	0.259	0.080	3.383	6.765
19-Dec	13.000	100.800	0.256	0.079	3.349	6.698
20-Dec	12.600	100.700	0.256	0.079	3.350	6.701
21-Dec	12.000	100.600	0.256	0.079	3.354	6.708
22-Dec	11.500	100.700	0.255	0.079	3.347	6.695

23-Dec	11.100	100.000	0.254	0.078	3.313	6.626
24-Dec	10.100	99.700	0.252	0.078	3.283	6.566
25-Dec	9.000	101.640	0.250	0.077	3.328	6.655
26-Dec	11.000	101.450	0.252	0.078	3.330	6.660
27-Dec	10.600	101.200	0.251	0.077	3.310	6.621
28-Dec	13.400	100.900	0.254	0.078	3.316	6.632
29-Dec	15.200	101.500	0.254	0.078	3.315	6.629
30-Dec	18.000	100.800	0.256	0.079	3.291	6.583
31-Dec	22.000	100.400	0.260	0.081	3.296	6.591
1-Jan	17.200	100.100	0.257	0.079	3.293	6.586
2-Jan	18.100	100.800	0.256	0.079	3.290	6.581
3-Jan	22.000	100.400	0.259	0.080	3.280	6.560
4-Jan	25.000	100.100	0.258	0.080	3.222	6.444
5-Jan	23.000	100.500	0.255	0.079	3.211	6.422

Table 32- Experimental data obtained from FRP plastic tank hydrogen storage system.

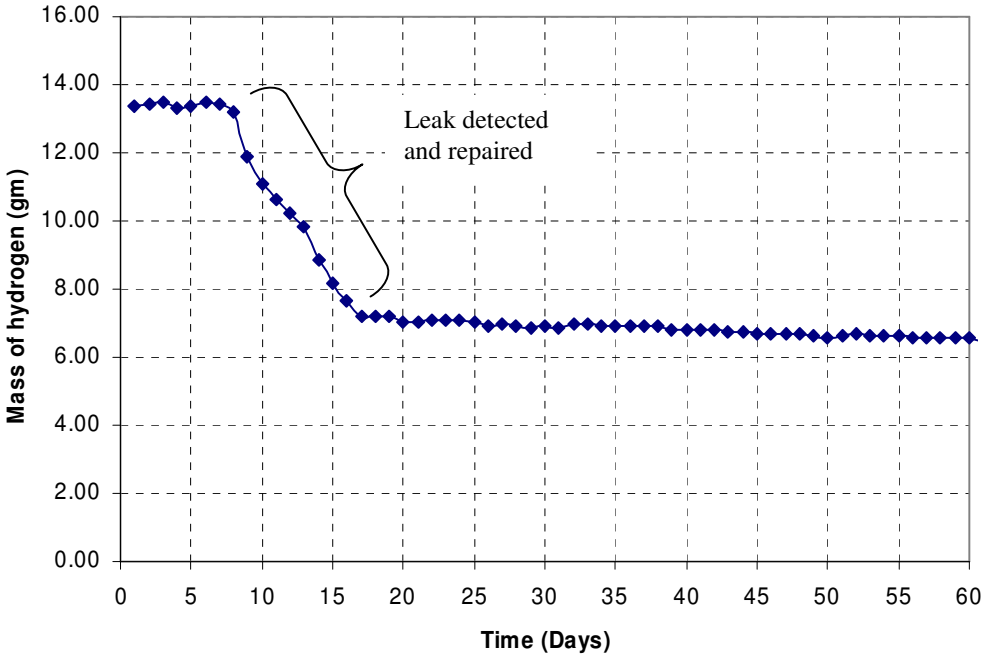

Figure 65- Mass of hydrogen present in the FRP storage tank plotted against time**.**

The initial mass of hydrogen present in the plastic tank at the beginning of the experiment was 0.007196 kg. After the observation period of 45 days the final mass of hydrogen left

in the water tank was 0.006422 kg. Hence the total loss over the period was 7.7 x 10^{-4} kg, or about 10.7 % of the initial mass.

The total loss of hydrogen over a period of 45 days was therefore in the order of 11%. This value compares with the 5 % loss estimated from theory.

The difference between the theoretical and practical loss rate of hydrogen stored is again most probably due to small mechanical leaks at fittings, valves, and the join between the top plate and the main part of the FRP tank. Since the hydrogen inlet point to the storage cylinder is always covered with water level, it is the escape of hydrogen through the outlet valve and fittings that could be main source of leakage.

6.5.2.5 Safety analysis

6.5.2.5.1 Potential source of ignition

The most common form of hazards that may arise with a fibre reinforced non-metallic tank, filled with hydrogen when left un-attended, can be the electrostatic sources of ignition. These hazards can be classified as follows:

- Lightning
- Static current
- Stray current

6.5.2.5.2 Lightning

Lightning posses of the greatest threat of potential hazard for the above ground hydrogen storage in fibre reinforced plastic tanks. The primary sources of development of static electricity in the atmosphere are the rain drops which induces an electrical field by splitting and bringing down the static charge of negative ions to the ground and leaving the positive ions in the cloud. As the cloud moves through the atmosphere, the section of

earth surface directly opposite to it follows the movement of the cloud with negative charge. When the electrostatic potential exceeds the di-electric potential of the air, the electrostatic discharge occurs in the form of lightening. If the above ground hydrogen storage equipment comes directly underneath the cloud and hence the lightening strike, it may be affected by the following ways:

Direct lightening primarily occurs when the gap between the cloud and the object (in this case storage equipment) on the earth surface narrows down. When this happens, a heavy ground current flows toward the impact point where the facilities or the equipments are in the path of a high lightening - caused current. The direct lightening results in generation of high temperature that can severely affect the objects in its path and ignite the flammable materials.

As a result of lightening, there is an abrupt change in the electrical field as it is collapsed by the sudden neutralisation of static charge. This abrupt change has the potential to induce a secondary spark at the equipment that is relatively remote from the actual site of the direct stroke.

6.5.2.5.3 *Static current*

As the rain drops separate the charges between a cloud and earth surface underneath, any adjacent cloud is induced with opposite charged due to polarisation of primary cloud. Hence the earth surface directly beneath these clouds is also oppositely charged. With the relative movement of these two clouds as the gap between them narrows down, an electrostatic discharge takes place between these two clouds in the form of Cloud-to-Cloud lightening. As the charge is neutralised at the clouds, the accumulated charge in the earth surface will neutralise by way of a passage of current through the conductor with the lowest path of resistance. These abrupt changes can induce a charge –causing sparks usually occur on an insulated metallic body.

A natural protection against the lightening damage is generated as the formation of cloud is accompanied with high humidity which acts as a bonding factor between surface bodies to the ground hence enhances the dissipation of static charge. The widely accepted artificial method against the damage is carried out by providing a metallic structure that is grounded sufficiently to safely dissipate the induced static charges. Non metallic structures can be protected from the direct stroke lightening by incorporating properly designed lightening rods, conducting masts or overhead wires. While ground mounted metallic fixed roof tanks are generally bonded top the ground hence dissipate direct stroke lightening, the fibre reinforced tanks (non metallic) must be protected against direct- stroke lightening rods or other means. However these tanks are known to ignite when flammable vapours are venting through the openings. In our case the flash back arrestor mounted at the hydrogen delivery point adequately acts as a protection.

If a forceful separation of the negatively charged electron from positively charged proton of an atom of a material, a static electrical field develops across it. The typical force includes mixing, flowing, pouring, pumping filtering or agitating materials that separates two similar or dissimilar materials. In case of gases contaminated with particles (metal scale and rust), liquid particles (e.g. paint spray, steam) and dust or fibres. The static electric charge generation is accelerated with the speed of separation (flow rate and turbulence), low conductivity materials and surface area of the interface (pipe or hose length). In case of our fibre reinforced plastic tank filled with hydrogen, the rate of hydrogen generation from the electrolyser bank is a potential source of accumulation of charge at the connecting pipes. But since the rate of production and hence flow rate is low this source of static charge accumulation can be neglected. Extreme temperatures with low humidity do have an enhancing impact on static charge accumulation. A spark results when the sudden breakdown in the insulating strength of the dielectric that separates the oppositely charged particles. In air the minimum spark voltage is approximately 350 volts for the shortest measurable gap. Hydrogen has a dielectric strength of 65% to that of air (i.e. 227.5 Volt) at the sea level (Lux 2001). Flammability of hydrogen air mixture depends on its vapour pressure, flash point and temperature.

Ignition by the static electricity may occur in the above ground hydrogen tank under the following conditions if

- enough accumulation of the charge occurs that enables itself to produce an incendiary spark,
- there is a spark gap and
- there is an ignitable hydrogen (with in flammable limit) exist in the spark gap.

By reducing the rate of static charge generation, static charge voltage may be prevented from reaching the sparking potential. By minimising the relative motion between two dissimilar molecules, the generation of static charge can be minimised. In case of above ground hydrogen storage a control over the generation of hydrogen can act as a regulating factor on static charge generation. Bonding and grounding can be done in order to dissipate the induced static charge hence spark between two conducting bodies. Bonding prevents accumulation of potential charge difference across the gap, which reduces the chances of formation of any incendiary spark. If earth is used as bonding factor it is called grounding which by passes any form of insulation.

6.5.2.5.4 *Stray currents*

Any electrical current flowing in the paths other than those provisions deliberately provided for it are called *stray currents*. Such path includes earth, pipelines and other metallic structures in contact with the earth. Stray currents can arise due to accidental faults in electrical power circuits, cathodic protection systems or galvanic currents generated from corrosion of buries metallic objects. Though the stray currents are not potentially danger enough to induce a spark across the air gap, intermittent charges can result in a spark that can ignite a flammable mixture if present. The commonly used pipelines are bonded at the separation points (valves and connectors) with a wire having low electrical resistivity. In case of metallic tanks cathodic protection system are generally provided against corrosion. A proper engineering study is required to determine

the exact size and location of the bonding to prevent the resultant static charge accumulation.

The storage system is self regulating in terms of pressure, but a pressure release valve at the top of the hydrogen storage cylinder is desirable in case the pipe connecting the tanks became blocked. An oxygen sensor in this cylinder connected to an alarm system if the oxygen concentration rose to near the lower flammability limit for hydrogen of 4% oxygen is also necessary. A flashback arrestor in the supply line to the fuel cell is a further sensible precaution, and of course no naked flames should be allowed near the storage system. The location of the hydrogen storage tank underground potentially has a strong safety advantage, particularly since in the Australian context hydrogen storages used for RAPS in many rural and remote areas must be able to withstand bushfires and lightning strikes.

6.5.2.6 Unit costs

This 225 litre experimental system can store 0.018 kg of hydrogen at atmospheric pressure, or the equivalent of just under 0.7 kWh of electrical energy. At a total cost of $US 500, the cost per kg comes out to be about $28 000, or $700/kWh. Much larger plastic storage tanks with capacities up to 45 000 litres are commercially available. Such a tank could store 3.7 kg of hydrogen, or 95 kWh of equivalent electrical energy, at atmospheric pressure. At a cost of $US 7500 such a system would have a unit storage cost of just over $US 2000 per kg or hydrogen or $US 80/kWh. If such tanks could be designed to store hydrogen at 2 bar, the costs are halved to $US 1000 per kg or $US 40/kWh. Hence the target cost of $US 500 is being approached. It might be attained with mass production of plastic tanks especially for hydrogen storage that could with stand pressures at 2 to 4 bar.

6.5.2.7 Design and procedural improvements

This water tank based hydrogen storage is designed for a low pressure (20 kPa) with relatively large volume (225 litres). However, the extra strength of FRP can possibly allow the storage of hydrogen at above 100 kPa. During the experiment, the pneumatic leak test was carried out at 7 psi that is almost, 50 kPa gauge pressure and it was able to withstand the applied pressure. There was a minor bulging of cover plate experienced particularly at leak tests. This indicates that at higher pressure the potential source of failure can be the joints between top cover plate and the tank. In order to avoid any such potential failures, the following improvements in design for the FRP tank hydrogen storage systems might be made:

- Avoiding the replacement of filter by the cover plate, that is a continuous container surface should be ordered from the manufacturer (no joints).
- The hydrogen exit pipe coming from below through water and rising to just below top of cylinder.
- Use of special sensitive hydrogen leak detectors around all joints. (ultrasonic leak detector, hydrogen sensors which triggers alarm etc)

6.5.3 Composite and metal cylinders

Composite and metal gas storage cylinders provide further options for low-cost hydrogen storage for stationary applications. Such cylinders, being widely used already for storing LPG up to 35 bar, have their own merits in terms of simple design, and ease of construction, and cost-effectiveness. As mentioned in chapter 2, in many remote stationary applications there is ample space and these low-pressure storage can be potentially attractive. PEM electrolysers can be used to produce and compress hydrogen directly for storage in these vessels.

Composite Scandinavia in 1989 became the first organisation to commercially produce composite cylinders for liquefied petroleum gases (LPG) storage. The composite cylinder is made of fibreglass-reinforced vinylester and weighs approximately 50% less than a conventional steel equivalent model.

Composite cylinders are formed by wrapping glass fibres around a mandrel in multiple directions (second two photos) and saturating the fibres with resin to create each half of the cylinder (REF). Next, appropriate holes are drilled in each half and the two halves are bonded together to create the cylinder. The process requires no liner as two halves are made by winding fibreglass before being injected with plastic under high pressure in a hermetic process. After hardening, the two halves are de-moulded and then joined using a specially-developed method. After initial inspection and pressure testing, the coloured casing and valves are assembled. The completed cylinders are pressure-tested with air are available in 5 kg, 10 kg and 14 kg sizes. Because of their translucency, lower weight, and lower maintenance requirements, they are much more customer-friendly. Their translucent property is beneficial for LPG storage as it allows visual inspection of actual storage level, for hydrogen storage that translucent property has no significance except it draws customer's attraction. One of the primary hall marks of these composite cylinders are their corrosion free nature as well as they incurs low-maintenance as just soap and water is needed to clean the outside of the cylinder. Generally air instead of water is used for pressure testing of a composite cylinder.

When subjected to heat and/or fire the cylinders' permeability increases. This allows the gas to seep through the walls slowly instead of releasing large amounts of gas through the valve. The average temperature of most fires is not hot enough to melt the glass fibres. All materials are permeable to certain degree, and composite materials are slightly more permeable than steel. The durable and lightweight composite cylinders are suitable for replacing traditional steel cylinders. Composite cylinders are increasingly being used for storing LPG at pressures of up to 35 bar. For hydrogen storage the cylinders can be derated to 20 bars (Pyle1997).

Low-carbon metal cylinders are commonly used for LPG and natural gases. Similar principles standards that are applicable to storage of LPG and natural gas in the low to medium pressure range can be implemented for hydrogen as well. Pyle (1997) has used steel LPG cylinders derated from their design pressure of 17 bar (for LPG use) to 8 bar for safe storage of hydrogen. Metal cylinders for storing hydrogen must be made of low carbon steel, so that they do not suffer from hydrogen embrittlement (Pyle 2003). The material of the tank should be of low-carbon steel and is thus resistant to hydrogen embrittlement. Pyle states that tanks made from steel with a high-carbon content, or which has been cold-rolled or cold-forged, or have weld hard spots in excess of about Vickers Hardness Number 260, should not be used for storage of hydrogen (Pyle 2003). Composite cylinders are particularly promising for hydrogen storage since they do not suffer from embrittlement. All valves and regulators used should of course be hydrogen compatible.

Storage of hydrogen as a compressed gas up to 20 bar in metal or composite cylinders would match well the capabilities of current-generation PEM electrolysers to generate hydrogen under pressure for direct storage without the need of an external compressor. This option could be very cost-effective, since the compression achievable by the PEM electrolysers would greatly reduce the storage volumes required, and the additional cost of an electrically driven compressor would be avoided, as would its electricity consumption that otherwise would significantly lower the net energy production of the system.

An 8000 litre metal cylinder for storing gas at pressures up to 20 bar today costs in the order of US$ 9000. If such a cylinder is used to store hydrogen at 20 bar, which should be obtainable directly from a PEM electrolyser, the cost would be just less than $700/kg (or $26/kWh), and hence it is approaching our target cost of $500/kg (or $20/kWh).

Hydrogen produced by a PEM electrolyser would need to be dried before entering a metal or composite cylinder for storage, and then probably humidified again before reuse in a fuel cell.

Cylinders would be fitted with a pressure release valve, and flashback arrestor in the supply line to the fuel cell. A sensor to measure oxygen concentration connected to an alarm system if the oxygen concentration rose to near the lower flammability limit of 4% oxygen would also be necessary. With proper safety equipment and procedures, such hydrogen storages should be as safe as the metal or composite LPG containers (Figure 66) commonly used at service stations, industrial plants, commercial establishments and many houses in areas not served by natural gas.

Figure 66- A composite cylinder originally designed for LP gases.

6.6 CONCLUSION

A number of options for storing hydrogen storage at relatively low pressure, especially those pressure ranges achievable using a PEM electrolyser without external compressor, are assessed in this chapter for RAPS applications. These options are:

- Acrylic cylinders (9.7 litre) for laboratory experiment use
- Fibre reinforced plastic water tanks (225 litre)
- Composite cylinders (for pressures up to 20 bar)
- Low-carbon steel (up to 20 bar) cylinders

The evaluative criteria used are mass and volumetric energy density, loss rate, hydrogen permeation, safety and cost per unit mass of hydrogen stored.

It was found that for the acrylic system the theoretical total loss of hydrogen over a period of 50 days would be 2.9% by mass, out of which 1.9 % is dissolved in water and 1% lost due to permeation through the walls of the cylinder. This theoretical value is much less than the actual experimentally measured loss of 22% by mass over the same period. The most likely explanation of this disparity is hydrogen leakage through the valve, connections, and possibly the glued joint between the acrylic top plate and the cylinder.

The evaluated theoretical total loss of hydrogen for the FRP water tank over 45 days was found to be around 5% by mass, with the vast majority of the loss due to hydrogen being dissolved in water. The actual permeation of hydrogen through the FRP water tank wall was calculated to be only just over 0.0018%. The actual experimental loss of hydrogen for FRP water tank over this period was measured to be almost 11% by mass. This much lower permeation as compared to acrylic cylinder is justified considering the fact that the permeability coefficient for FRP material is much lower than that of acrylic material. Again the difference between experimental and theoretical difference could be attributed to the existence of some leaks that might have escaped both the hydraulic and pneumatic testings.

Design improvements that would reduce the incidence of hydrogen leakage in cylinders of this kind are the following:

- Manufacturing a container with a seamless containment surface, that is, with no joins

- Drawing off hydrogen from a vertical pipe that enters the cylinder from a fitting at the bottom, and then rises through the water to just below the top surface of cylinder, thus avoiding the need for any fitting directly exposed to hydrogen at the top.
- Testing for leaks from the cylinder using sensitive hydrogen leak detectors before it is put into use, and sealing any leaks found.

A full safety regime must be implemented when storing hydrogen for use in solar-hydrogen RAPS systems. When using metal cylinders, existing safety regulations and standards relating to storing flammable gases such as LPG provide a useful starting point, but hydrogen-specific standards and regulations will be needed if solar-hydrogen systems are to be more widely used. Particular care must be taken to ensure against lightning strikes and build up of static charge when using plastic or composite cylinders for hydrogen storage. Also the risks to hydrogen storage systems of bushfires must be considered in fire-prone areas. Undergrounding of hydrogen storage tanks may be an option worthy of consideration in such areas.

7. TRIPLE BOTTOM LINE COMPARISON

7.1 RAPS SYSTEM TYPES TO BE COMPARED

A brief comparison of the solar-hydrogen systems investigated in this thesis with other types of RAPS systems is carried out in this chapter, using a triple bottom line evaluation methodology covering economic, social and environmental factors. Both technological and practical strengths and weakness of the solar hydrogen systems are identified. The main alternative stand-alone RAPS systems compared with solar -hydrogen system are:

- PV array + battery storage
- Diesel generator + battery storage
- PV array + diesel generator + battery storage

The triple bottom line evaluation methodology used is described in section7.2. Section 7.3 covers the economic evaluation, section 7.4 the environmental evaluation and section 7.5 the social evaluation. A summary of the overall triple bottom line evaluation is provided in section 7.6.

7.2 EVALUATION METHODOLOGY

7.2.1 Triple Bottom Line

The term 'Triple Bottom Line' was originally coined by John Elkington, co-founder of the business consultancy 'Sustainability' in 1994. Triple bottom line evaluation is one of the most comprehensive methodologies for assessing a technology, project or organisational performance in economic, environmental and social terms (Elkington 99). During the early 1990s the concepts of 'environmental economics'–including full-cost pricing, internalising environmental and social externalities, social benefit-cost analysis, social capital and environmental capital–began to be applied more widely by government

and mainstream businesses and industries (Elkington 99). In addition to the traditional financial bottom line, governmental and private sector organizations started to measure their environmental and social 'bottom' lines too.

The main criteria used in the brief triple bottom line evaluation of solar hydrogen RAPS systems and the alternatives in this chapter are the economic, environmental and social, dimensions

7.2.2 Economic

The economic comparisons of these systems are carried out in line with the lifecycle cost analysis of solar hydrogen systems conducted in chapter 5. The respective values and parameters for the different components are obtained from the literature (Ghosh *et al.* 2003; Kelowani *et al.* 2004; Akbarzadeh 1992).The final outcome of the earlier analysis – that is, average unit cost of energy (in $US/kWh) – is compared with the unit costs of energy estimated on a similar basis for conventional battery or diesel back-up RAPS systems.

Hence the economic evaluation is based on an average unit cost of the energy supplied by each option taking into account the full lifecyle of each component. This unit cost is estimated by converting the capital cost into an annualised cost using a capital recovery factor corresponding to the assumed lifetime of each component of the system and a real discount rate of 5% (as explained in chapter 5). This annualised capital cost is added to the total annual operating cost, and then divided by the annual energy supplied to find the average unit cost of energy.

7.2.3 Environmental

At present climate change and global warming are widely believed to be due to the results of increase in greenhouses gases, particularly carbon dioxide, in the atmosphere. Carbon dioxide emissions come largely from the burning of fossil fuels. In this chapter greenhouse emissions associated with the various RAPS options are compared. In addition brief mention is made of other key environmental impacts of the options.

7.2.4 Social

The main social factors considered are:

- Level of service provided, including reliability.
- User attitudes and experience
- Safety
- Regulations and standards

7.3 ECONOMIC EVALUATION

A detailed analysis of the unit cost of energy supplied by a stand-alone solar-hydrogen system to a remote household in south eastern Australia was conducted in chapter 5. The unit cost assumptions for the main components of the system made in this analysis are summarized again in Table 33. These assumptions were made on the basis of a search through available literature and through websites of various hydrogen and renewable energy technology manufacturers. The unit capital costs were then applied on a linear basis to the find the capital cost of the components given the size of each component. No account was taken of economics of scale.

As discussed in chapter 5 and chapter 6, a range of unit capital costs for the hydrogen storage system from an upper value of US$ 2000 /kg of H_2 down to a target value of US$ 500 /kg, is assumed.

System component	Relative cost of the components	Discount rate (d)	Annual Operation & Maintenance cost (percent of initial investment)	Life time(n)
	(US$)	(%)	(%)	(y)
Photovoltaic array	5000/kW	5	2	25
PEM Electrolyser	3000/kW	5	2	20
PEM Fuel cell	6000/kW	5	2	15
Balance of System	6000/Unit	5	2	25
Hydrogen Storage System	500 – 2000 /kgH2	5	2	25

Table 33- The economic assumptions incorporated in the modeling section.

The results obtained for the unit costs of energy from a solar-hydrogen system in this location are presented in Table 34. The unit cost was found to be US$ 2.45/kWh for the higher storage cost of US$ 2000 /kg, falling to US$ 1.5 / kWh for the lower storage cost of US$ 500 /kg. As expected these unit costs are very much higher than the present price of domestic electricity from the central grid in southern Australian (between $US 0.1 and 0.15 /kWh. But the solar-hydrogen system modeled here is completely standalone, and has zero greenhouse emissions.

The model used to analyse the solar-hydrogen RAPS system has also been used to estimate the costs of a comparable stand-alone PV – battery storage system, a diesel generator and battery system, and a PV – diesel generator – battery system, all supplying exactly the same daily load profile and annual electricity demand. For a diesel based system, the entire amount of load is provided by the fuel. With a fuel transportation cost of US$1.30/litre and a power output of 1kWh per liter of the fuel, a capital cost of US$980/kW yields a unit cost of power in the range of US$ 1.69-1.9/kWh.

On these assumptions, the unit cost of power for an equivalent standalone PV array and battery-storage system comes out the highest of all the options, at US$ 2.68-2.80/kWh, compared to US$ 1.69-1.90/kWh for the diesel generator and battery, and US$ 2.19-2.29/kWh for the combined PV – diesel generator – battery system (Table 29). The PV - battery system has such high costs since to guarantee the supply throughout the year, the PV array size has to be very large (60 m^2) since the batteries cannot store energy for a long period without substantial losses. Also even for a relatively small energy storage capacity of 0.25 kg equivalent of hydrogen batteries bank storage capacities of 6.25 kWh need to be employed.

The unit costs of the diesel generator and battery system are high because the fuel cost alone (US$ 1.3 /litre) delivered to remote areas contributes US$ 1.69-1.90/kWh, and the generator and batteries have a relatively short lifetime.

These cost estimates refer to a particular location and assumed daily load profile. They are also highly dependent on the assumptions made for unit capital and operating costs. As the insolation of a location increased, so the unit costs of energy from a solar-hydrogen system would fall accordingly. As further information on actual unit costs comes to hand, there will be a need to revise the estimates made. But the estimates here do give a reasonable indication of the unit cost of energy range that might be expected from solar-hydrogen systems and their main alternatives in remote applications.

Indeed the unit costs obtained here are comparable to those given in the recent literature. Shakya *et al*. (2005), for example, reported a unit cost of energy solar-hydrogen systems to be US$ 1.94 /kWh. Shakya also mentioned that a PV (60%) + Wind (40%) system would yield a unit cost of power supply of US$ 2/kWh and that a wind alone - hydrogen system could give a unit cost of US$ 2.53/kWh.

RAPS System options	Unit cost of power (US $)	Conditions
PV +H_2 system	1.5	For a unit storage cost of US$500/kg
	2.5	For a unit storage cost of US$2000/kg
PV alone + Battery	2.7-2.8	Deep-cycle batteries with a total storage capacity of 6.25 kWh. PV panel size 60 m^2
PV + Diesel Gen +Battery	2.2-2.3	Delivered fuel cost $1.30/litre. Battery storage capacity 3.12 kWh. PV area of 30 m^2
Diesel Gen + Battery	1.7-1.9	Delivered fuel cost $1.30/litre. Battery storage capacity 0.3 kWh.

Table 34- Comparisons of unit cost of power for RAPS options.

7.4 ENVIRONMENTAL

7.4.1 Types of environmental factors

Of late environmental pollution has started to make its impact felt across the world. Both the population and anthropogenic activities have caused considerable damage to the ecological balance and the environment as a whole. In the past decades conventional pollutants (i.e. SO_2, NOx, CO and particulates) have been subjected to control provisions and mechanisms. Recently global pollutants like CO_2 emissions has been given top priorities as the level rise in concentration of CO2 is the primary contribution to the global warming (Dincer 2002).

7.4.2 Greenhouse Gas Effect

The rise in earth's temperature due to the emissions of gases (i.e. CO_2, CH_4, CFCs, N_2O, and peroxyacetylnitrate) into the atmosphere is called the greenhouse effect. The term greenhouse effect was originally used to refer to the role of the entire atmosphere, mainly the water vapour and clouds, in keeping the surface temperature of the earth relatively stable and warm. But the rise in concentration of CO_2 in the atmosphere due to human activities, mainly burning of fossil fuels, contributes almost 50 % of the greenhouse effect (Dincer 2002). The rest of the greenhouse effect is primarily due to other gases, i.e. methane, chlorofluorocarbon, nitrogen dioxide, etc. Global warming and potentially catastrophic climate change due to the greenhouse effect is now of great international concern.

In the present case, it is therefore important to estimate the greenhouse gas emission impacts of each of the RAPS options considered.

The greenhouse gas emissions in terms of CO_2-equivalent levels that are caused by the various RAPS systems are compared in Table 35. For each litre of diesel fuel combusted 3.1 kg of CO_2-e is emitted to the atmosphere. Hence the diesel-battery combination would emit some 5.6 tonne of CO_2-e per year in supplying the total load of 1825 kWh of load, and assuming 1 litre of diesel is needed to generate 1 kWh (Akbarzadeh 1992). Similarly a 50% PV + 50% diesel system would emit half this amount, that is, just under 3 tonnes/year.

As expected the options relying solely on solar energy supply via PV panels have the lowest greenhouse emissions in usage, and are thus preferred from a greenhouse emission perspective.

RAPS Options	Green house emission	Total annual emissions
	(kg of CO_2/kWh)	(tonne of CO_2-e per yr)
PV +H_2 system	0	0
PV alone + Battery	0	0
PV + Diesel Generator +Battery	1.55	2.8
Diesel Generator + Battery	3.1	5.7

Table 35- Comparison of greenhouse gas emissions in operation for the various RAPS options.

These evaluated emissions ignore the fact that there are considerable 'embodied emissions' in the system components, that is, the associated emissions in making batteries, PV panels, diesel generators, PEM electrolysers and PEM fuel cells. A full lifecycle assessment of the options would therefore be useful, but such an assessment is beyond the scope of the present study.

7.4.3 Other environmental impacts

Hydrogen is one of the cleanest fuels (carbon free) as it generates water as the end product when used in fuel cells. Unlike fossil fuels, particular diesel or petrol, hydrogen does not produces any other harmful pollutants like SO_2, CO, CO_2 etc (Dincer 2002). Hence generation of hydrogen from renewable sources via electrolysis and subsequent use via fuel cell offers a complete pollution free form of energy utilisation.

The environmental impact due to the batteries depends upon the extent to which its constituent materials are collected and recycled. For a certain collection rate of batteries, all environmental impacts are minimised as the recycling rate increases. Hence it is always recommended to recycle the battery waste to the maximum possible extent. As it not only reduces the global warming but also minimises non-renewable resource depletion (Rydh and Sanden 2005).

A solar hydrogen system is completely silent while a diesel generator is noisy. Unlike conventional renewable source where power intermittent fluctuation is inevitable, hydrogen storage and power regeneration via fuel cell can balance out and hence provide a continuous uninterruptible power supply. Lack of recycling and re-use schemes for hydrogen technology at present can be regarded as a weakness (Zoulias *et al.* 2006). On the other hand hydrogen has an opportunity for reduction of environmental impact as well as minimising the usage of batteries and diesel generators.

7.5 SOCIAL EVALUATION

7.5.1 Social factors

The level of service provided to the users will shape the smooth acceptance of solar hydrogen system. At present both diesel and battery base storage systems are readily available in the market whereas solar hydrogen system requires greater penetration to the market. It should be mentioned that part of solar-hydrogen system's components particularly PV panel and the predicted low cost options of hydrogen storage can easily be traced in any market. It is the PEM electrolyser and fuel cell groups that need greater market support from the government.

Secondly user attitudes and experience to solar-hydrogen systems, a new technology with which consumers are not familiar, are important. The users of RAPS can be divided into three groups (Zoulias *et al*. 2006):

- Group A: high-cost grid-connected users,
- Group B: traditional remote area power supply (RAPS) users, and
- Group C: non-electrified users

Zoulias (*et al*. 2006) concludes that there is a potential for group A to opt for RAPS if the grid connection is too expensive for its maintenance and operation for the grid owner. Any segmentation of the cost from grid owner results in a high cost for these particular customers rendering RAPS or H-RAPS as an alternative option (Zoulias *et al*. 2006). Again the quality of the power supplied may not be up to the satisfaction of the customers. But the group B (conventional RAPS users) as well as group C (the non- electrified users), are

considered as the best potential market for the solar-hydrogen based RAPS. These two user groups will compare the hydrogen-based RAPS system with diesel generator sets and the alternative option of grid extension. The major market barrier is the initial high upfront cost for hydrogen based RAPS, which will deter the potential customers (Zoulias *et al.* 2006).

Also the end users do not posses the proper knowledge of available technology. Demand side managements and rational use of energy may allow hydrogen-based RAPS to be an attractive alternative compared to conventional RAPS or even grid extension. In most parts of Australia, the cost of grid extension for a distance of 1 km is around A$ 10,000 (RISE 2004: website).

Zoulias (*et al.* 2006) has identified that the residential power supply, agricultural activity, tourism sector, water desalination and treatment, back-up power systems, remote telecommunications, lighthouses and food processing establishments remote from the main grid as the main potential markets for hydrogen based RAPS systems.

User's attitude and preference for a solar hydrogen system over conventional RAPS system in general and diesel generator in particular revolves around their perception about hydrogen. Though at present solar hydrogen system offers a relatively higher unit cost of power supply ($US 1.5- $ 2.5/ kWh as compared to $1 /kWh for RAPS application), its emission free nature has the potential to attract an increasingly environment conscious public. As a precautionary measure, a special simple training of user is required for solar hydrogen system since it involves a flammable hydrogen gas.

The fear of risk or potential hazard associated with hydrogen usage can be attributed to the negative image created by the media in the past i.e. Hindenburg tragedy 1937, the 1986 challenger incident. Subsequent scientific investigations proved that on both the occasion hydrogen was not the cause of failure. Addison Bain, former manager of hydrogen Programs NASA, identified that it was the highly flammable cellulose nitride based external coating that caused the ignition due to an electrical storm. Unless such prejudices about hydrogen are removed, and both the public and Govt. decision makers are informed with proper safety issues related to hydrogen gas, the implementation of hydrogen technology is going to be significantly delayed (Garrity 2002). The level of service that can

be made available to the users by the government is one of the crucial factors that will shape its implementation in the market.

From a performance aspect the reliability of a solar hydrogen system is at par with most of the other RAPS system as it also uses same energy source i.e. PV panel. If extreme weather limits the PV panel output capacity for long enough, the stored hydrogen will be excessively utilised which may lead to disruption of the power supply continuity. The unpredictability of such a scenario can be played down by providing an extra tolerance to the hydrogen storage capacity.

The consumer desire and user acceptability of hydrogen technology needs to be fostered for the effective implementation of this technology. If the existing barriers are sorted out in a realistic manner this technology has the potential to reduce Australia's total reliance on coal, gasoline and natural gas, providing energy security. The US Government recently committed an extra US$1.2 billion to hydrogen research. Japan has launched a 20-year research program that is sending satellites into space in the hope that it can harvest solar energy and send it back to the earth by laser onto cells of Titania (TiO2). The European Commission has instituted an intense R&D program in pursuit of solar hydrogen. Iceland aims to be the world's first hydrogen economy.

Diesel and PV RAPS systems employing battery storage have been used for many years and users are familiar with these options. As a new technology, it will be important for the sellers and installers of solar-hydrogen based RAPS systems to build-up confidence in these systems with potential users. Reporting on successful applications over extended periods will be essential to build up this confidence.

As discussed in Chapters 3 and 6, ensuring solar-hydrogen systems are safe, and that users and the community have full confidence in the measures taken to minimize any risks are critical, if the technology is to be more widely deployed. The safety aspects of the four RAPS systems under consideration here are briefly summarised in Table 36.

Technological options	Primary Energy Storage Medium	Risks and prevention
• Solar PV + Battery	Battery (deep cycle)	Electrical short circuit. Toxicity of electrolyte and electrodes in battery, hence safe disposal or recycling are needed
• Diesel generator + Battery	Fuel	Flammable fuel for which the usual precautions must be taken. Local air pollution. Toxicity of electrolyte and electrodes in battery, hence safe disposal or recycling are needed
• Solar PV + Diesel generator + Battery	Fuel +Battery	Flammable fuel for which the usual precautions must be taken. PV does not posses any extra safety concerns. Toxicity of electrolyte and electrodes in battery, hence safe disposal or recycling are needed
• Soar PV + H_2 system (Investigated in this thesis)	Hydrogen	Ignition of hydrogen due to naked flame, sparks from static electrical discharge, lightning strikes. Full safety regimen for safe storage and usage of hydrogen must be employed. Special measures would be needed if storing hydrogen in areas prone to bush fires e.g. use of underground storages.

Table 36- Safety aspects of various RAPS system.

The solar PV +battery based RAPS system is associated with toxicity of battery waste material which requires recycling and safe disposal. Also these are a potential hazard of short circuit of the electrical system. In case of diesel generator + battery storage system, the safe storage of fuel may require extra safety precautions especially from potential ignition source, electrical spark or even lightning. It also causes noise and local-air pollution and hence is a potential health hazard. A solar PV coupled with diesel and battery system would draw same sort of safety precaution except it will cause less noise and local-air pollution as compared to diesel alone + battery system. In case of solar hydrogen system the hydrogen storage is the main component demanding specific safety assessment.

For remote areas, on open above ground hydrogen storage particularly in the proposed non metallic (composite or plastic fibre reinforced) tanks remains vulnerable to certain potential hazards like lightning and static electricity.

7.5.2 Regulations and Standards

At present various international efforts are underway to develop regulations and standards for hydrogen through the International Organisation of Standardisation (ISO), International Organisation of Electrotechnical commission (IEC) and World Forum for Harmonisation of Vehicle Regulations (US Department of Energy 2006: website).

ISO is a conglomerate of the national standards bodies of more than 140 countries. One of its primary objectives is to promote and facilitate exchange of scientific and technological activities through standardisation process. Three of ISO's technical committees – namely TC 22- Road Vehicles, TC 197- Hydrogen technologies and TC 58- Gas cylinders – are at present working on standards related to hydrogen and fuel cells.

The electrical interface to fuel cells is currently being developed by International Electrotechnical Committee. One of its technical committees, TC105, is specifically dealing with stationary fuel cell and power plants. Its working group includes terminology, fuel cell modules, safety, performance, installation and propulsion (US Department of Energy 2006: website). Within the UN Framework Group on Pollution and Energy (GRPE), Australia along with Japan and EU has recognised a need to harmonise the regulations relating vehicle, but at present there are no standards or provisions dedicated exclusively to hydrogen.

Putting in place an appropriate set of national and international standards and regulations relating to hydrogen production, storage and use in stationary applications will be a critical step in paving the way for deployment of solar-hydrogen systems for remote applications.

7.5 OVERVIEW OF TRIPLE BOTTOM LINE COMPARISON

An overview of the preliminary triple bottom comparison of solar-hydrogen RAPS systems with some of their main competitors is provided in Table 37. The solar hydrogen system gives a unit cost of power in the rage of US$ 1.5 - 2.45/kWh depending upon the unit storage cost of hydrogen which varies from US$2000/kg to US $500/kg. Initial investment cost is high yet the system has a low ongoing maintenance cost with a relatively long life time. From environmental aspect, the solar hydrogen system is the best option as compared to other diesel and battery based RAPS option. Though not much actual experience is known yet a solar hydrogen system can be placed on par with other RAPS alternative on a reliability scale. As a new system, it requires user education as well as regulation standards.

A diesel generator + battery storage system is found to be providing a unit cost of power in the range of US$1.69-1.90/kWh. Though initial investment cost is low it incurs substantial amount of fuel (diesel) cost. The fuel transportation cost varies grossly from location to location. For our calculation purpose a transportation cost of US1.3/litre was assumed. Also it causes maximum amount of emission i.e. 3 kg of CO_2 per kWh of power supplied. Unlike solar hydrogen system, this diesel +battery storage system is quite mature and requires less safety precautions with the exception of toxic waste of battery needs to be recycled.

A solar PV coupled with battery storage offers unit cost of power of US2.68-2.80 /kWh with an intermediate initial capital investment cost. It produces zero emission while in operation but there are some embodied emissions (emissions caused during manufacturing of the system components) which are ignored in the present analysis. It is becoming increasingly common among the RAPS users. Also at times a 50 % PV and 50% diesel generator are combined with a common battery storage bank which offers marginal improvement in unit cost of power (US2.19-2.26 /kWh) than that of a solar PV + battery system. Also a reduced level of noise and local air pollution together with less CO_2 emissions (1.55 kg/kWh) are found in such a system. It's also getting popular while the battery waste needs to be recycled or safely disposed off.

Option	Economics	Environmental impact	Social impact
Solar PV + hydrogen	Unit cost of US$1.5-2.45/ kWh. Initial high capital cost required for investment. Low ongoing maintenance cost. Long life time.	Zero greenhouse emissions in operation. Embodied emission in making the equipment*. No noise as system operation is quiet.	New system requiring user education, and regulations and standards on system performance and safety. Reliability should be on par with conventional RAPS system, though actual experience is required to prove this. Added safety precautions are required due to the hydrogen gas storage.
Diesel generator + battery	Unit cost of power is in the range of around US$1.69-1.90 /kWh Initial capital investment is relatively low. Incurs a Fuel transportation cost.	Emissions per kWh = 3 kg CO2-e. Local air pollution Embodied emissions in making equipment* Noisy. Toxicity of electrolyte and electrodes in battery, hence safe disposal or recycling are needed	Users are familiar with system Mature technology Frequent maintenance needed. Diesel engine and batteries may need replacing every 5–10 years. Proven safe operation, but electrical short circuit may occur
Solar PV + battery	Unit cost of power is US$ 2.68-2.80/kWh. Initial investment cost is higher than diesel system but less than solar hydrogen system.	Zero greenhouse emissions in operation. Embodied emission in making equipment* Toxicity of electrolyte and electrodes in battery, hence safe disposal or recycling are needed	Becoming increasingly common among users. Batteries likely to require frequent attention and replacement System can be reliable if adequate PV area and battery storage are installed. But high cost to ensure no periods of limited supply

Solar PV + battery + diesel generator	Unit cost of power US $2.19-2.26/kWh Initial investment cost is less than the PV alone system due to the reduced PV panel size. Diesel generator incurs added fuel transportation cost.	Emissions per kWh = 1.55 kg CO2-e. Local air pollution, but less than diesel – battery. Embodied emissions in making equipment* Batteries contain toxic materials, so must be disposed of safely or recycled (but less batteries needed than PV-battery	Becoming increasingly common among users. Batteries and diesel engine likely to require frequent maintenance, and replacement. System is noisy due to the diesel generator.

Table 37- Over all triple bottom line evaluation of RAPS systems.

8. CONCLUSIONS AND RECOMMENDATIONS

8.1 CONCLUSIONS

8.1.1 This thesis

The present thesis has focused exclusively on solar-hydrogen systems for remote area applications. The work presented in this thesis leads to a clearer understanding of the technical merits, and economic, environmental and social aspects, of solar-hydrogen systems for RAPS applications compared with the main alternatives. The solar radiation data incorporated in this work are specific to a south-eastern Australian location and the assumed cost factors are consistent with present market values of the system components.

In the present work, two experimental solar –hydrogen systems have been designed and constructed, and tested:

- A 50 W PEM electrolyser and 10 W PEM fuel cell system
- A 200 W PEM electrolyser and 500 W PEM fuel cell system

Experimental data obtained from the PEM electrolysers and PEM fuel cells have been compared with the manufacturers' predicted performances, and are used as key inputs to the computer modeling components of this study.

A mathematical model based on Excel spreadsheets and Visual Basic for determining the key characteristics of a solar photovoltaic - hydrogen system for RAPS, given the load to be met and the characteristics of the Proton Exchange Membrane (PEM) electrolyser and PEM fuel cell employed, has been developed. The primary objective of the model is to determine the size of each individual component of the solar-hydrogen system that yields the lowest unit cost of power supplied over a specified period. The model allows two different strategies for determining storage capacity to be compared: 'unconstrained storage', that is, allowing sufficient capacity to store all the hydrogen produced by excess PV power over load; and 'constrained storage', that is, limiting storage capacity to an economic minimum. The minimum unit costs of generated power can be evaluated for a

range of constrained-storage capacities assuming the unit cost of all other components, namely electrolyser, fuel cell, and balance of system, remain constant.

The model has been applied to a case study of electricity supply to a remote homestead in south-eastern Australia. All the major parameters such as electrical load requirement and solar radiation for the particular conditions are fed into the model. The model run is carried out for the unconstrained and constrained storage conditions. For each condition the cost of power generation is evaluated by varying the assumed hydrogen storage cost while keeping the rest of the assumed unit costs fixed to typical values found in the literature. In the unconstrained storage condition, a PV area of 18.3 m^2 is required and a storage capacity of 13.1 kg of hydrogen. A substantial amount of hydrogen storage between from summer to winter takes place. 42% of the annual load is met by the PV array and 58% by using hydrogen from storage in the fuel cell. The unit cost of power supplied varies from \$1.43/kWh for a unit storage cost of \$500/kg of hydrogen to \$2.42/kWh at \$2000/kg.

A number of experimental investigations for storing hydrogen storage at relatively low pressure, especially those pressure ranges achievable using a PEM electrolyser without external compressor, are reported such as

- Acrylic cylinders (9.7 litre) for laboratory experiment use
- Fibre reinforced plastic water tanks (225 litre)
- Composite cylinders (for pressures up to 20 bar)
- Low-carbon steel (up to 20 bar) cylinders

The acryclic cylinders and FRP water tank based hydrogen storage are assessed based on certain evaluative criteria, such as mass and volumetric energy density, loss rate, hydrogen permeation, safety and cost per unit mass of hydrogen stored. The theoretical loss of hydrogen for acrylic system over a period of 50 days was calculated to be around 3% by mass as against an experimentally measured loss of 22% over the same period. Similarly for the FRP water tank the theoretical loss of hydrogen over 45 days was found to be around 5% by mass while actual experimental loss of hydrogen over this period was measured to be almost 11%. Design improvements that would reduce the incidence of hydrogen leakage in cylinders are identified as follows

- Preferring a container with a seamless containment surface

- Avoiding any fitting directly exposed to the stored hydrogen by using a vertical pipe that enters the cylinder from a fitting at the bottom, and then rises through the water to just below the top surface of cylinder.
- Using sensitive hydrogen leak detectors sealing off any possible additional leaks that might have escaped hydraulic and pneumatic leak test.

A triple bottom line evaluation methodology covering economic, social and environmental factors was employed to assess both the technological strengths and weakness of solar-hydrogen system in comparison to other RAPS alternative. The solar hydrogen system gives a unit cost of power in the rage of US$ 1.5 - 2.45/kWh depending upon the unit storage cost of hydrogen which was taken as a variable ranging from US$2000/kg to US $500/kg. A diesel generator + battery storage system offers a unit cost of power in the range of US$1.69-1.90/kWh. A solar PV coupled with battery storage incurs unit cost of power of US2.68-2.80 /kWh with an intermediate initial capital investment cost. While solar-hydrogen and PV battery systems are pollution free (baring the embodied emissions), the diesel generator based systems causes maximum CO2 emissions i.e. 3 kg of CO2 for each kWh of diesel consumed. The solar hydrogen system being in a precommercial stage requires user education and new regulations and standards on system performance with added system. The hydrogen gas storage in particular requires added safety precautions.

8.1.2 Research Questions

Specifically the thesis has addressed the following research questions:

- What is the optimal design for a PEM-based solar hydrogen system to meet a given profile of annual electricity demand at a remote location?
- What is the most cost-efficient hydrogen storage option for small to medium-scale remote area application?
- How do solar hydrogen RAPS systems compare with the conventional diesel generator and PV- battery systems from the triple bottom line point of view?
- What improvements in cost and performance are required to make solar-hydrogen systems competitive with conventional RAPS technologies?
- Which system components in solar hydrogen RAPS systems require further R&D?

The conclusions drawn regarding these questions are now summarised.

8.1.3 Optimal design of solar hydrogen system?

From the model output, it was found that in the unconstrained storage condition a solar-hydrogen system to supply a 5 kWh daily load to a remote homestead in southern Australian would require a PV panel area of 18 m^2, a 1.7 kW electrolyser, a hydrogen storage capacity of 13 kg, and fuel cell size of 0.3 kW. Such systems would yield a unit cost of energy of US$ 2.45/ kWh. The same system with a future target unit storage cost of US$500/kg would offer a unit cost of energy of US$1.5/kWh. In the unconstrained storage condition all of the excess PV power is utilised by the electrolyser to generate hydrogen enabling the system to exploit fully seasonal energy storage from summer to winter. From an energy utilisation point of view, this option is always recommended.

8.1.4 Cost-efficient hydrogen storage option?

From the analysis conducted in this thesis, options for storing hydrogen in solar–hydrogen RAPS systems that are promising and merit further investigation are:

- Fibre reinforced plastic (FRP) tanks, built with a seamless wall (pressure range less than 5 bar)
- Composite gas cylinders (adapted from LPG-type cylinders) (up to 20 bar)
- Low-carbon steel tanks (up to 20 bar).

In addition further investigation into the use of metal hydrides and other solid storage media for hydrogen is required, given that the mass and volume constraints for such systems are generally much more relaxed in the case of stationary remote applications than they are in transport applications.

8.1.5 Triple bottom line comparison with alternatives?

In terms of economics, a solar-hydrogen system supplying 5 kWh/d in a south eastern Australian location offers a unit cost of energy in the range of US$1.5-2.5/ kWh depending on the assumed capital cost of storage (US$500/kg for the lower unit cost, US$2000 for the higher unit cost). This cost range compares with an estimated US$ 1.7-1.9 /kWh for a diesel generator – battery system, US$ 2.2-2.3 /kWh for a diesel generator – PV – battery system, and US$ 2.7-2.8 /kWh for a PV – battery system. Hence if the target storage cost of US$500/kg can be achieved, a solar-hydrogen system will become an economically attractive proposition.

From environmental aspect, the solar hydrogen system is the best option as compared to other diesel and battery based RAPS options, having zero greenhouse emissions in operation. But a full lifecycle assessment of all the options is required to estimate embodied greenhouse emissions associated with making system components and disposing or recycling them at the end of their lifetimes.

A key social impact is the level of safety of a solar-hydrogen system compared to the alternatives. Clearly a full safety regimen for safe storage and usage of hydrogen in RAPS systems must be introduced through a new set of standards and regulations. A program of user education will also be required covering potential benefits of solar-hydrogen systems, and safe operating practices. A properly designed solar-hydrogen system should be able to meet the end-use demand over a full year with a high level of reliability, and without requiring regular maintenance, though further field testing and proving of the technology is still required.

8.1.6 Improvements needed in cost and performance?

The main components of a solar-hydrogen RAPS systems requiring reductions in capital costs and if possible improved performance at the same time are the PV array, the PEM electrolyser, and the PEM fuel cell. In addition, the analysis here has identified the need for developing a safe hydrogen storage system suitable for RAPS applications, with very

low losses over periods of up to six months, which can be obtained for a capital cost of US$ 500/kg or less.

8.1.7 System components that require further R&D ?

The following components and design options for solar-hydrogen RAPS systems need further research and development:

- PV, PEM electrolysers, and PEM fuel cells, to reduce capital costs, improve energy efficiency and extend lifetimes
- The development of a hydrogen storage system suitable for RAPS applications with a capital cost of US$ 500/kg or less.
- The possibility of direct coupling a PV array to a PEM electrolyser (Paul and Andrews 2007) to avoid the need for an expensive dc-to-dc converter and maximum power point tracker
- The use of a unitised regenerative fuel cell instead of a separate electrolyser and fuel cell as it can function in either mode (Doddathimaiya and Andrews 2006)
- The use of the PEM electrolyser to pressurise hydrogen for storage without the need for an external mechanical compressor.
- The design of an overall control system for a solar-hydrogen system

8.2 RECOMMENDATIONS

The author would like to suggest following recommendations for future work on solar-hydrogen systems for RAPS.

- Further experimental testing of the 250 W electrolyser – 500 W fuel cell system should be carried out to measure its performance over an extended period.
- Consideration should be given to designing a heat recovery system to use the thermal output of the fuel cell for water heating purposes.
- The option of collecting the hydrogen that is ventilated to the atmosphere by the fuel cell during open-ended operation, and burning this to provide additional heat for the hot water system or any other auxiliary requirement.

- The modelling work on solar-hydrogen systems should be extended to include:
    - Running scenarios with a more realistic daily load profile that varies from day to day, and season to season, to investigate the effects on system sizing and economics
    - Further sensitivity testing of the results obtained for system component sizes for varying assumed costs of key components, especially the PEM electrolyser and fuel cell.
    - Incorporation into the model the effect of varying ambient temperature on the efficiency of the PV array.
- Research and development into a suitable control system for the overall solar-hydrogen-system should be conducted, covering:
    - Load splitting between final load and electrolyser
    - Switching between hydrogen production and hydrogen utilisation modes
    - Control of the fuel cell subsystem
    - Monitoring the amount of hydrogen in storage.
- Development work into hydrogen storage systems suitable for stationary applications that have a unit capital cost of US$ 500/kg of hydrogen storage should continue in order to exploit the full advantage of seasonal storage of hydrogen in solar-hydrogen RAPS systems. Options worthy of further investigation include:
    - Modified plastic water tanks for low-pressure storage using water displacement method, with walls free from joints and the hydrogen outlet taken from a pipe rising from the bottom of the tank through the water to the top
    - Medium-pressure composite gas cylinders
    - Metal hydrides, given that much lower gravimetric and volumetric densities may be practical in RAPS applications than in vehicles.
- The possible use of unitised regenerative fuel cells – a single cell that can operate in either electrolyser or fuel cell mode as required - solar-hydrogen RAPS systems to lower the combined cost of a separate electrolyser and fuel cell. This options is possible since the electrsolyser and fuel cell are never required to operate at the same time in a solar-hydrogen system of the type investigated in the present work.
- The triple bottom line evaluation of solar-hydrogen systems for RAPS with alternatives such as diesel or petrol generators, batteries with or without PV arrays

needs to be extended to cover a life cycle assessment, in particular of embodied greenhouse gas emissions, of all the main components of these systems.

REFERENCES

ACRE Green Paper 1997. Australian Cooperative Research Centre for Renewable Energy. *Sustainable energy Policy for Australia*.

Adriaens P, Cyndee L. Gruden and John Hull 2003. CICEET progress report . http://ciceet.unh.edu/progressreports/2003/3_2003/adraiens01/index.html visited on 15th Nov 2006.

Agbossou K, Kolhe M, Hamelin J, Bernier, E & Bose TK, 2004, 'Electrolytic Hydrogen Based Renewable Energy System with Oxygen Recovery and Re-utilization', *Renewable Energy*, vol. 29, no. 8, pp.1305-1318

Ahn, S-Y, Shin, S-J, Ha, HY, Hong, S-A, Lee, Y-C, Lim, TW & Oh, I-H 2002, 'Performance and lifetime analysis of the kW-class PEMFC stack', *Journal of Power Sources*, vol. 106, no. 1-2, pp. 295-303.

Akbarzadeh A, 1992, Fundamentals of Remote Area Power Supply Systems (Energy Victoria, Melbourne).

Aki, H, Yamamoto, S, Kondoh, J, Maeda, T, Yamaguchi, H, Murata, A & Ishii, I 2006, 'Fuel cells and energy networks of electricity, heat, and hydrogen in residential areas', *International Journal of Hydrogen Energy*, vol. 31, no. 8, pp. 967-80.

Al-Baghdadi, MARS 2005, 'Modelling of proton exchange membrane fuel cell performance based on semi-empirical equations', *Renewable Energy*, vol. 30, no. 10, pp. 1587-99.

Alcock J L, Shirvill L C, Cracknell R F, 2001, "Compilation of existing safety data on hydrogen and comparative fuels", European Integrated Hydrogen Project II, WP 5, ENK6-CT2000-00442**.**

Ali SM & Andrews J, 2005, '*Low-cost hydrogen storage options for solar hydrogen systems for remote area power supply*', in the proceedings of ANZSES, Nov 28-30 Dunedin, New Zeeland

Alkaner, S & Zhou, P 2006, 'A comparative study on life cycle analysis of molten carbon fuel cells and diesel engines for marine application', *Journal of Power Sources*, vol. 158, no. 1, pp. 188-99.

Alnatheer, O 2005, 'The potential contribution of renewable energy to electricity supply in Saudi Arabia', *Energy Policy*, vol. 33, no. 18, pp. 2298-312.

Andrews J, Doddathimmaiah AK, Ali S M, Akberzadeh A.2005, 'solar hydrogen systems for remote area power supply from a triple bottom line perspective', in the proceedings of *solar world congress*, Florida, USA.

Aurora P and Duffy J 2005, "Solar Hydrogen Fuel Cell Modelling", in the proceedings of the 2005 *Solar World Congress*, International Solar Energy Society.

Balachandran, U, Lee, TH, Wang, S & Dorris, SE 2004, 'Use of mixed conducting membranes to produce hydrogen by water dissociation', *International Journal of Hydrogen Energy*, vol. 29, no. 3, pp. 291-6.

Bao, C, Ouyang, M & Yi, B 2006, 'Analysis of the water and thermal management in proton exchange membrane fuel cell systems', *International Journal of Hydrogen Energy*, vol. 31, no. 8, pp. 1040-57.

Bao C, Ouyang M & Yi B 2006, 'Modeling and control of air stream and hydrogen flow with recirculation in a PEM fuel cell system--II. Linear and adaptive nonlinear control', *International Journal of Hydrogen Energy*, vol. 31, no. 13, pp. 1897-913.

Barbir F 2005,'PEM electrolysis for production of hydrogen from renewable energy sources', Solar Energy, vol. 78, pp. 661-669.

BCS, 2005 Fuel cell manual for 10 cell 10 W stacks.

Bechrakis, DA, McKeogh, EJ & Gallagher, PD 2006, 'Simulation and operational assessment for a small autonomous wind-hydrogen energy system', *Energy Conversion and Management*, vol. 47, no. 1, pp. 46-59.

Belkic, D 1999, 'Double detachment in collisions between protons and negative hydrogen ions', *Nuclear Instruments and Methods in Physics Research Section B: Beam Interactions with Materials and Atoms*, vol. 154, no. 1-4, pp. 62-72.

Benson R, Claude J, Hansen E and Sarantos C 2004 , Laboratory report, Material processing laboratory, Massachusetts Institute of Technology, USA. http://web.mit.edu/3.082/www/team3_s02/materials.html, website visited on January 2006

Berg, P, Novruzi, A & Promislow, K 2006, 'Analysis of a cathode catalyst layer model for a polymer electrolyte fuel cell', *Chemical Engineering Science*, vol. 61, no. 13, pp. 4316-31.

Bernay, C, Marchand, M & Cassir, M 2002, 'Prospects of different fuel cell technologies for vehicle applications', *Journal of Power Sources*, vol. 108, no. 1-2, pp. 139-52.

Betournay, MC, Bonnell, G, Edwardson, E, Paktunc, D, Kaufman, A & Lomma, AT 2004, 'The effects of mine conditions on the performance of a PEM fuel cell', *Journal of Power Sources*, vol. 134, no. 1, pp. 80-7.

Bischoff, M 2006, 'Large stationary fuel cell systems: Status and dynamic requirements', *Journal of Power Sources*, vol. 154, no. 2, pp. 461-6.

Blunk, R, Zhong, F & Owens, J 2006, 'Automotive composite fuel cell bipolar plates: Hydrogen permeation concerns', *Journal of Power Sources*, vol. 159, no. 1, pp. 533-42.

Bonville, LJ, Kunz, HR, Song, Y, Mientek, A, Williams, M, Ching, A & Fenton, JM 2005, 'Development and demonstration of a higher temperature PEM fuel cell stack', *Journal of Power Sources*, vol. 144, no. 1, pp. 107-12.

Borruto, A, Palma, F & Iavarone, M 2003, 'Hydrogen-steel interaction: relationship between variations of mechanical properties of AISI 304 steel and hydrogen content', *International Journal of Hydrogen Energy*, vol. 28, no. 8, pp. 881-7.

Busquet, S, Hubert, CE, Labbe, J, Mayer, D & Metkemeijer, R 2004, 'A new approach to empirical electrical modelling of a fuel cell, an electrolyser or a regenerative fuel cell', *Journal of Power Sources*, vol. 134, no. 1, pp. 41-8.

Carnes, B & Djilali, N 2006, 'Analysis of coupled proton and water transport in a PEM fuel cell using the binary friction membrane model', *Electrochimica Acta*, vol. 52, no. 3, pp. 1038-52.

Celik, AN 2003, 'Long-term energy output estimation for photovoltaic energy systems using synthetic solar irradiation data', *Energy*, vol. 28, no. 5, pp. 479-93.

Chan, SH, Xia, ZT & Wei, ZD 2006, 'Matching of critical parameters in a small non-pressurized non-humidified PEMFC stack', *Journal of Power Sources*, vol. 158, no. 1, pp. 385-91.

Chang, P, Kim, G-S, Promislow, K & Wetton, B 'Reduced dimensional computational models of polymer electrolyte membrane fuel cell stacks', *Journal of Computational Physics*, vol. In Press, Corrected Proof, p. 863.

Chang, PAC, St-Pierre, J, Stumper, J & Wetton, B 2006, 'Flow distribution in proton exchange membrane fuel cell stacks', *Journal of Power Sources*, vol. 162, no. 1, pp. 340-55.

Chisaka, M & Daiguji, H 2006, 'Effect of glycerol on micro/nano structures of catalyst layers in polymer electrolyte membrane fuel cells', *Electrochimica Acta*, vol. 51, no. 23, pp. 4828-33.

Choi, W, Howze, JW & Enjeti, P 2006, 'Development of an equivalent circuit model of a fuel cell to evaluate the effects of inverter ripple current', *Journal of Power Sources*, vol. 158, no. 2, pp. 1324-32.

Choi, KH, Park, DJ, Rho, YW, Kho, YT & Lee, TH 1998, 'A study of the internal humidification of an integrated PEMFC stack', *Journal of Power Sources*, vol. 74, no. 1, pp. 146-50.

Conibeer, GJ & Richards, BS 'A comparison of PV/electrolyser and photoelectrolytic technologies for use in solar to hydrogen energy storage systems', *International Journal of Hydrogen Energy*, vol. In Press, Corrected Proof.

Conte, M, Iacobazzi, A, Ronchetti, M & Vellone, R 2001, 'Hydrogen economy for a sustainable development: state-of-the-art and technological perspectives', *Journal of Power Sources*, vol. 100, no. 1-2, pp. 171-87.

Corbo, P, Corcione, FE, Migliardini, F & Veneri, O 2006, 'Experimental assessment of energy-management strategies in fuel-cell propulsion systems', *Journal of Power Sources*, vol. 157, no. 2, pp. 799-808.

Crank J 1968, *Diffusion in Polymers*, Academic Press, London.

Damen, K, Troost, Mv, Faaij, A & Turkenburg, W 2006, 'A comparison of electricity and hydrogen production systems with CO2 capture and storage. Part A: Review and selection of promising conversion and capture technologies', *Progress in Energy and Combustion Science*, vol. 32, no. 2, pp. 215-46.

Dincer I, 2002, 'Technical ,environmental and exergetic aspects of hydrogen energy systems', *International Journal of Hydrogen Energy,* vol. 27 pp.265-285

DOE (2003) "Hydrogen, Fuel Cells & Infrastructure Technologies Program", U.S. Department of Energy, Energy Efficiency and Renewable Energy.

Doukas, H, Patlitzianas, KD, Kagiannas, AG & Psarras, J 2006, 'Renewable energy sources and rationale use of energy development in the countries of GCC: Myth or reality?' *Renewable Energy*, vol. 31, no. 6, pp. 755-70.

Du, CY, Yang, T, Shi, PF, Yin, GP & Cheng, XQ 2006, 'Performance analysis of the ordered and the conventional catalyst layers in proton exchange membrane fuel cells', *Electrochimica Acta*, vol. 51, no. 23, pp. 4934-41.

Dunn S. 2000: Micropower: The Next Electrical Era. Worldwatch Paper 151. Worldwatch Institute, Washington D.C., US

Dunn S. 2001: *Hydrogen Futures*: *Towards a Sustainable Energy System Worldwatch Paper 157*. Worldwatch Institute, Washington D.C., US.

Elkington, J., 1999, *Cannibals with Forks: The Triple Bottom Line of 21st Century Business* (Capstone Publishing, Oxford).

Erdmann, G 2003, 'Future economics of the fuel cell housing market', *International Journal of Hydrogen Energy*, vol. 28, no. 7, pp. 685-94.

Faber, A, Idenburg, AM & Wilting, HC 2007, 'Exploring techno-economic scenarios in an input-output model', *Futures*, vol. 39, no. 1, pp. 16-37.

Feitelberg, AS & Rohr, J, Donald F. 2005, 'Operating line analysis of fuel processors for PEM fuel cell systems', *International Journal of Hydrogen Energy*, vol. 30, no. 11, pp. 1251-7.

Ferng, YM, Tzang, YC, Pei, BS, Sun, CC & Su, A 2004, 'Analytical and experimental investigations of a proton exchange membrane fuel cell', *International Journal of Hydrogen Energy*, vol. 29, no. 4, pp. 381-91.

Garrity, L 2002, *The Hydrogen Economy*, sustainability background paper, State Sustainability Strategy CD-ROM, Department of the Premier and Cabinet, Perth.

Ghosh, PC, Emonts, B & Stolten, D 2003, 'Comparison of hydrogen storage with diesel-generator system in a PV-WEC hybrid system', *Solar Energy*, vol. 75, no. 3, pp. 187-98.

Green, MA 2000, 'Photovoltaics: technology overview', *Energy Policy*, vol. 28, no. 14, pp. 989-98.

Grigoriev S A, Lyutikovaa E K, SMartemianovb, Fateeva VN 2007,' On the possibility of replacement of Pt by Pd in a hydrogen electrode of PEM fuel cells, *International Journal of Hydrogen Energy,* article on press.

Hamelin, J, Agbossou, K, Laperriere, A, Laurencelle, F & Bose, TK 2001, 'Dynamic behavior of a PEM fuel cell stack for stationary applications', *International Journal of Hydrogen Energy*, vol. 26, no. 6, pp. 625-9.

Han, J-N, Park, G-G, Yoon, Y-G, Yang, T-H, Lee, W-Y & Kim, C-S 2003, 'A new evaluation method of anode/cathode used for polymer electrolyte membrane fuel cell', *International Journal of Hydrogen Energy*, vol. 28, no. 6, pp. 609-13.

Hawkes, AD, Aguiar, P, Hernandez-Aramburo, CA, Leach, MA, Brandon, NP, Green, TC & Adjiman, CS 2006, 'Techno-economic modelling of a solid oxide fuel cell stack for micro combined heat and power', *Journal of Power Sources*, vol. 156, no. 2, pp. 321-33.

Hermann, A, Chaudhuri, T & Spagnol, P 2005, 'Bipolar plates for PEM fuel cells: A review', *International Journal of Hydrogen Energy*, vol. 30, no. 12, pp. 1297-302.

Hollmuller, P, Joubert, J-M, Lachal, B & Yvon, K 2000, 'Evaluation of a 5 kWp photovoltaic hydrogen production and storage installation for a residential home in Switzerland', *International Journal of Hydrogen Energy*, vol. 25, no. 2, pp. 97-109.

Hsieh, S-S, Feng, C-L & Huang, C-F 2006, 'Development and performance analysis of a H2/air micro PEM fuel cell stack', *Journal of Power Sources*, vol. 163, no. 1, pp. 440-9.

Hu, M, Sui, S, Zhu, X, Yu, Q, Cao, G, Hong, X & Tu, H 2006, 'A 10 kW class PEM fuel cell stack based on the catalyst-coated membrane (CCM) method', *International Journal of Hydrogen Energy*, vol. 31, no. 8, pp. 1010-8.

Hwang, J-J & Hwang, H-S 2002, 'Parametric studies of a double-cell stack of PEMFC using Grafoil(TM) flow-field plates', *Journal of Power Sources*, vol. 104, no. 1, pp. 24-32.

Hwang, JJ, Wang, DY & Shih, NC 2005, 'Development of a lightweight fuel cell vehicle', *Journal of Power Sources*, vol. 141, no. 1, pp. 108-15.

HYTREC report 2006, Hydrogen Technology Research Centre, http://www.hytrec.no/hvorfor2.aspx visited on Nov 2006

Inoue, G, Matsukuma, Y & Minemoto, M 2006, 'Effect of gas channel depth on current density distribution of polymer electrolyte fuel cell by numerical analysis including gas flow through gas diffusion layer', *Journal of Power Sources*, vol. 157, no. 1, pp. 136-52.

Inoue, G, Yoshimoto, T, Matsukuma, Y, Minemoto, M, Itoh, H & Tsurumaki, S 2006, 'Numerical analysis of relative humidity distribution in polymer electrolyte fuel cell stack including cooling water', *Journal of Power Sources*, vol. 162, no. 1, pp. 81-93.

IPCC 1995, *IPCC Guidelines for Greenhouse Gas Inventories-Volume 1: greenhouse gas inventory reporting instructions*, Intergovernmental Panel on Climate Change, Geneva

Isherwood, W, Smith, JR, Aceves, SM, Berry, G, Clark, W, Johnson, R, Das, D, Goering, D & Seifert, R 2000, 'Remote power systems with advanced storage technologies for Alaskan villages', *Energy*, vol. 25, no. 10, pp. 1005-20.

Ivy, J. (2004) 'Summary of electrolytic hydrogen production', *Milestone Completion Report*, NREL/MP-560-36734, National Renewable Energy Laboratory, September, http://www.nrel.gov/docs/fy04osti/36734.pdf visited on July 2006

Jarvis, LP, Atwater, TB, Plichta, EJ & Cygan, PJ 1998, 'Power assisted fuel cell', *Journal of Power Sources*, vol. 70, no. 2, pp. 253-7.

Johnson, R, Morgan, C, Witmer, D & Johnson, T 2001, 'Performance of a proton exchange membrane fuel cell stack', *International Journal of Hydrogen Energy*, vol. 26, no. 8, pp. 879-87.

Ju, H, Meng, H & Wang, C-Y 2005, 'A single-phase, non-isothermal model for PEM fuel cells', *International Journal of Heat and Mass Transfer*, vol. 48, no. 7, pp. 1303-15.

Jung, H-M, Lee, W-Y, Park, J-S & Kim, C-S 2004, 'Numerical analysis of a polymer electrolyte fuel cell', *International Journal of Hydrogen Energy*, vol. 29, no. 9, pp. 945-54.

Kaplanis, SN 2006, 'New methodologies to estimate the hourly global solar radiation; Comparisons with existing models', *Renewable Energy*, vol. 31, no. 6, pp. 781-90.

Kazim, A. 2005,"Exergoeconomic analysis of a PEM fuel cell at various operating conditions." *Energy Conversion and Management,* vol. 46, no.7-8, pp. 1073-1081.

Kim, SY & Kim, WN 'Effect of cathode inlet manifold configuration on performance of 10-cell proton-exchange membrane fuel cell', *Journal of Power Sources*, vol. In Press, Corrected Proof, p. 252.

Klemes, J, Bulatov, I & Cockerill, T 2007, 'Techno-economic modeling and cost functions of CO2 capture processes', *Computers & Chemical Engineering*, vol. 31, no. 5-6, pp. 445-55.

Koh, J-H, Hsu, AT, Akay, HU & Liou, M-F 2005, 'Analysis of overall heat balance in self-heated proton-exchange-membrane fuel cells for temperature predictions', *Journal of Power Sources*, vol. 144, no. 1, pp. 122-8.

Kolhe, M, Agbossou, K, Hamelin, J & Bose, TK 2003, 'Analytical model for predicting the performance of photovoltaic array coupled with a wind turbine in a stand-alone renewable energy system based on hydrogen', *Renewable Energy*, vol. 28, no. 5, pp. 727-42.

Koroneos, C, Dompros, A, Roumbas, G & Moussiopoulos, N 2004, 'Life cycle assessment of hydrogen fuel production processes', *International Journal of Hydrogen Energy*, vol. 29, no. 14, pp. 1443-50.

Kothare, MV 2006, 'Dynamics and control of integrated microchemical systems with application to micro-scale fuel processing', *Computers & Chemical Engineering*, vol. 30, no. 10-12, pp. 1725-34.

Larminie J, Dicks A, 2003. Fuel Cell Systems Explained. John Wiley & Sons, Ltd., Chichester.

Lee, JH & Lalk, TR 1998, 'Modeling fuel cell stack systems', *Journal of Power Sources*, vol. 73, no. 2, pp. 229-41.

Lee, JH, Lalk, TR & Appleby, AJ 1998, 'Modeling electrochemical performance in large scale proton exchange membrane fuel cell stacks', *Journal of Power Sources*, vol. 70, no. 2, pp. 258-68.

Lee, T-W, Hur, J, Lee, B-K & Won, C-Y 'Design of a fuel cell generation system using a PEMFC simulator', *Electric Power Systems Research*, vol. In Press, Corrected Proof, p. 355.

Lehman PA, Chamberlin CE, Pauletto G & Rocheleau MA 1994 'Operating experience with a Photovoltaic-hydrogen Energy System', Hydrogen '94: *The 10th World Hydrogen Energy Conference*, June 20-24, 1994, Cocoa Beach, Florida.

Li, X & Sabir, I 2005, 'Review of bipolar plates in PEM fuel cells: Flow-field designs', *International Journal of Hydrogen Energy*, vol. 30, no. 4, pp. 359-71.

Li, X, Cao, G-y & Zhu, X-j 2006, 'Modeling and control of PEMFC based on least squares support vector machines', *Energy Conversion and Management*, vol. 47, no. 7-8, pp. 1032-50.

Licht, S, Wang, B, Mukerji, S, Soga, T, Umeno, M & Tributsch, H 2001, 'Over 18% solar energy conversion to generation of hydrogen fuel; theory and experiment for efficient solar water splitting', *International Journal of Hydrogen Energy*, vol. 26, no. 7, pp. 653-9.

Lodhi, MAK 1997, 'Photovoltaics and hydrogen: Future energy options', *Energy Conversion and Management*, vol. 38, no. 18, pp. 1881-93.

Luo, Z, Li, D, Tang, H, Pan, M & Ruan, R 2006, 'Degradation behavior of membrane-electrode-assembly materials in 10-cell PEMFC stack', *International Journal of Hydrogen Energy*, vol. 31, no. 13, pp. 1831-7.

Lutz, AE, Larson, RS & Keller, JO 2002, 'Thermodynamic comparison of fuel cells to the Carnot cycle', *International Journal of Hydrogen Energy*, vol. 27, no. 10, pp. 1103-11.

Maharudrayya, S, Jayanti, S & Deshpande, AP 2006, 'Pressure drop and flow distribution in multiple parallel-channel configurations used in proton-exchange membrane fuel cell stacks', *Journal of Power Sources*, vol. 157, no. 1, pp. 358-67.

Malik, A 2007, 'Environmental challenge vis a vis opportunity: The case of water hyacinth', *Environment International*, vol. 33, no. 1, pp. 122-38.

Mankins, JC 1997, 'A fresh look at space solar power: New architectures, concepts and technologies', *Acta Astronautica*, vol. 41, no. 4-10, pp. 347-59.

Marchi, CS, Somerday, BP & Robinson, SL 2007, 'Permeability, solubility and diffusivity of hydrogen isotopes in stainless steels at high gas pressures', *International Journal of Hydrogen Energy*, vol. 32, no. 1, pp. 100-16.

McLellan, B, Shoko, E, Dicks, AL & Diniz da Costa, JC 2005, 'Hydrogen production and utilisation opportunities for Australia', *International Journal of Hydrogen Energy*, vol. 30, no. 6, pp. 669-79.

Mehta, V & Cooper, JS 2003, 'Review and analysis of PEM fuel cell design and manufacturing', *Journal of Power Sources*, vol. 114, no. 1, pp. 32-53.

Mennola, T, Mikkola, M, Noponen, M, Hottinen, T & Lund, P 2002, 'Measurement of ohmic voltage losses in individual cells of a PEMFC stack', *Journal of Power Sources*, vol. 112, no. 1, pp. 261-72.

Mert, SO, Dincer, I & Ozcelik, Z 2007, 'Exergoeconomic analysis of a vehicular PEM fuel cell system', *Journal of Power Sources*, vol. 165, no. 1, pp. 244-52.

Mishra, V, Yang, F & Pitchumani, R 2005, 'Analysis and design of PEM fuel cells', *Journal of Power Sources*, vol. 141, no. 1, pp. 47-64.

Moreira, J, Ocampo, AL, Sebastian, PJ, A. Smit, M, Salazar, MD, del Angel, P, Montoya, JA, Perez, R & Martinez, L 2003, 'Influence of the hydrophobic material content in the gas diffusion electrodes on the performance of a PEM fuel cell', *International Journal of Hydrogen Energy*, vol. 28, no. 6, pp. 625-7.

Nafeh A and Fahmy F 2002 *'Comparative Study between FLC and PI Controller Applied for MPPT of a PV System',* Electronics Research Institute and E. El-Zahab, Cairo University, EGYPT

NASA (1997) "Safety Standard for Hydrogen and Hydrogen Systems", Office of Safety and Mission Assurance, USA.

Nelson, DB, Nehrir, MH & Wang, C 2006, 'Unit sizing and cost analysis of stand-alone hybrid wind/PV/fuel cell power generation systems', *Renewable Energy*, vol. 31, no. 10, pp. 1641-56.

Onovwiona, HI, Ismet Ugursal, V & Fung, AS 2007, 'Modeling of internal combustion engine based cogeneration systems for residential applications', *Applied Thermal Engineering*, vol. 27, no. 5-6, pp. 848-61.

Oszcipok, M, Veda, M, Riemann, D & Geckeler, D 2006, 'Low temperature operation and influence parameters on the cold start ability of portable PEMFCs', *Journal of Power Sources*, vol. 154, no. 2, pp. 404-11.

Paul B and Andrews J 2007, 'Direct coupling of photovoltaic panels with PEM electrolyser in Solar-hydrogen systems', in the proceedings of the 3rd *IASTED Asian conference, Power and Energy Systems,* April 2-4, 2007

Park, J & Li, X 2007, 'An experimental and numerical investigation on the cross flow through gas diffusion layer in a PEM fuel cell with a serpentine flow channel', *Journal of Power Sources*, vol. 163, no. 2, pp. 853-63.

Passey, R., MacGill, I., Nolles, K. and Outhred, H. (2005) *The NSW Greenhouse Gas Abatement Scheme: An analysis of the NGAC Registry for the 2003 Compliance Period.* Discussion Paper DP_050405, Centre for Energy and Environmental Markets, University of NSW.

Pehnt, M 2001, 'Life-cycle assessment of fuel cell stacks', *International Journal of Hydrogen Energy*, vol. 26, no. 1, pp. 91-101.

Pei, P, Ouyang, M, Feng, W, Lu, L, Huang, H & Zhang, J 2006, 'Hydrogen pressure drop characteristics in a fuel cell stack', *International Journal of Hydrogen Energy*, vol. 31, no. 3, pp. 371-7.

Perz, EW & Bergmann, S 2007, 'A simulation environment for the techno-economic performance prediction of water and power cogeneration systems using renewable and fossil energy sources', *Desalination*, vol. 203, no. 1-3, pp. 337-45.

Pischinger, S, Schonfelder, C & Ogrzewalla, J 2006, 'Analysis of dynamic requirements for fuel cell systems for vehicle applications', *Journal of Power Sources*, vol. 154, no. 2, pp. 420-7.

Prasanna, M, Cho, EA, Kim, H-J, Oh, I-H, Lim, T-H & Hong, S-A 'Performance of proton-exchange membrane fuel cells using the catalyst-gradient electrode technique', *Journal of Power Sources*, vol. In Press, Corrected Proof, p. 252.

Priestnall, MA, Kotzeva, VP, Fish, DJ & Nilsson, EM 2002, 'Compact mixed-reactant fuel cells', *Journal of Power Sources*, vol. 106, no. 1-2, pp. 21-30.

Prince-Richard, S, Whale, M & Djilali, N 2005, 'A techno-economic analysis of decentralized electrolytic hydrogen production for fuel cell vehicles', *International Journal of Hydrogen Energy*, vol. 30, no. 11, pp. 1159-79.

Pukrushpan, J, Stefanopoulou, A, Varigonda, S, Eborn, J & Haugstetter, C 2006, 'Control-oriented model of fuel processor for hydrogen generation in fuel cell applications', *Control Engineering Practice*, vol. 14, no. 3, pp. 277-93.

Qi, Z, Tang, H, Guo, Q & Du, B 2006, 'Investigation on "saw-tooth" behavior of PEM fuel cell performance during shutdown and restart cycles', *Journal of Power Sources*, vol. 161, no. 2, pp. 864-71.

Raison, RJ 2006, 'Opportunities and impediments to the expansion of forest bioenergy in Australia', *Biomass and Bioenergy*, vol. 30, no. 12, pp. 1021-4.

Rajalakshmi, N, Raja, M & Dhathathreyan, KS 2002, 'Evaluation of current distribution in a proton exchange membrane fuel cell by segmented cell approach', *Journal of Power Sources*, vol. 112, no. 1, pp. 331-6.

Richards, BS & Conibeer, GJ 'A comparison of hydrogen storage technologies for solar-powered stand-alone power supplies: A photovoltaic system sizing approach', *International Journal of Hydrogen Energy*, vol. In Press, Corrected Proof.

Research Institute for Sustainable Energy 2007, http://www.rise.org.au visited on Jan 2007

Rowe, A & Li, X 2001, 'Mathematical modeling of proton exchange membrane fuel cells', *Journal of Power Sources*, vol. 102, no. 1-2, pp. 82-96.

Rydh, CJ & Sanden, BA 2005, 'Energy analysis of batteries in photovoltaic systems. Part II: Energy return factors and overall battery efficiencies', *Energy Conversion and Management*, vol. 46, no. 11-12, pp. 1980-2000.

Sanborn Scott, D 2004, 'Inside fuelcells', *International Journal of Hydrogen Energy*, vol. 29, no. 12, pp. 1203-11.

Santarelli, M & Macagno, S 2004, 'A thermoeconomic analysis of a PV-hydrogen system feeding the energy requests of a residential building in an isolated valley of the Alps', *Energy Conversion and Management*, vol. 45, no. 3, pp. 427-51.

Santarelli, M, Cali, M & Macagno, S 2004, 'Design and analysis of stand-alone hydrogen energy systems with different renewable sources', *International Journal of Hydrogen Energy*, vol. 29, no. 15, pp. 1571-86.

Santilli, RM & Shillady, DD 2000, 'A new isochemical model of the water molecule', *International Journal of Hydrogen Energy*, vol. 25, no. 2, pp. 173-83.

Schatz Energy Research Center, 2003, http://www.humboldt.edu/~serc/pr.html, website visited on 13th aug 2005.

Schucan, T, 2000, *'International energy agency hydrogen implementing agreement task 11: Integrated systems – Final report of subtask A : Case studies of Integrated Hydrogen energy systems*, viewed 8 March 2005,www.ieahia.org/pdfs/chapter11.pdf

Scherer, GWH & Newson, E 1998, 'Analysis of the seasonal energy storage of hydrogen in liquid organic hydrides', *International Journal of Hydrogen Energy*, vol. 23, no. 1, pp. 19-25.

Semelsberger, TA & Borup, RL 2005, 'Fuel effects on start-up energy and efficiency for automotive PEM fuel cell systems', *International Journal of Hydrogen Energy*, vol. 30, no. 4, pp. 425-35.

Shaahid, SM & Elhadidy, MA 'Technical and economic assessment of grid-independent hybrid photovoltaic-diesel-battery power systems for commercial loads in desert environments', *Renewable and Sustainable Energy Reviews*, vol. In Press, Corrected Proof, p. 333.

Shakya B D, Aye L and Musgrave P. (2005), "Technical Feasibility and Financial Analysis of Hybrid Wind-Photovoltaic System with Hydrogen Storage for Cooma", *Int J Hydrogen Energy* (30) 9-20

Shayegan, S, Hart, D, Pearson, P & Joffe, D 2006, 'Analysis of the cost of hydrogen infrastructure for buses in London', *Journal of Power Sources*, vol. 157, no. 2, pp. 862-74.

Pyle, W 2003,*Solar hydrogen Chronicle, A hands on guide to solar hydrogen fuel: production, purification ,storage, utilization*, Weelok Mountain Publications, Weelock VT USA

Sjardin, M, Damen, KJ & Faaij, APC 2006, 'Techno-economic prospects of small-scale membrane reactors in a future hydrogen-fuelled transportation sector', *Energy*, vol. 31, no. 14, pp. 2523-55.

Stamps, AT & Gatzke, EP 2006, 'Dynamic modeling of a methanol reformer--PEMFC stack system for analysis and design', *Journal of Power Sources*, vol. 161, no. 1, pp. 356-70.

Sustainable Energy Development Office, http://www1.sedo.energy.wa.gov.au/, website visited on 16th August 2006

Tanaka, T, Otsuka, K, Oyakawa, K & Watanabe, S 2005, 'Development of a performance test method for PEFC stack', *Journal of Power Sources*, vol. 147, no. 1-2, pp. 208-13.

Tanrioven, M & Alam, MS 2006, 'Reliability modeling and analysis of stand-alone PEM fuel cell power plants', *Renewable Energy*, vol. 31, no. 7, pp. 915-33.

Tawfik, H, Hung, Y & Mahajan, D 2007, 'Metal bipolar plates for PEM fuel cell--A review', *Journal of Power Sources*, vol. 163, no. 2, pp. 755-67.

Thomas C. E. and James, B. D. 1998. *Analysis of Utility Hydrogen Systems,* DOE Report, Contract No. ACG-8-18012-01.

Tina, G, Gagliano, S & Raiti, S 2006, 'Hybrid solar/wind power system probabilistic modelling for long-term performance assessment', *Solar Energy*, vol. 80, no. 5, pp. 578-88.

Tsuchiya, H & Kobayashi, O 2004, 'Mass production cost of PEM fuel cell by learning curve', *International Journal of Hydrogen Energy*, vol. 29, no. 10, pp. 985-90.

Tzimas E, Filiou C, Perves S D, Veyret J B 2003,'Hydrogen storage: state of art and future perspective, European Commission, Directorate general Joint Research Centre (DG JRC) Institute of Energy,Petten, Netherlands.

Ulleberg Ø, Miland, H. HYTREC wind/electrolysis system. Kjeller 2006-09-22. IFE/KR/F-2006/125

Verduzco, LE, Duffey, MR & Deason, JP 2007, 'H2POWER: Development of a methodology to calculate life cycle cost of small and medium-scale hydrogen systems', *Energy Policy*, vol. 35, no. 3, pp. 1808-18.

Vynnycky, M 'On the modelling of two-phase flow in the cathode gas diffusion layer of a polymer electrolyte fuel cell', *Applied Mathematics and Computation*, vol. In Press, Corrected Proof, p. 863.

Wagner, N & Schulze, M 2003, 'Change of electrochemical impedance spectra during CO poisoning of the Pt and Pt-Ru anodes in a membrane fuel cell (PEFC)', *Electrochimica Acta*, vol. 48, no. 25-26, pp. 3899-907.

Wagner, N & Gulzow, E 2004, 'Change of electrochemical impedance spectra (EIS) with time during CO-poisoning of the Pt-anode in a membrane fuel cell', *Journal of Power Sources*, vol. 127, no. 1-2, pp. 341-7.

Wallmark, C & Alvfors, P 2003, 'Technical design and economic evaluation of a stand-alone PEFC system for buildings in Sweden', *Journal of Power Sources*, vol. 118, no. 1-2, pp. 358-66.

Wang, Y & Wang, C-Y 2005, 'Transient analysis of polymer electrolyte fuel cells', *Electrochimica Acta*, vol. 50, no. 6, pp. 1307-15.

Wang, C, Mao, Z, Bao, F, Li, X & Xie, X 2005, 'Development and performance of 5 kw proton exchange membrane fuel cell stationary power system', *International Journal of Hydrogen Energy*, vol. 30, no. 9, pp. 1031-4.

WCED (World Commission on Environment and Development), *Our Common Future*. (Oxford University Press, Oxford, 1987).

Williams, MV, Kunz, HR & Fenton, JM 2004, 'Operation of Nafion(R)-based PEM fuel cells with no external humidification: influence of operating conditions and gas diffusion layers', *Journal of Power Sources*, vol. 135, no. 1-2, pp. 122-34.

Williams, MC, Strakey, JP & Surdoval, WA 2005, 'The U.S. Department of Energy, Office of Fossil Energy Stationary Fuel Cell Program', *Journal of Power Sources*, vol. 143, no. 1-2, pp. 191-6.

Wolf, J., *MRS Bulletin*, 2002, September, p. 684

Yan, W-M, Chen, F, Wu, H-Y, Soong, C-Y & Chu, H-S 2004, 'Analysis of thermal and water management with temperature-dependent diffusion effects in membrane of proton exchange membrane fuel cells', *Journal of Power Sources*, vol. 129, no. 2, pp. 127-37.

Yang, J, Cermakova, J, Uchytil, P, Hamel, C & Seidel-Morgenstern, A 2005, 'Gas phase transport, adsorption and surface diffusion in a porous glass membrane', *Catalysis Today*, vol. 104, no. 2-4, pp. 344-51.

Yoon, Y-G, Park, G-G, Yang, T-H, Han, J-N, Lee, W-Y & Kim, C-S 2003, 'Effect of pore structure of catalyst layer in a PEMFC on its performance', *International Journal of Hydrogen Energy*, vol. 28, no. 6, pp. 657-62.

You, L & Liu, H 2001, 'A parametric study of the cathode catalyst layer of PEM fuel cells using a pseudo-homogeneous model', *International Journal of Hydrogen Energy*, vol. 26, no. 9, pp. 991-9.

Yu, HM, Schumacher, JO, Zobel, M & Hebling, C 2005, 'Analysis of membrane electrode assembly (MEA) by environmental scanning electron microscope (ESEM)', *Journal of Power Sources*, vol. 145, no. 2, pp. 216-22.

Yuan, X, Sun, JC, Blanco, M, Wang, H, Zhang, J & Wilkinson, DP 2006, 'AC impedance diagnosis of a 500 W PEM fuel cell stack: Part I: Stack impedance', *Journal of Power Sources*, vol. 161, no. 2, pp. 920-8.

Zahedi, A 2006, 'Solar photovoltaic (PV) energy; latest developments in the building integrated and hybrid PV systems', *Renewable Energy*, vol. 31, no. 5, pp. 711-8.

Zhang X & Shi, P 2006, 'Nafion effect on dual-bonded structure cathode of PEMFC', *Electrochemistry Communications*, vol. 8, no. 10, pp. 1615-20.

Zhang, Y, Ouyang, M, Lu, Q, Luo, J & Li, X 2004, 'A model predicting performance of proton exchange membrane fuel cell stack thermal systems', *Applied Thermal Engineering*, vol. 24, no. 4, pp. 501-13.

Zhu, WH, Payne, RU & Tatarchuk, BJ 2006, 'Critical flow rate of anode fuel exhaust in a PEM fuel cell system', *Journal of Power Sources*, vol. 156, no. 2, pp. 512-9.

Zoulias, EI & Lymberopoulos, N 2007, 'Techno-economic analysis of the integration of hydrogen energy technologies in renewable energy-based stand-alone power systems', *Renewable Energy*, vol. 32, no. 4, pp. 680-96.

Zugel M and Blackledge S 2002: Clean Energy Solutions, *Energy Efficiency and Renewable Energy in New Mexico* NMPIRG Education Fund.

APPENDICES

A

Technical and production

• 1kg H2 = ~11500 L STP = 100 - 140km driving range

• 150cm tall, 20cm diameter bottle at 700bar = ~3kg H2 = 300km driving distance

• 5kg H2 is required for ~500km driving distance ICE cars

• 5kW water electrolyser, 7h operation = 1kg H2 = 100km driving range

• 360 litres H2 = 1kWh = 3.6MJ

• 1GJ = 277.8kWh = 100,000L H2 = 8.7kg H2

Hydrogen Conversions and Facts

• 1 mol of hydrogen = 2.0 grams = 22.4 standard litres

• Heat of combustion of hydrogen: 241.8 kilojoules / mol of H2 LHZ 15

British thermal units / gram of hydrogen

• 1 kilogram of hydrogen = 33.3 kilowatt-hours =0 .12 giga joules

• 1 standard of cubic foot H2 = 2.53 grams of H2 = 28.32 litres of H2 =.028 cubic metres of H2.

Other fuel comparisons

• 1 kilogram of gasoline = 13.0 kWh

• 1 kilogram of methanol = 5.58 kWh

• 1 kilogram of propane = 12.9 kWh

• 1 kilogram of ethanol = 7.49 kWh

• 1 kilogram of butane = 12.7 kWh

• 1 kilogram of natural gas CH4 = 13.88 kWh

Pressure

1 atmosphere = 1.01 bar = 14.7 pounds per square inch = 1x105 pascals

- Theoretically 1 liter of water can yield 1.24 Nm^3.But the actual water consumption requires 25% more water as a portion of water is lost in oxygen exhaust

Overview - Acrylic, General Purpose, Molded				**Date: 3/7/2006 6:24:25 AM**
KeyWords:				
PMMA; Polymethyl Methacrylate; Polymethylmethacrylate; Plastics, Polymers				
SubCat: Acrylic, Thermoplastic, Polymer				
Properties	**Value**	**Min**	**Max**	**Comment**
Physical				
Density, g/cc	--	1.15	1.19	Average = 1.18 g/cc; Grade Count = 51
Water Absorption, %	--	0.3	2	Average = 0.85%; Grade Count = 27
Moisture Absorption at Equilibrium, %	--	0.3	0.33	Average = 0.3%; Grade Count = 16
Linear Mold Shrinkage, cm/cm	--	0.003	0.0065	Average = 0.0047 cm/cm; Grade Count = 30
Melt Flow, g/10 min	--	0.9	27	Average = 6.2 g/10 min; Grade Count = 45
Mechanical				
Hardness, Rockwell M	--	63	97	Average = 90.6; Grade Count = 26
Tensile Strength, Ultimate, MPa	--	47	79	Average = 68.7 MPa; Grade Count = 41
Tensile Strength, Yield, MPa	--	55	85	Average = 73.5 MPa; Grade Count = 11
Elongation at Break, %	--	1	30	Average = 6%; Grade Count = 48
Elongation at Yield, %	--	4	5	Average = 4.5%; Grade Count = 11
Tensile Modulus, GPa	--	2.2	3.8	Average = 3.1 GPa; Grade Count = 33
Flexural Modulus, GPa	--	3	3.5	Average = 3.3 GPa; Grade Count = 23
Flexural Yield Strength, MPa	--	81	138	Average = 110 MPa; Grade Count = 31
Compressive Yield Strength, MPa	--	100	117	Average = 110 MPa; Grade Count=4
Shear Modulus, GPa	1.4	--	--	Grade Count = 3
Izod Impact, Notched, J/cm	--	0.12	0.2	Average = 0.16 J/cm; Grade Count = 23
Izod Impact, Unnotched, J/cm	2.7	--	--	Grade Count = 1
Charpy Impact, Unnotched, J/cm²	--	1.9	6	Average = 2.6 J/cm²; Grade Count = 16
Charpy Impact, Notched, J/cm²	--	0.2	0.4	Average = 0.24 J/cm²; Grade Count = 16
Gardner Impact, J	--	0.23	1.4	Average = 0.73 J; Grade Count = 7
Tensile Creep Modulus, 1 hour, MPa	--	1800	2700	Average = 2500 MPa; Grade Count = 9

Tensile Creep Modulus, 1000 hours, MPa	--	1200	1800	Average = 1600 MPa; Grade Count = 10
Electrical				
Electrical Resistivity, ohm-cm	--	1.00E+14	1.00E+15	Average = 1e+15 ohm-cm; Grade Count = 20
Surface Resistance, ohm	--	1.00E+14	1.00E+16	Average = 2E+15 ohm; Grade Count = 19
Dielectric Constant	--	2.8	4	Average = 3.2; Grade Count = 23
Dielectric Constant, Low Frequency	--	3	4	Average = 3.5; Grade Count = 23
Dielectric Strength, kV/mm	--	17.7	60	Average = 28.8 kV/mm; Grade Count = 31
Dissipation Factor	--	0.03	0.55	Average = 0.064; Grade Count = 20
Dissipation Factor, Low Frequency	--	0.04	0.55	Average = 0.07; Grade Count = 20
Comparative Tracking Index, V	600	--	--	Grade Count=16
Thermal				
CTE, linear 20°C, µm/m-°C	--	60	130	Average = 72.9 µm/m-°C; Grade Count=27
Specific Heat Capacity, J/g-°C	--	1.46	1.47	Average = 1.5 J/g-K; Grade Count = 10
Thermal Conductivity, W/m-K	--	0.19	0.24	Average = 0.2 W/m-K; Grade Count = 11
Melting Point, °C	130	--	--	Grade Count = 3
Maximum Service Temperature, Air, °C	--	41	103	Average = 85.8°C; Grade Count = 47
Deflection Temperature at 0.46 MPa (66 psi), °C	--	80	103	Average = 94.1°C; Grade Count=18
Deflection Temperature at 1.8 MPa (264 psi), °C	--	41	100	Average = 86.5°C; Grade Count=47
Vicat Softening Point, °C	--	47	117	Average = 94.2°C; Grade Count = 42
Glass Temperature, °C	--	100	105	Average = 100°C; Grade Count = 4
Flammability, UL94	HB	--	--	Grade Count = 36
Oxygen Index, %	18	--	--	Grade Count = 7
Optical				
Refractive Index	--	1.49	1.498	Average = 1.49; Grade Count = 25
Haze, %	--	1	96	Average = 33.2%; Grade Count = 10
Transmission, Visible, %	--	80	93	Average = 89.2%; Grade Count = 42
Processing				
Processing Temperature, °C	--	243	250	Average = 240°C; Grade Count = 6

Table 38– Properties of acrylic material (polymethylmethacylate)

C

SOLAR RADIATION CALCULATIONS:

The total hourly solar radiation (I_T) on the PV panel is evaluated from the following equation:

$$I_T = I_b R_b + I_d R_d + (I_b + I_d) R_r \quad \text{[Eq 1]}$$

Where, $R_d = \frac{1+\cos\beta}{2}$, the tilt factor for diffuse radiation

$R_r = \rho\frac{1-\cos\beta}{2}$, the tilt factor for ground reflected radiation

β = the tilt angle of the PV panel

ρ = the ground reflectivity

The tilt factor for direct solar radiation R_b can be defined as:

$$R_b = \frac{\sin\delta\sin(\Phi-\beta)+\cos\delta\cos\omega.\cos(\Phi-\beta)}{\sin\Phi\sin\delta+\cos\phi\cos\delta\cos\omega} \quad \text{[Eq 2]}$$

where Φ = local latitude angle, $\omega = \frac{(12-t)\pi}{12}$ is the hour angle (in radian) and is a function of time in hour. The declination angle

$$\delta = \frac{\pi}{180}23.45\sin\left[\frac{2\pi}{365}(284+j_d\right] \quad \text{[Eq 3]}$$

where j_d is the Julian day of the year. The clearness index k_t is expressed as

$$k_t = \frac{I_g}{I_o} \quad \text{[Eq 4]}$$

where I_g = global solar radiation on a horizontal surface,

I_o = the extra-terrestrial solar radiation.

$$I_o = H_{sc}\left[1+0.033\cos\left(\frac{2\pi j_d}{365}\right)\right](\sin\phi\sin\delta+\cos\phi\cos\delta\cos\omega) \quad \text{[Eq 5]}$$

where H_{sc}=1367 W/m^2 is the solar constant.

The instantaneous diffuse solar radiation (I_d) can also be assumed as follows:

$$I_d = I_g(1-1.13k_t), \quad \text{[Eq 6]}$$

where k_t being the clearness index.

The ratio of daily solar radiation (H_t) at an angle of tilt β and the global solar radiation (H_g) on a horizontal surface can be expressed as

$$\frac{H_T}{H_g} = \left(1 - \frac{H_d}{H_g}\right) R_{bd} + \frac{H_d}{H_g} R_d + R_r, \qquad \text{[Eq 7]}$$

where H_d is the daily diffuse solar insolation on a horizontal surface and the R_{bd} is the tilt factor

$$R_{bd} = \frac{\omega \sin\delta \sin(\phi - \beta) + \cos\delta \sin\omega_{st} \cos(\phi - \beta)}{\omega_s \sin\phi \sin\delta + \cos\phi \cos\delta \sin\omega_{st}}, \qquad \text{[Eq 8]}$$

where $\omega_s = \cos^{-1}(-\tan\phi \tan\delta)$, is the sunrise angle and $\omega_{st} = \cos^{-1}[-\tan(\phi - \beta)\tan\delta]$, is sunset angle. The hourly solar radiation (I_b) on a horizontal surface can be expressed as:

$$I_b = I_{bn} \cos\theta_z, \qquad \text{[Eq 9]}$$

where I_{bn} is the direct solar radiation incident normal to the PV panel. And the θ_z is the angle of incidence with reference to the horizon and it is evaluated as from the following equation:

$$\cos\theta_z = \sin\phi \sin\delta + \cos\phi \cos\delta \cos\omega \qquad \text{[Eq 10]}$$

Putting the value of eq 2.10 in eq 2.9, the hourly solar radiation, I_b can be evaluated as:

$$I_b = I_{bn}(\sin\phi \sin\delta + \cos\phi \cos\delta \cos\omega) \qquad \text{[Eq 11]}$$

The daily direct solar radiation (H_b) incident on a horizontal surface for a clear sunny day can be taken as the integral of I_b from sunrise (-ω) to sunset (+ω):

$$H_b = \frac{12}{\pi} I_{bn} \int_{-\omega_s}^{+\omega_s} (\sin\phi \sin\delta + \cos\phi \cos\delta \cos\omega) d\omega. \qquad \text{[Eq 12]}$$

The hourly direct solar radiation (I_b) on a horizontal surface at an hour angle ω is obtained as:

$$I_b = \frac{\pi}{24}(H_g - H_d) \frac{(\sin\phi \sin\delta + \cos\phi \cos\delta \cos\omega)}{(\omega_s \sin\phi \sin\delta + \cos\phi \cos\delta \sin\omega_s)} \qquad \text{[Eq 13]}$$

The hourly diffuse solar radiation (I_d) on a flat surface at an hour angle ω can be derived by using from daily diffuse solar radiation (H_d):

$$I_b = \frac{\pi}{24} H_d \left(\frac{\cos\omega - \cos\omega_s}{\sin\omega_s - \omega_s \cos\omega_s} \right) \qquad \text{[Eq.14]}$$

Also hourly diffuse solar radiation can be derived from clearness index k_t. The value of k_t is the ratio of daily solar radiation on a horizontal surface over the solar radiation on a flat extra terrestrial surface. Hence

$$k_t = \frac{H_g}{H_0} \qquad \text{[Eq 15]}$$

where H_0 is the daily solar insolation on an extra-terrestrial flat surface

$$H_0 = \frac{24}{\pi} H_{sc} \left[1 + 0.033 \cos\left(\frac{2\pi j_d}{365} \right) \right] \left(\cos\phi \cos\delta \sin\omega_s + \omega_s \sin\phi \sin\delta \right) \qquad \text{[Eq 16]}$$

These above set of equations can be used to derive hourly solar radiation on a horizontal surface. The PV arrays are assumed to be placed tilted to the angle of local latitude (for Melbourne it is 38° towards north). The energy efficiency of the panel is affected by the ambient temperature and is governed by the following equations:

$$I_b = \frac{\pi}{24} (H_g - H_d) \frac{\left(\sin\phi \sin\delta + \cos\phi \cos\delta \cos\omega \right)}{\left(\omega_s \sin\phi \sin\delta + \cos\phi \cos\delta \sin\omega_s \right)}$$

$$\eta_{pv} = \eta_{ref} \left[1 - B\left(T_{pv} - T_{ref} \right) \right]$$